



TECHNISCHE UNIVERSITÄT  
**ILMENAU**

---

Research Reports from the Communications Research Laboratory at  
Ilmenau University of Technology

---

**Signal Processing for Multicell Multiuser MIMO Wireless  
Communication Systems**

**Gerald Chetachi Nwalozie**



Technische Universität Ilmenau  
Fakultät für Elektrotechnik und Informationstechnik  
Institut für Informationstechnik  
Fachgebiet Nachrichtentechnik



# Signal Processing for Multicell Multiuser MIMO Wireless Communication Systems

Gerald Chetachi Nwalozie  
Dissertation zur Erlangung des  
akademischen Grades Doktor-Ingenieur (Dr.-Ing)

Anfertigung im: Fachgebiet Nachrichtentechnik  
Institut für Informationstechnik  
Fakultät für Elektrotechnik und Informationstechnik

Gutachter: Univ.-Prof. Dr.-Ing. Martin Haardt  
Prof. André L. F. de Almeida, Federal University of Ceará, Fortaleza, Brazil  
Prof. Dr.-Ing. Marius Pesavento, Technische Universität Darmstadt

Vorgelegt am: 20. 08. 2024

Verteidigt am: 14. 11. 2024

DOI: 10.22032/dbt.63971

URN: urn:nbn:de:gbv:ilm1-2024000430

## ACKNOWLEDGEMENTS

I would like to express my gratitude to Univ.- Prof. Martin Haardt for giving me an opportunity to work on this topic under his supervision. His questions, useful suggestions, and expertise have enhanced my work greatly, both academically and professionally.

I would also like to express my gratitude to Prof. André de Almeida for all of the fruitful discussions and ideas he gave me over the past years. All of these discussions were really helpful in further improving my research work. I would also like to thank Prof. Dr.-Ing. Marius Pesavento and Prof. André de Almeida for volunteering to review the thesis.

I also owe a lot of tributes to Dr. Khaled Nafez Rauf Ardah for his patience, motivation, enthusiasm, and immense knowledge, for providing me with better insights into future research directions, and also helping me out on numerous occasions whenever I was stuck at some point. I also owe a debt of gratitude to my colleagues in the Communication Research Laboratory. Particularly, I would love to thank Dr. Marjan Maleki, Dr. Liana Khamidullina, Alla Manina, Sepideh Gherekhloo, Damir Rakhimov, Joseph Kibugi Chege, Mikus Grasis, Dr. Mike Wolf, and Marko Hennhöfer. I appreciate every technical or private discussion and exchange of ideas over the past years.

I acknowledge the financial support from Nnamdi Azikiwe University Nigeria, under NEEDS Assessment Fund.

Lastly, I would like to thank my family. None of this would have been achieved without your support. Their infallible love and support have always been my strength. Their patience and sacrifice will remain my inspiration throughout my life. To my beloved sister in heaven, thank you so much for all your prayers and support to me, it is unfortunate that you are not here today to witness this. I would also like to express my deep appreciation to my beloved wife for her eternal support and understanding of my goals and aspirations. Her patience and sacrifice will remain my inspiration throughout my life. Without her help, I would not have been able to complete much of what I have done and become who I am. Finally, a few compliments to my son David Chinedum Chetachi. His innocent smile and cute little gestures have brought so much happiness and joy into my life.



---

## ABSTRACT

Multi-user multi-antenna wireless communication systems have become essential due to the widespread of smart applications and the use of the Internet. Ultra-dense deployment of small cell networks has been recognized as an effective way to meet the exponentially growing mobile data traffic and to accommodate increasingly diversified mobile applications for beyond 5G and future wireless networks. Small cells using low-power nodes are meant to be deployed in hot spots, where the number of users varies strongly with time and between adjacent cells. As a result, small cells are expected to have burst-like traffic, which makes the static time division duplex (TDD) frame configuration strategy, where a common TDD pattern is selected for the whole network, not able to meet the users' requirements and the traffic fluctuations. Dynamic TDD (DTDD) technology which allows the cells to independently adapt their TDD pattern based on the current traffic demand and interference status has been proposed as a solution to satisfy the asymmetric and dynamic traffic demand of small cells. However, one major issue arising from the deployment of small cells with multiple-input multiple-output (MIMO) and DTDD technologies is cross-link interference which severely degrades the system's performance if not properly managed. One encouraging solution is the deployment of reconfigurable intelligent surface (RIS) to flexibly reconfigure the signal propagation and/or the wireless channels between the base stations (BS) and the user equipment (UE). An RIS is a planar surface composed of a large number of low-cost passive reflecting elements, the phase shifts of the RIS elements can be adjusted to meet a certain cost function, e.g., the reflected signals add constructively at the intended users and/or destructively at the unintended users.

In the *first* part of this thesis we study the integration of an RIS in a multicell multiuser MIMO wireless communication system and propose novel non-iterative algorithms for efficient mitigation of the cross-link interference and maximization of the system-wide spectral efficiency. Furthermore, to reduce the high signaling overhead involved in such a centralized scheme in the collection of all the channel state information (CSI) at the central processing unit (CPU), a novel distributed coordinated beamforming algorithm based on the alternating direction method of multipliers (ADMM) technique is proposed. The design objective is to maximize the minimum

signal-to-interference-plus-noise ratio (SINR) of the downlink users while satisfying the total power constraint of the downlink BSs and guaranteeing that the maximum interference seen by the uplink users due to the transmission of the downlink cells is below a pre-defined level. Moreover, to further reduce the complexity involved in the joint design of the transmit beamforming vectors and RIS reflection coefficients, we exploit the decoupled nature of the signal-to-leakage-plus-noise ratio (SLNR) maximization problem which allows for a characterization of the solution to the multi-user beamforming problem in terms of generalized eigenvectors. To this end, we propose a low-complexity and non-iterative algorithm for the design of the RIS reflection vector and the Rayleigh-Ritz method for the design of the transmit beamforming vectors. Additionally, we consider the design of robust beamforming vectors that minimize the total transmit power of the downlink cells while satisfying the users' quality-of-service (QoS) targets in the presence of channel estimation errors. Robust beamforming is considered for the conventional worst-case formulation which has deterministic upper bounds on the norms of the channel estimation errors. We also consider a probabilistic-constrained optimization, based on the statistical channel error model. To this end, we adopt an S-procedure and a Bernstein-type inequality to reformulate the problems into tractable ones. Moreover, we propose two alternating optimization (AO) based algorithms using relaxed semidefinite programming (SDP) to solve these two problems. The evaluations of all the proposed algorithms are carried out using a numerical analysis that shows the effectiveness and performance superiority of the proposed algorithms, as compared to baseline algorithms, in terms of achievable rates, power efficiencies, convergence rate, and complexity. This implies that for the current and future wireless communication systems, the integration of RISs in a DTDD system has the potential to mitigate cross-link interference and the algorithms proposed in this thesis are especially appropriate.

In the *second* part of this thesis we carry out a preliminary investigation on the concept of near-field beamforming. As a result of the combination of massive MIMO and operation at mmWave frequencies, communicating devices will operate in the near-field of the BS antenna. We exploit the distance discrimination potential of the near-field beamforming from a communication perspective to facilitate the deployment of high-rate multi-user MIMO millimeter wave systems. We investigate the system's performance using several precoding schemes. Our numerical results demonstrate a significant performance improvement due to the capability of the near-field beamforming to support reliable communications even for devices that are located in the same angular direction which corresponds to the "worst case" situation. Furthermore, we study the robust near-field beamforming design. We consider a robust near-field beamforming

algorithm that is robust with respect to unknown BS antenna array aperture perturbations. We analytically derive the bounds on the perturbations of the steering vector as a function of the known norm of the coordinate displacements for the worst-case robust beamforming scheme. The evaluations of the proposed algorithm are carried out using a numerical analysis that shows the effectiveness and performance superiority of the proposed robust near-field algorithm in comparison with other benchmark schemes. We have proposed and implemented signal processing algorithms for multicell multi-user MIMO wireless communication systems. The algorithms are implemented to address some of the requirements for future wireless cellular networks. These include enhanced spectral and energy efficiencies, reduced latency, and greater flexibility in traffic handling. Our numerical results demonstrate the benefits of our proposed algorithms in addressing these requirements. Therefore, these algorithms are suitable for beyond 5G and future wireless networks. As a result, the work in this thesis is invaluable for network operators, network planners, and the research community.

---

## ZUSAMMENFASSUNG

Drahtlose Mehrnutzer-Mehrantennen-Kommunikationssysteme sind aufgrund der weiten Verbreitung aufgrund der weiten Verbreitung intelligenter Anwendungen und der Nutzung des Internets unverzichtbar geworden. Der extrem dichte Ausbau von Kleinzellennetzen ist als wirksames Mittel erkannt worden, um den exponentiell wachsenden mobilen Datenverkehr zu bewältigen und zunehmend diversifizierte mobilen Anwendungen für die Zeit nach 5G und künftige drahtlose Netzwerke. Kleinzellen mit Niedrig sind für den Einsatz in Hotspots gedacht, in denen die Anzahl der Nutzer zeitlich stark schwankt stark mit der Zeit und zwischen benachbarten Zellen schwankt. Infolgedessen wird erwartet, dass kleine Zellen Dies macht die statische Zeitduplex (TDD)-Rahmenkonfiguration, bei der ein gemeinsamer figurationsstrategie, bei der ein gemeinsames TDD-Muster für das gesamte Netz gewählt wird, nicht in der Lage ist, die Anforderungen der Nutzer und die Verkehrsschwankungen zu erfüllen. Die dynamische TDD-Technologie (DTDD), die es den Zellen ermöglicht, ihr TDD-Muster auf der Grundlage der aktuellen Verkehrsnachfrage und des Interferenzstatus selbständig anzupassen, wurde als Lösung vorgeschlagen, um die asymmetrische und dynamische Verkehrsnachfrage von kleinen Zellen zu befriedigen. Ein großes Problem beim Einsatz von Kleinzellen mit MIMO- (Multiple-Input Multiple-Output) und DTDD-Technologien ist jedoch die Cross-Link-Interferenz, die die Leistung des Systems stark beeinträchtigt, wenn sie nicht ordnungsgemäß verwaltet wird. Eine vielversprechende Lösung ist der Einsatz rekonfigurierbarer intelligenter Oberflächen (RIS) zur flexiblen Neukonfiguration der Signalausbreitung und/oder die drahtlosen Kanäle zwischen den Basisstationen (BS) und den Benutzergeräten (UE) flexibel zu rekonfigurieren. Ein RIS ist eine ebene Fläche, die aus einer großen Anzahl kostengünstiger passiver reflektierender Elemente besteht. Die Phasenverschiebungen der RIS-Elemente können so eingestellt werden, dass sie eine bestimmte Kostenfunktion erfüllen, z. B. dass die reflektierten Signale bei den beabsichtigten Benutzern konstruktiv und/oder bei den unbeabsichtigten Benutzern destruktiv wirken.

Im ersten Teil dieser Arbeit untersuchen wir die Integration eines RIS in ein drahtloses Mehrzellen-MIMO-Kommunikationssystem und schlagen neuartige nicht-iterative Algorithmen zur effizienten Minderung der Cross-Link-Interferenz und Maximierung

---

der systemweiten spektralen Effizienz vor. Um den hohen Signalisierungsaufwand zu reduzieren, der bei einem solchen zentralisierten Schema mit der Sammlung aller Kanalzustandsinformationen (CSI) in der zentralen Verarbeitungseinheit (CPU) verbunden ist, wird ein neuartiger verteilter koordinierter Strahlformungsalgorithmus vorgeschlagen, der auf der ADMM-Technik (Alternating Direction Method of Multipliers) basiert. Das Ziel des Entwurfs ist die Maximierung des minimalen Signal-Störungsplus-Rausch-Verhältnis (SINR) der Downlink-Benutzer bei gleichzeitiger Einhaltung der Gesamtleistungsbeschränkung der Downlink-BS und Gewährleistung, dass die maximale Interferenz, die die Uplink-Benutzer aufgrund der Übertragung der Downlink-Zellen wahrnehmen, unter einem unter einem vordefinierten Wert liegt. Um die Komplexität des gemeinsamen Entwurfs der Vektoren für die Sendestrahlformung und der RIS-Reflexionskoeffizienten weiter zu reduzieren, nutzen wir die entkoppelte Natur des Problems der Maximierung des Signal-Leck-Rausch-Verhältnisses (SLNR), das eine Charakterisierung der Lösung des Mehrbenutzer-Strahlformungsproblems in Form von verallgemeinerten Eigenvektoren ermöglicht. Zu diesem Zweck schlagen wir einen nicht-iterativen Algorithmus mit geringer Komplexität für den Entwurf des RIS-Reflexionsvektors und die Rayleigh-Ritz-Methode für den Entwurf der Sendestrahlformungsvektoren vor. Darüber hinaus betrachten wir den Entwurf von robusten Beamforming-Vektoren, die die Gesamtsendeleistung der Downlink-Zellen minimieren und gleichzeitig die Dienstgüteziele der Nutzer in Anwesenheit von Kanalschätzungsfehlern erfüllen. Robustes Beamforming wird für die konventionelle Worst-Case-Formulierung betrachtet, die deterministische obere Schranken für die Normen der Kanalschätzungsfehler hat. Obergrenzen für die Normen der Kanalschätzungsfehler hat. Wir betrachten auch eine wahrscheinlichkeitsbeschränkte Optimierung, die auf einem statistischen Kanalfehlermodell basiert. Zu diesem Zweck setzen wir ein S-Verfahren und eine Ungleichung vom Bernstein-Typ ein, um die Probleme in vertretbare Probleme umzuformulieren. Außerdem schlagen wir zwei auf alternierender Optimierung (AO) basierende Algorithmen vor, die entspannte semidefinite Programmierung (SDP) verwenden, um diese beiden Probleme zu lösen. Die Bewertung aller vorgeschlagenen Algorithmen erfolgt anhand einer numerischen Analyse, die die Effektivität und Leistungsüberlegenheit der vorgeschlagenen Algorithmen zeigt, im Vergleich zu den Basisalgorithmen in Bezug auf die erreichbaren Raten, die Leistungseffizienz, die Konvergenzrate und die Komplexität. Dies impliziert, dass die Integration von RISs in ein DTDD-System das Potenzial hat, Cross-Link-Interferenzen in aktuellen und zukünftigen drahtlosen Kommunikationssystemen abzuschwächen, und dass die in dieser Arbeit vorgeschlagenen Algorithmen besonders geeignet sind.

---

Im zweiten Teil dieser Arbeit führen wir eine Voruntersuchung zum Konzept des Nahfeld-Beamforming durch. Als Ergebnis der Kombination von Massive MIMO und dem Betrieb bei mmWave-Frequenzen werden kommunizierende Geräte im Nahfeld der BS-Antenne arbeiten. Wir nutzen das Entfernungsunterscheidungspotenzial der Nahfeld-Strahlformung aus einer Kommunikationsperspektive, um den Einsatz von hochratigen Multinutzer-MIMO-Millimeterwellensystemen zu erleichtern. Wir untersuchen die Leistung des Systems unter Verwendung verschiedener Vorcodierungsverfahren. Unsere numerischen Ergebnisse zeigen eine signifikante Leistungsverbesserung aufgrund der Fähigkeit des Nahfeld-Beamforming. Die numerischen Ergebnisse zeigen eine deutliche Leistungsverbesserung, die auf die Fähigkeit der Nahfeld-Strahlformung zurückzuführen ist, eine zuverlässige Kommunikation selbst für Geräte zu unterstützen, die sich in der gleichen Winkelrichtung befinden, was dem schlimmsten Fall entspricht. Außerdem untersuchen wir das robuste Nahfeld-Beamforming-Design. Wir betrachten ein robustes Nahfeld-Beamforming Algorithmus, der gegenüber unbekanntem BS-Antennengruppen-Apertur-Störungen robust ist. Wir leiten analytisch die Grenzen für die Störungen des Steuerungsvektors als Funktion der bekannten Norm der Koordinatenverschiebungen für das robuste Strahlformungsschema im schlimmsten Fall ab. Die Bewertung des vorgeschlagenen Algorithmus erfolgt anhand einer numerischen Analyse, die die Effektivität und Leistungsüberlegenheit des vorgeschlagenen robusten Nahfeld-Algorithmus im Vergleich zu anderen Benchmark-Verfahren zeigt. Wir haben Signalverarbeitungsalgorithmen für drahtlose Mehrzellen-Mehrbenutzer-MIMO-Kommunikationssysteme vorgeschlagen und implementiert. Die Algorithmen wurden implementiert, um einige der Anforderungen für zukünftige drahtlose zellulare Netzwerke zu erfüllen. Dazu gehören eine verbesserte spektrale und energetische Effizienz, geringere Latenzzeiten und eine größere Flexibilität bei der Verkehrsabwicklung. Unsere numerischen Ergebnisse zeigen die Vorteile der von uns vorgeschlagenen Algorithmen bei der Bewältigung dieser Anforderungen. Daher sind diese Algorithmen für 5G und zukünftige drahtlose Netzwerke geeignet. Daher ist die Arbeit in dieser Arbeit von unschätzbarem Wert für Netzbetreiber, Netzplaner und die Forschungsgemeinschaft.

# CONTENTS

<b>Contents</b> . . . . .	ix
<b>List of Figures</b> . . . . .	xii
<b>1. Introduction and scope of the thesis</b> . . . . .	1
1.1 Motivation and state of the art . . . . .	1
1.2 Major Contributions and Outline . . . . .	8
1.3 Matrix Properties and Notation . . . . .	12
<b>2. Overview of Reconfigurable Intelligent Surfaces</b> . . . . .	13
2.1 Introduction . . . . .	13
2.2 Architecture of RIS . . . . .	14
2.2.1 Passive RIS . . . . .	14
2.2.2 Semi-Passive RIS . . . . .	16
2.3 Optimization of RIS Reflection . . . . .	17
2.3.1 RIS-aided SISO System . . . . .	17
2.3.2 RIS-aided MISO System . . . . .	20
2.3.3 RIS-aided MIMO System . . . . .	22
2.4 Benefits of RIS-aided Wireless Communications . . . . .	24
2.5 Applications of RIS in Wireless Communications . . . . .	25
2.6 Practical Challenges . . . . .	29
2.6.1 RIS Channel Acquisition . . . . .	29
2.6.2 Practical RIS Deployment . . . . .	32
2.7 RIS versus Relay . . . . .	32
<b>3. Reflection Design Methods for RIS-Aided Dynamic TDD Systems</b> . . . . .	35
3.1 Introduction . . . . .	35
3.2 Chapter Contributions and Organization . . . . .	36
3.3 System Model . . . . .	37
3.4 Problem Formulation . . . . .	42
3.5 Proposed RIS Reflection Design Methods . . . . .	43
3.5.1 Method 1 . . . . .	45
3.5.2 Method 2 . . . . .	46
3.6 Active Beamforming Design . . . . .	47
3.6.1 Transmit beamforming design . . . . .	47
3.6.2 Receive beamforming design . . . . .	48
3.7 Complexity analysis . . . . .	48
3.8 Numerical Results . . . . .	49

3.9	Chapter Conclusions . . . . .	52
<b>4.</b>	<b>An ADMM approach for Distributed Coordinated Beamforming for RIS-aided DTDD Systems . . . . .</b>	<b>53</b>
4.1	Introduction . . . . .	53
4.2	Chapter Contributions and Organization . . . . .	55
4.3	System Model . . . . .	55
4.4	Problem Formulation . . . . .	58
4.5	Transmit Beamforming Design . . . . .	58
4.5.1	Centralized Algorithm . . . . .	59
4.5.2	Distributed Algorithm . . . . .	60
4.6	RIS Reflection Matrix Design . . . . .	66
4.7	Backhaul Signaling and Per-BS complexity Analysis . . . . .	71
4.8	Numerical Results . . . . .	72
4.9	Chapter Conclusions . . . . .	74
<b>5.</b>	<b>Leakage-Based Coordinated beamforming for RIS-aided DTDD Systems . . . . .</b>	<b>76</b>
5.1	Introduction . . . . .	76
5.2	Chapter Contributions and Organization . . . . .	77
5.3	System Model . . . . .	78
5.4	Problem Formulation . . . . .	80
5.4.1	RIS Reflection Design Method . . . . .	81
5.4.2	Transmit Beamforming Design . . . . .	84
5.5	Complexity analysis . . . . .	85
5.6	Numerical Results . . . . .	85
5.7	Chapter Conclusions . . . . .	89
<b>6.</b>	<b>Robust Beamforming for RIS-Aided Dynamic TDD Systems . . . . .</b>	<b>90</b>
6.1	Introduction . . . . .	90
6.2	Chapter Contributions and Organization . . . . .	92
6.3	System Model . . . . .	94
6.4	Worst-case Robust (WCR) Beamforming Design . . . . .	97
6.5	Probabilistic-Constrained Robust (PCR) Optimization . . . . .	106
6.6	Complexity Analysis . . . . .	115
6.7	Numerical Results . . . . .	118
6.8	Chapter Conclusions . . . . .	127
<b>7.</b>	<b>Near Field Beamforming for MU-MIMO Millimeter Wave Communication System . . . . .</b>	<b>128</b>
7.1	Introduction . . . . .	128
7.2	Chapter Contributions and Organization . . . . .	129
7.3	System Model . . . . .	130
7.4	Precoding Methods . . . . .	132
7.4.1	MU-MISO transmission . . . . .	132
7.4.2	MU-MIMO transmission . . . . .	135
7.5	Numerical Results . . . . .	135
7.6	Chapter Conclusions . . . . .	140

<b>8. Robust Near Field Beamforming for Millimeter Wave Communication Systems with Aperture Perturbations</b> . . . . .	141
8.1 Introduction . . . . .	141
8.2 Chapter Contributions and Organization . . . . .	142
8.3 System Model . . . . .	143
8.4 Aperture Perturbation Model . . . . .	145
8.5 Problem Formulation . . . . .	148
8.6 Worst-Case Robust beamforming . . . . .	149
8.7 Numerical Results . . . . .	150
8.8 Conclusions . . . . .	156
<b>9. Conclusions and future work</b> . . . . .	157
9.1 Future works . . . . .	160
9.1.1 Acquisition of channel state information . . . . .	160
9.1.2 Orthogonal frequency-division multiplexing System . . . . .	160
9.1.3 Integration of double RISs . . . . .	161
9.1.4 Effects of CSI estimation error on Near-field beamforming . . . . .	161
<b>Appendix A. Symbols and Notation</b> . . . . .	162
<b>Appendix B. Acronyms</b> . . . . .	163
<b>Appendix C. Convex Optimization</b> . . . . .	166
C.1 Convex Sets . . . . .	166
C.2 Convex Functions . . . . .	168
C.3 Convex Optimization Problem . . . . .	169
C.4 Second-order Cone Programming . . . . .	171
C.4.1 Formulating Problems as SOCP . . . . .	173
C.5 Semidefinite Programming . . . . .	175
C.6 Optimization Problems of Real Functions in Complex Variables . . . . .	178
<b>Appendix D. Proofs and Derivations</b> . . . . .	182
D.1 Detailed explanation of the S-procedure . . . . .	182
D.2 Detailed explanation of Bernstein-type inequality . . . . .	184
D.3 Rayleigh Quotient and Eigenvalue Problem . . . . .	186
D.3.1 Generalized Eigenvalue Optimization . . . . .	188
D.4 Detailed Expansion of the Power Constraints in WCR and PCR Methods . . . . .	189
D.4.1 Power Constraints in WCR method . . . . .	189
D.4.2 Power Constraints in PCR . . . . .	190
D.5 Complexity Analysis for WCR and PCR Designs in Chapter 6 . . . . .	191
D.5.1 Worst-case Complexity Analysis . . . . .	192
D.5.2 Probabilistic-constrained Complexity Analysis . . . . .	192
<b>Bibliography</b> . . . . .	194
<b>Erklärung</b> . . . . .	209

## LIST OF FIGURES

1.1	Different generations of mobile cellular systems. . . . .	2
1.2	Interference scenario in DTDD system . . . . .	6
2.1	An RIS with $M_S$ passive reflecting elements . . . . .	15
2.2	An RIS with some active reflecting elements . . . . .	16
2.3	An RIS-aided SISO communication system . . . . .	17
2.4	An RIS-aided MISO communication system . . . . .	21
2.5	An RIS-aided MIMO communication system . . . . .	23
2.6	RIS for coverage extension . . . . .	25
2.7	RIS-assisted physical layer security . . . . .	25
2.8	RIS for improving channel rank . . . . .	25
2.9	RIS for interference suppression . . . . .	25
3.1	An RIS-aided DTDD system comprising $Q = 4$ cells. . . . .	38
3.2	Configuration and orientation of the ULA at the BS. . . . .	40
3.3	Configuration and orientation of the uniform rectangular structure at the RIS. . . . .	41
3.4	SE versus DL SNR, assuming $M_S = 256$ and $M_T = 16$ . . . . .	50
3.5	SE versus DL SNR, (DL+UL) assuming $M_S = 256$ and $M_T = 16$ . . . . .	50
3.6	SE versus number of antennas $M_T$ for $M_S = 252$ . . . . .	51
3.7	SE versus number of RIS elements $M_S$ for $M_T = 16$ , assuming DL SNR = 10 dB . . . . .	51
4.1	An RIS-aided DTDD system comprising $Q = 4$ cells. . . . .	56
4.2	Flow chart for the implementation of the AO-ADMM algorithm. . . . .	70
4.3	Convergence behaviour of the AO-ADMM for different $P$ , assuming $\rho = 0.5$ . Note $\rho$ is the penalty parameter as given in (4.24). . . . .	72
4.4	Convergence behaviour of the AO-ADMM algorithm for different $\rho$ , assuming that $P = 5$ dB. . . . .	73
4.5	Minimum SE versus the maximum transmit power, $\rho = 0.5$ . . . . .	74
5.1	SLNR versus DL transmit power, assuming $M_S = 256$ and $M_T = 16$ . . . . .	87

5.2	System-wide SE versus DL SNR, assuming $b = 2$ . . . . .	88
5.3	SE versus DL SNR, for different quantization bits $b$ . . . . .	88
6.1	An RIS-aided DTDD system without direct links. . . . .	95
6.2	Flow chart for the implementation of the WCR AO-based algorithm. . . . .	105
6.3	Flow chart for the implementation of the PCR AO-based algorithm. . . . .	114
6.4	Number of FLOPs vs. number of transmit antennas, $M_T$ for $M_S = 12$ . . . . .	117
6.5	Number of FLOPs vs. number of RIS elements, $M_S$ for $M_T = 6$ . . . . .	117
6.6	Average total transmit power vs. target SINR for both methods. . . . .	120
6.7	DL sum rate, assuming SINR target $\gamma = 6$ dB, $M_S = 12$ , and $M_T = 6$ . . . . .	120
6.8	Average total transmit power vs. number of RIS elements $M_S$ , assuming SINR target = 6 dB and $M_T = 6$ . . . . .	121
6.9	Total DL cells leakage power. . . . .	122
6.10	Histogram of DL transmit power. . . . .	124
6.11	Histogram of achieved SINR. . . . .	125
6.12	Histogram of DL leakage power. . . . .	126
7.1	MU-MIMO near-field configuration with ULA at the BS, $\phi_{UE}^{(k)} = \phi_{UE}, \forall k$ . . . . .	131
7.2	Beam pattern for MRT. Left: Beam pattern vs. distance. Right: Beam pattern vs. angle. . . . .	136
7.3	Beam pattern vs. distance. Left: ZF. Right: MMSE. . . . .	137
7.4	Achievable rate for MU-MISO setup ( $M_T = 128, M_R = 1, K = 5$ ). . . . .	137
7.5	Achievable rate for MU-MIMO setup ( $M_T = 128, M_R = 4, K = 5$ ). . . . .	138
7.6	Achievable rate vs array size ( $M_T d$ ) for MU-MIMO setup ( $M_R = 4, K =$ $5$ ). . . . .	139
7.7	Non-zero singular values vs distance. . . . .	139
8.1	Configuration and Orientation of URA at the BS . . . . .	144
8.2	Bounds of the perturbation for each axis of URA at the BS . . . . .	146
8.3	Output SINR versus SNR, $N_s = 1000$ . . . . .	151
8.4	Output SINR versus $N_s$ , SNR = -15 dB . . . . .	152
8.5	Transmit power versus SINR, $N_s = 1000$ . . . . .	153
8.6	Histogram of minimized interference power. . . . .	154
8.7	Histogram of achieved desired power. . . . .	155
C.1	Graphical representation of a convex function, (adapted from [131] ) . . . . .	168
C.2	Second-order cone . . . . .	172

# 1. INTRODUCTION AND SCOPE OF THE THESIS

The exploration of signal processing techniques for multicell multi-user MIMO systems is motivated by the need to address the challenges of modern wireless communication networks, due to the rapid advancement in technology and the emergence of diverse mobile applications. These challenges include the demand for higher data rates, interference management, resource optimization, and dynamic communication requirements. As a result, providing high spectral and energy efficiency in wireless communication systems has recently received a lot of attention. This chapter provides a high-level overview of the techniques that have been implemented to address these demands, such techniques include antenna diversity schemes, multiple-input multiple-output (MIMO) concepts, millimeter wave (mmWave) communications, beamforming techniques, and network densification. Furthermore, in this chapter, the open questions as well as the contributions of the current work are discussed.

## 1.1 Motivation and state of the art

Generally, a signal is defined as any time-varying physical process intended to convey information. It is a mathematical representation of any physical energy that is a function of one or more independent variables such as pressure, position, distance, time, etc., that contain some information. Some typical examples of signals are audio, video, sensor data, images, and many other types of data, including noise which however contains unwanted information. The representation, transformation, processing, analysis, and manipulation of analog and digital signals are the core functions of signal processing. There is a wide range of typical applications in which signal processing techniques are used, these include speech recognition, video and audio processing, telecommunications, image processing, biomedical engineering, financial engineering, and control systems. Some of the specific tasks in signal processing include filtering, noise reduction, amplification, compression, and feature extraction to detect patterns. Particularly, in telecommunications, signal processing techniques are used to transmit,

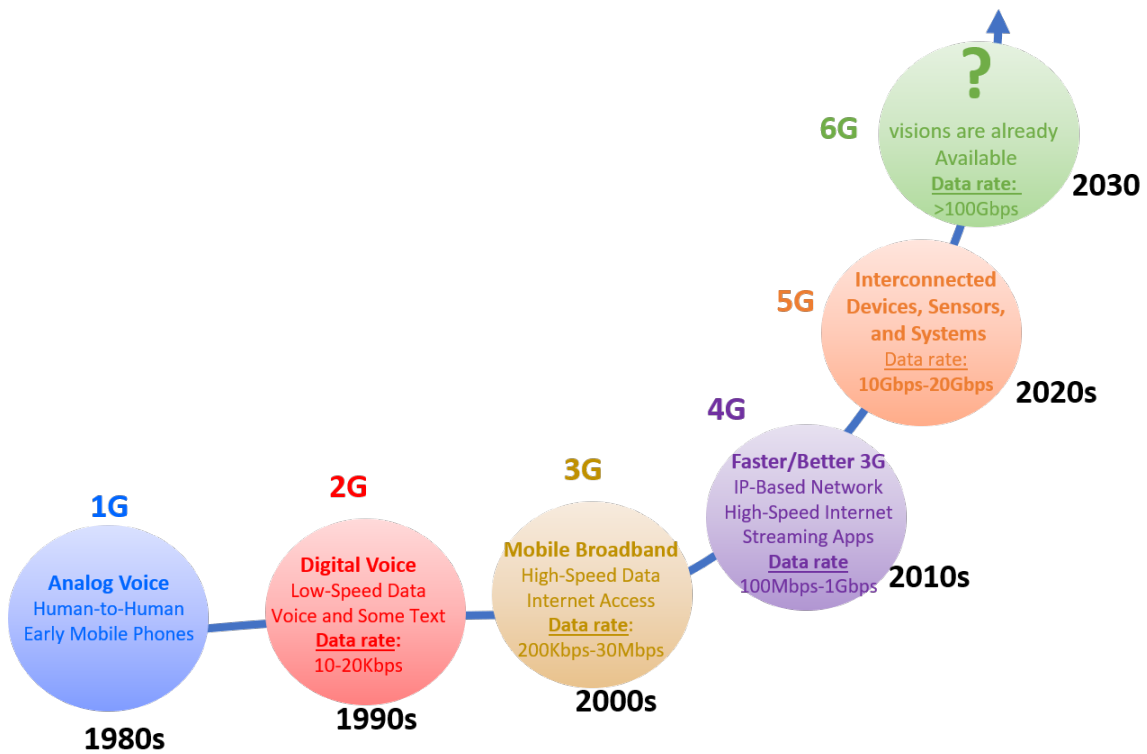


Fig. 1.1: Different generations of mobile cellular systems.

receive, and process signals over communication channels. Such techniques include modulation, demodulation, error correction, and signal amplification.

The abstract representation of signals in digital form is both simple and powerful, making it very convenient for use in many applications. As a result, digital signal processing techniques that deal specifically with the representation and manipulation of signals in a digital format are very important in many applications. In the last few decades, digital signal processing techniques have played a crucial role in the development and advancement of modern communication systems. Generally, starting from the second-generation (2G) to the current fifth-generation (5G) cellular systems, digital signal processing techniques have helped to transform modern wireless communication systems as can be seen in Fig. 1.1 [1, 2]. This has resulted in an exponential growth in the number of mobile subscribers, connected devices, and the amount of data sent and received [3]. This exponential growth is projected to be even higher for the beyond fifth-generation (B5G) and sixth-generation (6G) networks as a result of the widespread use of mobile internet and smart applications such as smart cities, smart buildings, augmented reality, internet of things (IoT), and smart homes [4].

Therefore, future wireless communication technologies should be able to satisfy the continuously increasing traffic demand and the high demand for quality of service (QoS)

by the consumers. Such QoS includes the demand for high throughput, high reliability, and low latency and jitter. As a result, there has been increased research focus in the area of developing new signal processing techniques for different air interfaces, for the B5G and 6G wireless systems. There are different requirements these new techniques are expected to meet, such as fast switching between downlink and uplink for time division duplex (TDD) systems, ultra-low latency transmissions for long and short data bursts, enhanced Mobile Broadband (eMBB), and high data rates [5]. Unfortunately, major capacity and performance limitations of wireless communication systems are a result of the unpredictability of the wireless propagation environment and the shortage of spectrum. Therefore, new signal processing techniques have been implemented to address these shortcomings, such as antenna diversity schemes, multiple-input multiple-output (MIMO) concept, millimeter wave (mmWave) communications, beamforming techniques, and network densification. In the following, we will give a comprehensive review of these techniques.

Antenna diversity is one of the techniques that is employed to improve the reliability of a wireless channel and increase the overall average received signal power. This is achieved by making use of more than one antenna to transmit or receive signals from different propagation paths in order to compensate for the multipath interference [6]. In wireless communications, the received signal strength varies strongly due to the effect of multipath propagation and interference on the link quality. Therefore, implementing antenna diversity schemes in such scenarios improves the reliability of a wireless channel. There are different forms of antenna diversity, including spatial diversity where multiple antenna elements occupy separate locations, polarization diversity where multiple antennas provide two or more different polarizations, and pattern diversity where directional antennas discriminate over angle space [6].

MIMO systems achieve a high spectral efficiency by using multiple antennas and spatial processing. Spatial multiplexing MIMO technique, in which the multiple data streams are divided into different substreams and transmitted by every transmit antenna, takes full advantage of the channel's spatial dimension and can significantly improve the spectral efficiency of a wireless link compared to traditional single-antenna systems [7]. The MIMO system offers the following advantages which include, array gain, interference reduction, and diversity gain. In addition to the benefit obtainable by the use of multiple antennas at the transmitter and the receiver, the MIMO systems also offer spatial multiplexing gain compared to traditional antenna array systems [8]. In wireless networks, using different phases and amplitudes to transmit the same data signal from all antennas can result in a high signal power for the intended user. This is achieved by coherently adding all the signal components, whereas low interference

is achieved at the non-intended user by destructively adding all the signal components [9, 10]. This constructive and/or destructive manipulation of the signal components can be realized by using linear or non-linear transmission techniques [11]. In terms of channel capacity gain, the non-linear techniques have been shown to outperform linear techniques. Unfortunately, the non-linear techniques have a high complexity compared with the linear techniques. As a result, the linear transmission beamforming techniques have gained more interest [11–13]. In a wireless network, the base station (BS) using the same radio resources can serve user equipments (UEs) located in different geographical spaces simultaneously. This is known as space-division multiple access (SDMA). In such a scenario, one or multiple beamforming vectors are designed and assigned to each UE and can be matched to the UE's channel.

Beamforming is a technique that is both versatile and powerful. It can be used in receiving, transmitting, or relaying signals of interest in a spatially selective manner in the presence of noise and interference. Beamforming can be performed at the BS to serve multiple users simultaneously and efficiently, as well as at the UE to improve the signal reception. In wireless communication systems, various performance criteria are used for the design of beamforming vectors. Some of these optimization criteria include the maximization of the signal-to-interference-plus-noise ratio (SINR), the minimization of the transmit power, interference nulling, the maximization of the signal-to-noise ratio (SNR), the maximization of the spectral efficiency, the maximization of the minimum SINR to achieve fairness among users, and robustness to channel uncertainty [14–16]. Maximizing the received signal power at the intended UE in a single-user MIMO (SU-MIMO) system can be implemented using a traditional beamforming scheme such as zero-forcing (ZF), minimum mean squared error (MMSE), and successive interference cancellation. Though there are significant benefits of MIMO in SU-MIMO system, these benefits would be higher when multi-user MIMO (MU-MIMO) is considered. Therefore, the issue of MIMO in multi-user systems is much more compelling. MU-MIMO can be considered on both the uplink and downlink [9, 10, 17]. The goal is to serve multiple users at the same time on the same resources. As a result, several beamforming schemes have been proposed to increase the signal power at the intended user and reduce interference to non-intended users for MU-MIMO systems. These include ZF, block diagonalization (BD), regularized BD, maximum ratio transmission (MRT), MMSE, weighted MMSE schemes, etc., [9, 13, 18, 19]. For instance, in a noise-limited system also known as the low signal-to-noise ratio (SNR) regime, the maximum ratio transmission (MRT) is the optimal transmit beamforming. The MRT scheme does not attempt to cancel the multi-user interference, rather its main objective is to maximize the signal power at the intended UE. Furthermore, for an interference-limited system,

which is the high-SNR regime the ZF scheme is the optimal transmit beamforming, to eliminate the interference-leakage to the non-intended UEs [9]. Regrettably, these schemes are far from optimal in the moderate SNR regime. Therefore, in the literature, there have been different iterative algorithms proposed to optimize the transmit beamforming vectors using different system optimization criteria. Such as the maximization of the SINR, MMSE criteria, and weighted sum rate [14, 15].

Additionally, deploying more BSs per area which allows the reuse of system resources is another way to improve the throughput of the cellular network. This is known as the densification of communication networks. Nonetheless, there are some concerns with this scheme, such as inter-cell interference issues, high cost of deployment, and unsuitability for high-speed UEs as they would have to switch the serving BS very often. In a multi-cell system, signals transmitted in one cell are observed as interference at other cells. One method to mitigate this interference is to use frequency-selective small cells. As a result, the deployment of small cells was introduced by the 3rd generation partnership project (3GPP) long-term evolution (LTE)-Advanced also known as 4G [20]. In comparison with the macro cells, the small cells have low operational cost and low hardware complexity. The range of the small cells is usually from ten meters to a few hundred meters and they operate at 3.5 GHz band [20, 21]. To further increase the system coverage, throughput, and capacity of the cellular system, these small cells are meant to be deployed in hot spots within the coverage area of the macro cell.

Generally, wireless networks operate in half-duplex (HD) such as TDD or frequency division duplex (FDD). In TDD the transmission for the uplink (UL) and downlink (DL) is carried on the same carrier frequency but in different time slots. Whereas in FDD, separate frequency channels are used for the UL and DL transmissions. These frequency channels in a FDD system are separated by a guard band. TDD has some notable advantages over FDD in terms of low power requirements, frequency diversity, lower hardware complexity, and unpaired band allocation [22, 23]. However, the most important advantage of TDD over FDD is the concept of channel reciprocity among the links's channel characteristics. This is as a result of the usage of the same carrier frequency for both the DL and UL transmissions. It is important to state that in a TDD system, only the physical channels are reciprocal, the radio frequency (RF) chains need to be calibrated. For small cell cellular systems, TDD is the widely used mode of transmission because of power consumption, spectrum efficiency, cost-effectiveness, interference mitigation, and a small round-trip propagation delay associated with the small cells. The TDD configuration in LTE-advanced networks is assumed to be a fixed TDD pattern [20]. However, in a static TDD system, the UL/DL changes are

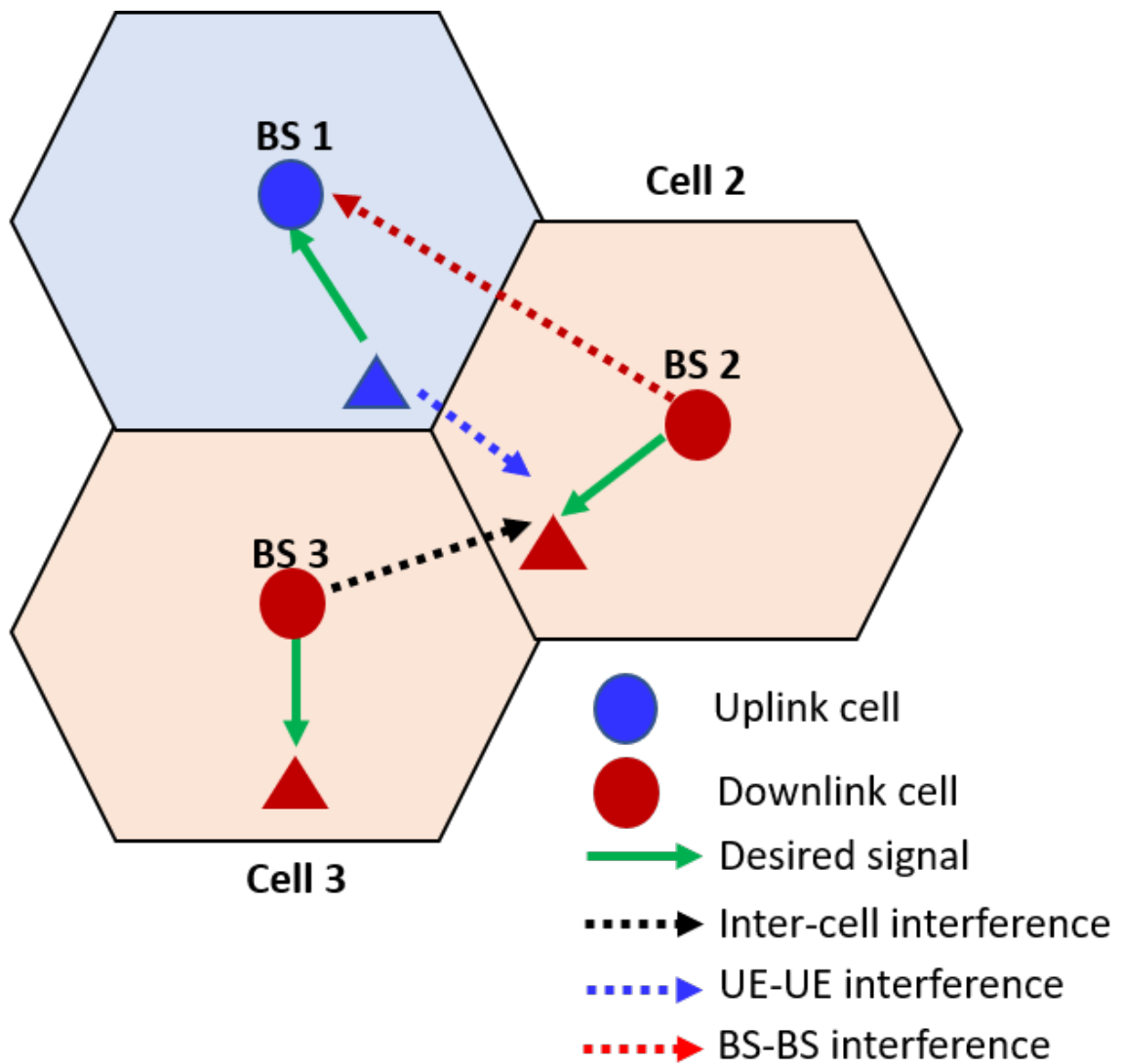


Fig. 1.2: Interference scenario in DTDD system

only possible at the subframe level. This cannot be rapidly modified to match the instantaneous traffic demands in those small cells. Therefore, in [24] this rigid scheme is broken, for 5G networks, and a dynamic TDD (DTDD) scheme was introduced to cope with traffic fluctuations. DTDD is a flexible form of the TDD scheme that enables cells to independently set the UL/DL configuration in each slot based on the prevailing traffic demands and interference levels [25]. Therefore, it has been shown in [25] and [26] that DTDD can greatly improve spectrum usage and reduce network latency. However, due to the coexistence of neighboring cells operating in different link directions in DTDD, this gives rise to additional BS-to-BS and UE-to-UE interference among other forms impairment as shown in Fig. 1.2. This cross-link interference severely degrades the system's performance. Hence, interference management in a DTDD system is essential.

As a result, there have been several approaches proposed to deal with this cross-link interference, such as clustering schemes, time slot allocation algorithms, and power control solutions [25]. The authors in [27], proposed to group several cells into a cluster according to some metric(s), where cells in the same cluster adopt the same TDD configuration. In [28], the authors proposed dynamic time slot allocation for an adaptive and flexible interference avoidance scheme. The work in [29] used adaptive power control techniques to reduce and compensate the cross-link interference. However, these solutions do not benefit from multi-antenna capabilities in order to mitigate interference. In the case of MIMO systems, Jayasinghe et al. [30] proposed a solution for the maximization of the weighted sum rate. The work in [31] proposed an interference alignment-based solution for a limited scenario formed by three cells and one user per cell. Nevertheless, interference management strategies in DTDD systems are more complicated than those in static TDD systems due to the cross-link interference. Therefore, the development of an efficient cross-link interference management scheme for DTDD systems is necessary.

Reconfigurable intelligent surfaces (RISs) have gained significant attention recently, as a low-cost and compact transformational technology for future wireless systems [32–34]. An RIS is a planar surface composed of a large number of passive reflecting elements that are closely packed together and a smart controller. Each of the reflecting elements is capable of controlling the phase and/or amplitude of the incident waveform independently [32, 33, 35]. By strategically deploying RISs in wireless networks and intelligently coordinating their reflections it is possible to flexibly reconfigure the signal propagation and/or the wireless channels between the transmitters and the receivers to achieve desired realizations or distributions, e.g., the reflected signals can add constructively at the intended users and/or destructively at the unintended users [33]. Due to these potentials, RIS-aided communication systems have received significant attention in the last few years, where various RIS-aided communication systems have been studied, such as millimeter-wave (mmWave) communications, cognitive radio, and unmanned aerial vehicle (UAV) communications [36–40]. Designing RIS elements with wideband characteristics and ensuring efficient control mechanisms for adjusting their properties across different frequency bands is a significant challenge [33]. In this thesis, Chapter 2 elaborates more on RISs, their fundamentals, architectures, and practical constraints.

Motivated by the inherent benefits of the RIS and the need to design and implement efficient interference management schemes for DTDD systems, this thesis exploits the advantages offered by DTDD along with the potential benefits of the RIS to mitigate the cross-link interference in a DTDD system. However, to the best of the author's

knowledge, there has been no work so far considering the integration of both techniques in the literature. Therefore, we consider the following open problems, how to jointly design the reflection coefficient of the RIS and the transmit beamforming vector to minimize the cross-link interference in a DTDD system and to reduce the signaling overhead involved in the collection of the channel state information (CSI) at the central processing unit (CPU). Additionally, the open problem of reducing the complexity involved in the design of transmit beamforming vectors for an RIS-aided DTDD system and the joint design of the RIS reflection coefficient and transmit beamforming vectors that are robust against CSI errors are considered. For B5G and 6G networks, an RIS-aided DTDD system has many potential use cases. It is ideal for areas with high user density and where demand for wireless connectivity is high or access to cell towers is difficult. Such as shopping malls, entertainment complexes and venues, stadiums, healthcare organizations, and manufacturing facilities.

Furthermore, motivated by the promising potential of the solution of the exploitation of higher frequencies in conjunction with large-scale antenna arrays at the BS. This thesis considers the efficient deployment of a high-rate MU-MIMO mmWave communication system by exploiting the distance-discriminating capability of near-field beamforming. At the same time, due to the potentially large size of antenna arrays operating at mmWave frequencies, there might be different reasons for the emergence of perturbations in the aperture geometry. These inevitable aperture deformations of the BS antenna array degrade the overall performance of the communication system. Motivated by this and the performance potential of near-field communications, this thesis studies the robust near-field beamforming designs that are robust against BS antenna array aperture perturbations.

## 1.2 Major Contributions and Outline

Motivated by the previously presented state-of-the-art, the contributions of this thesis are organized into nine chapters.

Chapter 2 provides a general overview of the fundamental concepts of RIS technology, its benefits, use cases, and applications in future 5G and 6G networks. In addition, the channel estimation problem and the beamforming optimization methods using RISs are discussed where we present the current state-of-the-art model for RIS-aided wireless communications. The overall aim of this chapter is to familiarize the readers, who are new to the subject, with the essentials of RIS technology.

In Chapter 3, we consider an RIS-aided multicell system model that takes into

account both prevailing traffic conditions and multicell BS-to-BS and UE-to-UE interference levels. The chapter addresses the issue of joint optimization of the transmit beamforming and the passive beamforming for an RIS-aided DTDD wireless system, to minimize the cross-link interference and maximize the system-wide spectral efficiency. However, the problem is shown to be non-convex as a result of the coupling of the optimization variables and the constant modulus constraints of the RIS. Therefore, we propose two non-iterative methods to design the RIS reflection vector to maximize the system spectral efficiency, while reducing the cross-link interference. Numerical results show the efficiency of the proposed methods compared to some baseline schemes. It is shown that the integration of an RIS in DTDD systems has a great potential to improve the communication efficiency while reducing the impact of cross-link interference. Chapter 3 is based on the following peer-reviewed conference publication:

G. C. Nwalozie, K. Ardah, and M. Haardt, "Reflection Design methods for Reconfigurable Intelligent Surfaces-aided Dynamic TDD Systems," in *Proc. of 12th IEEE Sensor Array and Multichannel Signal Processing Workshop (SAM 2022)*, Trondheim Norway, June 2022 [41].

Chapter 4 considers a decentralized coordinated algorithm for an RIS-aided DTDD wireless communication system. The motivation for this chapter is to reduce the high signaling overhead involved in collecting all the channel state information at the central processing unit regarding the centralized solution for the active beamforming design as presented in Chapter 3. To this end, a distributed coordinated beamforming based on the alternating direction method of multipliers (ADMM) is proposed in this chapter. A Semidefinite Programming (SDP) technique (explained in Appendix C.5) is adopted for the design of the passive reflection matrix of the RIS. Our design objective is to maximize the minimum SINR of the downlink users while satisfying the total power constraint of the downlink base stations and guaranteeing that the maximum interference seen by the uplink users due to the transmission of the downlink cells is below a pre-defined level. Our numerical results demonstrate that the proposed algorithm converges to the centralized solution in a reasonable number of iterations (within 10-15 iterations) as shown in Figure 4.3. Chapter 4 is based on the following peer-reviewed conference publication:

G. C. Nwalozie and M. Haardt, "Distributed Coordinated Beamforming for RIS-aided Dynamic TDD Systems," in *Proc. of 26th International ITG Workshop on Smart Antennas and 13th Conference on Systems, Communications, and Coding (WSA and SCC 2023)*, Braunschweig, Germany, March 2023 [42].

In Chapter 5, we jointly optimize the base station transmit precoders and the RIS reflection vector to maximize the sum signal-to-leakage-plus-noise ratio (SLNR), with

the objective of improving the communication efficiency while reducing the impact of cross-link interference. This is motivated by the need to reduce the complexity involved in the design of the transmit beamforming vectors. The SLNR is a reasonable metric to balance the complexity and performance in massive MIMO systems and leads to an optimal closed-form characterization of the BS precoders. The proposed method does not impose a condition on the relation between the number of transmit and receive antennas, and it also avoids noise enhancement. Our numerical results demonstrate a significant performance improvement using the proposed method as compared to some baseline schemes. Chapter 5 is based on the following peer-reviewed conference publication:

G. C. Nwalozie and M. Haardt, “Leakage-based Coordinated Beamforming for RIS-aided Dynamic TDD Systems,” in *Proc. of 31st European Signal Processing Conference (EUSIPCO 2023)*, Helsinki, Finland, September 2023 [43].

Motivated by the fact that the performance improvements obtainable from the joint design of transmit and passive beamforming vectors for an RIS-aided DTDD wireless system heavily depend on the accuracy of the CSI, Chapter 6 considers robust transmission strategies for an RIS-aided wireless system with imperfect CSI. Due to estimation errors and limited feedback channels, the transmitters can never have perfect CSI. The problem is formulated as a sum-power minimization problem for the downlink cells under individual users’ SINR constraints, interference temperature constraints for the uplink cells, and unit-modulus constraints of the RIS in the presence of CSI errors. We consider the statistical CSI imperfection and the bounded CSI imperfection models. We adopt the S-procedure (explained in Appendix D.1) to reformulate the bounded CSI model-based design problem and the Bernstein-type inequality (explained in Appendix D.2) to reformulate the statistical CSI model-based design problem into tractable problems. The resulting problems can be solved efficiently. Numerical results are presented showing that the outage probability-based approach outperforms that of the bounded design. Chapter 6 is based on the following peer-reviewed conference publications:

G. C. Nwalozie and M. Haardt, “Robust beamforming for RIS-aided Dynamic TDD Systems,” in *Proc. of 31st European Signal Processing Conference (EUSIPCO 2023)*, Helsinki, Finland, September 2023 [44].

G. C. Nwalozie and M. Haardt, “Probabilistic-Constrained Robust beamforming for RIS-aided Dynamic TDD Systems,” in *Proc. of 19th International Symposium on Wireless Communication Systems (ISWCS 2024)*, Rio de Janeiro, Brazil, July 2024 [45].

Chapter 7 studies near-field beamforming for a multi-user multiple-input multiple-

output (MU-MIMO) millimeter wave (mmWave) communication system. We exploit the distance discrimination potentials of the near-field beamforming to facilitate an efficient deployment of high-rate multi-user downlink MIMO mmWave systems. To this end, we investigate the performance of the near-field beamforming using several precoding schemes. Our numerical results demonstrate a significant performance improvement due to the capability of the near-field beamforming to support reliable communications even for devices that are located in the same angular direction which corresponds to the “worst case” situation. In the case of a far-field scenario, users that are located in the same angular direction cannot be separated. Chapter 7 is based on the following peer-reviewed conference publication:

G. C. Nwalozie, D. Rakhimov, and M. Haardt, “Near-field beamforming for MU-MIMO millimeter wave communication system,” in *Proc. of 31st European Signal Processing Conference (EUSIPCO 2023)*, Helsinki, Finland, September 2023 [46].

Motivated by the performance potentials of near-field communications and the inevitable aperture deformations of the BS antenna array that degrade the overall performance of the communication system, Chapter 8 studies robust near-field beamforming designs that are robust against BS antenna array aperture perturbations. We analytically derive the bounds on the perturbations of the steering vector as a function of the known norm of the coordinate displacements for the worst-case robust beamforming scheme. Our simulation results confirm that the proposed robust near-field algorithm outperforms the other benchmark schemes. Chapter 8 is based on the following peer-reviewed conference publication:

G. C. Nwalozie, D. Rakhimov, and M. Haardt, “Robust near-field beamforming for millimeter wave communication systems with aperture perturbation,” in *Proc. of 49th IEEE International Conference on Acoustics, Speech, and Signal Processing (ICASSP 2024)*, Seoul, Korea, April 2024 [47].

Finally, we conclude this thesis and present the future work in Chapter 9. In Appendix A, we list the symbols and the used notation. Some acronyms used in this thesis are provided in Appendix B. Furthermore, in Appendix C some important concepts and the basis of convex optimization are presented. Moreover, Appendix D provides a detailed explanation for the S-procedure and Bernstein-type inequalities.

### 1.3 Matrix Properties and Notation

The following matrix properties are used in this thesis

$$\text{vec}(\mathbf{A}\text{diag}(\mathbf{b})\mathbf{C}) = (\mathbf{C}^\top \diamond \mathbf{A})\mathbf{b} \quad (1.1)$$

$$(\mathbf{A}\mathbf{C}) \diamond (\mathbf{B}\mathbf{E}) = (\mathbf{A} \otimes \mathbf{B})(\mathbf{C} \diamond \mathbf{E}) \quad (1.2)$$

$$\mathbf{x}^\text{H} \mathbf{A} \mathbf{x} = \text{Tr}(\mathbf{A} \mathbf{x} \mathbf{x}^\text{H}) \quad (1.3)$$

$$\text{Tr}(\mathbf{A}^\text{H} \mathbf{B}) = \text{vec}^\text{H}(\mathbf{A}) \text{vec}(\mathbf{B}) \quad (1.4)$$

$$\text{vec}(\mathbf{A}\mathbf{B}\mathbf{C}) = (\mathbf{C}^\top \otimes \mathbf{A}) \text{vec}(\mathbf{B}) \quad (1.5)$$

$$(\mathbf{A} \otimes \mathbf{A})(\mathbf{C} \otimes \mathbf{D}) = \mathbf{A}\mathbf{C} \otimes \mathbf{B}\mathbf{D} \quad (1.6)$$

$$\text{Tr}(\mathbf{A}\mathbf{B}\mathbf{C}\mathbf{D}) = \text{Tr}(\mathbf{C}\mathbf{D}\mathbf{A}\mathbf{B}) \quad (1.7)$$

**Notation.** This thesis uses vectors and matrices as lowercase and uppercase boldface letters, respectively. The notation  $\diamond$  is used to denote the Khatri-Rao product, while  $\otimes$  is used to denote the Kronecker product. The transpose and the conjugate transpose (Hermitian) of  $\mathbf{X}$  are represented by  $\mathbf{X}^\top$  and  $\mathbf{X}^\text{H}$ , respectively. The  $\text{diag}(\mathbf{x})$  forms a matrix by placing  $\mathbf{x}$  on its main diagonal, and  $\text{vec}(\mathbf{X})$  vectorizes  $\mathbf{X}$  by stacking its columns on top of each other. Moreover,  $\mathbb{H}^{n \times n}$  stands for the set of  $n \times n$  complex Hermitian matrices. For a matrix  $\mathbf{A} \in \mathbb{H}^{n \times n}$ , we write  $\mathbf{A} \succeq \mathbf{0}$  and  $\mathbf{A} \succ \mathbf{0}$  to denote that  $\mathbf{A}$  is positive semidefinite and positive definite, respectively. Moreover,  $\text{Tr}(\mathbf{A})$ ,  $\lambda_{\max}(\mathbf{A})$ , and  $\lambda_{\min}(\mathbf{A})$  denote the trace, maximum eigenvalue, and minimum eigenvalue of  $\mathbf{A}$ , respectively. Furthermore,  $\mathbf{I}_n$  denotes the  $n \times n$  identity matrix, while  $\|\cdot\|$ ,  $\|\cdot\|_F$ ,  $\text{Pr}\{\cdot\}$  represent the Euclidean norm, matrix Frobenius norm, and probability function, respectively. For a complex  $\mathbf{A}$ , we use  $\text{Re}\{\mathbf{A}\}$  and  $\text{Im}\{\mathbf{A}\}$  to denote its real and imaginary parts, respectively.

## 2. OVERVIEW OF RECONFIGURABLE INTELLIGENT SURFACES

This chapter reviews the fundamental concepts of reconfigurable intelligent surfaces (RISs) technology, its benefits, use cases, hardware architecture, challenges, and applications in B5G and 6G networks. In addition, the passive beamforming design methods as well as the current state-of-the-art model for RIS-aided wireless communications are discussed. Next, we compare the RIS technology with active relay which is a related technology, underlining the major differences as well as the RIS's competitive advantage over active relay.

### 2.1 Introduction

Reconfigurable intelligent surfaces (RISs), also known as intelligent reflecting surfaces (IRSs), have recently emerged as a promising technology for B5G and 6G wireless communication. An RIS is a planar surface composed of a large number of passive reflecting elements that are closely packed together and a smart controller. The smart controller is used to reconfigure the phase shift and/or the amplitude of the RIS elements. Each of the reflecting elements is capable of controlling the phase and/or amplitude of the incident waveform independently [32, 33, 35]. By strategically deploying RISs in wireless networks and intelligently coordinating their reflections, it is possible to flexibly reconfigure the signal propagation and/or the wireless channels between the transmitters and the receivers to achieve the desired improvement in the channel characteristics. For example, these reflections can be smartly controlled to add constructively at the intended users and/or destructively at the unintended users. Thus, signal processing using RISs represents a unique approach to fundamentally tackle the problem of wireless channel fading impairment and interference, which could potentially result in a quantum leap improvement in wireless communication capacity and reliability [48–50]. The promising potentials of RIS for future wireless networks have motivated extensive research recently. Detailed overviews or surveys of the existing research work on RISs and their variants, such as RISs deployment, implementation, channel modeling,

applications, etc., are provided in the following review papers [33, 35, 51–54].

The RIS's primary function is to add various customizable paths to an uncontrollable communication channel, depending on the number of reflecting elements. They allow the user to have channel characteristics that are favourable to combat path loss and other losses. Hence, an RIS performs passive beamforming where an array gain is achieved by applying a phase shift to different reflecting elements, which results in constructive interference. As a result of this array gain, the SNR of the received signal is proportional to the square of the number of reflecting elements in the RIS [51, 55].

## 2.2 Architecture of RIS

### 2.2.1 Passive RIS

The reconfigurability potential of the RIS can be achieved by using any device capable of electronic phase-changing. This includes positive-intrinsic-negative (PIN) diodes, micro-electromechanical system (MEMS) switches, and field-effect transistors (FETs). A typical hardware architecture of a fully passive RIS is shown in Fig. 2.1, each of the reflecting elements of the RIS contains a PIN diode which controls the phase response. Through the control of the biasing voltage of the PIN diode, it can be turned ON and OFF. As a result, a subsequent phase shift of  $\pi$  in radians to the incident signal is achieved. Hence, by setting the respective biasing voltage via the smart controller, different phase shifts can be realized independently for the RIS's elements. A variable resistor load can effectively be used to control the reflection amplitude [56]. This allows for more flexibility in shaping the reflected signal to achieve various communication objectives effectively. Furthermore, the smart controller attached to the RIS is responsible for triggering and determining the reflection adaptation, which can be accomplished through a field-programmable gate array (FPGA) [57]. Through wired or wireless backhaul/control links, this RIS smart controller acts as a gateway to communicate with other network components (e.g., BSs/access points (APs) and user terminals). Due to its passive structure without the use of any transmit radio frequency (RF) chains, it has a low energy consumption and a low cost. RISs are generally of low profile as they can be discreetly integrated into various environments, and they can be made to be conformal to various objects. Therefore, they can be easily deployed on several structures such as roadside billboards, indoor walls, vehicle windows highway polls, and building facades [33, 48, 58].

Mathematically, the reflection vector for the given RIS with  $M_S$  reflecting elements

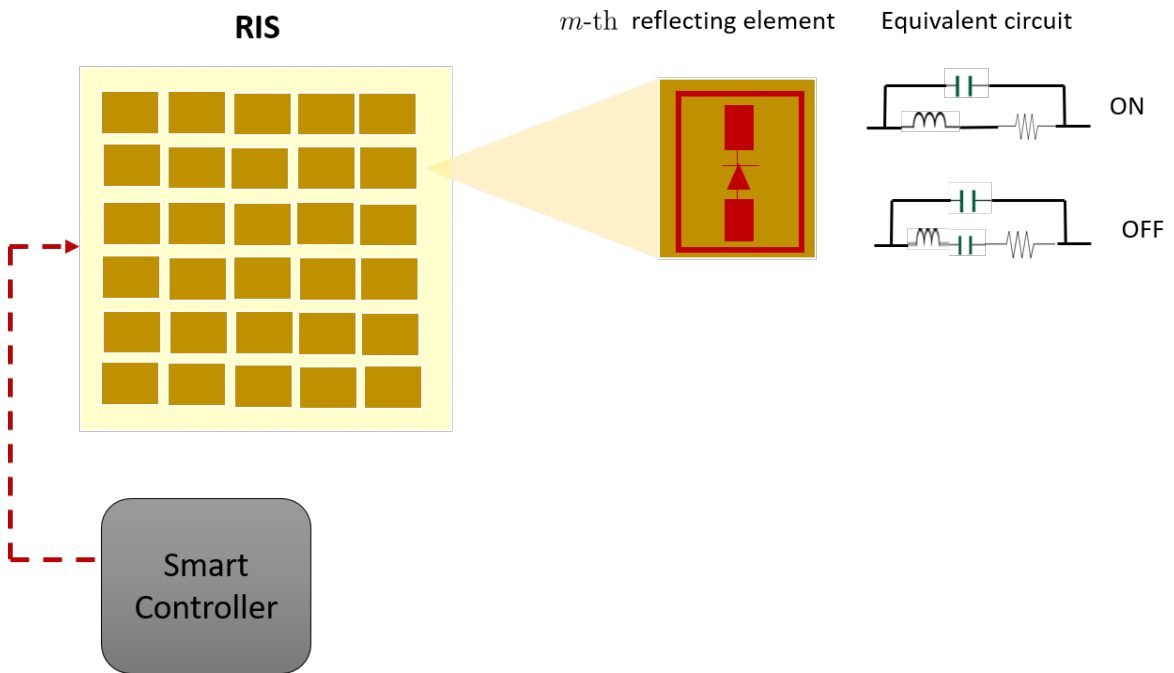


Fig. 2.1: An RIS with  $M_S$  passive reflecting elements

is given as

$$\boldsymbol{\theta} = [\beta_1 e^{j\phi_1}, \dots, \beta_{M_S} e^{j\phi_{M_S}}]^T \in \mathbb{C}^{M_S}, \quad (2.1)$$

where  $\beta_m \in [0, 1]$  denotes the closed interval between 0 and 1 which represents the reflection amplitude of the  $m$ th element of the RIS. Furthermore,  $\phi_m \in [0, 2\pi]$  denotes the closed interval between 0 and  $2\pi$  that represents the phase shift associated with the  $m$ th element of the RIS. The reflection amplitude is typically the measurement of the amount of energy of the impinging signal that is reflected, with  $\beta_m = 0$  representing absorption of the impinging signal whereas  $\beta_m = 1$  signifies full reflection. In the literature, the maximum value is usually adopted for  $\beta_m$ , i.e.,  $\beta_m = 1$  [33, 48]. The continuous tuning of the reflection coefficient is beneficial for improving communication performance, but it is difficult to implement due to the need for higher-resolution (high-precision) reflecting elements and more complex hardware design. Therefore, the element design becomes more difficult because of its limited size, and it also demands more controlling pins at the RIS controller to manage the necessary PIN diodes. For practical RISs that typically have a large number of reflecting elements, it is more cost-effective to only implement discrete and finite amplitude/phase-shift levels that only require a small number of control bits for each element [34, 59, 60].

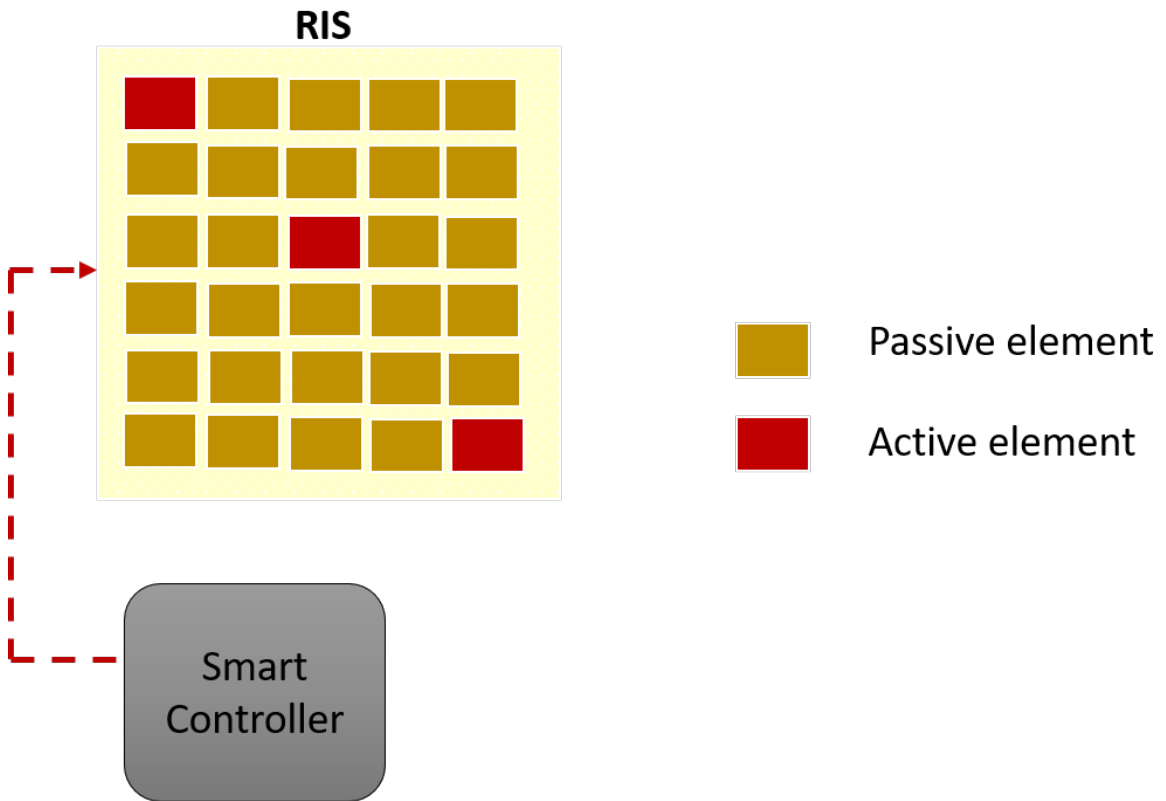


Fig. 2.2: An RIS with some active reflecting elements

### 2.2.2 Semi-Passive RIS

As a result of the unavailability of RF chains in a fully passive RIS, the CSI acquisition problem becomes more difficult because only the cascaded channel, i.e., the BS-RIS-UE equivalent channel, is available at the receiver side. However, it has been shown in [49, 61] that the optimal phase-shift configuration for the RIS elements is determined by the angles of the combined channel between the RIS and the BS and the RIS and the user without the phase shift of the RIS, so it is not necessary to separate them. Nonetheless, to enhance the channel estimation for RIS-aided communication systems a few of the RIS elements are mounted with dedicated RF chains. This setup is known as the semi-passive RIS and it is shown in Fig. 2.2. These active elements are used for processing the received pilot signals. As a result, the semi-passive RIS operates in two different modes namely channel sensing mode and reflection mode [39, 62–67]. In the channel sensing mode, the active elements are activated to receive the pilot signals from the BS to estimate the BS-RIS and the RIS-UE channels at the RIS while the other reflecting elements are turned OFF. In the reflecting mode, the sensors are deactivated, and the RIS reflector elements are activated to reflect the data signals from the BS to enhance communication.

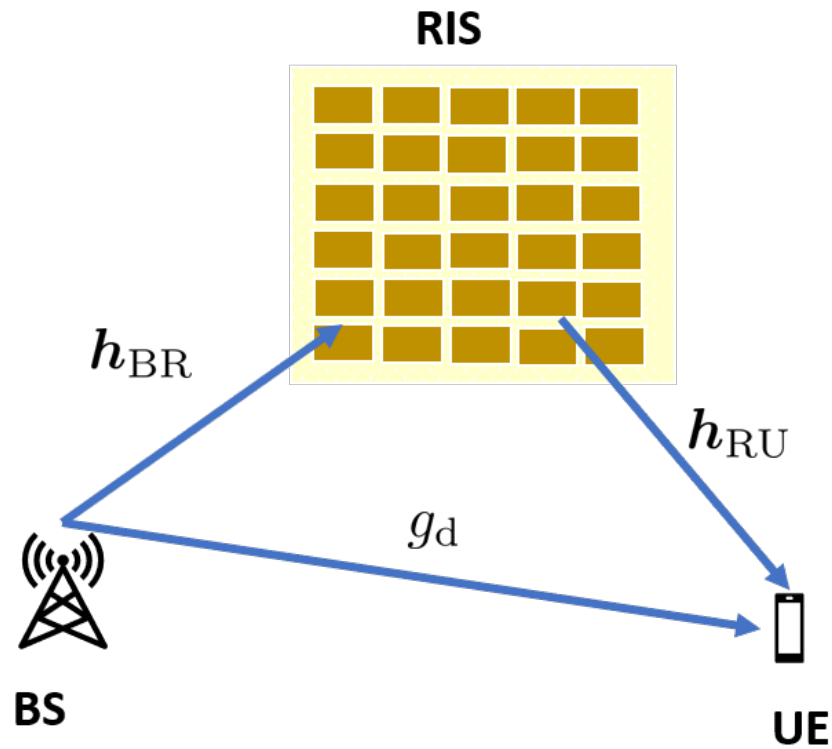


Fig. 2.3: An RIS-aided SISO communication system

## 2.3 Optimization of RIS Reflection

Next, this section discusses the optimization of passive reflection for RIS-aided wireless communication systems, and review the state-of-the-art solutions. For brevity, we consider a narrow-band system for a single-user single-input single-output (SISO), multiple-input single-output (MISO), and MIMO communication system with flat-fading channels in Sections 2.3.1, 2.3.2, and 2.3.3, respectively.

### 2.3.1 RIS-aided SISO System

Let us consider an RIS-aided SISO communication system as shown in Fig. 2.3, where the BS and the UE are each equipped with a single antenna. The RIS is equipped with  $M_S$  passive reflecting elements. The baseband equivalent channels for the BS-RIS link, RIS-UE link, and the BS-UE are given as  $\mathbf{h}_{BR} \in \mathbb{C}^{M_S \times 1}$ ,  $\mathbf{h}_{RU} \in \mathbb{C}^{M_S \times 1}$ , and  $g_d \in \mathbb{C}$  respectively. Using the RIS reflection model given in (2.1) the received signal at the UE is given as

$$y = (\mathbf{h}_{RU}^H \mathbf{\Theta} \mathbf{h}_{BR} + g_d) \sqrt{P_t} x + z, \quad (2.2)$$

where  $\Theta = \text{diag}(\boldsymbol{\theta})$  is the RIS reflection diagonal matrix and  $\boldsymbol{\theta}$  is the reflection vector of the RIS given in (2.1). Furthermore,  $x$  is the information signal modeled by an independent and identically distributed (i.i.d.) random variable with zero mean and unit variance,  $P_t$  is the transmit power at the BS, and  $z$  denotes additive white Gaussian noise (AWGN) at the user receiver modeled as a circularly symmetric complex Gaussian (CSCG) random variable with zero mean and variance  $\sigma^2$ . Therefore, the received SNR at the UE is written as

$$\gamma = \frac{P_t |\mathbf{h}_{\text{RU}}^H \Theta \mathbf{h}_{\text{BR}} + g_d|^2}{\sigma^2} \quad (2.3a)$$

$$= \frac{P_t \left( \left| \sum_{m=1}^{M_S} h_{\text{RU}}^*(m) \beta_m e^{j\phi_m} h_{\text{BR}}(m) + g_d \right|^2 \right)}{\sigma^2}, \quad (2.3b)$$

where  $h_{\text{RU}}(m)$  and  $h_{\text{BR}}(m)$  denote the  $m$ -th element of the  $\mathbf{h}_{\text{RU}}$  and  $\mathbf{h}_{\text{BR}}$  vectors, respectively. For the RIS-aided SISO communication system, the objective is to maximize the achievable data rate given as

$$\text{SE} = \log_2(1 + \gamma), \quad (2.4)$$

or equivalently the SNR, by optimizing the passive reflection coefficients of the RIS. The resulting optimization problem can be written as [33]

$$\max_{\boldsymbol{\theta}, \boldsymbol{\beta}} \left| \sum_{m=1}^{M_S} h_{\text{RU}}^*(m) \beta_m e^{j\phi_m} h_{\text{BR}}(m) + g_d \right|^2 \quad (2.5a)$$

$$\text{s.t. } 0 \leq \phi_m < 2\pi, m = 1, \dots, M_S \quad (2.5b)$$

$$0 \leq \beta_m \leq 1, m = 1, \dots, M_S, \quad (2.5c)$$

where we define  $\boldsymbol{\beta} = [\beta_1, \dots, \beta_{M_S}]^T \in \mathbb{C}^{M_S \times 1}$  and  $\boldsymbol{\theta} = [\phi_1, \dots, \phi_{M_S}]^T \in \mathbb{C}^{M_S \times 1}$ . It is evident from (2.5) that the amplitude coefficient that will result in the maximization of the SNR is given as  $\beta_m = 1, \forall m \in M_S$ .

The maximum SNR is achieved when the RIS-assisted channels have the same phase as the direct channel [68]. Therefore, the solution for the optimal phase-shift is given as [33]

$$\phi_m^{(\text{opt})} = \text{mod}[\psi - (\varphi_m + \xi_m)], \quad (2.6)$$

where  $\varphi_m$ ,  $\xi_m$ , and  $\psi$  are the phases of  $h_{\text{RU}}^*(m)$ ,  $h_{\text{BR}}(m)$ , and  $g_d$ , respectively. Then, the maximum received signal at the receiver obtained after back substitution is given

in (2.7)

$$\begin{aligned}
y &= \left( \sum_{m=1}^{M_S} |h_{\text{RU}}(m)||h_{\text{BR}}(m)|e^{j(\varphi_m+\xi_m+\psi-(\varphi_m+\xi_m))} + |g_d|e^{j\psi} \right) \sqrt{P_t}x + z, \\
&= \left( \sum_{m=1}^{M_S} |h_{\text{RU}}(m)||h_{\text{BR}}(m)|e^{j\psi} + |g_d|e^{j\psi} \right) \sqrt{P_t}x + z \\
&= \left( \sum_{m=1}^{M_S} |h_{\text{RU}}(m)||h_{\text{BR}}(m)| + |g_d| \right) e^{j\psi} \sqrt{P_t}x + z
\end{aligned} \tag{2.7}$$

Then, the maximum SNR is given as

$$\gamma = \frac{P_t (M_S g_{\text{refl}} + g_d)^2}{\sigma^2}, \tag{2.8}$$

where  $g_{\text{refl}} = \frac{1}{M_S} \sum_{m=1}^{M_S} |h_{\text{RU}}(m)||h_{\text{BR}}(m)|$ . Assuming that the direct BS-UE link is unavailable and considering only the RIS-assisted channels for i.i.d. Rayleigh fading, then as  $M_S \rightarrow \infty$  the asymptotic receiver power according to (2.8) is approximately given as [48, 69, 70]

$$P_r \approx M_S^2 \frac{P_t \pi^2 \varrho_{h_{\text{BR}}}^2 \varrho_{h_{\text{RU}}}^2}{16}, \tag{2.9}$$

where  $P_r$  denotes the receive power and  $\varrho_{h_{\text{BR}}}^2$ , and  $\varrho_{h_{\text{RU}}}^2$  represent the average power for each entry of  $\mathbf{h}_{\text{RU}}^H$  and  $\mathbf{h}_{\text{BR}}$  respectively.

*Proof.* Using the solution for the optimal phase shift for the RIS given in (2.6), then we could write the RIS-assisted channel as

$$|\mathbf{h}_{\text{RU}}^H \mathbf{\Theta} \mathbf{h}_{\text{BR}}| = \sum_{m=1}^{M_S} |h_{\text{RU}}(m)||h_{\text{BR}}(m)| = M_S g_{\text{refl}}, \tag{2.10}$$

and as a result, the received power  $P_r$  at the receiver is given as

$$P_r = P_t \left| \sum_{m=1}^{M_S} |h_{\text{RU}}(m)||h_{\text{BR}}(m)| \right|^2 = P_t M_S^2 g_{\text{refl}}^2. \tag{2.11}$$

Since  $h_{\text{RU}}(m) \sim \mathcal{CN}(0, \varrho_{h_{\text{RU}}}^2)$ , the real and imaginary parts are real independent iden-

tically distributed (i.i.d.) Gaussian random variables, i.e.,

$$\operatorname{Re}\{h_{\text{RU}}(m)\} \sim \mathcal{CN}\left(0, \varrho_{h_{\text{RU}}}^2/2\right), \quad (2.12)$$

$$\operatorname{Im}\{h_{\text{RU}}(m)\} \sim \mathcal{CN}\left(0, \varrho_{h_{\text{RU}}}^2/2\right). \quad (2.13)$$

As a result,  $|h_{\text{RU}}(m)|$  is a Rayleigh fading channel with the following mean  $\frac{\sqrt{\pi}\varrho_{h_{\text{RU}}}}{2}$ . Similarly,  $|h_{\text{BR}}(m)|$  is a Rayleigh fading channel with the following mean  $\frac{\sqrt{\pi}\varrho_{h_{\text{BR}}}}{2}$ . Therefore, we have

$$\mathbb{E}\{|h_{\text{RU}}(m)||h_{\text{BR}}(m)|\} = \frac{\pi\varrho_{h_{\text{RU}}}\varrho_{h_{\text{BR}}}}{4}. \quad (2.14)$$

Since  $\frac{1}{M_{\text{S}}}\sum_{m=1}^{M_{\text{S}}}|h_{\text{RU}}(m)||h_{\text{BR}}(m)| \rightarrow \pi\varrho_{h_{\text{RU}}}\varrho_{h_{\text{BR}}}/4$ , and from the Law of Large numbers, as  $M_{\text{S}} \rightarrow \infty$ , then it follows that (2.11) can be written as

$$P_{\text{r}} \rightarrow \frac{P_{\text{t}}M_{\text{S}}^2\pi^2\varrho_{h_{\text{BR}}}^2\varrho_{h_{\text{RU}}}^2}{16}. \quad (2.15)$$

□

This shows that with a sufficiently large number of reflecting elements  $M_{\text{S}}$ , the UE receive power increases *quadratically* with  $M_{\text{S}}$ , i.e., on the order of  $\mathcal{O}(M_{\text{S}}^2)$  [33, 48].

Furthermore, it is important to note that from the optimization problem given in (2.5), the design of the optimal RIS reflection coefficients does not depend on the individual RIS-assisted channels, i.e.,  $\mathbf{h}_{\text{BR}}$  and  $\mathbf{h}_{\text{RU}}$ . Rather, this depends on the combined channel via the RIS which is given as  $(\operatorname{diag}(\mathbf{h}_{\text{BR}}^{\text{H}})\mathbf{h}_{\text{RU}})$ . This observation is generally true for RIS-assisted communication systems and thus can be exploited to further simplify the channel estimation problem for RIS-assisted communication systems.

### 2.3.2 RIS-aided MISO System

In this section, we consider a single-user RIS-aided MISO system as shown in Fig. 2.4, where the BS has  $M_{\text{T}}$  antennas and a single antenna at the UE. Therefore, the BS-RIS channel matrix is written as  $\mathbf{H}_{\text{BR}} \in \mathbb{C}^{M_{\text{S}} \times M_{\text{T}}}$ , and the BS-UE channel is written as  $\mathbf{g}_{\text{d}} \in \mathbb{C}^{M_{\text{T}} \times 1}$ . In a similar manner, the SNR maximization problem can be formulated as

$$\max_{\mathbf{f}, \boldsymbol{\theta}} |(\mathbf{h}_{\text{RU}}^{\text{H}}\boldsymbol{\Theta}\mathbf{H}_{\text{BR}} + \mathbf{g}_{\text{d}}^{\text{H}})\mathbf{f}|^2 \quad (2.16a)$$

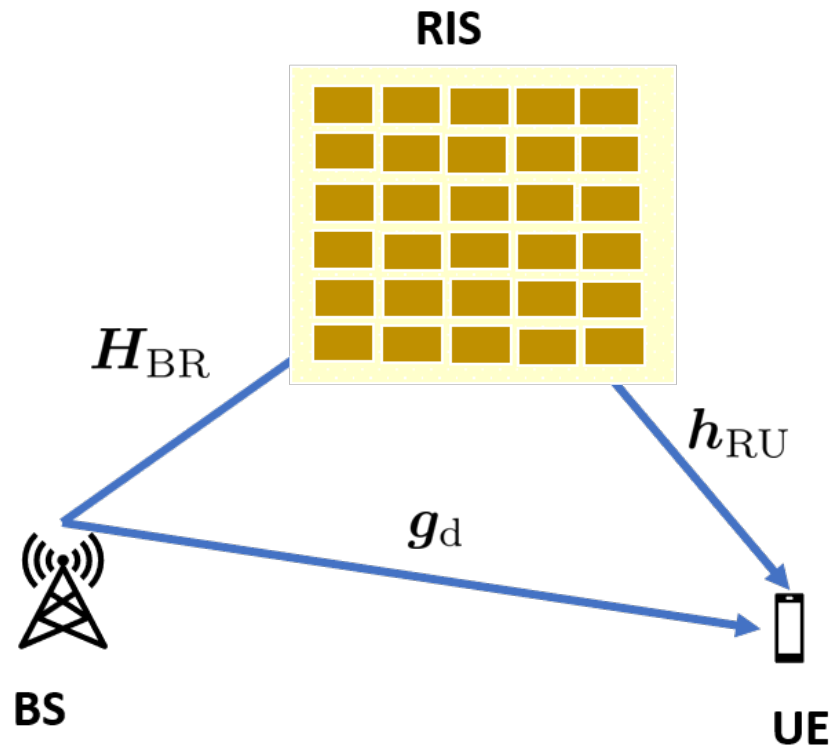


Fig. 2.4: An RIS-aided MISO communication system

$$\text{s.t. } \|\mathbf{f}\|^2 \leq P_t, \quad (2.16b)$$

$$0 \leq \theta_m < 2\pi, \forall m \in M_S, \quad (2.16c)$$

where  $\mathbf{f} \in \mathbb{C}^{M_T \times 1}$  denotes the transmit beamforming vector at the BS and  $\Theta = \text{diag}(\boldsymbol{\theta})$  is the RIS reflection matrix. When the BS-UE direct link is much stronger than the RIS-assisted channels, it is intuitive for the BS to form a beam towards the UE directly. However, in situations where the direct link is severely obstructed then it is preferable for the BS to exploit the reconfigurable potential of the RIS to serve the UE by steering the beam toward the RIS. The optimization problem given in (2.16) is regrettably non-convex due to the non-concave nature of the objective function with respect to the optimization variables  $\boldsymbol{\theta}$  and  $\mathbf{f}$ . Due to this coupling between the variables, an alternating optimization (AO) approach is proposed in [48, 71] to solve the problem given in (2.16) sub-optimally. Particularly, the main idea of the AO approach is to fix the transmit beamforming vector  $\mathbf{f}$ , and the phase shifts are obtained by solving the resulting problem. Then, with a fixed  $\boldsymbol{\theta}$ , the transmit beamforming solution is obtained. The above procedure is repeated until the solution has converged which indicates that at least a locally optimal solution to problem (2.16) is attained. We note that the same formulation and solution is applicable in the uplink communication

between the UE and the BS with multiple antennas. Such a system is known as a single-input multiple-output (SIMO) system.

Several works in the literature proposed different approaches for the joint transmit and passive beamforming design for RIS-aided single-user MISO/SIMO systems. The authors in [72] propose a deep learning-based scheme for optimizing the RIS phase shift matrix (considering maximum reflection, i.e.,  $\beta_m = 1, m = 1, \dots, M_S$ ) for a single-user MISO system. In the work, a customized deep neural network (NN) is trained offline by adopting the unsupervised learning approach, which can make real-time predictions when deployed online. From the numerical results, it is observed that there is slight performance degradation when compared with the semi-definite relaxation (SDR) approach proposed in [71]. In [73], similarly, a deep learning-based approach is proposed that tunes the RIS phase shift matrix in real-time for an RIS-aided MISO system with the availability of the line of sight (LOS) link  $\mathbf{g}_d \in \mathbb{C}^{M_T}$  between the BS and the UE. The simulation results show that the proposed approach has a comparable performance to the conventional approaches and also has a reduced computation complexity.

### 2.3.3 RIS-aided MIMO System

Next, we consider an RIS-aided MIMO system in this section with multiple antennas at both the BS and UE (see Fig. 2.5). Unlike the SISO/MISO/SIMO systems considered above, the optimization of the passive RIS phase shift in the MIMO case is, however, more challenging. This is due to the fact that the optimization process needs to take into account the multi-antenna channels and/or multi-path channels. As a result, the RIS reflection needs to be jointly optimized alongside the transmit covariance matrix at the BS in order to achieve the capacity of such a system [74]. Particularly in this case, the BS-RIS, RIS-UE, and BS-UE channels are respectively denoted as  $\mathbf{H}_{BR} \in \mathbb{C}^{M_S \times M_T}$ ,  $\mathbf{H}_{RU} \in \mathbb{C}^{M_R \times M_S}$ , and  $\mathbf{G}_d \in \mathbb{C}^{M_R \times M_T}$ , where  $M_R$  is the number of antennas at the UE. Similarly, considering maximum reflection at all the reflecting elements of the RIS (i.e.,  $\beta_m = 1, m = 1, \dots, M_S$ ) and continuous phase shift, the optimization problem for the capacity can be written as

$$\max_{\boldsymbol{\Theta}, \boldsymbol{\Sigma}} \log_2 \det \left( \mathbf{I}_{N_t} + \frac{\mathbf{H}\boldsymbol{\Sigma}\mathbf{H}^H}{\sigma^2} \right) \quad (2.17a)$$

$$\text{s.t. } 0 \leq \theta_m < 2\pi, \forall m \in M_S, \quad (2.17b)$$

$$\beta_m = 1, \forall m \in M_S, \quad (2.17c)$$

$$\text{Tr}(\boldsymbol{\Sigma}) \leq P_t, \boldsymbol{\Sigma} \succeq \mathbf{0}, \quad (2.17d)$$

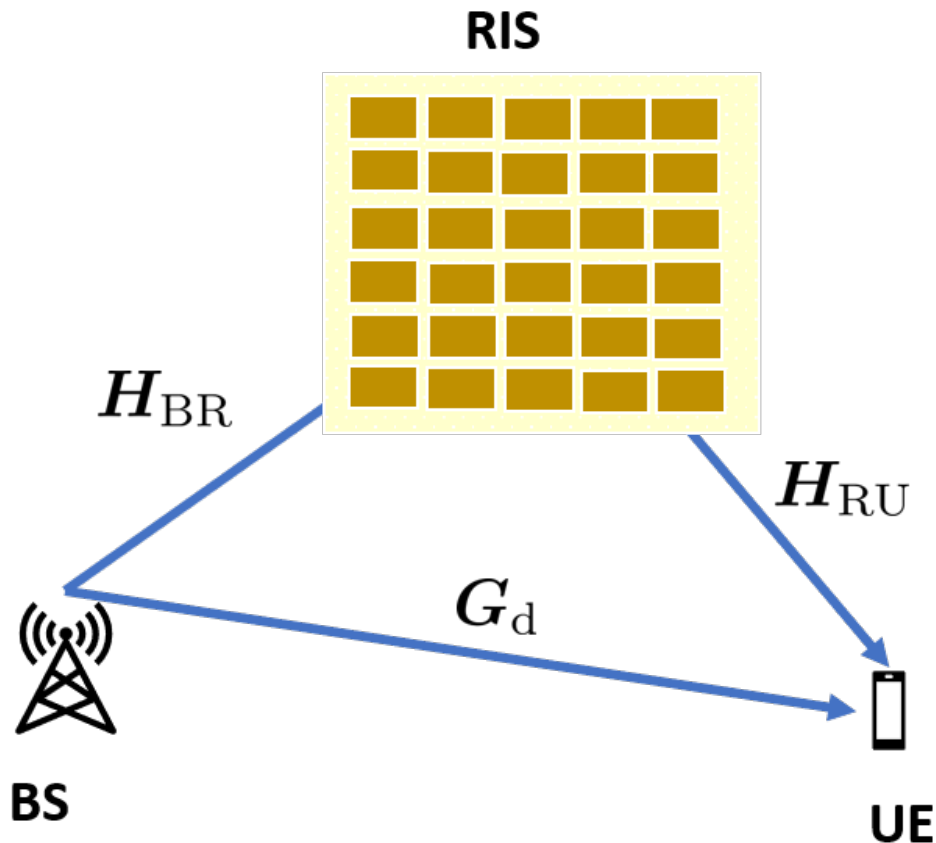


Fig. 2.5: An RIS-aided MIMO communication system

where  $\mathbf{H} = (\mathbf{H}_{RU}\Theta\mathbf{H}_{BR} + \mathbf{G}_d)$  is the overall effective channel and the positive semidefinite matrix  $\Sigma \in \mathbb{C}^{M_T \times M_T}$  denotes the transmit covariance matrix at the BS. Due to the non-concavity of the MIMO channel capacity with respect to  $\Sigma$  and  $\Theta$ , the optimization problem in (2.17) is non-convex.

In the literature, different strategies have been proposed by different authors for optimizing the RIS phase shift matrix in RIS-aided MIMO systems. For example, in [75], a low-complexity framework is proposed for the design of the RIS phase shift based on the maximization of the average received SNR. In [76], the authors adopted an RIS phase shift selection algorithm to optimize the RIS phase-shifts for multi-user MISO systems (virtually MIMO). A different scheme to enhance the overall channel power of a single-user MIMO system is proposed in [77]. The numerical results show that the rank of the channel matrix in LOS environments is increased by the incorporation of the RIS and the achievable rate is improved by supporting spatial multiplexing. The work in [78] focuses on optimizing the RIS phase shift matrix to improve the rank of the channel and improve the spectral efficiency of a point-to-point MIMO system with LOS. The authors in [74] proposed an efficient AO-based algorithm to iteratively

solve the problem given in (2.17), by fixing other variables and optimizing the transmit covariance matrix or one RIS element's phase shift at each time. The simulation results show that the proposed algorithms achieve superior rate performance over various benchmark schemes with or without RIS. The computational complexity is polynomial in terms of  $M_S$ ,  $M_T$ , and  $M_R$  [74].

## 2.4 Benefits of RIS-aided Wireless Communications

The integration of RISs in wireless communication systems offers the following appealing advantages. RISs can enhance the spectral efficiency of the wireless network by creating a virtual LOS link between the BS and the UEs to smartly and passively reflect the impinging waveform to bypass obstacles [33, 79]. The spectral efficiency enhancement becomes significant when obstacles, such as high-rise buildings block the LOS link between the BS and the UE as shown in Fig. 2.6.

As shown in Fig. 2.7, RISs can enhance the communication secrecy by dynamically tuning the wireless system in such a way as to eliminate the received signal at the unauthorized user (Eve) and enhance the received SNR at the authorized UE [80–82]. In Fig. 2.8, RISs are used to increase the channel rank at the desired UE by adding extra signal paths toward the desired direction in order to improve the channel rank condition [78].

Equally, RISs can refine the channel statistics and/or distribution, for instance, they can transform a Rayleigh fading channel to a Rician fading channel for ultra-high reliability [83]. In wireless communication networks, RISs can enhance the received SNR at the desired UE by performing constructive and destructive interference nulling/cancellation as shown in Fig. 2.9. This is achieved by properly designing the reflection coefficients of the RIS to create a "signal hotspot" and "interference-free zone" around a cell-edge user. Without the RIS the cell-edge user experiences high signal attenuation as a result of the co-channel interference it suffers from its neighboring cell as well as its serving BS. Furthermore, RISs operate in full-duplex (FD) and support full-band transmission as they only reflect electromagnetic waves. Therefore, RISs can be integrated transparently into wireless networks, providing great flexibility and compatibility with existing wireless systems as an auxiliary device [33, 84]. In summary, the efficient integration of RISs into wireless communication systems offers both new possibilities as well as challenges, which deserve new and further research.

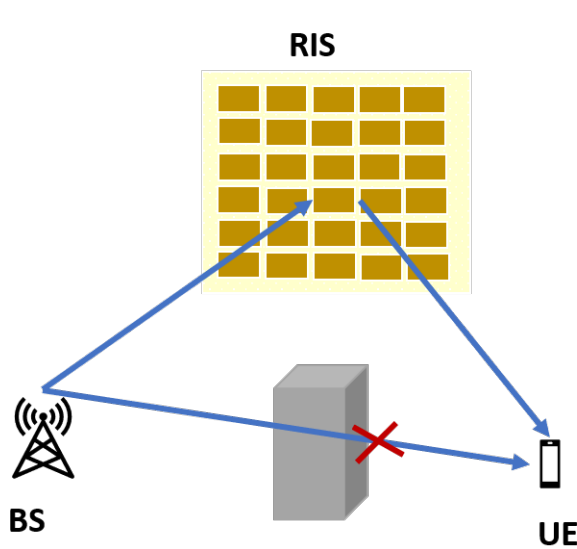


Fig. 2.6: RIS for coverage extension

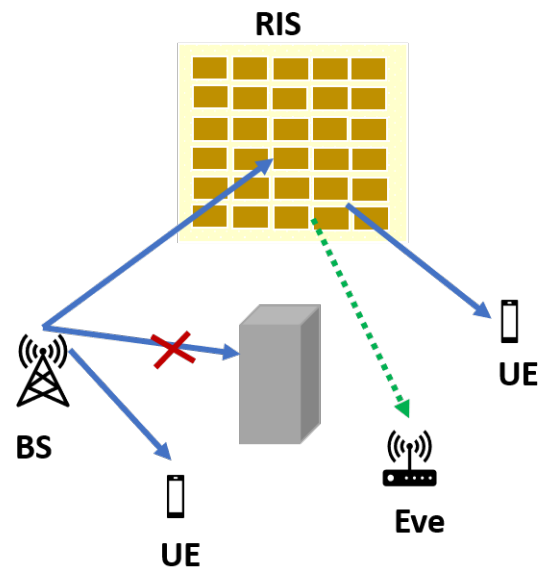


Fig. 2.7: RIS-assisted physical layer security

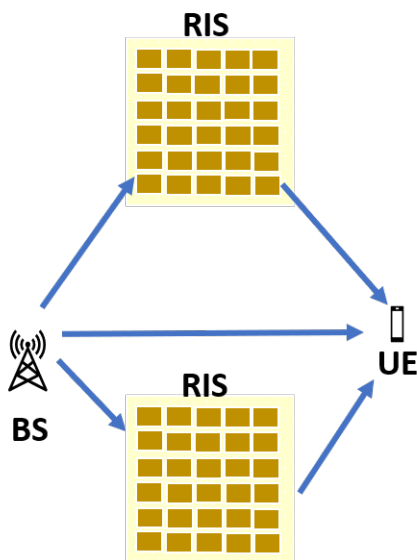


Fig. 2.8: RIS for improving channel rank

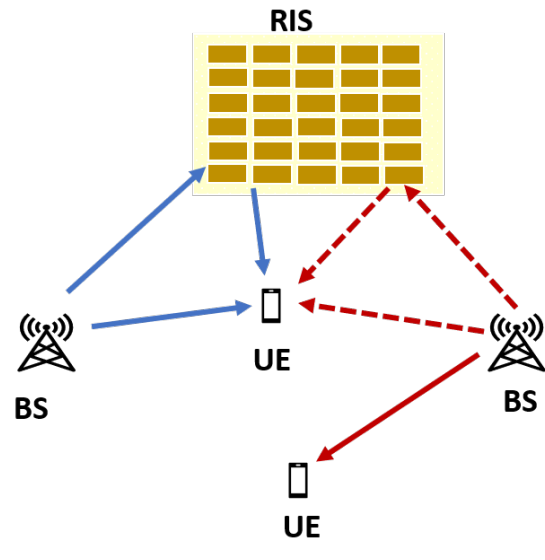


Fig. 2.9: RIS for interference suppression

## 2.5 Applications of RIS in Wireless Communications

Considering the enormous benefits offered by the RISs, numerous studies are being conducted in several application scenarios on the potential enhancement of RIS-assisted wireless communication systems. In the literature, the most frequently considered improvement metrics are maximizing the SNR and the overall energy/spectral efficiency, interference suppression, minimizing the transmit power, and improving the physical layer security.

The authors in [85] consider a multi-user SISO RIS-assisted system with a LOS

link. The work adopted the received SINR as the metric that is optimized at the receiver in the presence of interfering signals. To address the issue, the authors introduced intelligent spectrum learning, which uses an offline-trained convolutional neural network (CNN) at the RIS controller to extract the interfering signals directly from the user's signals. Hence, by configuring an active/inactive binary status of the RIS elements, a distributed control algorithm is proposed to maximize the received SINR. Here, each RIS element can have two possible states: ON and OFF. The ON status indicates that the RIS element is ON, which implies that it reflects the incident signals with continuous phase shifts, while the OFF indicates that the RIS element is OFF, which means that it does not reflect any signals. Simulation results demonstrate an improvement in performance using this deep-learning approach.

To enhance the received signal power at the UE, the work in [71] employs a single RIS with  $M_S$  passive elements to aid downlink communication in a MISO system. The aim is to maximize the SNR by optimizing the BS's transmit beamforming and the RIS's reflection coefficients. The authors adopted the AO approach to iteratively adjust the transmit and passive beamforming strategies. To obtain the BS's beamforming vector, the maximum-ratio transmission strategy is proposed based on the RIS's passive beamforming. The RIS's passive beamforming is coordinated with the direct channel to boost the received signal power. Numerical results show that compared to non-RIS-assisted MISO systems, the SNR at the receiver increases on the order of  $M_S^2$  when  $M_S$  reflecting elements are used in the RIS. In [86], the application of multiple RISs to assist MISO mmWave wireless communications is studied. By utilizing the joint optimization of transmit and passive beamforming, the work demonstrated that the RIS can increase the received signal power and extend the network coverage by providing alternative signal paths.

A multi-user MISO system with an RIS-assisted LOS between a common access point (AP) and the users is considered in [58]. In particular, a practical phase shift model that captures the phase-dependent amplitude variation in the element-wise reflection design at the RIS is proposed. This is different from the ideal phase shift model for the RIS, which assumes that regardless of the phase shifts of the RIS elements they achieve full signal reflection. An AO algorithm is proposed to find sub-optimal solutions to the optimization problem of minimizing the total transmit power at the AP. This is achieved by jointly designing the AP transmit precoder and the RIS phase-shift matrix, subject to the users' individual SINR constraints. The simulation results demonstrate the asymptotic performance loss of the optimized RIS-assisted system when implemented with an ideal phase shift model, and the gains that can be achieved by optimizing using the practical phase shift model under consideration. In [87], the

authors examined the asymptotic achievable rate in an RIS-aided downlink MISO system. The system model focuses on a common BS that is transmitting to  $K$  users using time-division multiple access (TDMA) to serve one user in each time slot. The optimality of the asymptotic performance was analyzed by considering the practical limitations of RISs, such as practical reflection coefficients (i.e., when the practical phase shift model is considered for the RIS), when multiple RISs are deployed in a scheme where some users are RIS-aided and others are not. The results are analyzed using the symbol-error rate (SER) and the ergodic capacity, and compared to a baseline strategy without RIS and the AO algorithm proposed in [58]. The ergodic capacity is the maximum mutual information averaged over all channel states. It implies that the ergodic capacity is the result of infinitely long realizations of the channels [16].

The application of the RIS for suppressing inter-cell interference and improving the communication performance of cell-edge users has been examined in several studies. For example, the work in [88] proposed a resource allocation framework to enhance the SE for a multi-cell non-orthogonal multiple access (NOMA) network with a single RIS. The RIS is configured to suppress the inter-cell interference, by properly adjusting its phase shifts. Furthermore, [89] investigates the phase-shift response to the incident signals at different frequencies. The authors studied an RIS-assisted communication where different BSs operating at different operated by the same provider, concurrently serve the UEs in their cells. The authors provide a practical frequency-dependent RIS reflection model. Subsequently, the maximization of the sum rate by minimizing the transmit power is investigated. Extensive numerical results demonstrate the significant performance improvement of the proposed scheme in terms of power saving and rate enhancement. The work in [90] shows that in an RIS-aided multi-cell MISO system, the minimum SINR can be maximized by using SOCP and SDR techniques to optimize the transmit and passive beamforming vectors. For the max-min fairness problem considered, a weighting factor  $\alpha_i \geq 0, i = 1, \dots, K$  is adopted, where  $K$  is the number of users. This weight parameter characterizes the fairness among the users, with a larger value of  $\alpha_i$  indicating that the  $i$  user has a higher priority in transmission. The authors propose an algorithm that utilizes successive convex approximation (SCA) to tackle the beamforming optimization problem, which requires less computational complexity than the SDR-based scheme. Compared to conventional cases without the RIS, the proposed algorithm can significantly increase the minimum-weighted-SINR in the RIS-aided communication system, as shown by the numerical results.

The authors in [91] investigate the tradeoff between energy efficiency (EE) and SE on the uplink of an RIS-aided MU-MIMO system that is equipped with discrete phase shifters. The EE is defined as the number of bits that can be sent over a unit of power

consumption, i.e.,  $EE = W \frac{SE}{P_{\text{total}}}$  [bits/joules], where  $W$  is the transmission bandwidth and  $SE$  is the spectral efficiency as defined in (2.4). Moreover,  $P_{\text{total}}$  is the sum of the power consumed in sending the bits. This includes, the static circuit power dissipated at UE, RIS energy consumption which is directly proportional to the number of RIS elements, per-unit hardware-dissipated power at the RIS, and the transmit power amplifier adopted at UE. The transmission strategy design takes into account the partial CSI of the cascaded channels and assumes a non-line-of-sight (NLOS) model between both ends. The partial CSI implies that the instantaneous CSI of the slow varying BS-RIS channel is perfectly known, whereas for the fast varying RIS-UE channel the statistical CSI is available. The RIS reflection coefficients design and the precoding design for users are implemented to maximize resource efficiency (RE). The RE is a performance metric given in [92] that is flexible enough to balance the EE and SE for both continuous and discrete-phase shifts at the RIS. An optimization framework that utilizes the AO approach is proposed to tackle the optimization problem by creating an iterative MMSE method that is combined with a projected gradient (PG). The efficiency of the optimized framework for RE maximization is demonstrated by the simulation results.

In [93], the use of RISs to improve anti-jamming communication performance to reduce jamming interference is investigated by properly adjusting the RIS elements in a multi-user MISO system under NLOS conditions between the users and the BS. The problem is formulated as a joint optimization of power allocation at the BS and the RIS phase-shift matrix, taking into account the requirements for QoS for legitimate users. The work mainly focused on the joint optimization of the power allocation and the passive beamforming of the RIS, so the transmit beamforming vector is set by maximizing output SINR. The authors proposed a fuzzy win or learn fast-policy hill-climbing (FWoL-FPHC) algorithm to jointly optimize the anti-jamming power allocation and the RIS phase-shift matrix. From the numerical results it is shown that the proposed anti-jamming learning-based approach can efficiently improve the RIS-assisted system performance as well as the transmission protection level and have a better performance when compared with the mmWave massive MIMO approach given in [94].

The authors in [95] show that by adapting the RIS's reflection coefficients, the physical layer communications can be secured from the attacks from eavesdroppers. This is achieved by simultaneously creating directive beams to enhance the performance at the intended user and steering nulls towards the eavesdropper. The RIS is placed next to a legitimate receiver and via the joint optimization of the RIS phase shift matrix and the transmit beamformer of the legitimate transmitter, the secrecy rate

at the legitimate receiver is enhanced. The secrecy rate is defined as the amount of information securely sent over a wireless communication channel per time unit [96]. Similar work in [97] investigates the security gain at malicious terminals in MIMO systems, where information leakage can be suppressed through the transmit and passive beamforming design of the RIS. In [98], the system secrecy rate is maximized subject to the unit modulus constraints of the RIS and power constraint at the source. The authors develop an efficient AO-based algorithm, where the solutions to the transmit covariance of the source and the passive beamforming of the RIS are achieved in closed form and semi-closed form, respectively. Theoretically, the authors demonstrated that the convergence of the proposed algorithm is guaranteed.

Generally, it has been shown that RISs have the potential to become an effective tool for improving future wireless communications by intelligently reconfiguring the signal reflections in an uncontrollable wireless channel in favour of network performance [32, 71]. This can potentially benefit a wide range of vertical industries in 5G/6G such as transportation, manufacturing, smart city, etc., [33, 35]. It is important to point out that despite the fact that the above-mentioned scenarios are under discussion, it may take some time to complete the standardization process of RISs for 5G and 6G networks. In the meantime, there are several ongoing pilot projects launched to advance research in this new field [99].

## 2.6 Practical Challenges

Notwithstanding all the benefits derivable in RIS-aided wireless communication systems by the joint optimization of the transmit beamforming of the BS and the passive beamforming of the RIS, there are still some challenges to the practical implementation of RIS-aided wireless communication systems which also require attention. In the following, we present some of the challenges as well as some of the possible solutions to mitigate these challenges.

### 2.6.1 RIS Channel Acquisition

A major challenge in RIS-assisted communications is the acquisition of CSI. Generally, in an RIS-aided communication system, the effective optimization of the RIS phase shift matrix relies on the available CSI of all the channels considered. In such a system, three channels must be estimated: the BS-UE, BS-RIS, and RIS-UE channel [100]. The BS-UE channel can easily be estimated using any conventional channel estimation scheme. However, due to the passive nature of the RIS, the estimation of the BS-RIS

and RIS-UE channels creates a huge bottleneck for the system. Therefore, for such a system the acquisition of the CSI is typically carried out at the communication ends, i.e., at the transmitter or at the receiver. As a result of this, there is a degradation in the accuracy of channel estimation. Also, such an approach has a high computational complexity and high power requirements when considering large RISs. Furthermore, there is a large overhead for CSI acquisition due to the fact that the large number of scattering elements it comprises leads to a proportional amount of channel parameters to be estimated. Therefore, efficient channel estimation schemes are still open issues that need to be addressed for RIS-assisted communication systems as conventional methods are not feasible. One of the possible solutions, however, may be the use of low-power sensors that can be powered by energy-harvested modules—embedded through the RIS.

Currently, there are two main configurations for channel estimation in the available literature for RIS-assisted systems. They are the semi-passive and fully passive architectures as discussed in Section 2.2. In the semi-passive configuration, a few active elements can estimate only the DL or UL CSI of the BS-RIS or the UE-RIS links; and channel reciprocity can be leveraged to obtain the reverse links only in TDD systems [39,66]. However, in an FDD system such CSI is not available, thereby making channel estimation in FDD systems infeasible for a semi-passive configuration.

In a fully passive RIS-aided communication system, where the RIS has no radio-frequency chains, channel estimation is a challenging task since it involves the estimation of multiple channels simultaneously. Due to its passive nature, an RIS cannot send and receive pilot symbols and has no signal processing capability to estimate the channels. One practical approach considered in the literature is to estimate the cascaded BS-RIS-UE channel at the UE on the DL, and the cascaded UE-RIS-BS channel at the BS on the UL, respectively. With regards to the joint optimization of the passive and transmit beamforming for RIS-aided networks, when compared to that on their corresponding links the CSI on the cascaded links is generally sufficient and without loss of optimality [49,61]. It is important to mention that this approach, is applicable to both TDD and FDD systems, unlike the case of a semi-passive configuration. Even though, due to channel reciprocity only the uplink or downlink cascaded channels need to be estimated in the TDD case [33,35]. In some of the existing literature on channel estimation for the fully passive configuration for RIS-aided communication systems, the ON/OFF channel estimation protocol see [101,102], or some variants of the ON/OFF channel estimation protocol [103,104] is used. The ON/OFF protocol involves turning OFF (no reflection) the RIS reflecting elements to estimate the direct wireless channel and turning it ON (full reflection) to estimate the RIS-assisted channels by canceling

the interference from the direct channel since it is known from the previous step. The channel estimation scheme in these works has a high training overhead and a high computational complexity since the schemes require that the number of pilots is at least equal to the number of RIS elements [100, 101, 105]. Several approaches have been examined to solve these problems, including using the low-rank nature of mmWave channels and exploiting the multidimensional (i.e., tensor) structure of the received signals.

In [37, 103, 106, 107], the low-rank nature of the mmWave channels is exploited where the CSI acquisition is formulated as a sparse-recovery problem and compressed sensing tools are adopted. These are known to require a few measurements to have an accurate estimate to solve the problem. The authors in [108] express the received signal in an RIS-aided MIMO communication system as a 3-way tensor. This 3-way tensor accepts a canonical polyadic (CP) decomposition. The CP decomposition, equally referred to as CANDECOMP (canonical decomposition) and PARAFAC (parallel factors), is a tensor decomposition technique that expresses a multi-dimensional tensor as the sum of the minimum number of rank-one tensors [108–110]. Therefore, the authors adopted tensor-based signal processing tools to implement efficient channel estimation schemes [108]. In comparison with matrix-based methods, tensor-based signal processing methods have fundamental advantages over their bilinear (matrix) counterparts, as they can improve the identifiability of the parameters due to the powerful uniqueness properties of tensor decompositions [109–112].

The work in [113] shows that the low-rank nature of mmWave MIMO channels enables the received training signals to be written as a low-rank multiway tensor that admits a CP or a PARAFAC decomposition. Utilizing such a structure, the authors proposed a tensor-based RIS channel estimation method. The authors used the alternating least squares (ALS) method to estimate the factor matrices of the resulting tensor. In [114], a PARAFAC-based channel estimation framework for RIS-empowered communications was proposed. Leveraging the tensor structure of the unknown channels, the authors adopted ALS and the vector approximate message passing algorithms to estimate the unknown channel matrices. Despite the availability of a variety of research papers in the existing literature devoted to the issue of CSI acquisition in RIS-aided communication systems, however, an efficient channel estimation method that would achieve high estimation accuracy with low training overhead remains an open and important issue with regards to RIS-aided communication systems.

## 2.6.2 Practical RIS Deployment

The deployment strategy adopted for any RIS-assisted communication system is an important factor that needs to be considered. Since the deployment strategy adopted has a significant impact on the realizations/distributions of all RIS-reflected channels it also affects its fundamental performance limit. Similarly, from the implementation perspective, the deployment of the RIS should also take into account the various practical factors such as the QoS demand of the UEs (see Section 1.1), the spatial distribution of the UEs, the deployment cost of the RIS, the operational cost, the propagation environment, and the space constraints [33,35]. Equally, the deployment of the RIS should also consider the location availability, the inter-cell interference in cellular networks, etc. Hence, autonomous deployments for RIS-assisted systems are still an open challenge. Autonomous deployment denotes a scenario where the RISs are self-configuring and energy self-sufficient. This implies that they are equipped with built-in sensing (RF power detector) and energy-harvesting capabilities. As a result, they can sense and decode the RF signals and make local decisions. Therefore, this eliminates the need for the control channel and operator management [115,116].

Additionally, the issue of path loss is another challenge in RIS-aided communication systems. Typically, in such a system, transmitted signals will experience larger path loss and due to the passive nature of the RIS (without RF chains), it cannot add any power gain to the overall signal strength to compensate for the power loss. However, the above issues are minimal in a semi-passive RIS configuration when compared with a fully passive one. Therefore, with regards to the implementation strategy the fully passive RIS configuration is preferred for system applications where power efficiency is the main consideration, whereas the semi-passive configuration is used for system applications that require additional power gain. For RIS-assisted systems to fully reap the benefits of the RIS, additional research is required to deal with the issue of energy efficiency, resource allocation, and secure transmission.

## 2.7 RIS versus Relay

RISs have the potential of dynamically tuning the highly probabilistic wireless environment into a partially deterministic one [32,35,71]. Another possible method used in the literature to avoid the unreliability of high-frequency channels is the deployment of relays. With the use of relays, a single NLOS link can effectively be turned into multiple LOS links [117]. Relays are active devices that are equipped with active electronic components such as power amplifiers for signal transmission, low-noise

amplifiers, digital-to-analog converters, and analog-to-digital converters. Equally, the relay requires a dedicated source of power for its operation, the relays can operate in HD as well as in FD modes. In the following, the key similarities and differences between RISs and relays in terms of hardware complexity, achievable rate, noise, and power budget are discussed.

Due to the fact that the relays require several electronic components and a dedicated power source for operation, the deployment of relays in wireless networks may result in higher capital expenditure and an increase in power consumption in the network. These are further increased when relays are used to realize multi-antenna designs at sub-millimeter and millimeter wave frequency bands [118]. The system hardware complexity is even higher when the relays are operated in the FD mode because of the requirement to eliminate the loop-back self-interference in the system. This is accomplished via the use of specifically designed antennas and sophisticated analog/digital signal processing methods. However, RISs can be deployed with much lower energy and hardware cost because an RIS is a planar surface that is comprised of a large number of passive reflecting elements without requiring any transmit RF chain. Furthermore, RISs operate in FD mode, support full-band transmission, and are free from self-interference. Therefore, they do not require any sophisticated techniques for self-interference cancellation [33, 35].

In terms of achievable rate, the duplexing protocol adopted for the relay-aided systems determines the achievable rate. HD-based relay-aided systems suffer from a low spectral efficiency since the spectral efficiency is usually scaled down by a factor of two because different physical resources are used for the data transmitted by the relay and the transmitter. In FD mode the spectral efficiency is not scaled down by a factor of two, however as discussed above, a FD-based relay-aided system is affected by the residual loop-back self-interference which impairs the receiver. On the contrary, RISs are configured to operate with peculiar reflections and it is not affected by the HD constraint and the loop-back self-interference. Therefore, they have the potential to provide a better achievable rate than relays. Moreover, the RIS reflection coefficients can be designed in such a way that they optimally combine the received signals from the RIS and the transmitter thus resulting in an improved spectral efficiency.

Furthermore, due to the fact that several electronic components are used in the relays, there is an unavoidable presence of additive noise that affects the performance of the relay negatively. Relay-aided systems suffer from antenna noise amplification. The impact of the residual loop-back self-interference in FD-based relay systems causes additional degradation in the system performance. In comparison, since the RISs passively reflect impinging waveforms they cannot regenerate or amplify the signals.

Therefore, RISs are not affected by additive noise. However, the performance of the RIS may be impaired by phase noise [33, 49]. Moreover, in relay-aided systems an independent source of power is required to power the electronic components and to transmit signals. However, RISs can be implemented with fully passive components while only using low-power active components such as switches or varactors to ensure their reconfigurability [51]. Due to the above encouraging advantages of RISs over relays, it is justified to say that RIS-assisted transmission may outperform relay-assisted transmission for a sufficiently large RIS [33, 51]. Therefore, RISs are envisaged to be suitably deployed massively in wireless networks to significantly improve their energy and spectral efficiency cost-effectively.

In this chapter, we have given a detailed overview of RISs, their hardware implementation, benefits, various use cases in wireless communications, and their implementation challenges. In the succeeding chapters, we adopt a fully passive RIS architecture and their inherent benefits. This will be used for further interference mitigation and improvement of the system-wide spectral efficiency of a narrow-band, flat-fading DTDD wireless communication system.

## 3. REFLECTION DESIGN METHODS FOR RIS-AIDED DYNAMIC TDD SYSTEMS

Motivated by the fact that the RIS is capable of turning the dynamic wireless environment into a partially deterministic space by adaptively altering the propagation of the reflected signal, this chapter considers the joint optimization of the transmit and passive beamforming for an RIS-aided DTDD wireless system. The goal is to minimize the cross-link interference and maximize the system-wide spectral efficiency. The problem is non-convex as a result of the coupling between the optimization variables and the constant modulus constraints of the RIS. Therefore, to obtain a solution we propose two different novel non-iterative algorithms for solving the problem. Our simulation results show that the proposed algorithms have a better sum rate performance as compared to a DTDD system without RIS. This shows that the integration of the RIS in a DTDD system has the potential to mitigate cross-link interference which is one of the major bottlenecks in a DTDD system.

### 3.1 Introduction

Ultra-dense small cell network deployment is one of the key techniques to meet the exponential growth of traffic demands for B5G and future wireless networks. Small cells using low-power nodes are meant to be deployed in hot spots, where the number of users varies strongly with time and between adjacent cells [119]. As a result, small cells are expected to have burst-like traffic, which makes the static TDD frame configuration strategy, where a common TDD pattern is selected for the whole network, unable to meet the users' requirements and the traffic fluctuations. This inadvertently leads to a high drop rate for the small cells. Dynamic TDD has been proposed as a solution to satisfy the asymmetric and dynamic traffic demand of small cells [25]. In DTDD, each cell is allowed to dynamically reconfigure its TDD pattern based on its instantaneous traffic demand and/or interference status. In [120], the DTDD system performance was evaluated with different performance metrics, and it was found that the DTDD system provides a significant improvement in throughput as compared to the static

TDD.

The main challenge brought by DTDD is the cross-link interference issue, because adjacent cells may use at a given time different TDD frame configurations according to traffic needs, thereby giving rise to opposite transmission directions among neighboring cells. There are two kinds of cross-link interference: BS-to-BS and UE-to-UE interference, which may degrade the system performance significantly. Among the two, the BS-to-BS interference is extremely detrimental due to the large transmit power at the BS and LOS propagation characteristics. Therefore, there is a need to develop an efficient cross-link interference management scheme.

RISs have gained significant attention as a cost-effective solution to improve the current and future wireless networks [32, 33, 35, 113, 121]. In a passive RIS-aided communication system, where the RIS has no radio-frequency chains, the phase shifts of the RIS elements can be adjusted to meet a certain cost function, e.g., the reflected signals add constructively at the intended users and/or destructively at the unintended users [33]. Due to these potentials, there has been increased research interest in RIS-aided communication systems in the last few years, where various RIS-aided communication systems have been studied, such as mmWave communications, cognitive radio, and UAV communications [36–40].

In this chapter, we consider an RIS-aided DTDD system controlled by a central processing unit (CPU) to investigate the potential benefits of employing the RIS to improve communication efficiency while reducing the impact of cross-link BS-to-BS interference. We propose two different novel non-iterative algorithms for solving the resulting problem. Moreover, we assume that the small cells directions are optimized *a priori*, e.g., using the proposed cell reconfiguration method in [122], and are known at the CPU.

## 3.2 Chapter Contributions and Organization

Our main contribution in this chapter is in the design of the passive RIS reflection coefficient vector, where two low-complexity and non-iterative methods are proposed to design the RIS reflection coefficient vector with the objective of maximizing the system SE, while effectively eliminating the cross-link BS-to-BS interference.

- The first algorithm designs a single RIS passive reflection vector for the cells in the considered DTDD system by maximizing the power of the desired users and ensuring reduced multi-user interference.

- The second algorithm designs the RIS passive reflection vector to maximize each cell's desired user signal power independently and ensure zero multi-user interference towards the other cells in the DTDD system. This is achieved by designing the RIS reflection coefficient vector to maximize only the desired signal power in each cell at a time. While other users' channels in the DTDD system relative to the given cell are projected to the null space of the desired user. As a result, the cross-link and intercell interference are eliminated and the system-wide SE is maximized. Results from our numerical analysis show that the algorithm based on the second approach outperforms that of the first algorithm.
- On the other hand, we adopt the classical ZF and MMSE schemes for the design of active transmit and receive beamforming vectors at the BSs, respectively. Equally, we analyze the computational complexity of the proposed solutions. Detailed simulation results are provided showing the efficiency of the proposed RIS reflection design methods as compared to some baseline methods. Specifically, it is shown that the integration of RISs in DTDD systems has a great potential in improving communication spectral efficiency by providing alternative and extra communication links, while at the same time reducing the impact of the cross-link BS-to-BS interference. The concept of reflection design methods for RIS-aided DTDD systems presented in this chapter has been published in [41].

The rest of the chapter is organized as follows, the system model is presented in Section 3.3, while the SE maximization problem is formulated in Section 3.4. In Section 3.5 the proposed RIS reflection design methods are presented, and the design of the transmit and receive beamforming vectors are considered in Section 3.6. Complexity analysis is considered in Section 3.7, while our numerical results and chapter conclusions are presented in Sections 3.8 and 3.9, respectively.

### 3.3 System Model

In this chapter, we consider an RIS-aided mmWave DTDD system consisting of  $Q$  small cells, where each cell has a BS with a uniform linear array (ULA) of  $M_T$  antennas serving a single UE<sup>1</sup> that is equipped with a single-antenna. As shown in Fig. 3.1, we assume that the communication is aided by an RIS with  $M_S$  passive reflecting elements uniformly arranged on a rectangular surface. The RIS has  $M^h$  and  $M^v$  elements in the horizontal and vertical directions, respectively, as shown in Fig. 3.3. Therefore,  $M_S = M^h \cdot M^v$ . A CPU controls the BSs and the RIS via backhaul connections.

---

<sup>1</sup> The extension of our proposed solution to multi-user scenarios is straightforward.

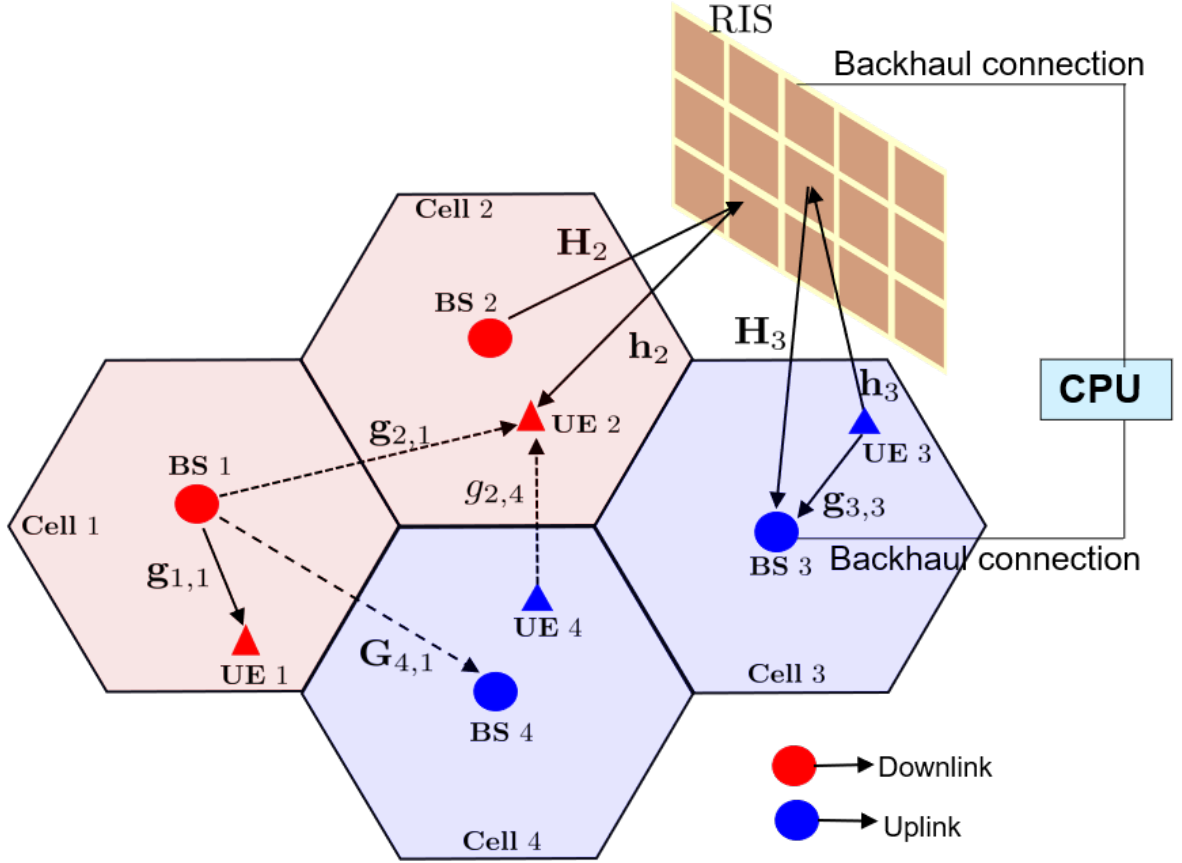


Fig. 3.1: An RIS-aided DTDD system comprising  $Q = 4$  cells.

Similar to [33], we note that the negligible strength of the signals reflected two or more times by the RIS is ignored due to path loss.

Let  $\mathcal{Q} \triangleq \{1, \dots, Q\}$  denote the set of BSs (cells). At the considered time instant, we assume that there are  $|\mathcal{Q}^{\text{ul}}|$  cells operating in the UL direction and  $|\mathcal{Q}^{\text{dl}}|$  cells operating in the DL direction, such that  $|\mathcal{Q}^{\text{ul}}| + |\mathcal{Q}^{\text{dl}}| = Q$  and  $\mathcal{Q}^{\text{ul}} \cap \mathcal{Q}^{\text{dl}} = \emptyset$ . Note that  $|\mathcal{X}|$  denote the cardinality of set  $\mathcal{X}$ , i.e., the number of elements in set  $\mathcal{X}$ . Let  $\mathbf{H}_q \in \mathbb{C}^{M_S \times M_T}$  be the channel matrix from the  $q$ th BS to the RIS,  $\mathbf{h}_q \in \mathbb{C}^{M_S}$  be the channel vector from the  $q$ th UE to the RIS,  $\mathbf{G}_{r,q} \in \mathbb{C}^{M_T \times M_T}$  be the channel matrix from the  $q$ th BS to the  $r$ th BS,  $\mathbf{g}_{r,q} \in \mathbb{C}^{M_T}$  be the channel vector from the  $q$ th BS to the  $r$ th UE, and  $g_{r,q} \in \mathbb{C}$  be the channel scalar from  $q$ th UE to the  $r$ th UE. Then, the received signal by the UE in the  $q$ th DL cell, i.e.,  $q \in \mathcal{Q}^{\text{dl}}$ , can be expressed as

$$y_q^{(\text{dl})} = \sum_{\forall k \in \mathcal{Q}^{\text{dl}}} (\mathbf{h}_{q,k}^{\text{BS-UE}})^T \mathbf{f}_k x_k + \sum_{\forall r \in \mathcal{Q}^{\text{ul}}} h_{q,r}^{\text{UE-UE}} \sqrt{p_r^{\text{ul}}} x_r + z_q, \quad (3.1)$$

where

$$\mathbf{h}_{q,k}^{\text{BS-UE}} = (\mathbf{h}_q^T \Theta \mathbf{H}_k + \mathbf{g}_{q,k}^T)^T, \quad (3.2)$$

is the effective BS-UE channel, i.e., the effective channel from the BS in the  $k$ th DL cell to the  $q$ th UE in the  $q$ th DL cell and

$$h_{q,r}^{\text{UE-UE}} = \mathbf{h}_q^{\text{T}} \mathbf{\Theta} \mathbf{h}_r + g_{q,r}, \quad (3.3)$$

is the effective UE-UE channel, i.e., the effective channel from the  $r$ th UE in the  $r$ th UL cell to the  $q$ th UE in the  $q$ th DL cell. Moreover,  $\mathbf{\Theta} = \text{diag}(\boldsymbol{\theta})$  is the RIS reflection diagonal matrix,  $\boldsymbol{\theta} = [\beta_1 e^{j\phi_1}, \dots, \beta_{M_S} e^{j\phi_{M_S}}]^{\text{T}} \in \mathbb{C}^{M_S}$ , where  $\beta_m \in [0, 1]$  and  $\phi_m \in [0, 2\pi]$  denote the amplitude and phase shift associated with the  $m$ th element of the RIS, respectively. We assume that  $\beta_m = 1, \forall m$  in this work to maximize the signal reflection [32]. Equally,  $\mathbf{f}_k \in \mathbb{C}^{M_T}$  is the transmit precoding vector with  $\|\mathbf{f}_k\|_2^2 = p_k^{\text{dl}}$ ,  $x_k$  is the zero mean transmit symbol such that  $\mathbb{E}\{|x_k|^2\} = 1$ ,  $z_q$  is additive white Gaussian noise with variance  $\sigma_q^2$ , and  $p_r^{\text{X}}$  is the transmit power in the  $X \in \{\text{dl}, \text{ul}\}$  direction. Therefore, the SINR of the  $q$ th UE,  $q \in \mathcal{Q}^{\text{dl}}$ , is given as

$$\Gamma_q^{(\text{dl})} = \frac{|(\mathbf{h}_{q,q}^{\text{BS-UE}})^{\text{T}} \mathbf{f}_q|^2}{\sum_{\substack{\forall k \in \mathcal{Q}^{\text{dl}} \\ k \neq q}} |(\mathbf{h}_{q,k}^{\text{BS-UE}})^{\text{T}} \mathbf{f}_k|^2 + \sum_{\forall r \in \mathcal{Q}^{\text{ul}}} |h_{q,r}^{\text{BS-UE}}|^2 p_r^{\text{ul}} + \sigma_q^2}. \quad (3.4)$$

On the other hand, the received signal at the  $r$ th UL BS, i.e.,  $r \in \mathcal{Q}^{\text{ul}}$ , after the receive combining, can be expressed as

$$y_r^{(\text{ul})} = \sum_{\forall j \in \mathcal{Q}^{\text{ul}}} \mathbf{w}_r^{\text{H}} \mathbf{h}_{r,j}^{\text{BS-UE}} \sqrt{p_j^{\text{ul}}} x_j + \sum_{\forall q \in \mathcal{Q}^{\text{dl}}} \mathbf{w}_r^{\text{H}} \mathbf{H}_{r,q}^{\text{BS-BS}} \mathbf{f}_q x_q + \tilde{z}_r, \quad (3.5)$$

where

$$\mathbf{H}_{r,q}^{\text{BS-BS}} = \mathbf{H}_r^{\text{T}} \mathbf{\Theta} \mathbf{H}_q + \mathbf{G}_{r,q}, \quad (3.6)$$

and  $\mathbf{w}_r \in \mathbb{C}^{M_T}$  is the receive beamforming vector with  $\|\mathbf{w}_r\|_2^2 = 1$ ,  $\tilde{z}_r = \mathbf{w}_r^{\text{H}} \mathbf{z}_r$  with  $\mathbf{z}_r \in \mathbb{C}^{M_T}$  being the additive white Gaussian noise with variance  $\sigma_r^2$ . Therefore, the SINR for the  $r$ th UE,  $r \in \mathcal{Q}^{\text{ul}}$ , is given as

$$\Gamma_r^{(\text{ul})} = \frac{|\mathbf{w}_r^{\text{H}} \mathbf{h}_{r,r}^{\text{BS-UE}}|^2 p_r^{\text{ul}}}{\sum_{\substack{\forall j \in \mathcal{Q}^{\text{ul}} \\ j \neq r}} |\mathbf{w}_r^{\text{H}} \mathbf{h}_{r,j}^{\text{BS-UE}}|^2 p_j^{\text{ul}} + \sum_{\forall q \in \mathcal{Q}^{\text{dl}}} |\mathbf{w}_r^{\text{H}} \mathbf{H}_{r,q}^{\text{BS-BS}} \mathbf{f}_q|^2 + \sigma_r^2}. \quad (3.7)$$

From the above, the system-wide spectral efficiency for the DTDD system is given as

$$\text{SE} = \sum_{\forall q \in \mathcal{Q}^{\text{dl}}} \log_2 \left( 1 + \Gamma_q^{(\text{dl})} \right) + \sum_{\forall r \in \mathcal{Q}^{\text{ul}}} \log_2 \left( 1 + \Gamma_r^{(\text{ul})} \right). \quad (3.8)$$

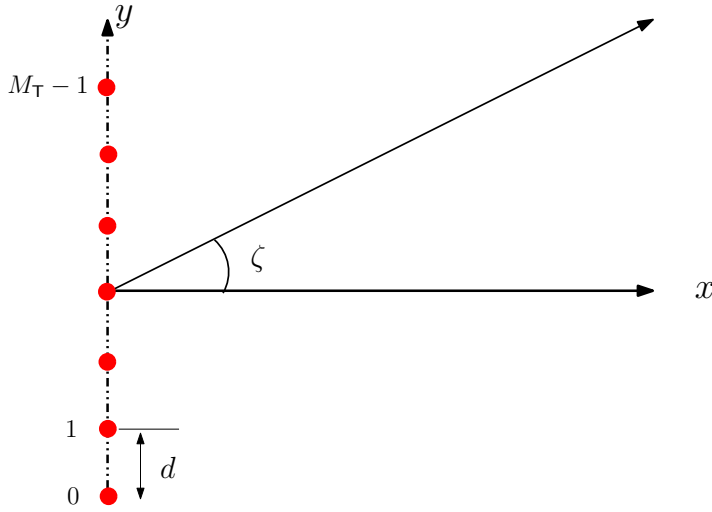


Fig. 3.2: Configuration and orientation of the ULA at the BS.

In this chapter, following [36, 37, 113] we assume that the above-defined channels are modeled according to the geometric channel model [123–125], where every channel is modeled as a summation of  $L \ll \max\{M_S, M_T\}$  paths, each has a distinctive direction-of-departure (DoD) and/or direction-of-arrival (DoA) and a complex path gain. For simplicity, in this chapter we use the same value of  $L$  for all the channels. The channel  $\mathbf{H}_q$  is given as

$$\mathbf{H}_q = \sqrt{\frac{M_S M_T}{L}} \sum_{\ell=1}^L \alpha_\ell \mathbf{a}_R(\mu_\ell^h, \mu_\ell^v) \mathbf{a}_T^T(\psi_\ell), \quad (3.9)$$

where  $\alpha_\ell$  denotes the complex-valued channel gain of the  $\ell$ th path,  $\psi_\ell$  is the spatial frequency of the  $\ell$ th path at the transmit array of the BS, and  $\mathbf{a}_T(\psi_\ell) \in \mathbb{C}^{M_T \times 1}$  is the array steering vector with a Vandermonde structure (due to the ULA assumption at the BS). The steering vector  $\mathbf{a}_T(\psi_\ell)$  is given as

$$\mathbf{a}_T(\psi_\ell) = [1 \quad e^{-j\psi_\ell} \quad \dots \quad e^{-j(M_T-1)\psi_\ell}]^T \in \mathbb{C}^{M_T \times 1}. \quad (3.10)$$

The spatial frequency  $\psi_\ell$  is defined as  $\psi_\ell = 2\pi \frac{d}{\lambda} \sin(\zeta_\ell)$ , where  $d$  is the inter-element spacing,  $\lambda$  is the signal wavelength, and  $\zeta_\ell \in [-90^\circ, 90^\circ]$  is the DoD in the angular domain at the BS as shown in Fig. 3.2. Furthermore, the receive 2D array steering vector at the RIS is given as

$$\mathbf{a}_R(\mu_\ell^h, \mu_\ell^v) = \mathbf{a}_R(\mu_\ell^h) \diamond \mathbf{a}_R(\mu_\ell^v) \in \mathbb{C}^{M_S \times 1}, \quad (3.11)$$

where  $\mu_\ell^h$  and  $\mu_\ell^v$  are the receive spatial frequencies of the  $\ell$ th path at the RIS. The array steering vectors  $\mathbf{a}_R(\mu_\ell^h) \in \mathbb{C}^{M^h \times 1}$  and  $\mathbf{a}_R(\mu_\ell^v) \in \mathbb{C}^{M^v \times 1}$  have the following

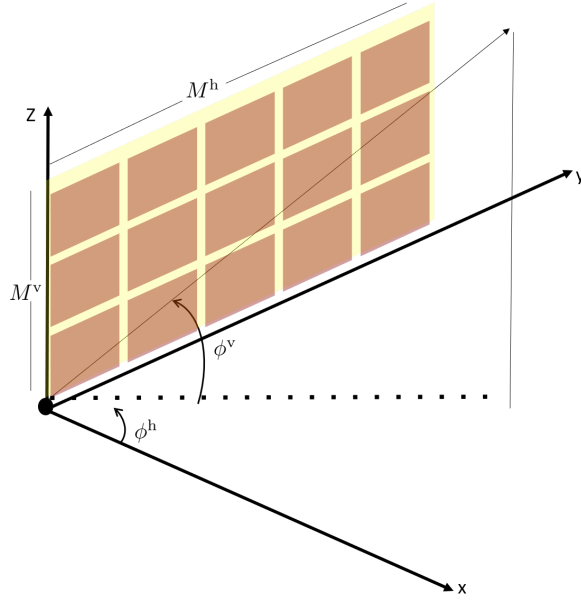


Fig. 3.3: Configuration and orientation of the uniform rectangular structure at the RIS.

structures

$$\mathbf{a}_R(\mu_\ell^h) = \left[ 1 \quad e^{-j\mu_\ell^h} \quad \dots \quad e^{-j(M^h-1)\mu_\ell^h} \right]^T \in \mathbb{C}^{M^h \times 1}, \quad (3.12)$$

$$\mathbf{a}_R(\mu_\ell^v) = \left[ 1 \quad e^{-j\mu_\ell^v} \quad \dots \quad e^{-j(M^v-1)\mu_\ell^v} \right]^T \in \mathbb{C}^{M^v \times 1} \quad (3.13)$$

The receive spatial frequencies are respectively defined as

$$\mu_\ell^h = 2\pi \frac{d}{\lambda} \cos(\phi_\ell^h) \quad (3.14)$$

$$\mu_\ell^v = 2\pi \frac{d}{\lambda} \sin(\phi_\ell^h) \cos(\phi_\ell^v), \quad (3.15)$$

where  $\phi_\ell^h \in [-180^\circ, 180^\circ]$  and  $\phi_\ell^v \in [-90^\circ, 90^\circ]$ , are the azimuth and elevation angles of the  $\ell$ th path at the RIS, respectively, as shown in Fig. 3.3. Equally, the channel  $\mathbf{h}_q$  between the RIS and the  $q$ th UE,  $q \in \mathcal{Q}^{\text{dl}}$ , is given as

$$\mathbf{h}_q = \sqrt{M_S/L} \sum_{\ell=1}^L \beta_\ell \mathbf{a}_T(\eta_\ell^h, \eta_\ell^v), \quad (3.16)$$

where  $\beta_\ell$  is the complex-valued channel gain of the  $\ell$ th path,  $\mathbf{a}_T(\eta_\ell^h, \eta_\ell^v)$  is the transmit array steering vector at the RIS,  $\eta_\ell^h$  and  $\eta_\ell^v$  are the transmit spatial frequencies of the  $\ell$ th path at the RIS. Note that  $\mathbf{a}_T(\eta_\ell^h, \eta_\ell^v)$ ,  $\eta_\ell^h$ , and  $\eta_\ell^v$  are similarly defined as  $\mathbf{a}_R(\mu_\ell^h, \mu_\ell^v)$ ,  $\mu_\ell^h$ , and  $\mu_\ell^v$  above.

Additionally, the channel  $\mathbf{G}_{r,q}$  between the  $r$ th BS,  $r \in \mathcal{Q}^{\text{ul}}$ , and the  $q$ th BS,

$q \in \mathcal{Q}^{\text{dl}}$ , is given as

$$\mathbf{G}_{r,q} = \sqrt{M_{\text{T}}^2/L} \sum_{\ell=1}^L \xi_{\ell} \mathbf{a}_{\text{R}}(\vartheta_{\ell}) \mathbf{a}_{\text{T}}^{\text{T}}(\varpi_{\ell}) \in \mathbb{C}^{M_{\text{T}} \times M_{\text{T}}} \quad (3.17)$$

where  $\xi_{\ell}$  is the complex-valued channel gain of the  $\ell$ th path and  $\mathbf{a}_{\text{R}}(\vartheta_{\ell}) \in \mathbb{C}^{M_{\text{T}} \times 1}$  and  $\mathbf{a}_{\text{T}}(\varpi_{\ell}) \in \mathbb{C}^{M_{\text{T}} \times 1}$  are the array steering vectors with Vandermonde structures at the  $r$ th BS in the UL and the  $q$ th BS in the DL, respectively. Equally,  $\vartheta_{\ell}$  and  $\varpi_{\ell}$  are the spatial frequencies of the  $\ell$ th path at the  $r$ th BS,  $r \in \mathcal{Q}^{\text{ul}}$  and the  $q$ th BS,  $q \in \mathcal{Q}^{\text{dl}}$ , respectively. The steering vectors  $\mathbf{a}_{\text{T}}(\varpi_{\ell})$  and  $\mathbf{a}_{\text{R}}(\vartheta_{\ell})$  are given as

$$\mathbf{a}_{\text{T}}(\varpi_{\ell}) = [1 \quad e^{-j\psi_{\ell}} \quad \dots \quad e^{-j(M_{\text{T}}-1)\varpi_{\ell}}]^{\text{T}} \in \mathbb{C}^{M_{\text{T}} \times 1}, \quad (3.18)$$

$$\mathbf{a}_{\text{R}}(\vartheta_{\ell}) = [1 \quad e^{-j\vartheta_{\ell}} \quad \dots \quad e^{-j(M_{\text{T}}-1)\vartheta_{\ell}}]^{\text{T}} \in \mathbb{C}^{M_{\text{T}} \times 1}. \quad (3.19)$$

The spatial frequencies  $\varpi_{\ell}$  and  $\vartheta_{\ell}$  are defined as  $\varpi_{\ell} = 2\pi \frac{d}{\lambda} \sin(\zeta_{\ell})$  and  $\vartheta_{\ell} = 2\pi \frac{d}{\lambda} \sin(\varphi_{\ell})$ , respectively. Equally,  $\vartheta_{\ell} \in [-90^{\circ}, 90^{\circ}]$  and  $\varpi_{\ell} \in [-90^{\circ}, 90^{\circ}]$  are the DoA and DoD of the  $\ell$ th path at the  $r$ th BS,  $r \in \mathcal{Q}^{\text{ul}}$  and the  $q$ th BS,  $q \in \mathcal{Q}^{\text{dl}}$ , respectively. Similarly, the direct channel between the  $q$ th BS,  $q \in \mathcal{Q}^{\text{dl}}$  and the  $q$ th UE,  $q \in \mathcal{Q}^{\text{dl}}$ ,  $\mathbf{g}_q$  is given as

$$\mathbf{g}_q = \sqrt{M_{\text{T}}/L} \sum_{\ell=1}^L \kappa_{\ell} \mathbf{a}_{\text{T}}(\nu_{\ell}), \quad (3.20)$$

where  $\kappa_{\ell}$  is the complex-valued channel gain of the  $\ell$ th path and the array steering vector  $\mathbf{a}_{\text{T}}(\nu_{\ell})$  and the spatial frequency  $\nu_{\ell}$  at the BS and are similarly defined as  $\mathbf{a}_{\text{T}}(\varpi_{\ell})$  and  $\varpi_{\ell}$  above. Under this assumption, we have that  $\text{rank}\{\mathbf{H}_q\} \leq L, \forall q$  and  $\text{rank}\{\mathbf{G}_{r,q}\} \leq L, \forall r, q$ . Moreover, we assume block fading channels. This implies that the channels change over time but are constant during the duration of the coherence time. Signal transmission is carried within this channel coherence period. Also, these channels have been estimated and known at the BSs through the CPU.

### 3.4 Problem Formulation

The main goal of this chapter is to design the passive reflection coefficient vector  $\boldsymbol{\theta}$  of the RIS and the active transmit beamforming vectors  $\mathbf{f}_q, \forall q \in \mathcal{Q}^{\text{dl}}$ , and receive beamforming vectors  $\mathbf{w}_r, \forall r \in \mathcal{Q}^{\text{ul}}$ , of the BSs to maximize the system SE, which can

be formulated as

$$\max_{\mathbf{f}_q, \forall q \in \mathcal{Q}^{\text{dl}}, \mathbf{w}_r, \forall r \in \mathcal{Q}^{\text{ul}}, \boldsymbol{\theta}} \text{SE} \quad (3.21\text{a})$$

$$\text{s.t.} \quad \|\mathbf{f}_q\|_2^2 = p_q^{\text{dl}}, \forall q \in \mathcal{Q}^{\text{dl}} \quad (3.21\text{b})$$

$$|[\boldsymbol{\theta}]_m|^2 = 1, m = 1, \dots, M_S, \quad (3.21\text{c})$$

where the SE is defined in (3.8). Furthermore, (3.21b) is the DL transmit power constraint and (3.21c) are the constant modulus constraints (CMCs) for the RIS reflection coefficients. Problem (3.21) is non-convex due to its joint optimization of the optimization variables  $(\mathbf{f}_q, \mathbf{w}_r, \boldsymbol{\theta})$  and the CMCs in (3.21c). To obtain a low-complexity solution, we propose in the following non-iterative sub-optimal solutions by decoupling the optimization between the problem variables. Specifically, given the channel matrices, we propose two solution methods for the design of the RIS passive reflection coefficient vector  $\boldsymbol{\theta} \in \mathbb{C}^{M_S}$ . In the first algorithm we intuitively design the RIS reflection coefficient vector to mitigate the cross-link interference and maximize the SE. However, to reduce overhead and complexity, we propose a heuristic approach in designing the RIS reflection coefficient vector in order to address the issue of the cross-link interference and further improve the system performance. After that, for a given  $\boldsymbol{\theta}$ , we design the BSs' transmit and receive active beamformers  $\mathbf{f}_q, \forall q \in \mathcal{Q}^{\text{dl}}$ , and  $\mathbf{w}_r, \forall r \in \mathcal{Q}^{\text{ul}}$ , using the classical ZF and MMSE methods, respectively.

### 3.5 Proposed RIS Reflection Design Methods

In the following, two non-iterative heuristic solutions are proposed for the design of the RIS reflection coefficient vector  $\boldsymbol{\theta} \in \mathbb{C}^{M_S}$ . The RIS reflection coefficient vector  $\boldsymbol{\theta} \in \mathbb{C}^{M_S}$  is designed in such a way as to enhance communication efficiency and mitigate the impact of cross-link interference in the DTDD system. To begin, we first note that from (1.1) the vectorized form of the above-defined effective channels in (3.2), (3.3),

and (3.6) can be expressed, respectively, as

$$\mathbf{h}_{q,k}^{\text{BS-UE}} = \underbrace{(\mathbf{H}_k^{\text{T}} \diamond \mathbf{h}_q^{\text{T}})}_{\mathbf{H}_{q,k}^{\text{BS-UE}}} \boldsymbol{\theta} + \mathbf{g}_{q,k}, \quad (3.22)$$

$$h_{q,r}^{\text{UE-UE}} = \underbrace{(\mathbf{h}_r^{\text{T}} \diamond \mathbf{h}_q^{\text{T}})}_{(\mathbf{h}_{q,r}^{\text{UE-UE}})^{\text{T}}} \boldsymbol{\theta} + g_{q,r}, \quad (3.23)$$

$$\text{vec}\{\mathbf{H}_{r,q}^{\text{BS-BS}}\} = \underbrace{(\mathbf{H}_q^{\text{T}} \diamond \mathbf{H}_r^{\text{T}})}_{\mathbf{H}_{r,q}^{\text{BS-BS}}} \boldsymbol{\theta} + \text{vec}\{\mathbf{G}_{r,q}\}, \quad (3.24)$$

where  $\mathbf{H}_{q,k}^{\text{BS-UE}} \in \mathbb{C}^{M_{\text{T}} \times M_{\text{S}}}$ ,  $\mathbf{H}_{r,q}^{\text{BS-BS}} \in \mathbb{C}^{M_{\text{T}}^2 \times M_{\text{S}}}$ , and  $\mathbf{h}_{q,r}^{\text{UE-UE}} \in \mathbb{C}^{M_{\text{S}} \times 1}$  are the RIS-assisted composite channels. Note that  $\text{rank}\{\mathbf{H}_{q,k}^{\text{BS-UE}}\} \leq L$ ,  $\text{rank}\{\mathbf{H}_{r,q}^{\text{BS-BS}}\} \leq L^2$ , and  $\text{rank}\{\mathbf{h}_{q,r}^{\text{UE-UE}}\} = 1$ . Moreover, from the signal models in (3.1) and (3.5), we know that the effective channels  $\{\mathbf{h}_{q,k}^{\text{BS-UE}}\}$  carry the desired signals (DS) for  $q = k$  and the inter-cell interference (ICI) signals for  $q \neq k$ , while  $\{\mathbf{H}_{r,q}^{\text{BS-BS}}, \mathbf{h}_{q,r}^{\text{UE-UE}}\}$  carry the cross-link (CL) interference signals between the UL and DL cells i.e.,  $r \in \mathcal{Q}^{\text{ul}}$  and  $q \in \mathcal{Q}^{\text{dl}}$ . Therefore, we define the following matrices

$$\mathbf{D}_{\text{DS}}^{\text{BS-UE}} = \text{stack}\{\mathbf{H}_{q,q}^{\text{BS-UE}}\}_{\forall q \in \mathcal{Q}} \in \mathbb{C}^{Q \cdot M_{\text{T}} \times M_{\text{S}}} \quad (3.25)$$

$$\mathbf{C}_{\text{DL-ICI}}^{\text{BS-UE}} = \text{stack}\{\mathbf{H}_{q,k}^{\text{BS-UE}}\}_{\forall k, q \in \mathcal{Q}^{\text{dl}}, k \neq q} \in \mathbb{C}^{(|\mathcal{Q}^{\text{dl}}| - 1) \cdot M_{\text{T}} \times M_{\text{S}}} \quad (3.26)$$

$$\mathbf{C}_{\text{UL-ICI}}^{\text{BS-UE}} = \text{stack}\{\mathbf{H}_{q,k}^{\text{BS-UE}}\}_{\forall k, q \in \mathcal{Q}^{\text{ul}}, k \neq q} \in \mathbb{C}^{(|\mathcal{Q}^{\text{ul}}| - 1) \cdot M_{\text{T}} \times M_{\text{S}}} \quad (3.27)$$

$$\mathbf{C}_{\text{DL-CL}}^{\text{BS-BS}} = \text{stack}\{\mathbf{H}_{r,q}^{\text{BS-BS}}\}_{\forall r \in \mathcal{Q}^{\text{ul}}, \forall q \in \mathcal{Q}^{\text{dl}}} \in \mathbb{C}^{(|\mathcal{Q}^{\text{dl}}|) \cdot M_{\text{T}}^2 \times M_{\text{S}}} \quad (3.28)$$

$$\mathbf{C}_{\text{UL-CL}}^{\text{UE-UE}} = \text{stack}\{(\mathbf{h}_{q,r}^{\text{UE-UE}})^{\text{T}}\}_{\forall r \in \mathcal{Q}^{\text{ul}}, \forall q \in \mathcal{Q}^{\text{dl}}} \in \mathbb{C}^{|\mathcal{Q}^{\text{ul}}| \times M_{\text{S}}} \quad (3.29)$$

where we define  $\mathbf{A} = \text{stack}\{\mathbf{A}_i\}_{\forall i \in \mathcal{I}} = \begin{bmatrix} \mathbf{A}_1, \\ \vdots, \\ \mathbf{A}_{|\mathcal{I}|} \end{bmatrix}$ , i.e., a function that stacks the input

matrices on top of each other.

From the above, this chapter proposes to design the RIS reflection coefficient vector  $\boldsymbol{\theta} \in \mathbb{C}^{M_{\text{S}}}$  to ensure maximum power to the desired UEs in the DTDD system while ensuring zero interference conditions to the unintended UEs in the system. The problem can be expressed as given in (3.30),

$$\max_{\boldsymbol{\theta}} \quad \|\mathbf{D}_{\text{DS}}^{\text{BS-UE}} \boldsymbol{\theta}\|_2^2 \quad (3.30\text{a})$$

$$\text{s.t.} \quad |[\boldsymbol{\theta}]_m|^2 = 1, \quad m = 1, \dots, M_{\text{S}} \quad (3.30\text{b})$$

$$\mathbf{C}_{\text{INT}}\boldsymbol{\theta} = \mathbf{0}, \quad (3.30c)$$

where  $\mathbf{D}_{\text{DS}}^{\text{BS-UE}}$  is a matrix that contains all the channels of the desired users in the DTDD system as defined in (3.25) and  $\mathbf{C}_{\text{INT}} = \text{stack}\{\mathbf{C}_{\text{DL-ICI}}^{\text{BS-UE}}, \mathbf{C}_{\text{UL-ICI}}^{\text{BS-UE}}, \mathbf{C}_{\text{DL-CL}}^{\text{BS-BS}}, \mathbf{C}_{\text{UL-CL}}^{\text{UE-UE}}\}$  is a block matrix containing all the interference channel matrices in the DTDD system. The constraint in (3.30c) is the multi-user zero interference condition. The problem in (3.30) is non-convex due to CMCs in (3.21c). In the following, we propose two non-iterative solutions to obtain a feasible and efficient RIS reflection coefficient vector.

**Remark 1:** Given the above mmWave channel modeling, the following inequality holds true:

$$R_c \triangleq \text{rank}\{\mathbf{C}_{\text{INT}}\} \leq L_{\text{DL-ICI}}^{\text{BS-UE}} + L_{\text{UL-ICI}}^{\text{BS-UE}} + L_{\text{DL-CL}}^{\text{BS-BS}} + L_{\text{UL-CL}}^{\text{UE-UE}}, \quad (3.31)$$

where  $L_{\text{DL-ICI}}^{\text{BS-UE}} \leq (|\mathcal{Q}^{\text{dl}}|^2 - |\mathcal{Q}^{\text{dl}}|)L$ , from (3.26),  $L_{\text{UL-ICI}}^{\text{BS-UE}} \leq (|\mathcal{Q}^{\text{ul}}|^2 - |\mathcal{Q}^{\text{ul}}|)L$ , from (3.27),  $L_{\text{DL-CL}}^{\text{BS-BS}} \leq |\mathcal{Q}^{\text{dl}}||\mathcal{Q}^{\text{ul}}|L^2$ , from (3.28), and  $L_{\text{UL-CL}}^{\text{UE-UE}} \leq |\mathcal{Q}^{\text{dl}}||\mathcal{Q}^{\text{ul}}|$ , from (3.29).

### 3.5.1 Method 1

In this method, we relax the CMCs in (3.21c). As a result, the problem in (3.30) can be written as

$$\max_{\boldsymbol{\theta}} \quad \|\mathbf{D}_{\text{DS}}^{\text{BS-UE}}\boldsymbol{\theta}\|_2^2 \quad (3.32a)$$

$$\text{s.t.} \quad \mathbf{C}_{\text{INT}}\boldsymbol{\theta} = \mathbf{0} \quad (3.32b)$$

$$\|\boldsymbol{\theta}\|_2^2 = 1. \quad (3.32c)$$

A direct solution to (3.32) is given as

$$\boldsymbol{\theta}^{\text{FD-1}} = \mathbf{V}_{\text{INT}}^{\text{NS}} \mathbf{v}_{\text{max}}^{\text{DS}} \in \mathbb{C}^{M_S}, \quad (3.33)$$

where  $\mathbf{V}_{\text{INT}}^{\text{NS}} \in \mathbb{C}^{M_S \times (M_S - R_c)}$  holds the basis for the null-space (NS)<sup>2</sup> of  $\mathbf{C}_{\text{INT}} \in \mathbb{C}^{I \times M_S}$ , which can be obtained from the singular value decomposition (SVD) of  $\mathbf{C}_{\text{INT}}$  [13], where  $I = Q(M_T^2 + M_T + 1)$  and  $R_c$  is the rank of  $\mathbf{C}_{\text{INT}}$  according to (3.31). Furthermore,  $\mathbf{v}_{\text{max}}^{\text{DS}} \in \mathbb{C}^{(M_S - R_c) \times 1}$  is the right singular vector corresponding to the maximum singular value of  $\mathbf{D}_{\text{DS}}^{\text{BS-UE}} \mathbf{V}_{\text{INT}}^{\text{NS}} \in \mathbb{C}^{QM_T \times (M_S - R_c)}$ . Therefore, a solution to

<sup>2</sup> The dimensionality constraint for the existence of the null-space is overcome by exploiting the low-rank structure of the mmWave channel whose rank is dependent on the number of propagation paths  $L$  instead of depending on the number of transmit antenna  $M_T$  or the number of RIS elements  $M_S$ .

(3.30) which satisfies the CMCs in (3.21c) is given as

$$\boldsymbol{\theta}^{\text{CMC-1}} \leftarrow \text{P}(\boldsymbol{\theta}^{\text{FD-1}}), \quad (3.34)$$

where  $\text{P}(z_i) = \frac{z_i}{|z_i|}$  is the element-wise projection function.

### 3.5.2 Method 2

In the previous method, we designed the RIS reflection coefficient vector centrally for all the cells in the DTDD system to maximize the desired UEs' powers. However, to further improve the performance of the system, in this method, we propose a heuristic method to perform the desired UE's power maximization optimization in (3.32) individually for the different cells in the DTDD system. First, we assume that  $\boldsymbol{\theta}$  is decomposed into  $Q$  sub-vectors as

$$\boldsymbol{\theta} = \boldsymbol{\theta}_1 + \boldsymbol{\theta}_2 + \cdots + \boldsymbol{\theta}_Q \in \mathbb{C}^{M_S}, \quad (3.35)$$

where  $Q$  is the total number of cells in the DTDD system,  $\boldsymbol{\theta}_q \in \mathbb{C}^{M_S}$ , and  $\|\boldsymbol{\theta}_q\|_2^2 = 1, \forall q$ . Given the above decomposition, we propose to design the  $q$ th sub-vector  $\boldsymbol{\theta}_q$  as

$$\max_{\boldsymbol{\theta}_q} \quad \|\mathbf{H}_{q,q}^{\text{BS-UE}} \boldsymbol{\theta}_q\|_2^2 \quad (3.36a)$$

$$\text{s.t.} \quad \|\boldsymbol{\theta}_q\|_2^2 = 1 \quad (3.36b)$$

$$\boldsymbol{\Pi}_q^{\text{INT}} \boldsymbol{\theta}_q = \mathbf{0}, \quad (3.36c)$$

where  $\mathbf{H}_{q,q}^{\text{BS-UE}} \in \mathbb{C}^{M_T \times M_S}$  is the RIS-assisted composite channel for the desired user in the  $q$ th cell as given in (3.22) and  $\boldsymbol{\Pi}_q^{\text{INT}} = \text{stack}\{\mathbf{D}_{\text{DS-INT}}^{\text{BS-UE}}, \mathbf{C}_{\text{INT}}\}$  is the total interference block matrix specific to the  $q$ th cell and

$$\mathbf{D}_{\text{DS-INT}}^{\text{BS-UE}} = \text{stack}\{\mathbf{H}_{r,r}^{\text{BS-UE}}\}_{\forall r \in Q, r \neq q} \in \mathbb{C}^{(Q-1)M_T \times M_S} \quad (3.37)$$

i.e., a matrix containing all blocks of  $\mathbf{D}_{\text{DS}}^{\text{BS-UE}}$  in (3.25) except for the  $q$ th sub-block. Note that  $R_\pi \triangleq \text{rank}\{\boldsymbol{\Pi}_q^{\text{INT}}\} \leq \text{rank}\{\mathbf{C}_{\text{INT}}\} + L_{\text{DS-INT}}^{\text{BS-UE}}$ , where  $L_{\text{DS-INT}}^{\text{BS-UE}} \leq (Q-1)L$ . A solution to the  $q$ th sub-problem in (3.36) is given as

$$\boldsymbol{\theta}_q^{\text{FD-2}} = \mathbf{V}_{\text{INT},q}^{\text{NS}} \mathbf{v}_{\text{max},q}^{\text{BS-UE}} \in \mathbb{C}^{M_S}, \quad (3.38)$$

where  $\mathbf{V}_{\text{INT},q}^{\text{NS}} \in \mathbb{C}^{M_S \times (M_S - R_\pi)}$  holds the basis for the null-space (NS) of  $\boldsymbol{\Pi}_q^{\text{INT}} \in \mathbb{C}^{I_q \times M_S}$ , and  $\mathbf{v}_{\text{max},q}^{\text{BS-UE}} \in \mathbb{C}^{(M_S - R_\pi) \times 1}$  is the right singular vector corresponding to the maximum singular value of  $\mathbf{H}_{q,q}^{\text{BS-UE}} \mathbf{V}_{\text{INT},q}^{\text{NS}} \in \mathbb{C}^{M_T \times (M_S - R_\pi)}$ , where  $I_q = Q(M_T^2 + 2M_T + 1) - M_T$  and  $R_\pi$  is the rank of the  $\boldsymbol{\Pi}_q^{\text{INT}}$  matrix.

Let  $\Theta^{\text{FD-2}} = [\boldsymbol{\theta}_1^{\text{FD-2}}, \dots, \boldsymbol{\theta}_Q^{\text{FD-2}}] \in \mathbb{C}^{M_S \times Q}$  denote a matrix that has the designed  $\boldsymbol{\theta}_q^{\text{FD-2}}, \forall q \in Q$  vectors in its columns. Then, it can be easily shown that

$$\mathbf{D}_{\text{DS}}^{\text{BS-UE}} \Theta^{\text{FD-2}} = \begin{bmatrix} \mathbf{e}_1 & \cdots & \mathbf{0} \\ \vdots & \ddots & \vdots \\ \mathbf{0} & \cdots & \mathbf{e}_Q \end{bmatrix} \in \mathbb{C}^{QM_T \times Q}, \quad (3.39)$$

where the diagonal elements  $\mathbf{e}_q = \mathbf{H}_{q,q}^{\text{BS-UE}} \boldsymbol{\theta}_q \in \mathbb{C}^{M_T}$  represent the respective output from the RIS for the cells. Let

$$\boldsymbol{\theta}^{\text{FD-2}} = \frac{\boldsymbol{\theta}_1^{\text{FD-2}} + \dots + \boldsymbol{\theta}_Q^{\text{FD-2}}}{\|\boldsymbol{\theta}_1^{\text{FD-2}} + \dots + \boldsymbol{\theta}_Q^{\text{FD-2}}\|}, \quad (3.40)$$

then we have,

$$\mathbf{D}_{\text{DS}}^{\text{BS-UE}} \boldsymbol{\theta}^{\text{FD-2}} = \text{stack}\{\bar{\mathbf{e}}_1, \dots, \bar{\mathbf{e}}_Q\}, \quad (3.41)$$

where  $\bar{\mathbf{e}}_q = \frac{\mathbf{e}_q}{\|\boldsymbol{\theta}_1^{\text{FD-2}} + \dots + \boldsymbol{\theta}_Q^{\text{FD-2}}\|}$ . This justifies our proposed heuristic approach for designing the reflection coefficient vector in (3.35). Finally, to satisfy the constant modulus constraints of in (3.21c), we apply the projection function as

$$\boldsymbol{\theta}^{\text{CMC-2}} \leftarrow \text{P}(\boldsymbol{\theta}^{\text{FD-2}}). \quad (3.42)$$

## 3.6 Active Beamforming Design

### 3.6.1 Transmit beamforming design

For a given  $\boldsymbol{\theta}$ , e.g.,  $\boldsymbol{\theta} \in \{\boldsymbol{\theta}^{\text{CMC-1}}, \boldsymbol{\theta}^{\text{CMC-2}}\}$ , we design the transmit beamforming vectors  $\mathbf{f}_q, \forall q \in \mathcal{Q}^{\text{dl}}$ . Specifically, the  $q$ th transmit beamforming vector for the  $q$ th DL BS,  $\mathbf{f}_q, q \in \mathcal{Q}^{\text{dl}}$ , is designed to satisfy the following interference condition

$$\Upsilon_q \mathbf{f}_q = \mathbf{0}, \forall q \in \mathcal{Q}^{\text{dl}}, \quad (3.43)$$

where  $\Upsilon_q = \text{stack}\{\Upsilon_q^{\text{ICI}}, \Upsilon_q^{\text{BS-BS}}\}$  is a matrix collecting the *direct* interference channels relative to the  $q$ th UE, where

$$\Upsilon_q^{\text{ICI}} = \text{stack}\{\mathbf{g}_{k,q}^{\text{T}}\}_{\forall r \in \mathcal{Q}^{\text{dl}}, k \neq q} \in \mathbb{C}^{(|\mathcal{Q}^{\text{dl}}|-1) \times M_T} \quad (3.44)$$

$$\Upsilon_q^{\text{BS-BS}} = \text{stack}\{\mathbf{G}_{r,q}\}_{\forall r \in \mathcal{Q}^{\text{ul}}} \in \mathbb{C}^{|\mathcal{Q}^{\text{ul}}| M_T \times M_T}. \quad (3.45)$$

which satisfies  $R_v \triangleq \text{rank}\{\Upsilon_q\} \leq (|\mathcal{Q}^{\text{dl}}| - 1) + |\mathcal{Q}^{\text{ul}}|L$ . Given  $\Upsilon_q$ , the  $q$ th transmit vector  $\mathbf{f}_q, q \in \mathcal{Q}^{\text{dl}}$ , is given as

$$\mathbf{f}_q = \frac{\bar{\mathbf{f}}_q}{\|\bar{\mathbf{f}}_q\|_2} \sqrt{p_q^{\text{dl}}}, \quad (3.46)$$

where  $\bar{\mathbf{f}}_q = \mathbf{V}_q^{\text{NS}} \mathbf{v}_{\text{max},q}$ , in which  $\mathbf{V}_q^{\text{NS}} \in \mathbb{C}^{M_T \times (M_T - R_v)}$  holds the basis for the null-space of  $\Upsilon_q \in \mathbb{C}^{I_v \times M_T}$ , while  $\mathbf{v}_{\text{max},q} \in \mathbb{C}^{(M_T - R_v) \times 1}$  is the right singular vector corresponding to the maximum singular value of  $(\mathbf{h}_{q,q}^{\text{BS-UE}})^T \mathbf{V}_q^{\text{NS}}$ , where  $I_v = (|\mathcal{Q}^{\text{dl}}| - 1) + |\mathcal{Q}^{\text{ul}}|M_T$  and  $R_v$  is the rank of the  $\Upsilon_q$  matrix.

### 3.6.2 Receive beamforming design

For a given  $\boldsymbol{\theta}$ , e.g.,  $\boldsymbol{\theta} \in \{\boldsymbol{\theta}^{\text{CMC-1}}, \boldsymbol{\theta}^{\text{CMC-2}}\}$ , and  $\mathbf{f}_q, \forall q \in \mathcal{Q}^{\text{dl}}$ , we design the receive beamforming vectors at the UL BSs,  $\mathbf{w}_r, \forall r \in \mathcal{Q}^{\text{ul}}$ . To design  $r$ th receive beamforming vector  $\mathbf{w}_r, r \in \mathcal{Q}^{\text{ul}}$ , we adopt the MMSE scheme [126], which is given as

$$\mathbf{w}_{\text{MMSE},r} = \frac{\mathbf{B}_r^{-1} \mathbf{h}_{r,r}^{\text{BS-UE}}}{\|\mathbf{B}_r^{-1} \mathbf{h}_{r,r}^{\text{BS-UE}}\|_2}, \forall r \in \mathcal{Q}^{\text{ul}}, \quad (3.47)$$

where

$$\mathbf{B}_r = \sum_{\forall j \in \mathcal{Q}^{\text{ul}}} p_r^{\text{ul}} \mathbf{h}_{r,j}^{\text{BS-UE}} (\mathbf{h}_{r,j}^{\text{BS-UE}})^H + \sum_{\forall q \in \mathcal{Q}^{\text{dl}}} \mathbf{H}_{r,q}^{\text{BS-BS}} \mathbf{f}_{\text{ZF},q} (\mathbf{H}_{r,q}^{\text{BS-BS}} \mathbf{f}_{\text{ZF},q})^H + \sigma_r^2 \mathbf{I}_{M_T}. \quad (3.48)$$

## 3.7 Complexity analysis

Since the complexity of computing the SVD of a  $m \times n$  matrix, with  $m \geq n$ , is on the order of  $\mathcal{O}\{n^2\}^3$  [127], then the complexity of calculating  $\boldsymbol{\theta}^{\text{CMC-1}}$  is on the order of  $\mathcal{O}\{M_S^2\}$ ,  $\boldsymbol{\theta}^{\text{CMC-2}}$  is on the order of  $\mathcal{O}\{QM_S^2\}$ , and the transmit precoding vectors  $\mathbf{f}_q, \forall q \in \mathcal{Q}^{\text{dl}}$ , is on the order of  $\mathcal{O}\{|\mathcal{Q}^{\text{dl}}|M_T^2\}$  [127]. Moreover, the complexity of calculating the decoding vectors  $\mathbf{w}_r, \forall r \in \mathcal{Q}^{\text{ul}}$ , is on the order of  $\mathcal{O}\{|\mathcal{Q}^{\text{ul}}|M_T^3\}$ , since the complexity of computing the inverse of a  $n \times n$  matrix is on the order of  $\mathcal{O}\{n^3\}$  [127].

<sup>3</sup> The Big  $\mathcal{O}$  notation is a mathematical notation used in computer science to describe the time or space complexities of algorithms. It gives the upper bound or the worst-case scenario of the complexity [127].

### 3.8 Numerical Results

In this section, we show simulation results to evaluate the performance of our proposed methods as compared to baseline schemes. We consider a system with  $Q = 4$  cells, as shown in Fig. 3.1, where  $|\mathcal{Q}^{\text{dl}}| = 2$  and  $|\mathcal{Q}^{\text{ul}}| = 2$ . We set  $p_r^{\text{ul}} = 23\text{dBm}$  and assume that the number of channels paths  $L = 4$ ,  $\{\alpha_\ell, \beta_\ell, \xi_\ell, \kappa_\ell\} \sim \mathcal{CN}(0, 1)$ , and the corresponding DoDs and/or DoAs are uniformly distributed with  $[-\frac{\pi}{2}, \frac{\pi}{2}]$ . We normalize every channel path gains so that  $\mathbb{E}\{\|\mathbf{H}_q\|_{\text{F}}^2\} = M_{\text{T}}M_{\text{S}}$ ,  $\mathbb{E}\{\|\mathbf{G}_{r,q}\|_{\text{F}}^2\} = M_{\text{T}}^2$ ,  $\mathbb{E}\{\|\mathbf{h}_q\|_{\text{F}}^2\} = M_{\text{S}}$ , and  $\mathbb{E}\{\|\mathbf{g}_{r,q}\|_{\text{F}}^2\} = M_{\text{T}}$ . Furthermore, for our initial experiments  $M_{\text{T}} = 16$ , for all the BSs in the DTDD system and  $M_{\text{S}} = 256$  are used. With the above simulation parameters then  $I$  and  $R_{\text{c}}$  in Section 3.5.1 are given as  $I = Q(M_{\text{T}}^2 + M_{\text{T}} + 1) = 1092$  and  $R_{\text{c}} = 4L + 4L^2 + 4 = 84$ , respectively. Then, the matrix that spans the null-space of  $\mathbf{C}_{\text{INT}}$  is  $\mathbf{V}_{\text{INT}}^{\text{NS}} \in \mathbb{C}^{256 \times 172}$ . Similarly,  $I_q$  and  $R_{\pi}$  in Section 3.5.2 are given as  $I_q = Q(M_{\text{T}}^2 + 2M_{\text{T}} + 1) - M_{\text{T}} = 1140$  and  $R_{\pi} = 7L + 4L^2 + 4 = 96$ , respectively. Therefore, the matrix that spans the null-space of  $\mathbf{\Pi}_{\text{INT},q}^{\text{NS}}$  becomes  $\mathbf{V}_{\text{INT},q}^{\text{NS}} \in \mathbb{C}^{256 \times 160}$ . Additionally,  $I_v$  and  $R_v$  in Section 3.6.1 are given as  $I_v = (|\mathcal{Q}^{\text{dl}}| - 1) + |\mathcal{Q}^{\text{ul}}|M_{\text{T}} = 33$  and  $R_v = 9$ , respectively. Moreover, the matrix that spans the null-space of  $\mathbf{\Upsilon}_q$  is  $\mathbf{V}_q^{\text{NS}} \in \mathbb{C}^{16 \times 7}$ .

We include results for the following two baseline cases:

- **Random**, where the entries of the RIS reflection coefficient vector are designed randomly as  $[\boldsymbol{\theta}]_{[m]} = e^{j\phi_m}, \forall m$ , with  $\phi_m \sim \mathcal{U}(-\pi, \pi)$ ,
- **No RIS**, the case where no RIS is deployed, i.e.,  $[\boldsymbol{\theta}]_{[m]} = 0, \forall m$ .

In Fig. 3.4, we show the SE versus the DL SNR, while assuming that the RIS has  $M_{\text{S}} = 256$  passive reflecting elements and each BS has  $M_{\text{T}} = 16$  antennas. We plot the achievable SE of the DL and the UL cells separately and then combined them in Fig. 3.5 to better understand the difference between the proposed and the baseline methods. From the figures, we can clearly see that Method 2 has a better SE performance compared to Method 1 and the other two baseline schemes, while both the proposed methods have significantly better performance compared to the Random RIS scenarios. This is due to the heuristic approach adopted for the design of the RIS reflection coefficient vector in Method 2.

We note that from figures there is a performance degradation between the full digital solution and the solution that satisfies the CMCs for the proposed methods. This performance degradation could be seen as a tradeoff in solving the non-convex CM constraints using convex relaxation technique. The performance loss is higher

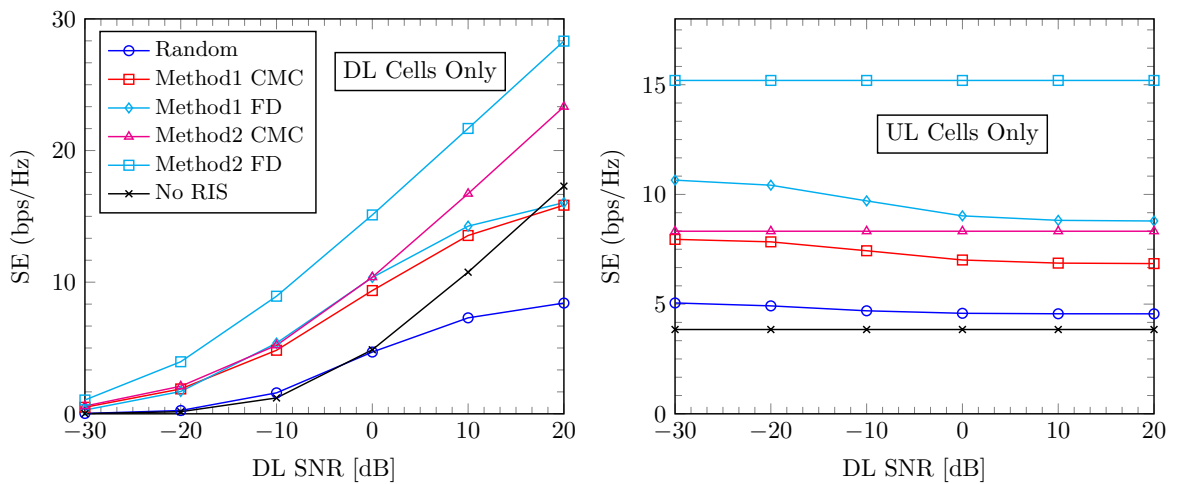


Fig. 3.4: SE versus DL SNR, assuming  $M_S = 256$  and  $M_T = 16$ .

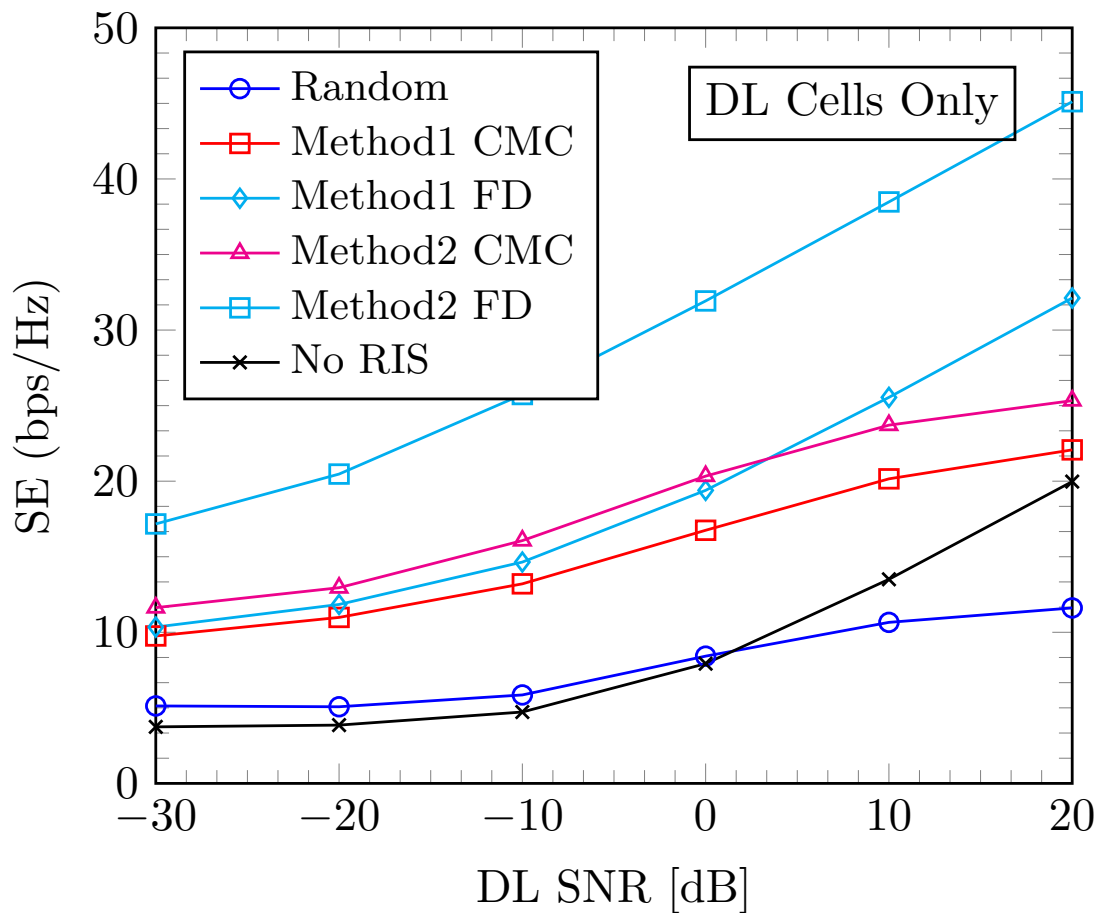
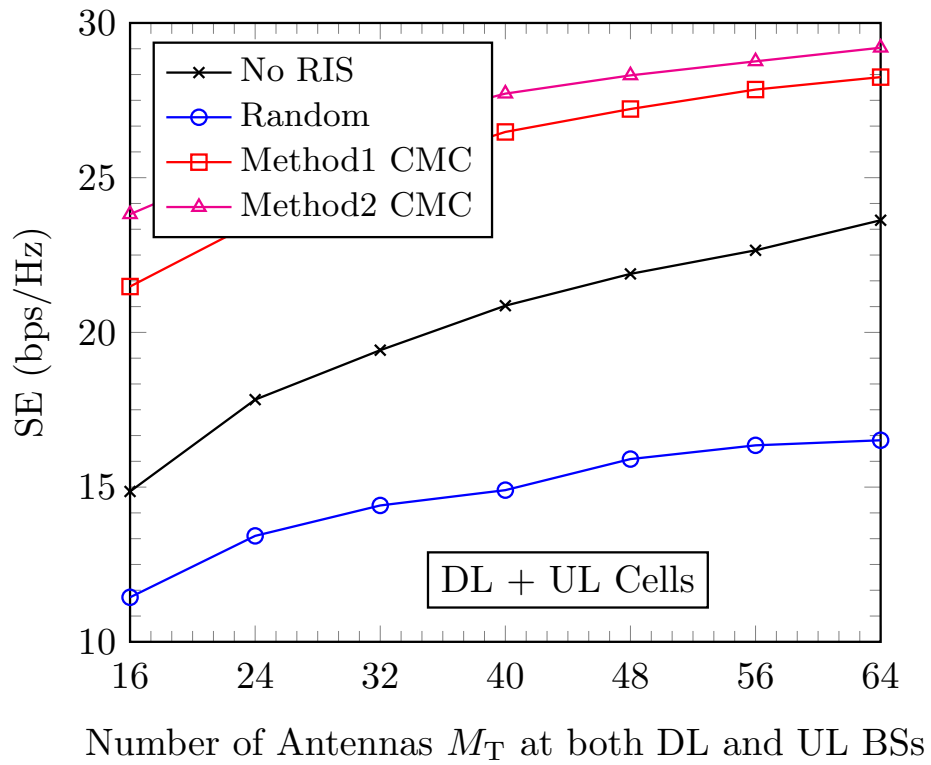
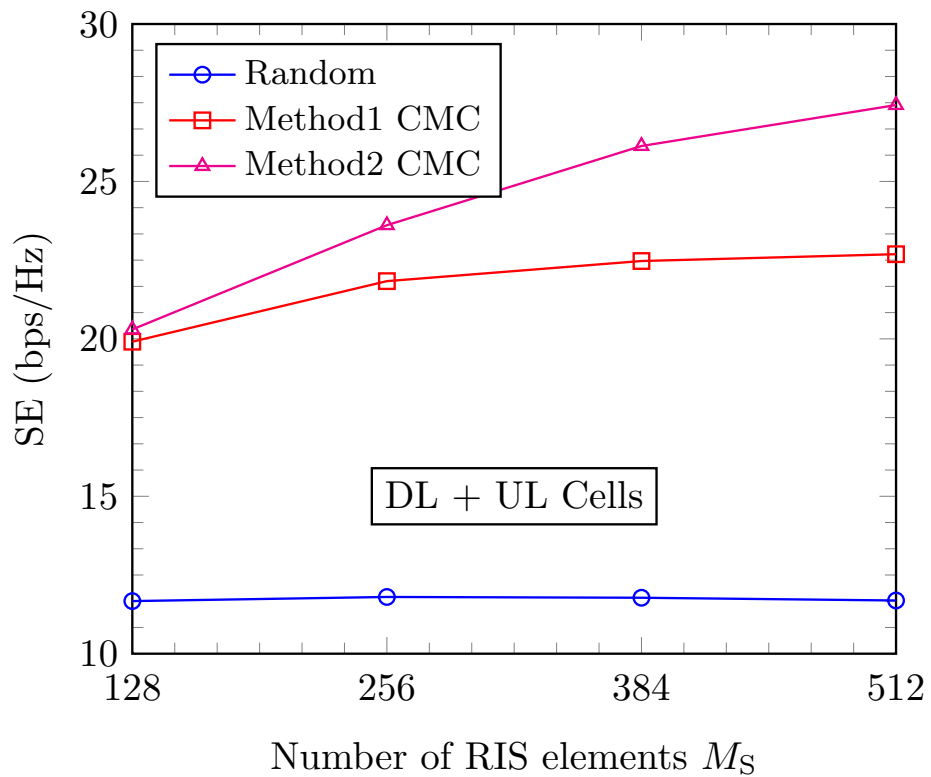


Fig. 3.5: SE versus DL SNR, (DL+UL) assuming  $M_S = 256$  and  $M_T = 16$ .

is higher in the UL cells, which is as a result of the BS-BS cross-link interference. This cross-link interference is higher compared to the UE-UE cross-link interference due to the high transmitting power of the BSs compared to that of the UE. The results show the benefits of the intelligent spectrum control of the RIS in a DTDD system

Fig. 3.6: SE versus number of antennas  $M_T$  for  $M_S = 252$ Fig. 3.7: SE versus number of RIS elements  $M_S$  for  $M_T = 16$ , assuming DL SNR = 10 dB

with regards to reducing the impact of the cross-links interference thereby improving communication efficiency.

Next, we evaluate the impact of the number of antennas at each of the DL and UL BSs and the number of elements of the RIS on the achievable rate of the DTDD system, considering only the solution that satisfies the CMCs condition. In Fig. 3.6 we observe that Method 2 has a better performance output compared to the other methods as the number of antennas increases. The Random scheme has the worst performance output with the increase in the number of antennas. This shows that the passive beamforming gain of the RIS is advantageous when the reflection coefficient vector of the RIS is designed to achieve a certain design function. If not, the RIS will act as an additional source of interference in the system.

Equally, we see that the performance advantage of Method 2 compared to the other methods increases as the number of the RIS elements  $M_S$  increases in Fig. 3.7. Similarly, the performance of the Random scheme does not improve with an increase in the number of elements of the RIS, which supports the fact that there is little passive beamforming gain derivable with the random phase shift implementation for the RIS.

We note that the proposed solutions are heuristic and lead to sub-optimal solutions with reduced complexity. Therefore, there is still the need to carry out further research to develop and implement a solution that will result in a better solution, equally, there is a need to carry out a performance complexity analysis of such a solution to discover the trade-off between the better solution and the complexity involved. Furthermore, additional research is required in order to extend the proposed methods in this chapter to a wideband system.

### 3.9 Chapter Conclusions

In this chapter, we have considered the transmit and passive beamforming design problem in an RIS-aided DTDD wireless network to maximize the system's spectral efficiency. We have proposed centralized low-complexity and non-iterative solutions for the design of the RIS reflection coefficient vector. We have assumed that the channels are perfectly known at the BSs through the CPU. The effect of channel estimation errors will be considered in Chapter 6 of this thesis. The provided simulation results have shown that the integration of RISs in DTDD systems has a great potential in improving communication spectral efficiency by providing alternative and extra communication links, while at the same time reducing the impact of the cross-link BS-to-BS interference.

## 4. AN ADMM APPROACH FOR DISTRIBUTED COORDINATED BEAMFORMING FOR RIS-AIDED DTDD SYSTEMS

In Chapter 3 RIS-aided DTDD systems have been proposed as a solution to meet the traffic fluctuations of small cells and to tune the wireless propagation channels in real-time. In this chapter, we focus on reducing the high signaling overhead involved in the collection of all the channel state information (CSI) at the CPU for an RIS-aided DTDD system. This signaling overhead makes the implementation of the centralized approach presented in Chapter 3 to be impractical. We propose a decentralized coordinated beamforming based on the alternating direction method of multipliers (ADMM). Our numerical results demonstrate that the distributed algorithm converges to the centralized solution after a few iterations. Equally, the distributed solution has a lower signaling overhead compared to the centralized solution.

### 4.1 Introduction

Due to the rapid advancement in technology and the emergence of diverse mobile applications, there is a massive increase in mobile data traffic generation and demand for higher data rates for B5G wireless communication systems. The deployment of small cell networks has emerged as an effective way to meet the exponential growth of traffic demands for 5G and future wireless networks [119]. In a TDD system, the BSs alternate time periods when they receive signals from their served users on the UL, or transmit to users on the DL. However, in advanced long-term evolution (A-LTE) networks, a fixed configuration of the TDD periods is used, to be chosen among a given set. In the new radio (NR) standard for 5G networks, this rigid scheme is broken, and DTDD [24] enables cells to independently set the UL/DL configuration in each slot. DTDD has been proposed as a solution to satisfy the asymmetric and dynamic traffic demand of small cells [25]. In a DTDD-enabled wireless communication

system, each cell individually decides its schedule for the uplink and downlink mode operation across different time slots, based on its instantaneous traffic demand and/or interference status [120].

However, the main challenge brought by DTDD is the cross-link interference issue, because adjacent cells may use at a given time different TDD frame configurations according to traffic needs, thereby giving rise to opposite transmission directions among neighboring cells. There are two kinds of cross-link interference: base station-to-base station (BS-to-BS) and user equipment-to-user equipment (UE-to-UE) interference, which may degrade the system performance significantly. Between the two, the BS-to-BS interference is extremely detrimental due to the large transmit power and LOS propagation characteristics. Some techniques have been proposed to mitigate cross-link interference, including clustering schemes, power control solutions, and time slot allocation algorithms. In [27], a cell clustering scheme was proposed by grouping a number of cells into a cluster according to some metric(s), where cells in the same cluster adopt the same TDD configuration. In [28], the authors proposed dynamic time slot allocation for an adaptive and flexible interference avoidance scheme. The work in [29] used adaptive power control techniques to reduce and compensate for cross-link interference. However, these solutions do not benefit from multi-antenna capabilities in order to mitigate interference. In the case of MIMO systems, Jayasinghe et al.[30] proposed a solution for the maximization of the weighted sum rate. The work in [31] proposed an interference alignment-based solution for a limited scenario formed by three cells and one user per cell.

Interference management strategies in DTDD systems are more complicated than those in static TDD systems due to the cross-link interference. Therefore, there is a need to develop an efficient cross-link interference management scheme.

RISs have gained significant attention recently, as a low-cost and compact transformational technology for future wireless systems [32–34]. In a passive RIS-aided communication system, where the RIS has no radio-frequency chains, the phase shifts of the RIS elements can be adjusted to meet a certain cost function, e.g., the reflected signals add constructively at the intended users and/or destructively at the unintended users. In Chapter 3 and [41], we demonstrated that the intelligent spectrum control of the RIS can be exploited for interference management in an RIS-aided DTDD system. However, such an implementation may be impractical as a result of the high signaling overhead involved in the collection of all the channel state information at the CPU. To address this issue, we propose a distributed algorithm using the ADMM [128] technique for RIS-aided DTDD wireless networks. ADMM is a powerful decomposition technique that blends the superior convergence properties of dual decomposition and

the numerical robustness of augmented Lagrangian methods [128].

## 4.2 Chapter Contributions and Organization

Motivated by the intelligent spectrum control of a DTDD system by the RIS, this chapter proposes an alternating optimization (AO) based algorithm for the design of the transmit beamforming vectors and passive reflection coefficients for an RIS-aided DTDD system. The design objective is to maximize the minimum SINR of the DL users while satisfying the total power constraint of the DL BSs and guaranteeing that the maximum interference seen by the UL users due to the transmission of the DL cells is below a pre-defined level. First, for a given RIS reflection vector a centralized algorithm is proposed for the design of the transmit beamforming vectors according to [129]. Then, we propose a distributed algorithm for the design of the transmit beamforming vectors based on ADMM [128] that can be implemented in a distributed manner at each DL BS with a reasonable amount of information exchange between the coupled DL BSs.

Next, with the designed beamforming vectors, we adopt the SDP technique for the design of the passive reflection coefficients of the RIS. We consider the discrete phase-shift model for the RIS. Moreover, we assume that the directions of the small cells have been optimized *a priori*, e.g., using the proposed cell reconfiguration method in [122], and are known at the CPU. The concept of an ADMM approach for distributed coordinated beamforming for RIS-aided DTDD systems presented in this chapter has been published in [42].

The rest of the chapter is organized as follows. The system model is presented in Section 4.3, while the maximization of the minimum SINR problem is formulated in Section 4.4. In Section 4.5 the proposed distributed approach for the design of the transmit beamforming vectors of the DL BSs is presented, and the design of the RIS reflection vector is considered in Section 4.6. Backhaul signaling and a per-BS complexity analysis are considered in Section 4.7, while our numerical results and chapter conclusions are presented in Sections 4.8 and 4.9, respectively.

## 4.3 System Model

In this chapter, we consider an RIS-aided mmWave DTDD system consisting of  $Q$  small cells, where each cell has a BS with a ULA of  $M_T$  antennas serving  $K$  single antenna UEs. We assume that the communication is aided by an RIS with  $M_S$  passive

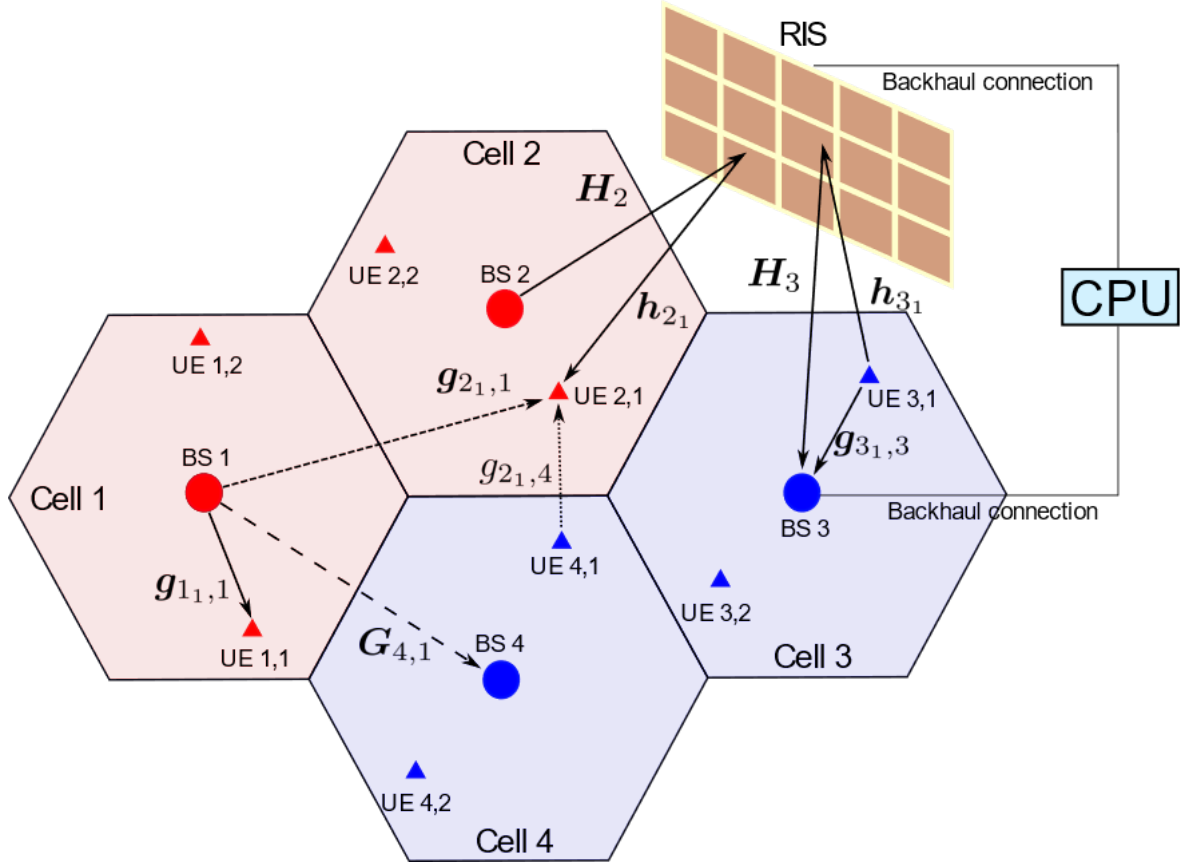


Fig. 4.1: An RIS-aided DTDD system comprising  $Q = 4$  cells.

reflecting elements uniformly arranged on a rectangular surface. The RIS has  $M^h$  and  $M^v$  elements in the horizontal and vertical directions, respectively, as shown in Fig. 3.3. Therefore,  $M_S = M^h \cdot M^v$ . The BSs and the RIS are controlled by a CPU via backhaul connections as illustrated in Fig. 4.1. Let  $\mathcal{Q} \triangleq \{1, \dots, Q\}$  and  $\mathcal{K} \triangleq \{\mathcal{K}_1, \dots, \mathcal{K}_Q\}$  denote the set of all BSs (cells) and UEs, respectively, whereas  $\mathcal{K}_q$  denotes the set of UEs served by the  $q$ th BS. At the considered time instant, we assume that there are  $|\mathcal{Q}^{\text{ul}}|$  cells operating in the UL direction and  $|\mathcal{Q}^{\text{dl}}|$  cells operating in the DL direction, such that  $|\mathcal{Q}^{\text{ul}}| + |\mathcal{Q}^{\text{dl}}| = Q$  and  $\mathcal{Q}^{\text{ul}} \cap \mathcal{Q}^{\text{dl}} = \emptyset$ . Equally, we assume that there are  $|\mathcal{K}^{\text{ul}}|$  and  $|\mathcal{K}^{\text{dl}}|$  UEs in the UL and DL direction, respectively, such that  $|\mathcal{K}^{\text{ul}}| + |\mathcal{K}^{\text{dl}}| = QK$  and  $\mathcal{K}^{\text{ul}} \cap \mathcal{K}^{\text{dl}} = \emptyset$ . Note that  $|\mathcal{X}|$  denote the cardinality of set  $\mathcal{X}$ , i.e., the number of elements in set  $\mathcal{X}$ .

Let  $\mathbf{H}_q \in \mathbb{C}^{M_S \times M_T}$  be the channel matrix from the  $q$ th DL BS,  $q \in \mathcal{Q}^{\text{dl}}$ , to the RIS,  $\mathbf{h}_{qk} \in \mathbb{C}^{M_S}$  be the channel vector from the RIS to the  $k$ th UE in the  $q$ th DL cell,  $q \in \mathcal{Q}^{\text{dl}}$ . Equally, let  $\mathbf{G}_{r,q} \in \mathbb{C}^{M_T \times M_T}$  be the channel matrix from the  $q$ th DL BS,  $q \in \mathcal{Q}^{\text{dl}}$ , to the  $r$ th UL BS,  $r \in \mathcal{Q}^{\text{ul}}$ . Furthermore,  $\mathbf{g}_{qk,q} \in \mathbb{C}^{M_T}$  is the channel vector from the  $q$ th BS,  $q \in \mathcal{Q}^{\text{dl}}$ , to the  $k$ th UE in  $q$ th DL cell, and  $g_{qk,rj} \in \mathbb{C}$  is the channel scalar from the  $j$ th UE in the  $r$ th UL cell,  $r \in \mathcal{Q}^{\text{ul}}$ , to the  $k$ th UE in the  $q$ th DL cell,

$q \in \mathcal{Q}^{\text{dl}}$ . Denote  $b$  as the number of quantization bits of the RIS, such that the number of phase levels is  $2^b$ . The resulting discrete phase shifts of the RIS are expressed as

$$\mathcal{F} \triangleq \left\{ 0, \frac{2\pi}{2^b}, 2\frac{2\pi}{2^b}, \dots, (2^b - 1)\frac{2\pi}{2^b} \right\}. \quad (4.1)$$

The SINR of the  $k$ th UE in the  $q$ th DL cell, i.e.,  $q \in \mathcal{Q}^{\text{dl}}$ , can be expressed as

$$\Gamma_{q_k}^{(\text{dl})} = \frac{|(\mathbf{h}_{q_k,q}^{\text{BS-UE}})^{\text{H}} \mathbf{f}_{q_k}|^2}{\sum_{\substack{j \in \mathcal{K}_q^{\text{dl}} \\ j \neq k}} |(\mathbf{h}_{q_k,q}^{\text{BS-UE}})^{\text{H}} \mathbf{f}_{q_j}|^2 + \sum_{\substack{n \in \mathcal{Q}^{\text{dl}} \\ n \neq q}} \sum_{i \in \mathcal{K}_n^{\text{dl}}} |(\mathbf{h}_{q_k,n}^{\text{BS-UE}})^{\text{H}} \mathbf{f}_{n_i}|^2 + \beta_{q_k}}, \quad (4.2)$$

where

$$\mathbf{h}_{q_k,q}^{\text{BS-UE}} = (\mathbf{h}_{q_k}^{\text{H}} \mathbf{\Theta} \mathbf{H}_q + \mathbf{g}_{q_k,q}^{\text{H}})^{\text{H}} \quad (4.3)$$

is the effective BS-UE channel,  $\mathbf{\Theta} = \text{diag}(\boldsymbol{\theta})$  is the RIS reflection diagonal matrix,  $\boldsymbol{\theta} = [X_1 e^{j\phi_1}, \dots, X_{M_S} e^{j\phi_{M_S}}]^{\text{T}} \in \mathbb{C}^{M_S}$ , where  $X_m \in [0, 1]$  and  $\phi_m \in \mathcal{F}$  denote the amplitude and phase shift associated with the  $m$ th element of the RIS, respectively. We assume that  $X_m = 1, \forall m$  in this work to maximize the signal reflection [32]. Also,  $\mathbf{f}_{q_k} \in \mathbb{C}^{M_T}$  is the transmit precoding vector with  $\|\mathbf{f}_{q_k}\|_2^2 = p_{q_k}^{\text{dl}}$ . Additionally,  $\beta_{q_k} = \alpha_{q_k} + \sigma_{q_k}^2$ , where

$$\alpha_{q_k} = \sum_{r \in \mathcal{Q}^{\text{ul}}} \sum_{j \in \mathcal{K}_r^{\text{ul}}} |h_{q_k,r_j}^{\text{UE-UE}}|^2 p_{r_j}^{\text{ul}}, \quad (4.4)$$

is the cross-link interference from the UL UEs, whereas,  $h_{q_k,r_j}^{\text{UE-UE}} = \mathbf{h}_{q_k}^{\text{H}} \mathbf{\Theta} \mathbf{h}_{r_j} + g_{q_k,r_j}$  and  $\sigma_{q_k}^2$  is noise variance. We assume that  $\alpha_{q_k}$  is known at the  $q$ th DL BS.

Furthermore, the total received BS-BS interference power at the  $r$ th UL BS, i.e.,  $r \in \mathcal{Q}^{\text{ul}}$ , from the DL BSs, can be expressed as

$$\text{IP}_r = \sum_{\forall q \in \mathcal{Q}^{\text{dl}}} \sum_{k \in \mathcal{K}_q^{\text{dl}}} \|\mathbf{H}_{r,q}^{\text{BS-BS}} \mathbf{f}_{q_k}\|^2, \quad (4.5)$$

where

$$\mathbf{H}_{r,q}^{\text{BS-BS}} = \mathbf{H}_r^{\text{H}} \mathbf{\Theta} \mathbf{H}_q + \mathbf{G}_{r,q}, \quad (4.6)$$

is the effective BS-BS channel.

In this chapter, we assume that the above-defined channels are estimated in advance,

e.g., by using the approach in [37].

## 4.4 Problem Formulation

In this chapter, we jointly optimize the passive reflection vector  $\boldsymbol{\theta}$  of the RIS and the active transmit beamforming vectors  $\mathbf{f}_{qk}$ ,  $\forall k \in \mathcal{K}_q^{\text{dl}}, \forall q \in \mathcal{Q}^{\text{dl}}$ , of the DL BSs to improve the communication performance. To provide fairness among the DL UEs, we consider the maximization of the minimum SINR of the DL UEs subject to per BS power constraints and the condition that the maximum interference received by each UL cell is less than a QoS imposed threshold  $\tau_r$ . Moreover, we assume the constant modulus constraints (CMCs) for the RIS reflection coefficients as given in (4.7d). Hence, the system-wide optimization problem is given as

$$\max_{\mathbf{f}, \boldsymbol{\theta}} \min_{q_k} \Gamma_{q_k}^{(\text{dl})} \quad (4.7a)$$

$$\text{s.t.} \quad \sum_{k \in \mathcal{K}_q^{\text{dl}}} \|\mathbf{f}_{qk}\|_2^2 \leq p_q^{\text{dl}}, \forall q \in \mathcal{Q}^{\text{dl}} \quad (4.7b)$$

$$\sum_{\forall q \in \mathcal{Q}^{\text{dl}}} \sum_{k \in \mathcal{K}_q^{\text{dl}}} \|\mathbf{H}_{r,q}^{\text{BS-BS}} \mathbf{f}_{qk}\|^2 \leq \tau_r, \forall r \in \mathcal{Q}^{\text{ul}} \quad (4.7c)$$

$$|[\boldsymbol{\theta}]_m|^2 = 1, \quad m = 1, \dots, M_S, \quad (4.7d)$$

$$\phi_m \in \mathcal{F}, \quad (4.7e)$$

where  $p_q^{\text{dl}}$  is the maximum transmit power allowed for  $q$ th DL BS and  $\tau_r$  is the predefined interference threshold to guarantee a certain QoS of the UL cells. Problem (4.7) is non-convex due to its joint optimization of the optimization variables  $(\mathbf{f}_{qk}, \boldsymbol{\theta})$ , the CMCs in (4.7d) and the constraint in (4.7e). Therefore, we adopt the AO framework to decouple and simplify the design of the transmit beamforming vectors and the passive RIS reflection vector. In the following using the AO approach, we update the active transmit beamforming vectors and the passive RIS reflection vector sequentially.

## 4.5 Transmit Beamforming Design

For a given  $\boldsymbol{\theta}$ , we design the transmit beamforming vectors  $\mathbf{f}_{qk}$ ,  $\forall k \in \mathcal{K}_q^{\text{dl}}, \forall q \in \mathcal{Q}^{\text{dl}}$ , as the solution to the problem given as

$$\max_{\mathbf{f}, \boldsymbol{\theta}} \min_{q_k} \Gamma_{q_k}^{(\text{dl})} \quad (4.8a)$$

$$\text{s.t.} \quad \sum_{k \in \mathcal{K}_q^{\text{dl}}} \|\mathbf{f}_{qk}\|_2^2 \leq p_q^{\text{dl}}, \quad \forall q \in \mathcal{Q}^{\text{dl}} \quad (4.8\text{b})$$

$$\sum_{\forall q \in \mathcal{Q}^{\text{dl}}} \sum_{k \in \mathcal{K}_q^{\text{dl}}} \|\mathbf{H}_{r,q}^{\text{BS-BS}} \mathbf{f}_{qk}\|^2 \leq \tau_r, \quad \forall r \in \mathcal{Q}^{\text{ul}}. \quad (4.8\text{c})$$

Problem (4.8) can be recast in the epigraph form (explained in Appendix C.3) as

$$\max_{\mathbf{f}, \varphi} \quad \varphi \quad (4.9\text{a})$$

$$\text{s.t.} \quad \Gamma_{qk}^{(\text{dl})} \geq \varphi \quad (4.9\text{b})$$

$$\sum_{k \in \mathcal{K}_q^{\text{dl}}} \|\mathbf{f}_{qk}\|_2^2 \leq p_q^{\text{dl}}, \quad \forall q \in \mathcal{Q}^{\text{dl}} \quad (4.9\text{c})$$

$$\sum_{\forall q \in \mathcal{Q}^{\text{dl}}} \sum_{k \in \mathcal{K}_q^{\text{dl}}} \|\mathbf{H}_{r,q}^{\text{BS-BS}} \mathbf{f}_{qk}\|^2 \leq \tau_r, \quad \forall r \in \mathcal{Q}^{\text{ul}}, \quad (4.9\text{d})$$

where  $\varphi$  is an auxiliary variable representing the SINR constraint.

### 4.5.1 Centralized Algorithm

A centralized solution to (4.9) can be obtained using the bisection method [129, 130]. The bisection method is used to find the roots of a polynomial function. It bisects the interval and selects a sub-interval within which the root must lie iteratively for further processing. A simple one-dimensional bisection search will efficiently find the required  $\varphi$ . In (4.9), the inequality constraints can be expressed as a generalized inequality with respect to the second-order cone program (SOCP) and can be solved using any SOCP solver [131, 132]. The key step in solving problem (4.9) in a centralized manner is to solve a SOCP which has a high computational cost. Following [129] the centralized approach is summarized in Algorithm 1, where the variables  $\text{SINR}_{\max}$  and  $\text{SINR}_{\min}$  define the range of the relevant SINR values, while  $\lambda \geq 0$  define the desired accuracy of the bisection method.

Specifically, the complexity of solving problem (4.9) in a centralized approach, for example, by using the interior point method (IPM) [131], is  $\mathcal{O}(|\mathcal{Q}^{\text{dl}}| M_{\text{T}}^3 |\mathcal{K}^{\text{dl}}|^3)$  which is an excessively high implementation cost in the case of large networks. Therefore, the centralized solution is impractical as a result of the high signaling overhead involved in the collection of all the channel state information at the CPU. Hence, to reduce the signaling overhead and the workload on the CPU, in the following, we propose a distributed algorithm based on the ADMM approach [128].

**Algorithm 1: Centralized Algorithm**


---

**Data:**  $\varphi_{\min} = \text{SINR}_{\min}, \varphi_{\max} = \text{SINR}_{\max}, \lambda \geq 0$   
**Result:**  $\varphi, \mathbf{f}_{q_k}$ , where  $\mathbf{f}_{q_k}$  is the last feasible solution of (4.9)

- 1 **while**  $|\varphi_{\max} - \varphi_{\min}| \geq \lambda$  **do**
- 2      $\varphi \leftarrow (\varphi_{\max} + \varphi_{\min})/2;$
- 3     With the obtained  $\varphi$  solve the resulting feasibility problem of (4.9);
- 4     **if** *Problem status is feasible for the given  $\varphi$*  **then**
- 5          $\varphi_{\min} \leftarrow \varphi;$
- 6     **else**
- 7          $\varphi_{\max} \leftarrow \varphi;$
- 8     **end**
- 9 **end**

---

### 4.5.2 Distributed Algorithm

#### Review of ADMM

ADMM is a powerful dual decomposition technique that is well suited for distributed constrained optimization problems. One of the major benefits of the ADMM schemes is that it is a powerful decomposition technique that combines the superior convergence properties of the dual decomposition method and the numerical robustness of augmented Lagrangian method. [128]. Therefore, ADMM has been established to be more numerically stable, faster in convergence, and can converge under more general conditions than the dual decomposition method (see Appendix C.3), e.g., without the requirements of strict convexity or finiteness of the objective function [128].

To illustrate the idea of ADMM, let us consider the following convex optimization problem [128, 133],

$$\min_{\mathbf{x} \in \mathbb{R}^n, \mathbf{z} \in \mathbb{R}^m} F(\mathbf{x}) + G(\mathbf{z}) \quad (4.10a)$$

$$\text{s.t. } \mathbf{x} \in \mathcal{S}_1, \mathbf{z} \in \mathcal{S}_2, \quad (4.10b)$$

$$\mathbf{z} = \mathbf{A}\mathbf{x}, \quad (4.10c)$$

where  $F : \mathbb{R}^n \mapsto \mathbb{R}$  and  $G : \mathbb{R}^m \mapsto \mathbb{R}$  are convex functions,  $\mathbf{A}$  is an  $m \times n$  matrix, and  $\mathcal{S}_1 \subset \mathbb{R}^n$  and  $\mathcal{S}_2 \subset \mathbb{R}^m$  are nonempty polyhedral sets (explained in (C.1.6) of Appendix C.1). For simplicity, we have considered a real-valued optimization problem. However, the complex-valued extension is discussed in Appendix C.6. Assume that problem (4.10) is solvable and strong duality holds (see Appendix C.3). ADMM

considers the following penalty-augmented problem

$$\min_{\mathbf{x} \in \mathbb{R}^n, \mathbf{z} \in \mathbb{R}^m} F(\mathbf{x}) + G(\mathbf{z}) + \frac{\rho}{2} \|\mathbf{A}\mathbf{x} - \mathbf{z}\|^2 \quad (4.11a)$$

$$\text{s.t. } \mathbf{x} \in \mathcal{S}_1, \mathbf{z} \in \mathcal{S}_2, \quad (4.11b)$$

$$\mathbf{z} = \mathbf{A}\mathbf{x}, \quad (4.11c)$$

where  $\rho \geq 0$  is the penalty parameter. It is easy to see that (4.11) is essentially equivalent to (4.10) owing to (4.11c). The penalty term  $\frac{\rho}{2} \|\mathbf{A}\mathbf{x} - \mathbf{z}\|^2$  brings strict convexity. Therefore, problem (4.11) is strictly convex with respect to either  $\mathbf{x}$  or  $\mathbf{z}$ .

The augmented Lagrangian of the above problem is given as

$$\mathcal{L}(\mathbf{x}, \mathbf{z}, \boldsymbol{\eta}) = F(\mathbf{x}) + G(\mathbf{z}) + \frac{\rho}{2} \|\mathbf{A}\mathbf{x} - \mathbf{z}\|^2 + \boldsymbol{\eta}^\top (\mathbf{A}\mathbf{x} - \mathbf{z}), \quad (4.12)$$

where  $\boldsymbol{\eta} \in \mathbb{R}^m$  is the dual variable or the Lagrangian multiplier associated with the constraint given in (4.11c). Given a dual variable  $\boldsymbol{\eta}$ , the problem is a convex problem and can be efficiently solved. Specifically, one can solve the following subproblems iteratively,

$$\mathbf{x}^{(i+1)} = \min_{\mathbf{x}} \mathcal{L}(\mathbf{x}, \mathbf{z}^{(i)}, \boldsymbol{\eta}^{(i)}), \quad (4.13a)$$

$$\mathbf{z}^{(i+1)} = \min_{\mathbf{z}} \mathcal{L}(\mathbf{x}^{(i+1)}, \mathbf{z}, \boldsymbol{\eta}^{(i)}), \quad (4.13b)$$

$$\boldsymbol{\eta}^{(i+1)} = \boldsymbol{\eta}^{(i)} + \rho(\mathbf{A}\mathbf{x}^{(i+1)} - \mathbf{z}^{(i+1)}). \quad (4.13c)$$

Here, starting with initial values for  $\mathbf{z}$  and  $\boldsymbol{\eta}$  the variable  $\mathbf{x}$  in (4.13a) is updated. The other variables are updated sequentially, in a similar manner until the stopping criterion is met. From the above, it is noted that the variables  $\mathbf{x}$  and  $\mathbf{z}$  are updated alternately, this accounts for the term alternating direction. ADMM can converge to the global optimum of the problem (4.10), the convergence properties of the ADMM are improved as compared to the dual decomposition method by utilizing the augmented Lagrangian [128]. The steps of the ADMM method [128],[134] are summarized in Algorithm 2.

### Applying ADMM to (4.9)

Applying the above concepts to problem (4.9), one can see that the solution is mainly composed of three iterative steps. The first step is a BS-wise step to update the local primal variables. The second step is a network-wise step to update the global variables. The third step is again a BS-wise step to update the local dual variables. To begin, we

---

**Algorithm 2: ADMM**


---

**Data:**  $\mathbf{A}$ ,  $i = 1, i_{\max}$ ,  $\rho \geq 0$ , and initialize  $\boldsymbol{\eta}^{(i)}$  and  $\mathbf{z}^{(i)}$  randomly  
**Result:**  $\mathbf{x}$ ,  $\boldsymbol{\eta}$ , and  $\mathbf{z}$   
**1 while** *not converged* or  $i < i_{\max}$  **do**  
**2**      $\mathbf{x}^{(i+1)} = \min_{\mathbf{x}} \mathcal{L}(\mathbf{x}, \mathbf{z}^{(i)}, \boldsymbol{\eta}^{(i)});$   
**3**      $\mathbf{z}^{(i+1)} = \min_{\mathbf{z}} \mathcal{L}(\mathbf{x}^{(i+1)}, \mathbf{z}, \boldsymbol{\eta}^{(i)});$   
**4**      $\boldsymbol{\eta}^{(i+1)} = \boldsymbol{\eta}^{(i)} + \rho(\mathbf{A}\mathbf{x}^{(i+1)} - \mathbf{z}^{(i+1)});$   
**5 end**

---

introduce slack variables which represent the local copies of the variables that couple all the DL BSs. The resulting equivalent problem is expressed as

$$\min -\varphi \quad (4.14a)$$

$$\text{s.t. } \tilde{\Gamma}_{qk}^{(\text{dl})} \geq \gamma_q \quad (4.14b)$$

$$\lambda_{n_j,q}^2 \geq \sum_{k \in \mathcal{K}_q^{\text{dl}}} |(\mathbf{h}_{n_j,q}^{\text{BS-UE}})^H \mathbf{f}_{qk}|^2, \forall j \in \mathcal{K}_n^{\text{dl}}, \forall n, q \in \mathcal{Q}^{\text{dl}}, n \neq q \quad (4.14c)$$

$$\phi_{r_j,q}^2 \geq \sum_{k \in \mathcal{K}_q^{\text{dl}}} \|\mathbf{H}_{r_j,q}^{\text{BS-BS}} \mathbf{f}_{qk}\|^2, \forall j \in \mathcal{K}_r^{\text{ul}}, \forall q \in \mathcal{Q}^{\text{dl}} \quad (4.14d)$$

$$\sum_{k \in \mathcal{K}_q^{\text{dl}}} \|\mathbf{H}_{r_j,q}^{\text{BS-BS}} \mathbf{f}_{qk}\|^2 + \sum_{\forall n \in \mathcal{Q}^{\text{dl}}, n \neq q} \bar{\phi}_{r_j,n}^2 \leq \tau_r, \forall r \in \mathcal{Q}^{\text{ul}} \quad (4.14e)$$

$$\sum_{k \in \mathcal{K}_q^{\text{dl}}} \|\mathbf{f}_{qk}\|_2^2 \leq p_q^{\text{dl}}, \forall q \in \mathcal{Q}^{\text{dl}} \quad (4.14f)$$

$$\lambda_{qk,n} = \mu_{qk,n}, \quad (4.14g)$$

$$\lambda_{n_j,q} = \mu_{n_j,q}, \forall j \in \mathcal{K}_n^{\text{dl}}, \forall n, q \in \mathcal{Q}^{\text{dl}}, n \neq q \quad (4.14h)$$

$$\phi_{r_j,q} = \psi_{r_j,q}, \forall j \in \mathcal{K}_r^{\text{ul}}, \forall q \in \mathcal{Q}^{\text{dl}} \quad (4.14i)$$

$$\phi_{r_j,n} = \psi_{r_j,n}, \forall j \in \mathcal{K}_r^{\text{ul}}, \forall n \in \mathcal{Q}^{\text{dl}} \quad (4.14j)$$

$$\gamma_q = \varphi, \quad (4.14k)$$

where

$$\tilde{\Gamma}_{qk}^{(\text{dl})} = \frac{|(\mathbf{h}_{qk,q}^{\text{BS-UE}})^H \mathbf{f}_{qk}|^2}{\sum_{j \in \mathcal{K}_q^{\text{dl}}, j \neq k} |(\mathbf{h}_{qk,q}^{\text{BS-UE}})^H \mathbf{f}_{qj}|^2 + \sum_{n \in \mathcal{Q}^{\text{dl}}, n \neq q} \lambda_{qk,n}^2 + \beta_{qk}},$$

and  $\gamma_q$ ,  $\lambda_{n_j,q}$ ,  $\lambda_{qk,n}$ ,  $\phi_{r_j,q}$ , and  $\phi_{r_j,n}$  are the newly introduced slack variables representing the local copies of the SINR variable, the interference generated by the BS in the  $q$ th DL cell to the  $j$ th UE in the  $n$ th DL cell, the interference at user  $q_k$  generated by the neighboring DL BSs  $n$  ( $n \neq q$ ), and the UL interference variable from the  $q$ th

and  $n$ th DL BSs, respectively. Furthermore,  $\varphi$ ,  $\mu_{qk,n}$ ,  $\mu_{n_j,q}$ ,  $\psi_{r_j,q}$ , and  $\psi_{r_j,n}$  are the respective global copies to satisfy equivalence between (4.9) and (4.14).

Next, for convenience, we include all the constraints that can be handled locally at the  $q$ th DL BS in the set  $\mathcal{W}_q$  which is defined as

$$\mathcal{W}_q = \left\{ \mathbf{F}_q, \boldsymbol{\lambda}_q, \boldsymbol{\phi}_q, \gamma_q \mid \tilde{\Gamma}_{qk}^{(\text{dl})} \geq \gamma_q, \sum_{k \in \mathcal{K}_q^{\text{dl}}} \|\mathbf{f}_{qk}\|_2^2 \leq p_q^{\text{dl}}, \phi_{r_j,q}^2 \geq \sum_{k \in \mathcal{K}_q^{\text{dl}}} \|\mathbf{H}_{r_j,q}^{\text{BS-BS}} \mathbf{f}_{qk}\|^2, \right. \\ \left. \lambda_{n_j,q}^2 \geq \sum_{k \in \mathcal{K}_q^{\text{dl}}} |(\mathbf{h}_{q,n_j}^{\text{BS-UE}})^H \mathbf{f}_{qk}|^2 \sum_{k \in \mathcal{K}_q^{\text{dl}}} \|\mathbf{H}_{r_j,q}^{\text{BS-BS}} \mathbf{f}_{qk}\|^2 + \sum_{\forall n \in \mathcal{Q}^{\text{dl}}, n \neq q} \bar{\phi}_{r_j,n}^2 \leq \tau_r \right\}. \quad (4.15)$$

Therefore, problem (4.14) can be compactly written as

$$\min_{\mathbf{F}_q, \boldsymbol{\lambda}_q, \boldsymbol{\phi}_q, \gamma_q, \varphi} - \varphi \quad (4.16a)$$

$$\text{s.t. } \{\mathbf{F}_q, \boldsymbol{\lambda}_q, \boldsymbol{\phi}_q, \gamma_q\} \in \mathcal{W}_q, \forall q \in \mathcal{Q}^{\text{dl}} \quad (4.16b)$$

$$\boldsymbol{\lambda}_q = \boldsymbol{\mu}_q, \forall q \in \mathcal{Q}^{\text{dl}}, \quad (4.16c)$$

$$\boldsymbol{\phi}_q = \boldsymbol{\psi}_q, \forall q \in \mathcal{Q}^{\text{dl}}, \quad (4.16d)$$

$$\gamma_q = \varphi, \forall q \in \mathcal{Q}^{\text{dl}}, \quad (4.16e)$$

where

$$\mathbf{F}_q = [\mathbf{f}_{q1}, \mathbf{f}_{q2}, \dots, \mathbf{f}_{q|\mathcal{K}_q^{\text{dl}}|}] \in \mathbb{C}^{M_T \times |\mathcal{K}_q^{\text{dl}}|} \quad (4.17)$$

$$\boldsymbol{\lambda}_q = [\{\lambda_{n_j,q}\}_{j \in \mathcal{K}_n^{\text{dl}}, n \in \bar{\mathcal{Q}}_q^{\text{dl}}}, \{\lambda_{qk,n}\}_{k \in \mathcal{K}_q^{\text{dl}}, n \in \bar{\mathcal{Q}}_q^{\text{dl}}}]^T \in \mathbb{C}^{a \times 1} \quad (4.18)$$

$$\boldsymbol{\mu}_q = [\{\mu_{n_j,q}\}_{j \in \mathcal{K}_n^{\text{dl}}, n \in \bar{\mathcal{Q}}_q^{\text{dl}}}, \{\mu_{qk,n}\}_{k \in \mathcal{K}_q^{\text{dl}}, n \in \bar{\mathcal{Q}}_q^{\text{dl}}}]^T \in \mathbb{C}^{a \times 1} \quad (4.19)$$

$$\boldsymbol{\phi}_q = [\{\phi_{r_j,q}\}_{j \in \mathcal{K}_r^{\text{ul}}, r \in \mathcal{Q}^{\text{ul}}, q \in \mathcal{Q}^{\text{dl}}}]^T \in \mathbb{C}^{b \times 1} \quad (4.20)$$

$$\boldsymbol{\psi}_q = [\{\psi_{r_j,q}\}_{j \in \mathcal{K}_r^{\text{ul}}, r \in \mathcal{Q}^{\text{ul}}, q \in \mathcal{Q}^{\text{dl}}}]^T \in \mathbb{C}^{b \times 1}, \quad (4.21)$$

$\mathbf{F}_q$  is the matrix that contains all the transmit beamforming vectors for all the UEs in the  $q$ th DL cell in its columns. Furthermore,  $\boldsymbol{\lambda}_q$  and  $\boldsymbol{\mu}_q$  are the transmitter-specific interference and consistency vectors, respectively; while the vectors  $\boldsymbol{\phi}_q$ , and  $\boldsymbol{\psi}_q$  are the transmitter-specific UL interference and consistency vectors, and  $\bar{\mathcal{Q}}_q^{\text{dl}} \triangleq \mathcal{Q}^{\text{dl}} \setminus q$ , i.e.,  $\bar{\mathcal{Q}}_q^{\text{dl}}$ , is the set including indices of all other DL BSs excluding the  $q$ th DL BS. The variables  $a$  and  $b$  are given as  $a = (|\mathcal{K}_q^{\text{dl}}| - 1) + (|\mathcal{Q}^{\text{dl}}|)(|\mathcal{K}_q^{\text{dl}}|)$  and  $b = (|\mathcal{Q}^{\text{ul}}|)(|\mathcal{K}_r^{\text{ul}}|)$ , respectively. Note that the consistency vectors are the vectors that satisfy equivalence

between (4.9) and (4.14). Furthermore, we define  $I_q(\mathbf{F}_q, \boldsymbol{\lambda}_q, \boldsymbol{\phi}_q, \gamma_q)$  as an indicator function given as

$$I_q(\mathbf{F}_q, \boldsymbol{\lambda}_q, \boldsymbol{\phi}_q, \gamma_q) = \begin{cases} 0, & (\mathbf{F}_q, \boldsymbol{\lambda}_q, \boldsymbol{\phi}_q, \gamma_q) \in \mathcal{W}_q \\ \infty, & \text{otherwise} \end{cases}. \quad (4.22)$$

It can easily be verified that  $\sum_{q \in \mathcal{Q}^{\text{dl}}} \gamma_q = |\mathcal{Q}^{\text{dl}}| \varphi$ . Therefore, problem (4.16) can be expressed equivalently as

$$\min_{\mathbf{F}_q, \boldsymbol{\lambda}_q, \boldsymbol{\phi}_q, \gamma_q, \varphi} \sum_{q \in \mathcal{Q}^{\text{dl}}} \left( -\frac{\gamma_q}{|\mathcal{Q}^{\text{dl}}|} + I_q(\mathbf{F}_q, \boldsymbol{\lambda}_q, \boldsymbol{\phi}_q, \gamma_q) \right) \quad (4.23a)$$

$$\text{s.t. } \boldsymbol{\lambda}_q = \boldsymbol{\mu}_q, \quad \forall q \in \mathcal{Q}^{\text{dl}} \quad (4.23b)$$

$$\boldsymbol{\phi}_q = \boldsymbol{\psi}_q, \quad \forall q \in \mathcal{Q}^{\text{dl}} \quad (4.23c)$$

$$\gamma_q = \varphi, \quad \forall q \in \mathcal{Q}^{\text{dl}}, \quad (4.23d)$$

According to the ADMM concept, we first form the augmented Lagrangian of (4.23), which is given as

$$\begin{aligned} \mathcal{L}_\rho(\mathbf{F}_q, \boldsymbol{\lambda}_q, \boldsymbol{\phi}_q, \gamma_q, \boldsymbol{\chi}_q, \boldsymbol{\xi}_q, \eta_q, \boldsymbol{\mu}_q, \boldsymbol{\psi}_q, \varphi) = & \\ & \sum_{q \in \mathcal{Q}^{\text{dl}}} \left( -\frac{\gamma_q}{|\mathcal{Q}^{\text{dl}}|} + I_q(\mathbf{F}_q, \boldsymbol{\lambda}_q, \boldsymbol{\phi}_q, \gamma_q) + \frac{\rho}{2} \left| \gamma_q - \varphi + \frac{1}{\rho} \eta_q \right|^2 + \frac{\rho}{2} \left\| \boldsymbol{\lambda}_q - \boldsymbol{\mu}_q + \frac{1}{\rho} \boldsymbol{\chi}_q \right\|_2^2 \right. \\ & \left. + \frac{\rho}{2} \left\| \boldsymbol{\phi}_q - \boldsymbol{\psi}_q + \frac{1}{\rho} \boldsymbol{\xi}_q \right\|_2^2 \right), \end{aligned} \quad (4.24)$$

where  $\rho \geq 0$  is the penalty parameter which helps to achieve numerical stability and faster convergence for the ADMM algorithm [128]. Note that the Lagrangian function (4.24) is completely separable between the DL BSs. Therefore, in the first step of each iteration of the ADMM algorithm, each  $q$  DL BS,  $\forall q \in \mathcal{Q}^{\text{dl}}$ , updates the local variables  $(\mathbf{F}_q^{(t+1)}, \boldsymbol{\lambda}_q^{(t+1)}, \boldsymbol{\phi}_q^{(t+1)}, \gamma_q^{(t+1)})$  by solving the following optimization problem

$$\min_{\mathbf{F}_q, \boldsymbol{\lambda}_q, \boldsymbol{\phi}_q, \gamma_q} -\frac{\gamma_q}{|\mathcal{Q}^{\text{dl}}|} + \frac{\rho}{2} \left| \gamma_q - \varphi^{(t)} + \frac{1}{\rho} \eta_q^{(t)} \right|^2 + \frac{\rho}{2} \varkappa_q(\boldsymbol{\lambda}_q, \boldsymbol{\phi}_q) \quad (4.25a)$$

$$\text{s.t. } \{\mathbf{F}_q, \boldsymbol{\lambda}_q, \boldsymbol{\phi}_q, \gamma_q\} \in \mathcal{W}_q, \quad (4.25b)$$

where the function  $\varkappa_q(\boldsymbol{\lambda}_q, \boldsymbol{\phi}_q)$  is defined as

$$\varkappa_q(\boldsymbol{\lambda}_q, \boldsymbol{\phi}_q) = \frac{\rho}{2} \left\| \boldsymbol{\lambda}_q - \boldsymbol{\mu}_q^{(t)} + \frac{1}{\rho} \boldsymbol{\chi}_q^{(t)} \right\|_2^2 + \frac{\rho}{2} \left\| \boldsymbol{\phi}_q - \boldsymbol{\psi}_q^{(t)} + \frac{1}{\rho} \boldsymbol{\xi}_q^{(t)} \right\|_2^2.$$

Problem (4.25) is non-convex due to the non-convex SINR constraint in the set  $\mathcal{W}_q$ .

However, for a fixed  $\gamma_q$ , the problem can be recast as a SOCP problem (explained in Appendix C.4), which can easily be solved by the CVX tool [135]. According to [136, Algorithm 2], we obtain the optimal  $\gamma_q^*$  used in solving for the other local variables of (4.25).

Next, the augmented Lagrangian function (4.24) is minimized over the global variables  $\boldsymbol{\mu}_q$ ,  $\boldsymbol{\psi}_q$ , and  $\varphi$  while all the other variables are fixed at their current values. This can be expressed as

$$\min_{\boldsymbol{\mu}_q, \boldsymbol{\psi}_q, \varphi} \sum_{q \in \mathcal{Q}^{\text{dl}}} \left( \frac{\rho}{2} \left| \gamma_q^{(t+1)} - \varphi + \frac{1}{\rho} \eta_q^{(t)} \right|^2 + \frac{\rho}{2} \left\| \boldsymbol{\lambda}_q^{(t+1)} - \boldsymbol{\mu}_q + \frac{1}{\rho} \boldsymbol{\chi}_q^{(t)} \right\|_2^2 \right. \quad (4.26a)$$

$$\left. + \frac{\rho}{2} \left\| \boldsymbol{\phi}_q^{(t+1)} - \boldsymbol{\psi}_q + \frac{1}{\rho} \boldsymbol{\xi}_q^{(t)} \right\|_2^2 \right). \quad (4.26b)$$

The problem in (4.26) is convex and separable in  $\{\boldsymbol{\mu}_q, \boldsymbol{\psi}_q\}_{q \in \mathcal{Q}^{\text{dl}}}$  and  $\varphi$  which are the optimization variables. Therefore, by setting the gradient of the cost function in (4.26) to zero with respect to the optimization variables, the global variables are updated as follows

$$\mu_{n_j, q}^{(t+1)} = \frac{1}{2} \left( \lambda_{n_j, q}^{(t+1)} + \bar{\lambda}_{q_k, n}^{(t+1)} \right), \quad (4.27a)$$

$$\psi_{r_j, q}^{(t+1)} = \frac{1}{|\mathcal{Q}^{\text{dl}}|} \left( \sum_{q \in \mathcal{Q}^{\text{dl}}} \left( \phi_{r_j, q}^{(t+1)} + \frac{1}{\rho} \xi_q^{(t)} \right) \right), \quad (4.27b)$$

$$\varphi^{(t+1)} = \frac{1}{|\mathcal{Q}^{\text{dl}}|} \left( \sum_{q \in \mathcal{Q}^{\text{dl}}} \left( \gamma_q^{(t+1)} + \frac{1}{\rho} \eta_q^{(t)} \right) \right). \quad (4.27c)$$

Note that (4.27) is updated after the DL BSs have exchanged their respective local variables.

Finally, each  $q$  DL BS,  $\forall q \in \mathcal{Q}^{\text{dl}}$ , updates the dual variables associated with the equality constraints as

$$\boldsymbol{\chi}_q^{(t+1)} = \boldsymbol{\chi}_q^{(t)} + \rho \left( \boldsymbol{\lambda}_q^{(t+1)} - \boldsymbol{\mu}_q^{(t+1)} \right), \quad (4.28)$$

$$\boldsymbol{\xi}_q^{(t+1)} = \boldsymbol{\xi}_q^{(t)} + \rho \left( \boldsymbol{\phi}_q^{(t+1)} - \boldsymbol{\psi}_q^{(t+1)} \right), \quad (4.29)$$

$$\eta_q^{(t+1)} = \eta_q^{(t)} + \rho \left( \gamma_q^{(t+1)} - \varphi^{(t+1)} \right). \quad (4.30)$$

We remark that the convergence of the ADMM scheme for convex problems has been established in [128, 137, 138] for non-convex problems.

## 4.6 RIS Reflection Matrix Design

With the obtained solution of problem (4.14), the second sub-problem of (4.9) becomes a feasibility check problem for finding the diagonal RIS phase shift matrix  $\Theta = \text{diag}\{\boldsymbol{\theta}\} \in \mathbb{C}^{M_S \times M_S}$ , with fixed  $\mathbf{F}_q$ ,  $q \in \mathcal{Q}^{\text{dl}}$ , and  $\varphi$ . Note that  $\mathbf{F}_q$  is the matrix that contains all the transmit beamforming vectors for all the UEs in the  $q$ th DL cell in its columns as given in (4.17). The feasibility check problem can be written as

$$\text{Find } \boldsymbol{\theta} \quad (4.31\text{a})$$

$$\text{s.t. } \Gamma_{q_k}^{(\text{dl})} \geq \varphi, \forall q \in \mathcal{Q}^{\text{dl}} \quad (4.31\text{b})$$

$$\sum_{\forall q \in \mathcal{Q}^{\text{dl}}} \sum_{k \in \mathcal{K}_q^{\text{dl}}} \|\mathbf{H}_{r,q}^{\text{BS-BS}} \mathbf{f}_{q_k}\|^2 \leq \tau_r \quad \forall r \in \mathcal{Q}^{\text{ul}} \quad (4.31\text{c})$$

$$|[\boldsymbol{\theta}]_m|^2 = 1, \quad m = 1, \dots, M_S, \quad (4.31\text{d})$$

$$\phi_m \in \mathcal{F}, \quad (4.31\text{e})$$

where  $\Gamma_{q_k}^{(\text{dl})}$  is defined in (4.2) as

$$\Gamma_{q_k}^{(\text{dl})} = \frac{|(\mathbf{h}_{q_k,q}^{\text{BS-UE}})^H \mathbf{f}_{q_k}|^2}{\sum_{\substack{j \in \mathcal{K}_q^{\text{dl}} \\ j \neq k}} |(\mathbf{h}_{q_k,q}^{\text{BS-UE}})^H \mathbf{f}_{q_j}|^2 + \sum_{\substack{n \in \mathcal{Q}^{\text{dl}} \\ n \neq q}} \sum_{i \in \mathcal{K}_n^{\text{dl}}} |(\mathbf{h}_{q_k,n}^{\text{BS-UE}})^H \mathbf{f}_{n_i}|^2 + \beta_{q_k}}$$

To extract the RIS reflection coefficient vector  $\boldsymbol{\theta}$  from the RIS-assisted channels in  $\Gamma_{q_k}^{(\text{dl})}$ , we apply a change of variable to  $\Gamma_{q_k}^{(\text{dl})}$ . As a result, the variable  $\Gamma_{q_k}^{(\text{dl})}$  can be expressed as

$$\Gamma_{q_k}^{(\text{dl})} = \frac{|\mathbf{a}_{q_k}^H \boldsymbol{\theta} + b_{q_k}|^2}{\|\mathbf{C}_{q_k} \boldsymbol{\theta} + \mathbf{d}_{q_k}\|^2 + \sigma_{q_k}^2}, \quad (4.32)$$

where

$$\mathbf{a}_{q_k} = \text{diag}(\mathbf{h}_{q_k,q}) \mathbf{H}_q \mathbf{f}_{q_k}, \in \mathbb{C}^{M_S \times 1} \quad (4.33)$$

$$b_{q_k} = \mathbf{g}_{q_k,q}^H \mathbf{f}_{q_k}, \quad (4.34)$$

$$\mathbf{d}_{q_k} = \text{stack}\{u_{q_k}^{\text{INTRA}}, u_{q_k}^{\text{ICI}}, u_{q_k}^{\text{CL}}\}, \in \mathbb{C}^{3 \times 1} \quad (4.35)$$

$$\mathbf{C}_{q_k} = \text{stack}\{(\mathbf{e}_{q_k}^{\text{INTRA}})^H, (\mathbf{e}_{q_k}^{\text{ICI}})^H, (\mathbf{e}_{q_k}^{\text{CL}})^H\} \in \mathbb{C}^{3 \times M_S}, \quad (4.36)$$

$\mathbf{a}_{q_k}$  is the RIS-assisted desired user signal for the  $k$ th UE in the  $q$ th DL cell,  $b_{q_k}$  is the direct desired user signal for the  $k$ th UE in the  $q$ th DL cell. Additionally,

the vector  $\mathbf{d}_{qk}$  is a vector that contains all the direct interference experienced by the  $k$ th UE in the  $q$ th DL cell on top of each other. This interference includes intra-cell interference from other UEs within the same cell, inter-cell interference from other DL cells, and cross-link interference from the UEs operating in the UL direction. Equally,  $\mathbf{C}_{qk}$  contains interference experienced by the  $k$ th UE in the  $q$ th DL cell on top of each other. Furthermore, these direct and RIS-assisted interference are respectively given as

$$u_{qk}^{\text{INTRA}} = \sum_{j \in \mathcal{K}_q^{\text{dl}}, j \neq k} \mathbf{g}_{qk,q}^{\text{H}} \mathbf{f}_{qj}, \quad (4.37a)$$

$$u_{qk}^{\text{ICI}} = \sum_{\substack{n \in \mathcal{Q}^{\text{dl}}, \\ n \neq q}} \sum_{i \in \mathcal{K}_n^{\text{dl}}} \mathbf{g}_{qk,n}^{\text{H}} \mathbf{f}_{ni}, \quad (4.37b)$$

$$u_{qk}^{\text{CL}} = \sum_{r \in \mathcal{Q}^{\text{ul}}} \sum_{j \in \mathcal{K}_r^{\text{ul}}} g_{qk,rj}, \quad (4.37c)$$

$$\mathbf{e}_{qk}^{\text{INTRA}} = \sum_{j \in \mathcal{K}_q^{\text{dl}}, j \neq k} \text{diag}(\mathbf{h}_{qk,q}) \mathbf{H}_q \mathbf{f}_{qj} \in \mathbb{C}^{M_S \times 1} \quad (4.37d)$$

$$\mathbf{e}_{qk}^{\text{ICI}} = \sum_{\substack{n \in \mathcal{Q}^{\text{dl}}, \\ n \neq q}} \sum_{i \in \mathcal{K}_n^{\text{dl}}} \text{diag}(\mathbf{h}_{qk,n}) \mathbf{H}_n \mathbf{f}_{ni} \in \mathbb{C}^{M_S \times 1} \quad (4.37e)$$

$$\mathbf{e}_{qk}^{\text{CL}} = \sum_{r \in \mathcal{Q}^{\text{ul}}} \sum_{j \in \mathcal{K}_r^{\text{ul}}} \text{diag}(\mathbf{h}_{qk,q}) \mathbf{h}_{rj,q} \in \mathbb{C}^{M_S \times 1} \quad (4.37f)$$

where we define  $\mathbf{X} = \text{stack}\{\mathbf{X}_i\}_{\forall i \in \mathcal{I}} = \begin{bmatrix} \mathbf{X}_1 \\ \vdots \\ \mathbf{X}_{|\mathcal{I}|} \end{bmatrix}$ , i.e., a function that stacks the input

matrices on top of each other. Similarly, to extract the RIS reflection coefficient vector from the constraint in (4.31c), we apply the vectorization operation given in (1.1) to the RIS-assisted component of (4.31c). As a result, (4.31c) can be expressed as

$$\|\mathbf{T}_{rq} \boldsymbol{\theta} + \boldsymbol{\omega}_{rq}\|^2 \leq \tau_r, \quad \forall r \in \mathcal{Q}^{\text{ul}}, \quad (4.38)$$

where

$$\mathbf{T}_{rq} = \sum_{\forall q \in \mathcal{Q}^{\text{dl}}} \sum_{k \in \mathcal{K}_q^{\text{dl}}} \left( \mathbf{f}_{qk}^{\text{T}} \mathbf{H}_q^{\text{T}} \diamond \mathbf{H}_r^{\text{H}} \right) \in \mathbb{C}^{M_T \times M_S} \quad (4.39a)$$

$$\boldsymbol{\omega}_{rq} = \mathbf{G}_{r,q} \mathbf{f}_{qk} \in \mathbb{C}^{M_T \times 1}. \quad (4.39b)$$

$\mathbf{T}_{rq}$  and  $\boldsymbol{\omega}_{rq}$  are the RIS-assisted and direct BS-BS cross-link interference experienced by the  $r$ th UL BS as a result of the transmissions of the  $q$ th DL BS. From the above, the feasibility check problem in (4.31) can be written as

$$\text{Find } \boldsymbol{\theta} \tag{4.40a}$$

$$\text{s.t. } \frac{|\mathbf{a}_{qk}^H \boldsymbol{\theta} + b_{qk}|^2}{\|\mathbf{C}_{qk} \boldsymbol{\theta} + \mathbf{d}_{qk}\|^2 + \sigma_{qk}^2} \geq \varphi, \forall q \in \mathcal{Q}^{\text{dl}} \tag{4.40b}$$

$$\|\mathbf{T}_{rq} \boldsymbol{\theta} + \boldsymbol{\omega}_{rq}\|^2 \leq \tau_r, \forall r \in \mathcal{Q}^{\text{ul}} \tag{4.40c}$$

$$|[\boldsymbol{\theta}]_{[m]}|^2 = 1, m = 1, \dots, M_S, \tag{4.40d}$$

$$\phi_m \in \mathcal{F}, \tag{4.40e}$$

Next, we exclude the limitation of the discrete phase shifts in  $\boldsymbol{\theta}$  and thereafter map the obtained continuous phase shifts to the nearest discrete phase value in  $\mathcal{F}$  as defined in (4.1), the resulting feasibility check problem is given as

$$\text{Find } \boldsymbol{\theta} \tag{4.41a}$$

$$\text{s.t. } \frac{|\mathbf{a}_{qk}^H \boldsymbol{\theta} + b_{qk}|^2}{\|\mathbf{C}_{qk} \boldsymbol{\theta} + \mathbf{d}_{qk}\|^2 + \sigma_{qk}^2} \geq \varphi, \forall q \in \mathcal{Q}^{\text{dl}} \tag{4.41b}$$

$$\|\mathbf{T}_{rq} \boldsymbol{\theta} + \boldsymbol{\omega}_{rq}\|^2 \leq \tau_r, \forall r \in \mathcal{Q}^{\text{ul}} \tag{4.41c}$$

$$|[\boldsymbol{\theta}]_{[m]}|^2 = 1, m = 1, \dots, M_S. \tag{4.41d}$$

Let us denote  $\varkappa$  as a new auxiliary variable, then (4.41) can be written as

$$\text{Find } \boldsymbol{\theta} \tag{4.42a}$$

$$\text{s.t. } \tilde{\boldsymbol{\theta}}^H \boldsymbol{\Sigma}_{qk} \tilde{\boldsymbol{\theta}} + |b_{qk}|^2 \geq \varphi \cdot (\tilde{\boldsymbol{\theta}}^H \boldsymbol{\Xi}_{qk} \tilde{\boldsymbol{\theta}} + \|\mathbf{d}_{qk}\|^2 + \sigma_{qk}^2), \tag{4.42b}$$

$$\tilde{\boldsymbol{\theta}}^H \boldsymbol{\Pi}_{rq} \tilde{\boldsymbol{\theta}} + \|\boldsymbol{\omega}_{rq}\|^2 \leq \tau_r, \forall r \in \mathcal{Q}^{\text{ul}} \tag{4.42c}$$

$$|[\boldsymbol{\theta}]_{[m]}|^2 = 1, m = 1, \dots, M_S, \tag{4.42d}$$

where  $\tilde{\boldsymbol{\theta}}$ ,  $\boldsymbol{\Sigma}_{qk}$ ,  $\boldsymbol{\Xi}_{qk}$ , and  $\boldsymbol{\Pi}_{rq}$  are defined respectively as

$$\tilde{\boldsymbol{\theta}} = \begin{bmatrix} \boldsymbol{\theta} \\ \varkappa \end{bmatrix} \in \mathbb{C}^{(M_S+1) \times 1} \tag{4.43a}$$

$$\boldsymbol{\Sigma}_{qk} = \begin{bmatrix} \mathbf{a}_{qk} \mathbf{a}_{qk}^H & \mathbf{a}_{qk} b_{qk}^* \\ \mathbf{a}_{qk}^H b_{qk} & 0 \end{bmatrix} \in \mathbb{C}^{(M_S+1) \times (M_S+1)} \tag{4.43b}$$

$$\boldsymbol{\Xi}_{qk} = \begin{bmatrix} \mathbf{C}_{qk}^H \mathbf{C}_{qk} & \mathbf{C}_{qk}^H \mathbf{d}_{qk} \\ \mathbf{d}_{qk}^H \mathbf{C}_{qk} & 0 \end{bmatrix} \in \mathbb{C}^{(M_S+1) \times (M_S+1)} \tag{4.43c}$$

$$\mathbf{\Pi}_{rq} = \begin{bmatrix} \mathbf{T}_{rq}^H \mathbf{T}_{rq} & \mathbf{T}_{rq}^H \boldsymbol{\omega}_{rq} \\ \boldsymbol{\omega}_{rq}^H \mathbf{T}_{rq} & 0 \end{bmatrix} \in \mathbb{C}^{(M_S+1) \times (M_S+1)}. \quad (4.43d)$$

Furthermore, we use the property given in (1.3). For example, the RIS-assisted desired user signal  $\tilde{\boldsymbol{\theta}}^H \boldsymbol{\Sigma}_{q_k} \tilde{\boldsymbol{\theta}}$  in (4.42) can be written as  $\tilde{\boldsymbol{\theta}}^H \boldsymbol{\Sigma}_{q_k} \tilde{\boldsymbol{\theta}} = \text{Tr}(\boldsymbol{\Sigma}_{q_k} \tilde{\boldsymbol{\theta}} \tilde{\boldsymbol{\theta}}^H)$ , where  $\text{Tr}(\cdot)$  is the trace operator. Next, we define the following rank-one matrix  $\boldsymbol{\Omega} = \tilde{\boldsymbol{\theta}} \tilde{\boldsymbol{\theta}}^H \in \mathbb{C}^{(M_S+1) \times (M_S+1)}$  such that  $\boldsymbol{\Omega} \succeq 0$ , i.e., the matrix is a positive semidefinite matrix. As a result, the feasibility check problem in (4.42) can be recast into a constrained SDP as

$$\text{Find } \boldsymbol{\Omega} \quad (4.44a)$$

$$\text{s.t. } \text{Tr}(\boldsymbol{\Sigma}_{q_k} \boldsymbol{\Omega}) + |b_{q_k}|^2 \geq \varphi \cdot \left( \text{Tr}(\boldsymbol{\Xi}_{q_k} \boldsymbol{\Omega}) + \|\mathbf{d}_{q_k}\|^2 \right), \quad (4.44b)$$

$$\text{Tr}(\mathbf{\Pi}_{rq} \boldsymbol{\Omega}) + \|\boldsymbol{\omega}_{rq}\|^2 \leq \tau_r, \quad \forall r \in \mathcal{Q}^{\text{ul}} \quad (4.44c)$$

$$[\boldsymbol{\Omega}]_{[m,m]} = 1, \quad m = 1, \dots, M_S + 1, \quad (4.44d)$$

$$\boldsymbol{\Omega} \succeq 0 \quad (4.44e)$$

$$\text{rank}\{\boldsymbol{\Omega}\} = 1. \quad (4.44f)$$

Finally, we adopt the SDR technique (see Appendix C.5) by relaxing the rank-one constraint in (4.44f) to recast problem (4.44) into a convex SDP which can be solved using the CVX tools.

$$\text{Find } \boldsymbol{\Omega} \quad (4.45a)$$

$$\text{s.t. } \text{Tr}(\boldsymbol{\Sigma}_{q_k} \boldsymbol{\Omega}) + |b_{q_k}|^2 \geq \varphi \cdot \left( \text{Tr}(\boldsymbol{\Xi}_{q_k} \boldsymbol{\Omega}) + \|\mathbf{d}_{q_k}\|^2 \right), \quad (4.45b)$$

$$\text{Tr}(\mathbf{\Pi}_{rq} \boldsymbol{\Omega}) + \|\boldsymbol{\omega}_{rq}\|^2 \leq \tau_r, \quad \forall r \in \mathcal{Q}^{\text{ul}} \quad (4.45c)$$

$$[\boldsymbol{\Omega}]_{[m,m]} = 1, \quad m = 1, \dots, M_S + 1, \quad (4.45d)$$

$$\boldsymbol{\Omega} \succeq 0, \quad (4.45e)$$

It is noted that the considered SDP problem in (4.45) has relaxed the rank-one constraint. However, the rank of the obtained solution may not be 1. If the rank is 1, then  $\boldsymbol{\theta}$  can be obtained by using an eigenvalue decomposition of  $\boldsymbol{\Omega}$ . Otherwise, we can use a rank-one approximation such as an eigenvalue decomposition-based approximation or Gaussian randomization (explained in Appendix C.5) to extract the  $\boldsymbol{\theta}$  that is feasible for the considered problem [139, 140]. However, it has been shown in [140] that the Gaussian randomization approach provides a better performance than the eigenvalue decomposition-based approximation.

The obtained continuous phase shifts given as  $\phi_m = \angle \boldsymbol{\theta}(m)$  are mapped to the

discrete ones. This operation can be expressed as

$$\tilde{\phi}_m = \underset{\phi \in \mathcal{F}}{\operatorname{argmin}} |\phi - \phi_m|, \quad (4.46)$$

where the periodicity with  $2\pi$  is taken into account.

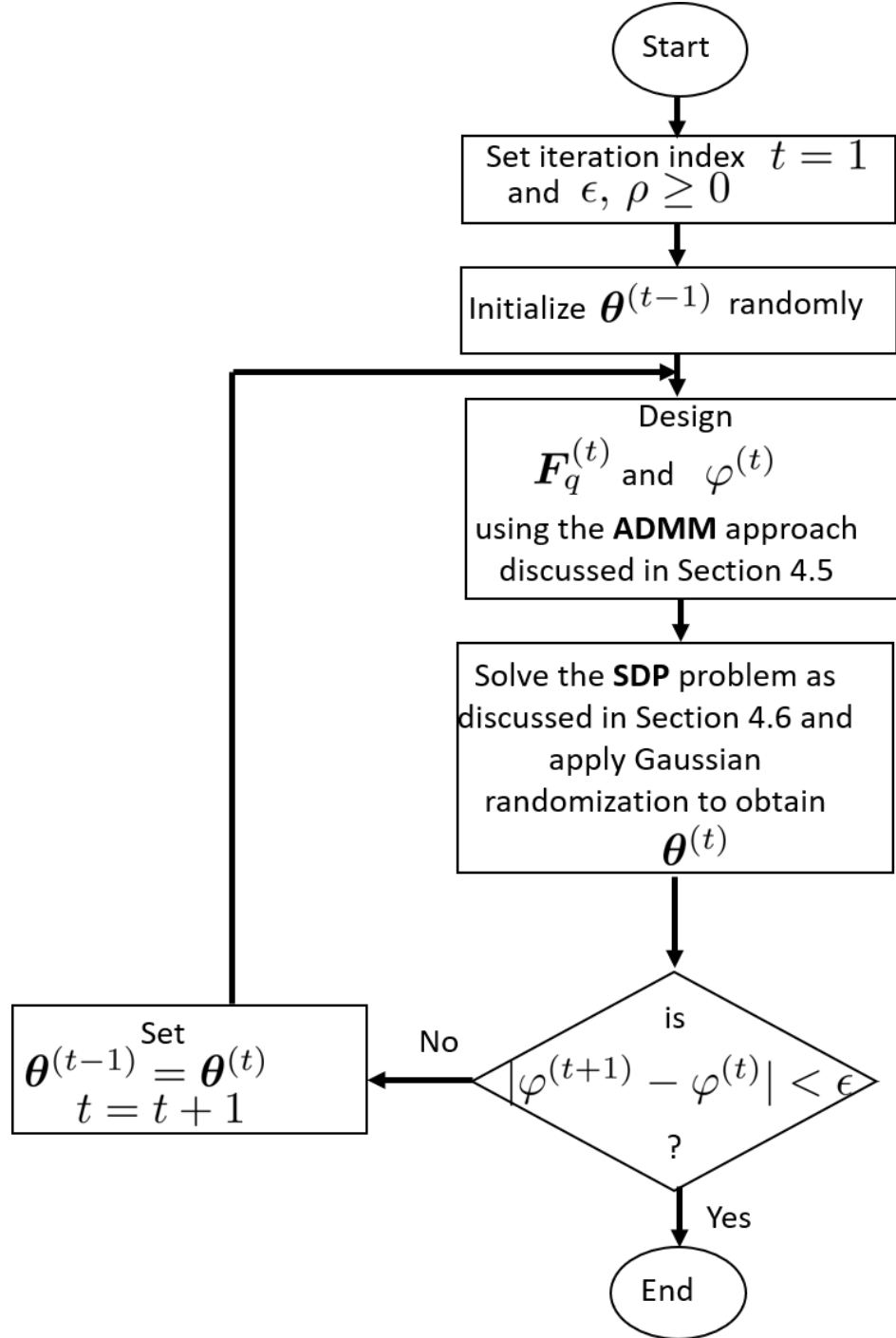


Fig. 4.2: Flow chart for the implementation of the AO-ADMM algorithm.

Next, the transmit beamforming vectors are updated using the  $\boldsymbol{\theta}$  designed in the previous step. The alternating optimization process continues until the difference between the consecutive value of the cost function  $\varphi$  as defined in (4.9) becomes smaller than a given threshold  $\epsilon > 0$ . The AO algorithm for the ADMM-based distributed coordinated beamforming is outlined in Algorithm 3 and Fig. 4.2.

---

**Algorithm 3: AO-ADMM**


---

**Data:**  $\epsilon, t, \rho \geq 0$ , and random  $\boldsymbol{\theta}$   
**Result:**  $\varphi, \mathbf{F}_q$ , and  $\boldsymbol{\theta}$

- 1 **for**  $t = 1 : 50$  **do**
- 2     Solve problem (4.9) for the given  $\boldsymbol{\theta}^{(t-1)}$ , using the ADMM approach to obtain  $\mathbf{F}_q^{(t)}$  and  $\varphi^{(t)}$ ;
- 3     With the fixed  $\mathbf{F}_q^{(t)}$  and  $\varphi^{(t)}$  solve the SDP problem in (4.45) and apply Gaussian randomization to obtain  $\boldsymbol{\theta}^{(t)}$ ;
- 4     **if**  $|\varphi^{(t+1)} - \varphi^{(t)}| < \epsilon$  **then**
- 5          $\boldsymbol{\theta} \leftarrow \boldsymbol{\theta}^{(t)}$ ;
- 6     **else**
- 7          $\boldsymbol{\theta}^{(t-1)} = \boldsymbol{\theta}^{(t)}$ ;
- 8          $t \leftarrow t + 1$ ;
- 9     **end**
- 10 **end**

---

## 4.7 Backhaul Signaling and Per-BS complexity Analysis

The ADMM-based solution for the design of the transmit beamforming vectors requires the  $q$ th DL BS to broadcast its local variables  $(\boldsymbol{\lambda}_q, \boldsymbol{\phi}_q, \gamma_q)$  to the coupled BSs, with a total of  $2|\mathcal{Q}^{\text{dl}}|(|\mathcal{Q}^{\text{dl}}| - 1)|\mathcal{K}_q^{\text{dl}}| + |\mathcal{Q}^{\text{dl}}|(|\mathcal{Q}^{\text{dl}}| - 1)|\mathcal{K}^{\text{ul}}| + 1$  real valued scalars per iteration. This leads to a reduced signaling/computational load on the CPU when compared with the centralized solution that requires each BS to exchange its local channel state information with all other BSs. The total number of real-valued scalars required to be sent in the centralized solution is  $2|\mathcal{K}^{\text{dl}}|M_{\text{T}}(|\mathcal{Q}^{\text{dl}}| - 1)|\mathcal{Q}^{\text{dl}}| + 2|\mathcal{Q}^{\text{dl}}|M_{\text{T}}^2(|\mathcal{Q}^{\text{dl}}| - 1)|\mathcal{Q}^{\text{ul}}|$ , for the exchange of the  $\mathbf{h}^{\text{BS-UE}}$  and  $\mathbf{H}^{\text{BS-BS}}$  effective channels, respectively defined in (4.3) and (4.6).

Furthermore, the per-iteration complexity of the ADMM-based solution is dominated by the complexity of solving (4.25) by each DL BS, which has 1 SOC of size  $(4|\mathcal{K}_q^{\text{dl}}| + 1)$ ,  $|\mathcal{K}_q^{\text{dl}}|$  SOC of size  $(2|\mathcal{K}_q^{\text{dl}}| + 2)$ ,  $|\mathcal{K}_q^{\text{dl}}|$  SOC of size  $(2|\mathcal{K}_q^{\text{dl}}| + 1)$ ,  $|\mathcal{Q}^{\text{dl}}|$  SOC of size  $(M_{\text{T}}|\mathcal{K}_q^{\text{dl}}| + 1)$ ,  $|\mathcal{Q}^{\text{dl}}|$  SOC of size  $(M_{\text{T}}|\mathcal{K}_q^{\text{dl}}| + |\mathcal{K}_q^{\text{dl}}| + 1)$ , and 1 SOC of size

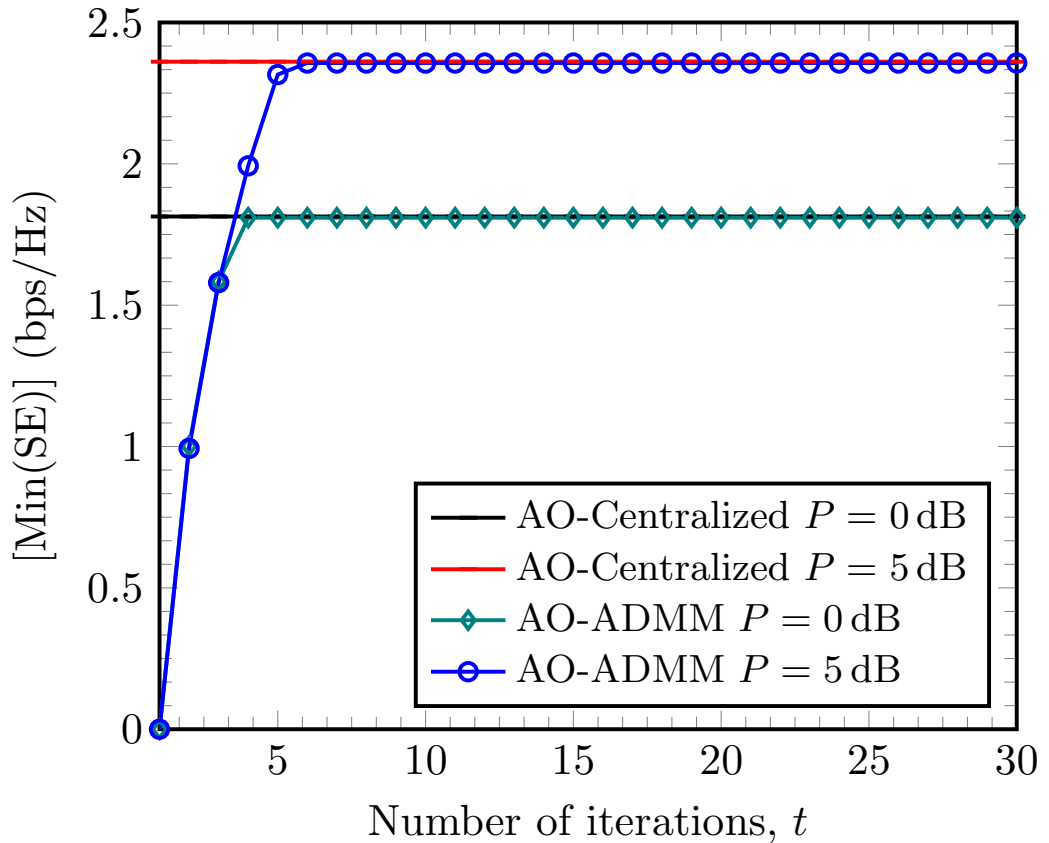


Fig. 4.3: Convergence behaviour of the AO-ADMM for different  $P$ , assuming  $\rho = 0.5$ . Note  $\rho$  is the penalty parameter as given in (4.24).

$(M_T |\mathcal{K}_q^{\text{dl}}| + 1)$ . The per-BS computational complexity can be computed using the complexity of a generic interior point method as given in [141, 142].

## 4.8 Numerical Results

In this section, we show simulation results to evaluate the performance of our proposed method as compared to the centralized baseline scheme given in Algorithm 1 of Section 4.5.1 [129]. We consider a system with  $Q = 4$  cells, as shown in Fig. 4.1, where  $|\mathcal{Q}^{\text{dl}}| = 2$  and  $|\mathcal{Q}^{\text{ul}}| = 2$ . We assume  $p_q^{\text{dl}} = P, \forall q \in \mathcal{Q}^{\text{dl}}, \sigma_1^2 = \dots = \sigma_K^2 = 1, p_r^{\text{ul}} = 23$  dBm,  $\tau_r = 4$  dB,  $\forall r \in \mathcal{Q}^{\text{ul}}$ , and  $\epsilon = 10^{-3}$ . Equally,  $|\mathcal{K}_q^{\text{dl}}| = 2, \forall q \in \mathcal{Q}^{\text{dl}}, |\mathcal{K}_r^{\text{dl}}| = 2, \forall r \in \mathcal{Q}^{\text{ul}}$ , and  $[M_S, M_T] = [256, 16]$ . We assume a Rician flat fading channel model such that, for example, the channel between the  $q$ th BS and the RIS is represented as

$$\mathbf{H}_q = \sqrt{\frac{\kappa}{\kappa + 1}} \mathbf{H}_q^{\text{LOS}} + \sqrt{\frac{1}{\kappa + 1}} \mathbf{H}_q^{\text{NLOS}}, \quad (4.47)$$

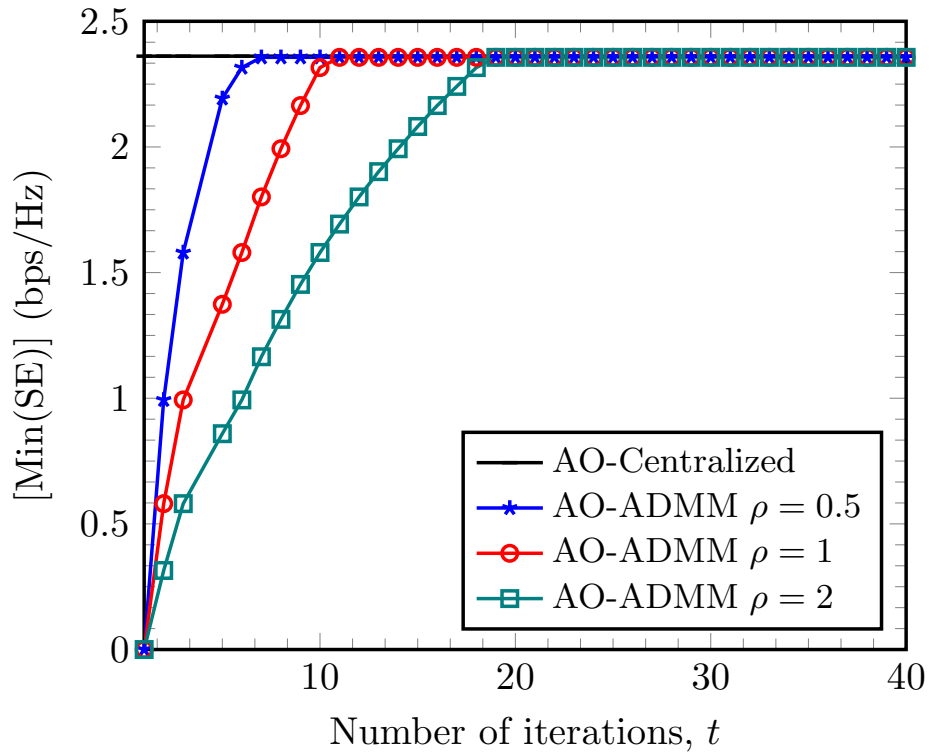


Fig. 4.4: Convergence behaviour of the AO-ADMM algorithm for different  $\rho$ , assuming that  $P = 5\text{dB}$ .

where  $\kappa \geq 0$  denotes the Rician  $\kappa$ -factor and  $\mathbf{H}_q^{\text{LOS}}$  denotes the channel associated with the LOS component which is modeled according to (3.9), while  $\mathbf{H}_q^{\text{NLOS}}$  represents the NLOS component, whose entries are independent and identically distributed (i.i.d.) and follow the complex Gaussian distribution with zero mean and unit variance. The other channels are modeled in a similar manner. In all our numerical experiments, we used the same value of  $\kappa = 2$  for all the channels for simplicity.

We study the achievable spectral efficiency using the maximization of the minimum SINR, expressed as  $\log_2(1 + \varphi)$ . Note that from  $\sum_{q \in \mathcal{Q}^{\text{dl}}} \gamma_q = |\mathcal{Q}^{\text{dl}}| \varphi$ , the global variable  $\varphi$  is the average SINR that is obtained independently by all the DL BSs. For performance comparison purposes, we include results for the case where problem (4.7) is solved by adopting an AO approach and problem (4.9) is solved according to the centralized approach in [129] while the SDP method is used to solve problem (4.31).

Fig. 4.3 shows the convergence behaviour of the proposed AO-ADMM solution for different maximum total transmit power  $P$  values while assuming that  $\rho = 0.5$ . It can be seen that the AO-ADMM solution converges to the AO-centralized solution within 10 iterations for the different maximum transmit power values considered. This confirms the practicality of the proposed design.

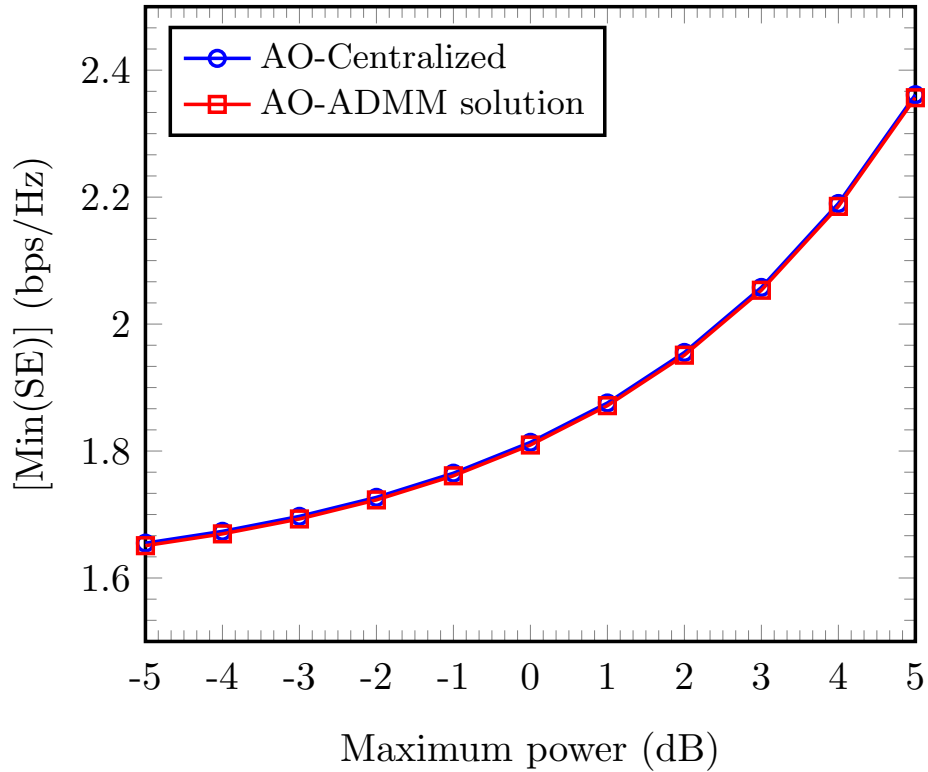


Fig. 4.5: Minimum SE versus the maximum transmit power,  $\rho = 0.5$ .

In Fig. 4.4 we investigate the convergence behaviour of the proposed AO-ADMM solution for different values of the penalty parameter  $\rho$  given in (4.24). The results show that for all considered values of  $\rho$ , the AO-ADMM solution converges to the AO-centralized solution within a few iterations. From the figure, we see that the AO-ADMM converges faster to the AO-centralized solution with the  $\rho = 0.5$ , and the convergence is slowest with  $\rho = 2$ . This shows that the rate of convergence depends on the value of  $\rho$  as it helps to achieve numerical stability and faster convergence.

Next, we compare the minimum spectral efficiency obtained using the AO-centralized solution and the AO-ADMM solution for different maximum total transmit power  $P$  values. Fig. 4.5 clearly shows that the AO-ADMM solution achieves the same performance as the AO-centralized solution for all values of the maximum total transmit power  $P$ .

## 4.9 Chapter Conclusions

In this chapter, we have considered an RIS-aided DTDD wireless network and utilized the alternating direction method of multipliers (ADMM) based distributed coordinated transmit beamforming to reduce the high signaling overhead involved in collecting

all the channel state information at the CPU and SDP for the design of the passive reflection matrix. To this end, an AO-ADMM algorithm was proposed. The simulation results demonstrate that after a few iterations, the AO-ADMM algorithm converges to the centralized solution. Furthermore, the distributed solution has a lower signaling overhead and complexity than the centralized solution.

## 5. LEAKAGE-BASED COORDINATED BEAMFORMING FOR RIS-AIDED DTDD SYSTEMS

In this chapter, we consider the discrete phase-shift model for the RIS and the concept of signal leakage for the design of the transmit beamforming for an RIS-aided DTDD system controlled by a CPU. Maximizing the signal-to-leakage-plus-noise ratio (SLNR) for all the users in the downlink cells is an efficient way of designing the transmit beamforming vectors because it limits the search space and also lowers the complexity involved in finding efficient transmit beamformers. The decoupled nature of the SLNR criterion allows for a characterization of the solution to the multi-user beamforming problem in terms of generalized eigenvalue problems. Numerical results show that the proposed algorithm achieves a satisfactory performance compared to other baseline schemes from the literature.

### 5.1 Introduction

Leveraging upon the intelligent spectrum control of the RIS, we have shown in the previous chapters that the cross-link BS-to-BS interference can be effectively mitigated by the joint design of active transmit beamforming vectors and the passive RIS reflection vector, thereby improving the overall system spectral efficiency for an RIS-aided DTDD system. However, due to the densification of the small cells and the required exchange of channel state information (CSI) in an RIS-aided DTDD system, there is still the need to carry out additional work to develop and implement solutions that will further reduce the complexity involved in the design of the passive and active beamforming in order to reduce the burden on the CPU and the backhaul connections to a greater extent.

To this end, in this chapter, we consider the discrete phase-shift model for the RIS and the concept of signal *leakage* for the design of the transmit beamforming for an RIS-aided DTDD system controlled by a CPU. Such a system is shown in Fig. 3.1. Maximizing the signal-to-leakage-and-noise ratio (SLNR) for all the users in

the downlink cells is an efficient way of designing the transmit beamforming vectors because it limits the search space and also lowers the complexity involved in finding efficient transmit beamformers [22, 143–145]. Moreover, in contrast to the ZF solution and the block diagonalization (BD) algorithm, the leakage scheme does not require any dimension condition on the number of transmit/receive antennas. The ZF solution and the BD algorithm require the number of transmit antennas at the base station to be greater than or equal to the sum of receive antennas of all users [13]. This condition is necessary in order to provide enough degrees of freedom for the ZF solution and the BD algorithm to force the multi-user interference to zero at each UE. The leakage-based solution further takes into account the influence of noise when designing the beamforming vectors. By doing so, the leakage-based solution outperforms ZF solutions even when the dimension requirement for zero-forcing solutions is satisfied [146].

The resulting optimization problem is solved by decoupling it among the variables, and we propose a low-complexity and non-iterative method, similar to the concept in Method 2 of Section 3.5 for the design of the RIS reflection vector and the Rayleigh-Ritz [127] method for the design of the transmit beamforming vectors. This is in contrast to the problem considered in Chapter 3 where the spectral efficiency is maximized based on the SINR and the continuous phase shifts are considered for the RIS. However, the SLNR is maximized in this chapter and the discrete phase-shift model for the RIS is considered. Moreover, we assume that the directions of operation of the small cells are known beforehand, i.e., we know the cells that are operating in the UL and DL, respectively. These directions are known at the CPU. The concept of leakage-based coordinated beamforming for RIS-aided DTDD systems has been published in [43].

## 5.2 Chapter Contributions and Organization

In this chapter, we address the issue of further reducing the complexity involved with the joint design of the transmit beamforming and the passive beamforming for an RIS-aided DTDD wireless system. We adopt the SLNR concept for the design of the transmit beamforming vectors of the DL cells in order to reduce the search space and also lower the complexity involved in finding efficient transmit beamformers. The decoupled nature of the SLNR criterion allows for a characterization of the solution to the multi-user beamforming problem in terms of generalized eigenvalue problems. The resulting optimization problem is solved by decoupling it among the variables, and we propose a low-complexity and non-iterative method for the design of the RIS reflection vector and the Rayleigh-Ritz method for the design of the transmit beamforming vectors.

The rest of the chapter is organized as follows. The system model is presented in Section 5.3, while the maximization of the sum SLNR problem formulation and proposed solution are considered in Section 5.4. In Section 5.5 the complexity analysis is carried out, and the numerical results are presented in Section 5.6. Chapter conclusions are presented in Section 5.7.

### 5.3 System Model

In this section, we consider an RIS-aided mmWave DTDD system consisting of  $Q$  small cells, where each cell has a BS with a ULA of  $M_T$  antennas serving a single UE<sup>1</sup> that is equipped with a single-antenna. As shown in Fig. 3.1, we assume that the communication is aided by an RIS with  $M_S$  passive reflecting elements uniformly arranged on a rectangular surface. The RIS has  $M^h$  and  $M^v$  elements in the horizontal and vertical directions, respectively, as shown in Fig. 3.3. Therefore,  $M_S = M^h \cdot M^v$ . Let  $\mathcal{Q} \triangleq \{1, \dots, Q\}$  denote the set of BSs (cells). At the considered time instant, we assume that there are  $|\mathcal{Q}^{\text{ul}}|$  cells operating in the uplink (UL) direction and  $|\mathcal{Q}^{\text{dl}}|$  cells operating in the downlink (DL) direction, such that  $|\mathcal{Q}^{\text{ul}}| + |\mathcal{Q}^{\text{dl}}| = Q$  and  $\mathcal{Q}^{\text{ul}} \cap \mathcal{Q}^{\text{dl}} = \emptyset$ . Note that  $|\mathcal{X}|$  denote the cardinality of set  $\mathcal{X}$ , i.e., the number of elements in set  $\mathcal{X}$ .

Let  $\mathbf{H}_q \in \mathbb{C}^{M_S \times M_T}$  be the channel matrix from the  $q$ th BS to the RIS,  $\mathbf{h}_q \in \mathbb{C}^{M_S}$  be the channel vector from the  $q$ th UE to the RIS,  $\mathbf{G}_{r,q} \in \mathbb{C}^{M_T \times M_T}$  be the channel matrix from the  $q$ th DL BS to the  $r$ th UL BS,  $\mathbf{g}_{q,q} \in \mathbb{C}^{M_T}$  be the channel vector from the  $q$ th BS to the  $q$ th UE in the  $q$ th DL cell, and  $g_{q,r} \in \mathbb{C}$  be the channel scalar from  $r$ th UL UE to the  $q$ th DL UE. Let us denote  $b$  as the number of quantization bits of the RIS, such that the number of phase levels is  $2^b$ . As in Chapter 4, the resulting discrete phase shifts of the RIS are expressed as

$$\mathcal{F} \triangleq \left\{ 0, \frac{2\pi}{2^b}, 2\frac{2\pi}{2^b}, \dots, (2^b - 1)\frac{2\pi}{2^b} \right\}. \quad (5.1)$$

The received signal by the UE in the  $q$ th DL cell, i.e.,  $q \in \mathcal{Q}^{\text{dl}}$ , can be expressed as

$$y_q^{(\text{dl})} = \sum_{\forall k \in \mathcal{Q}^{\text{dl}}} (\mathbf{h}_{q,k}^{\text{BS-UE}})^H \mathbf{f}_k x_k + \sum_{\forall r \in \mathcal{Q}^{\text{ul}}} h_{q,r}^{\text{UE-UE}} \sqrt{p_r^{\text{ul}}} x_r + z_q, \quad (5.2)$$

<sup>1</sup> The extension of our proposed solution to multi-user scenarios is straightforward.

where

$$\mathbf{h}_{q,k}^{\text{BS-UE}} = (\mathbf{h}_q^{\text{H}} \boldsymbol{\Theta} \mathbf{H}_k + \mathbf{g}_{q,k}^{\text{H}})^{\text{H}}, \quad (5.3)$$

$$h_{q,r}^{\text{UE-UE}} = \mathbf{h}_q^{\text{H}} \boldsymbol{\Theta} \mathbf{h}_r + g_{q,r}, \quad (5.4)$$

the vector in (5.3) represents the effective desired user channel, i.e., for  $q = k$  and/or effective inter-cell interference channel, i.e., for  $q \neq k$ . Furthermore, (5.4) represents the UE-UE cross-link interference from the UE in the  $r$ th UL cell to the UE in the  $q$ th DL cell. Moreover,  $\boldsymbol{\Theta} = \text{diag}(\boldsymbol{\theta})$  is the RIS reflection diagonal matrix,  $\boldsymbol{\theta} = [e^{j\phi_1}, \dots, e^{j\phi_{M_S}}]^{\text{T}} \in \mathbb{C}^{M_S}$  with  $\phi_m \in \mathcal{F}$ ,  $\mathbf{f}_k \in \mathbb{C}^{M_T}$  is the transmit precoding vector with  $\|\mathbf{f}_k\|_2^2 = p_k^{\text{dl}}$ ,  $x_k$  is the zero mean transmit symbol such that  $\mathbb{E}\{|x_k|^2\} = 1$ ,  $z_q$  is additive white complex Gaussian noise with zero mean and variance  $\sigma_q^2$ , and  $p_r^{\text{X}}$  is the transmit power in the  $X \in \{\text{dl}, \text{ul}\}$  direction. Then, the SINR at the UE in the  $q$ th DL cell is given as

$$\Gamma_q^{(\text{dl})} = \frac{|(\mathbf{h}_{q,q}^{\text{BS-UE}})^{\text{T}} \mathbf{f}_q|^2}{\sum_{\substack{\forall k \in \mathcal{Q}^{\text{dl}} \\ k \neq q}} |(\mathbf{h}_{q,k}^{\text{BS-UE}})^{\text{T}} \mathbf{f}_k|^2 + \sum_{\forall r \in \mathcal{Q}^{\text{ul}}} |h_{q,r}^{\text{BS-UE}}|^2 p_r^{\text{ul}} + \sigma_q^2}. \quad (5.5)$$

Equally, the total received BS-BS interference power at the  $r$ th UL BS, i.e.,  $r \in \mathcal{Q}^{\text{ul}}$ , from the DL BSs, can be expressed as

$$\text{IP}_r = \sum_{\forall q \in \mathcal{Q}^{\text{dl}}} \|\mathbf{H}_{r,q}^{\text{BS-BS}} \mathbf{f}_q\|^2, \quad (5.6)$$

where

$$\mathbf{H}_{r,q}^{\text{BS-BS}} = \mathbf{H}_r^{\text{H}} \boldsymbol{\Theta} \mathbf{H}_q + \mathbf{G}_{r,q}, \quad (5.7)$$

is the effective BS-BS cross-link interference channel between the  $q$ th BS operating in the DL and the  $r$ th BS in the UL.

In this chapter, we assume that the above-defined channels  $\{\mathbf{H}_q, \mathbf{h}_q, \mathbf{G}_{r,q}, \mathbf{g}_{r,q}, g_{r,q}\}$  are modeled according to the well-known mmWave Saleh-Valenzuela geometric channel model [123–125] as discussed in Section 3.2, where every channel is modeled as a summation of  $L \ll \max\{M_S, M_T\}$  paths, each has a distinctive DoD and/or DoA and a complex path gain. Under this assumption, we have that  $\text{rank}\{\mathbf{H}_q\} \leq L, \forall q$  and  $\text{rank}\{\mathbf{G}_{r,q}\} \leq L, \forall r, q$ . We assume the availability of the perfect CSI at the BSs. The CSI can be estimated using, for example, the channel estimation method in [37].

## 5.4 Problem Formulation

The main goal here is to design the passive reflection vector  $\boldsymbol{\theta} \in \mathbb{C}^{M_S}$  of the RIS and the active transmit beamforming vectors  $\mathbf{f}_q \in \mathbb{C}^{M_T}$ ,  $\forall q \in \mathcal{Q}^{\text{dl}}$ , of the DL BSs to maximize the sum SLNR. This is motivated by the need to reduce the complexity involved in designing the transmit beamforming vectors. As shown in [22, 143–145] the SLNR is a reasonable metric to balance the complexity and performance in massive MIMO systems and leads to an optimal closed-form characterization of the BS precoders. The SLNR-based problem can be formulated as

$$\max_{\mathbf{f}_q, \boldsymbol{\theta}} \sum_{q \in \mathcal{Q}^{\text{dl}}} \Omega_q^{(\text{dl})} \quad (5.8a)$$

$$\text{s.t. } \|\mathbf{f}_q\|_2^2 \leq p_q^{\text{dl}}, \forall q \in \mathcal{Q}^{\text{dl}} \quad (5.8b)$$

$$|[\boldsymbol{\theta}]_m|^2 = 1, m = 1, \dots, M_S, \quad (5.8c)$$

$$\phi_m \in \mathcal{F}, \quad (5.8d)$$

where (5.8b) is the DL transmit power constraint, (5.8c) are the CMCs for the RIS reflection coefficients, (5.8d) is the discrete phase constraint of the RIS, and  $\Omega_q^{(\text{dl})}$  denotes the SLNR at the  $q$ th DL cell, i.e.,  $q \in \mathcal{Q}^{\text{dl}}$ , which can be expressed as

$$\Omega_q^{(\text{dl})} = \frac{|(\mathbf{h}_{q,q}^{\text{BS-UE}})^H \mathbf{f}_q|^2}{\|\mathbf{A}_q \mathbf{f}_q\|^2 + \sigma_q^2}, \quad (5.9)$$

where

$$\mathbf{A}_q = \text{stack}\{\mathbf{A}_q^{\text{BS-UE}}, \mathbf{A}_q^{\text{BS-BS}}\} \in \mathbb{C}^{U \times M_T}, \quad (5.10)$$

is a matrix containing all the channels from the  $q$ th UE in the  $q$ th DL cell to other users in the DTDD system and  $U = |\mathcal{Q}^{\text{dl}}| - 1 + |\mathcal{Q}^{\text{ul}}| M_T$ . Furthermore,  $\mathbf{A}_q^{\text{BS-UE}} \in \mathbb{C}^{|\mathcal{Q}^{\text{dl}}|-1 \times M_T}$  is the inter-cell interference (leakage) experienced in the other DL cells as a result of the transmission in the  $q$ th DL cell, as defined in (5.11),

$$\mathbf{A}_q^{\text{BS-UE}} = \text{stack}\{(\mathbf{h}_{1,q}^{\text{BS-UE}})^H, \dots, (\mathbf{h}_{|\mathcal{Q}^{\text{dl}}|-1,q}^{\text{BS-UE}})^H, (\mathbf{h}_{|\mathcal{Q}^{\text{dl}}+1,q}^{\text{BS-UE}})^H\} \in \mathbb{C}^{(|\mathcal{Q}^{\text{dl}}|-1) \times M_T} \quad (5.11)$$

where for example,  $\mathbf{h}_{k,q}^{\text{BS-UE}} = \mathbf{h}_k^H \boldsymbol{\Theta} \mathbf{H}_q + \mathbf{g}_{k,q}^H$  is the effective interference (leakage) channel at the UE in the  $k$ th DL cell from the transmission of the  $q$ th DL cell. Moreover,

$\mathbf{A}_q^{\text{BS-BS}}$  is the cross-link interference (leakage) experienced by the UL BSs in the DTDD system due to the transmission in the  $q$ th DL cell as given in (5.12),

$$\mathbf{A}_q^{\text{BS-BS}} = \text{stack}\{\mathbf{H}_{1,q}^{\text{BS-BS}}, \dots, \mathbf{H}_{|\mathcal{Q}^{\text{ul}}|,q}^{\text{BS-BS}}\} \in \mathbb{C}^{|\mathcal{Q}^{\text{ul}}|M_{\text{T}} \times M_{\text{T}}}, \quad (5.12)$$

where  $\mathbf{H}_{r,q}^{\text{BS-BS}}$  is as defined in (5.7). We define  $\mathbf{X} = \text{stack}\{\mathbf{X}_i\}_{\forall i \in \mathcal{I}} = \begin{bmatrix} \mathbf{X}_1 \\ \vdots \\ \mathbf{X}_{|\mathcal{I}|} \end{bmatrix}$ , i.e., a

function that stacks the input matrices on top of each other.

We note that the difference between the SINR given in (5.5) and the SLNR given in (5.9) is that the denominator of (5.5) contains interference from other UEs in the DTDD system to the UE in the  $q$ th DL cell, whereas the denominator of (5.9) is the leakage to other UEs in the system from the BS in the  $q$ th DL cell. As a result, the SLNR in (5.9) have the same precoding vector  $\mathbf{f}_q$  in both the numerator and the denominator. This fact facilitates the solution of the problem.

To solve the non-convex problem (5.8), we propose in the following a non-iterative algorithm by decoupling the optimization between the problem variables. Specifically, given the channel matrices, we design the RIS passive reflection vector  $\boldsymbol{\theta} \in \mathbb{C}^{M_{\text{S}}}$ . After that, for a given  $\boldsymbol{\theta}$ , we design the BSs' transmit active beamformers  $\mathbf{f}_q \in \mathbb{C}^{M_{\text{T}}}$ , using the Rayleigh-Ritz method [127].

### 5.4.1 RIS Reflection Design Method

From (1.1), we first note that the vectorized form of the above-defined effective desired channel given in (5.3) and leakage channels in (5.7) can be expressed as

$$\mathbf{h}_{q,q}^{\text{BS-UE}} = \underbrace{(\mathbf{H}_q^{\text{T}} \diamond \mathbf{h}_q^{\text{T}})}_{\mathbf{H}_{q,q}^{\text{BS-UE}}} \boldsymbol{\theta} + \mathbf{g}_{q,q}, \quad \forall q \in \mathcal{Q}^{\text{dl}} \quad (5.13)$$

$$\mathbf{h}_{k,q}^{\text{BS-UE}} = \underbrace{(\mathbf{H}_q^{\text{T}} \diamond \mathbf{h}_k^{\text{T}})}_{\mathbf{H}_{k,q}^{\text{BS-UE}}} \boldsymbol{\theta} + \mathbf{g}_{k,q}, \quad \forall k, q \in \mathcal{Q}^{\text{dl}}, k \neq q \quad (5.14)$$

$$\text{vec}\{\mathbf{H}_{r,q}^{\text{BS-BS}}\} = \underbrace{(\mathbf{H}_q^{\text{T}} \diamond \mathbf{H}_r^{\text{T}})}_{\bar{\mathbf{H}}_{r,q}^{\text{BS-BS}}} \boldsymbol{\theta} + \text{vec}\{\mathbf{G}_{r,q}\}, \quad \forall r \in \mathcal{Q}^{\text{ul}}, \forall q \in \mathcal{Q}^{\text{dl}}, \quad (5.15)$$

where  $\mathbf{H}_{q,q}^{\text{BS-UE}} \in \mathbb{C}^{M_{\text{T}} \times M_{\text{S}}}$  is the desired channel in the  $q$ th DL cell,  $\mathbf{H}_{k,q}^{\text{BS-UE}} \in \mathbb{C}^{M_{\text{T}} \times M_{\text{S}}}$  is the DL leakage channel from the  $q$ th DL cell to other DL cells in the DTDD system, i.e.,  $\forall k, q \in \mathcal{Q}^{\text{dl}}, k \neq q$ , and  $\bar{\mathbf{H}}_{r,q}^{\text{BS-BS}} \in \mathbb{C}^{M_{\text{T}}^2 \times M_{\text{S}}}$  is the BS-BS leakage channel from the  $q$ th DL BS to  $r$ th UL BS. Note that  $\text{rank}\{\mathbf{H}_{k,q}^{\text{BS-UE}}\} \leq L$  and  $\text{rank}\{\bar{\mathbf{H}}_{r,q}^{\text{BS-BS}}\} \leq$

$L^2$  due to the channel model used. Considering only the RIS-assisted channels, we define the following matrices

$$\mathbf{D}_{\text{DS}}^{\text{BS-UE}} = \text{stack}\{\mathbf{H}_{q,q}^{\text{BS-UE}}\}_{\forall q \in \mathcal{Q}^{\text{dl}}} \in \mathbb{C}^{(|\mathcal{Q}^{\text{dl}}|) \cdot M_{\text{T}} \times M_{\text{S}}} \quad (5.16)$$

$$\mathbf{C}_{\text{DL-leak}}^{\text{BS-UE}} = \text{stack}\{\mathbf{H}_{k,q}^{\text{BS-UE}}\}_{\forall k,q \in \mathcal{Q}^{\text{dl}}, k \neq q} \in \mathbb{C}^{(|\mathcal{Q}^{\text{dl}}|-1) \cdot M_{\text{T}} \times M_{\text{S}}} \quad (5.17)$$

$$\mathbf{C}_{\text{UL-leak}}^{\text{BS-BS}} = \text{stack}\{\bar{\mathbf{H}}_{r,q}^{\text{BS-BS}}\}_{\forall r \in \mathcal{Q}^{\text{ul}}, \forall q \in \mathcal{Q}^{\text{dl}}} \in \mathbb{C}^{|\mathcal{Q}^{\text{ul}}| \cdot M_{\text{T}}^2 \times M_{\text{S}}}, \quad (5.18)$$

where  $\mathbf{D}_{\text{DS}}^{\text{BS-UE}}$  in (5.16) contains all the RIS-assisted composite desired user channels for all the DL UEs in the DTDD system. Additionally,  $\mathbf{C}_{\text{DL-leak}}^{\text{BS-UE}}$  in (5.17) contains all the RIS-assisted composite leakage channels to other DL UEs due to the transmission of the  $q$ th BS in the  $q$ th DL cell. Furthermore,  $\mathbf{C}_{\text{UL-leak}}^{\text{BS-BS}}$  in (5.18) contains all the RIS-assisted composite BS-BS leakage channels for all the UL BSs due to the transmission of the  $q$ th DL BS. From the above, we propose a heuristic method to design the RIS reflection vector  $\boldsymbol{\theta} \in \mathbb{C}^{M_{\text{S}}}$  similarly as discussed in Section 3.5 and in [41]. Therefore,  $\boldsymbol{\theta}$  is designed as a solution to

$$\max_{\boldsymbol{\theta}} \quad \|\mathbf{D}_{\text{DS}}^{\text{BS-UE}} \boldsymbol{\theta}\|_2^2 \quad (5.19\text{a})$$

$$\text{s.t.} \quad |[\boldsymbol{\theta}]_m|^2 = 1, \quad m = 1, \dots, M_{\text{S}}, \quad (5.19\text{b})$$

$$\phi_m \in \mathcal{F}, \quad (5.19\text{c})$$

$$\mathbf{C}_{\text{leak}} \boldsymbol{\theta} = \mathbf{0}, \quad (5.19\text{d})$$

where  $\mathbf{C}_{\text{leak}} = \text{stack}\{\mathbf{C}_{\text{DL-leak}}^{\text{BS-UE}}, \mathbf{C}_{\text{UL-leak}}^{\text{BS-BS}}\} \in \mathbb{C}^{J \times M_{\text{S}}}$  is the total leakage channel in the DTDD system due to the transmission of the  $q$ th DL BS, where  $J = M_{\text{T}}(|\mathcal{Q}^{\text{ul}}| \cdot M_{\text{T}} + (|\mathcal{Q}^{\text{ul}}| - 1))$ . The problem in (5.19) is non-convex due to the constraints in (5.19b) and (5.19c). In the following, we propose a low-complexity non-iterative sub-optimal solution to obtain a feasible and efficient RIS reflection vector.

**Remark 1:** Given the above mmWave channel model adopted in this chapter, the following inequality is satisfied:

$$\text{rank}\{\mathbf{C}_{\text{leak}}\} \leq L_{\text{DL-leak}}^{\text{BS-UE}} + L_{\text{UL-leak}}^{\text{BS-BS}}, \quad (5.20)$$

where  $L_{\text{DL-leak}}^{\text{BS-UE}} \leq (|\mathcal{Q}^{\text{dl}}|^2 - |\mathcal{Q}^{\text{dl}}|)L$ , from (5.17),  $L_{\text{UL-leak}}^{\text{BS-BS}} \leq |\mathcal{Q}^{\text{dl}}||\mathcal{Q}^{\text{ul}}|L^2$ , from (5.18).

We propose to relax (5.19b) and address the discrete non-convex constraint in (5.19c). To this end, we exclude the limitation of the discrete phase shifts and thereafter map the obtained continuous phase shifts to the nearest discrete phase value in  $\mathcal{F}$  as

defined in (5.1). The resulting problem is given as

$$\max_{\boldsymbol{\theta}} \quad \|\mathbf{D}_{\text{DS}}^{\text{BS-UE}} \boldsymbol{\theta}\|_2^2 \quad (5.21\text{a})$$

$$\text{s.t.} \quad \mathbf{C}_{\text{leak}} \boldsymbol{\theta} = \mathbf{0} \quad (5.21\text{b})$$

$$\|\boldsymbol{\theta}\|_2^2 = 1. \quad (5.21\text{c})$$

We propose to solve (5.21) by adopting a similar heuristic approach in Method 2 of Section 3.5. First, we assume that  $\boldsymbol{\theta}$  is decomposed into  $|\mathcal{Q}^{\text{dl}}|$  sub-vectors as

$$\boldsymbol{\theta} = \boldsymbol{\theta}_1 + \boldsymbol{\theta}_2 + \cdots + \boldsymbol{\theta}_{|\mathcal{Q}^{\text{dl}}|}, \quad (5.22)$$

where  $\|\boldsymbol{\theta}_q\|_2^2 = 1, \forall q$  and  $|\mathcal{Q}^{\text{dl}}|$  is the total number of cells operating in the DL. Given the above decomposition, we propose to design the  $q$ th sub-vector  $\boldsymbol{\theta}_q$  as

$$\max_{\boldsymbol{\theta}_q} \quad \|\mathbf{H}_{q,q}^{\text{BS-UE}} \boldsymbol{\theta}_q\|_2^2 \quad (5.23\text{a})$$

$$\text{s.t.} \quad \|\boldsymbol{\theta}_q\|_2^2 = 1 \quad (5.23\text{b})$$

$$\boldsymbol{\Sigma}_q^{\text{INT}} \boldsymbol{\theta}_q = \mathbf{0}, \quad (5.23\text{c})$$

where  $\boldsymbol{\Sigma}_q^{\text{INT}} = \text{stack}\{\mathbf{D}_{\text{DS-INT}}^{\text{BS-UE}}, \mathbf{C}_{\text{leak}}\}$  and

$$\mathbf{D}_{\text{DS-INT}}^{\text{BS-UE}} = \text{stack}\{\mathbf{H}_{k,q}^{\text{BS-UE}}\}_{\forall k,q \in \mathcal{Q}^{\text{dl}}, k \neq q}, \in \mathbb{C}^{(|\mathcal{Q}^{\text{dl}}|-1)M_{\text{T}} \times M_{\text{S}}} \quad (5.24)$$

i.e.,  $\mathbf{D}_{\text{DS-INT}}^{\text{BS-UE}}$  is a matrix containing all blocks of  $\mathbf{D}_{\text{DS}}^{\text{BS-UE}}$  in (5.16) except for the  $q$ th sub-block. Note that

$$R_{\Sigma_q} \triangleq \text{rank}\{\boldsymbol{\Sigma}_q^{\text{INT}}\} \leq \text{rank}\{\mathbf{C}_{\text{leak}}\} + L_{\text{DS-INT}}^{\text{BS-UE}}, \quad (5.25)$$

where  $L_{\text{DS-INT}}^{\text{BS-UE}} \leq (|\mathcal{Q}^{\text{dl}}| - 1)L$ . A solution to the  $q$ th sub-problem in (5.23) is given as

$$\boldsymbol{\theta}_q^{\text{FD}} = \mathbf{V}_{\text{INT},q}^{\text{NS}} \mathbf{v}_{\text{max},q}^{\text{BS-UE}} \in \mathbb{C}^{M_{\text{S}}}, \quad (5.26)$$

where  $\mathbf{V}_{\text{INT},q}^{\text{NS}} \in \mathbb{C}^{M_{\text{S}} \times (M_{\text{S}} - R_{\Sigma_q})}$  holds the basis for the null-space (NS) of  $\boldsymbol{\Sigma}_q^{\text{INT}}$ , which can be obtained from the singular value decomposition of  $\boldsymbol{\Sigma}_q^{\text{INT}}$  [13] and  $\mathbf{v}_{\text{max},q}^{\text{BS-UE}} \in \mathbb{C}^{(M_{\text{S}} - R_{\Sigma_q}) \times 1}$  is the right singular vector corresponding to the maximum singular value of  $\mathbf{H}_{q,q}^{\text{BS-UE}} \mathbf{V}_{\text{INT},q}^{\text{NS}} \in \mathbb{C}^{M_{\text{T}} \times (M_{\text{S}} - R_{\Sigma_q})}$ , where  $R_{\Sigma_q}$  is the rank of the  $\boldsymbol{\Sigma}_q^{\text{INT}}$  matrix.

The obtained continuous phase shifts given as  $\phi_m = \angle \boldsymbol{\theta}^{\text{FD}}(m)$  are mapped to the

discrete ones. This operation can be expressed as

$$\tilde{\phi}_m = \underset{\phi \in \mathcal{F}}{\operatorname{argmin}} |\phi - \phi_m|, \quad (5.27)$$

where the periodicity with  $2\pi$  is taken into account. Finally, to satisfy the constant modulus constraints in (5.19b), we apply the element-wise projection function as

$$\tilde{\boldsymbol{\theta}}^{\text{CMC}} \leftarrow \text{P} \left( \tilde{\boldsymbol{\theta}}^{\text{FD}} \right). \quad (5.28)$$

### 5.4.2 Transmit Beamforming Design

For a given  $\boldsymbol{\theta} \in \mathbb{C}^{M_S}$ , we design the transmit beamforming vectors  $\mathbf{f}_q \in \mathbb{C}^{M_T}, \forall q \in \mathcal{Q}^{\text{dl}}$ , as the solution to the problem given as

$$\max_{\mathbf{f}_q} \sum_{q \in \mathcal{Q}^{\text{dl}}} \Omega_q^{(\text{dl})} \quad (5.29a)$$

$$\text{s.t.} \quad \|\mathbf{f}_q\|_2^2 \leq p_q^{\text{dl}}, \forall q \in \mathcal{Q}^{\text{dl}}, \quad (5.29b)$$

where  $\Omega_q^{(\text{dl})}$  is the SLNR at the  $q$ th DL BS as defined in (5.9). The objective of the beamformer is to make the desired power as large as possible compared to the leakage power. Since (5.9) has the same transmit beamforming vector  $\mathbf{f}_q$  in its numerator and the denominator, it is easy to verify that we can decompose problem (5.29) into  $|\mathcal{Q}^{\text{dl}}|$  sub-problems which have simple closed-form solutions. The SLNR in (5.9) can be written as

$$\Omega_q^{(\text{dl})} = \frac{\mathbf{f}_q^H \mathbf{h}_{q,q}^{\text{BS-UE}} (\mathbf{h}_{q,q}^{\text{BS-UE}})^H \mathbf{f}_q}{\mathbf{f}_q^H (\mathbf{A}_q^H \mathbf{A}_q + \sigma_q^2 \mathbf{I}_{M_T}) \mathbf{f}_q}. \quad (5.30)$$

According to the generalized Rayleigh-Ritz quotient method (see Appendix D.3) [127], the optimal  $\mathbf{f}_q$  is given as

$$\mathbf{f}_q = \sqrt{p_q^{\text{dl}}} \mathbf{v}_{\max} \left\{ \left( \mathbf{A}_q^H \mathbf{A}_q + \sigma_q^2 \mathbf{I}_{M_T} \right)^{-1} \mathbf{h}_{q,q}^{\text{BS-UE}} (\mathbf{h}_{q,q}^{\text{BS-UE}})^H \right\}, \quad (5.31)$$

where the scaling factor  $\sqrt{p_q^{\text{dl}}}$  is used so that  $\mathbf{f}_q$  satisfies the power constraint in (5.29b) and the vector  $\mathbf{v}_{\max}\{\cdot\}$  is the eigenvector corresponding to the largest eigenvalue of the matrix. The eigenvector is normalized to unit norm, i.e.,  $\|\mathbf{v}_{\max}\|_2 = 1$ .

For comparison purposes, the ZF solution for the design of  $\mathbf{f}_q \in \mathbb{C}^{M_T}, \forall q \in \mathcal{Q}^{\text{dl}}$ ,

according to [143, 146] is given as

$$\mathbf{f}_q^{\text{ZF}} = \mathbf{\Upsilon}_q \mathbf{u}_q^{\text{max}} \in \mathbb{C}^{M_T \times 1}, \quad (5.32)$$

where  $\mathbf{\Upsilon}_q = \mathbf{I}_{M_T} - \mathbf{A}_q^+ \mathbf{A}_q \in \mathbb{C}^{M_T \times M_T}$  and  $\mathbf{u}_q^{\text{max}} \in \mathbb{C}^{M_T \times 1}$  is the right singular vector corresponding to the singular value of  $((\mathbf{h}_{q,q}^{\text{BS-UE}})^H \mathbf{\Upsilon}_q) \in \mathbb{C}^{1 \times M_T}$ , and  $\mathbf{A}_q^+$  is the pseudo-inverse of  $\mathbf{A}_q \in \mathbb{C}^{U \times M_T}$  as defined in (5.10). If  $\mathbf{A}_q$  is a tall matrix, then  $\mathbf{\Upsilon}_q = \mathbf{0}$ , as a result  $(\mathbf{h}_{q,q}^{\text{BS-UE}})^H \mathbf{\Upsilon}_q$  reduces to zero which suggests that  $\mathbf{f}_q^{\text{ZF}} = \mathbf{0}$ . This explains why the ZF solution is only applicable when the dimension condition [13] is satisfied. From our system model, for the problem in (5.32) to be well posed (i.e., in order for  $\mathbf{f}_q^{\text{ZF}}$  non-zero), we must have

$$M_T \geq |\mathcal{Q}^{\text{dl}}| - 1 + |\mathcal{Q}^{\text{ul}}| M_T. \quad (5.33)$$

However, this condition is not satisfied as  $\mathbf{A}_q$  is a tall matrix. This accounts for the poor performance of the ZF-based solutions in terms of the system-wide achievable spectral efficiency as shown in our numerical results.

## 5.5 Complexity analysis

Since the complexity of computing the SVD of a  $m \times n$  matrix, with  $m \geq n$ , is on the order of  $\mathcal{O}\{n^2\}$  [127], the complexity of calculating  $\tilde{\boldsymbol{\theta}}^{\text{CMC}}$  is on the order of  $\mathcal{O}\{|\mathcal{Q}^{\text{dl}}| M_T^2\}$ . The computational complexities of the leakage-based transmit precoding vector and that of the ZF solution are mainly due to the matrix inversion. The matrix inversion has a complexity of  $\mathcal{O}(n^3)$  [127]. Therefore, the computational complexity of the leakage-based transmit precoding vectors  $\mathbf{f}_q \in \mathbb{C}^{M_T}, \forall q \in \mathcal{Q}^{\text{dl}}$  is on the order of  $\mathcal{O}\{|\mathcal{Q}^{\text{dl}}| M_T^3\}$  [127]. Similarly, the computational complexity of the ZF solution  $\mathbf{f}_q^{\text{ZF}} \in \mathbb{C}^{M_T}, \forall q \in \mathcal{Q}^{\text{dl}}$  is  $\mathcal{O}\{|\mathcal{Q}^{\text{dl}}| M_T^3\}$ .

**Achievable sum rate:** We adopt the system-wide spectral efficiency (SE) as a performance evaluation metric. The system-wide SE for the RIS-aided DTDD system is given as

$$\text{SE} = \sum_{\forall q \in \mathcal{Q}^{\text{dl}}} \log_2 \left( 1 + \Gamma_q^{(\text{dl})} \right) + \sum_{\forall r \in \mathcal{Q}^{\text{ul}}} \log_2 \left( 1 + \Gamma_q^{(\text{ul})} \right). \quad (5.34)$$

## 5.6 Numerical Results

In this section, we show simulation results to evaluate the performance of our proposed method as compared to baseline schemes. We consider a system with  $Q = 4$  cells,

as shown in Fig. 3.1, where  $|\mathcal{Q}^{\text{dl}}| = 2$  and  $|\mathcal{Q}^{\text{ul}}| = 2$ . We assume that the RIS has  $M_{\text{S}} = 256$  passive reflecting elements and each BS has  $M_{\text{T}} = 16$  antennas. We set  $p_r^{\text{ul}} = 23$  dBm and assume that the number of channel paths  $L = 4$ , where the corresponding DoDs and/or DoAs are uniformly distributed in  $[-\frac{\pi}{2}, \frac{\pi}{2}]$ . With the above simulation parameters, the rank of  $\Sigma_q^{\text{INT}}$  and the matrix that spans the null-space of  $\Sigma_q^{\text{INT}}$  in Section 5.4.1 are given as  $R_{\Sigma_q} = 28$  and  $\mathbf{V}_{\text{INT},q}^{\text{NS}} \in \mathbb{C}^{256 \times 228}$ , respectively.

For performance comparison purposes, we include results for the following baseline cases:

1. **Baseline 1**, the SLNR-max problem (5.8) is solved by adopting an alternating optimization (AO) approach according to [147]. Here, the transmit beamforming vectors are designed according to (5.31), and the SQUAREM-MM algorithm is used to design the RIS reflection vector [147]. The obtained continuous phase shifts are then mapped to the nearest discrete phase.
2. **Baseline 2**, where the entries of the RIS reflection vector  $\boldsymbol{\theta} \in \mathbb{C}^{M_{\text{S}}}$  are designed as proposed in (5.23), and the transmit beamforming vector  $\mathbf{f}_q \in \mathbb{C}^{M_{\text{T}}}, \forall q \in \mathcal{Q}^{\text{dl}}$  is designed according to the ZF solution in (5.32).
3. **Baseline 3**, where we adopt the AO approach and use the SQUAREM-MM algorithm to design the RIS reflection vector as in [147]. Then we adopt the ZF scheme for the design of the transmit precoder  $\mathbf{f}_q \in \mathbb{C}^{M_{\text{T}}}, \forall q \in \mathcal{Q}^{\text{dl}}$ , for a given  $\boldsymbol{\theta} \in \mathbb{C}^{M_{\text{S}}}$ .

In Fig. 5.1, we present the performance result of the proposed scheme in terms of the SLNR with respect to the DL transmit power while assuming that the RIS has  $M_{\text{S}} = 256$  passive reflecting elements and each BS has  $M_{\text{T}} = 16$  antennas. We present simulation results for two cases; when the discrete phase shifts of the RIS, i.e., when the constraint in (5.19c) is satisfied, and the ideal RIS case (continuous phase shifts). The number of quantization bits used for the discrete phase levels is  $b = 2$ . From the figure, we observe that the proposed method outperforms Baseline 1, as a result of our adopted low-complexity non-iterative design method for the reflection vector of the RIS. We observe that there is a performance gap in the SLNR performance between the ideal case and the discrete case for the considered schemes. This performance gap is due to the quantization error, which is the difference between the continuous phase shifts and the nearest discrete phase shifts.

In Fig. 5.2, we show the achievable SE versus the DL SNR for all the cells in the DTDD system, while assuming that the RIS has  $M_{\text{S}} = 256$  passive reflecting elements and each BS has  $M_{\text{T}} = 16$  antennas. The number of quantization bits used for the

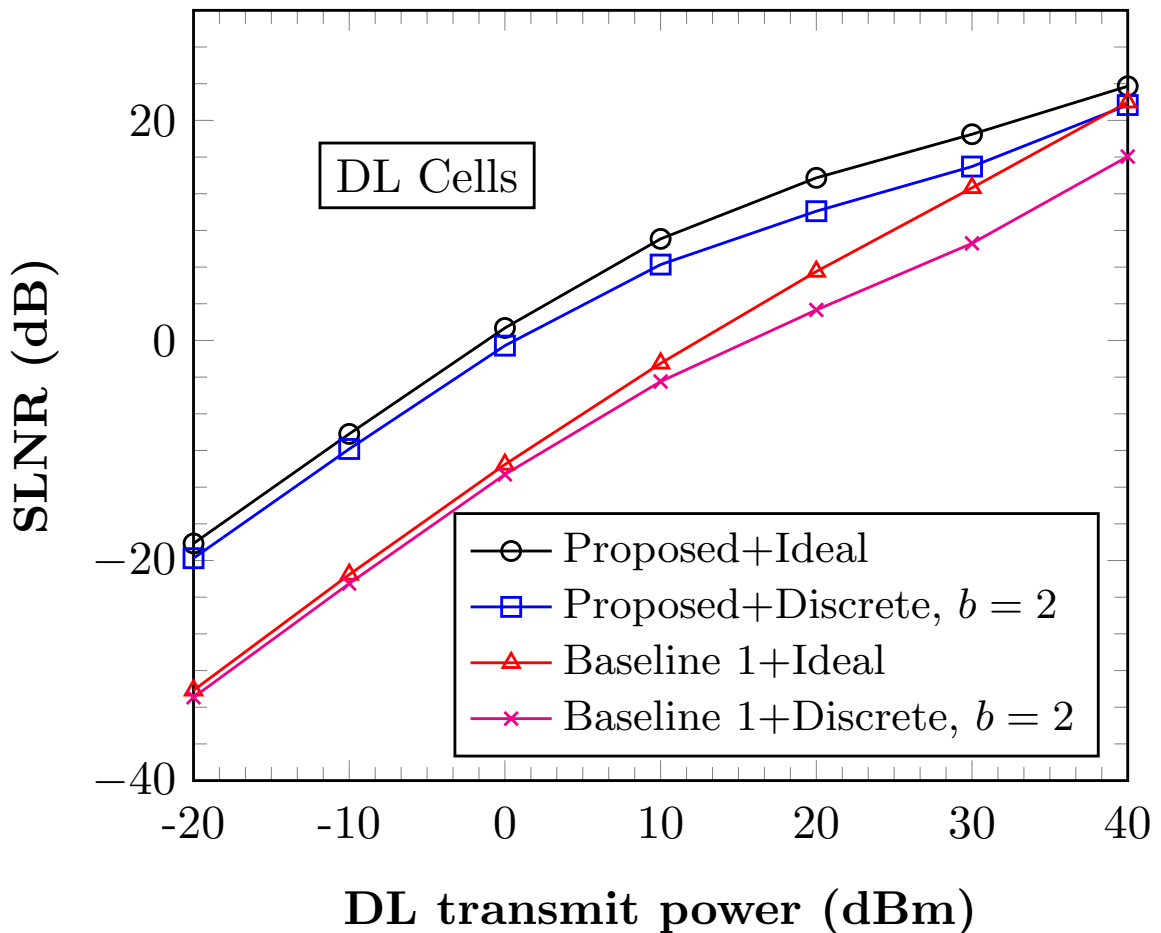
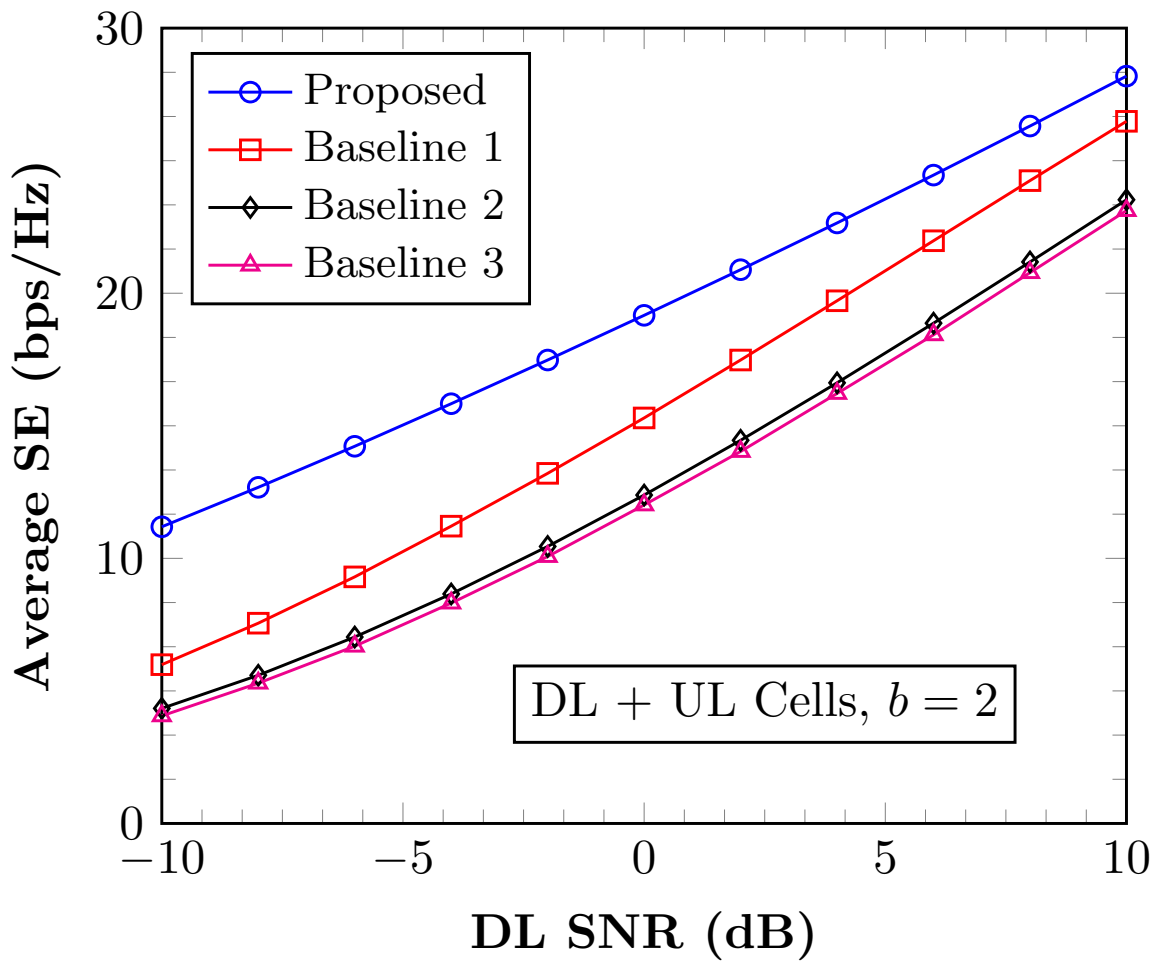
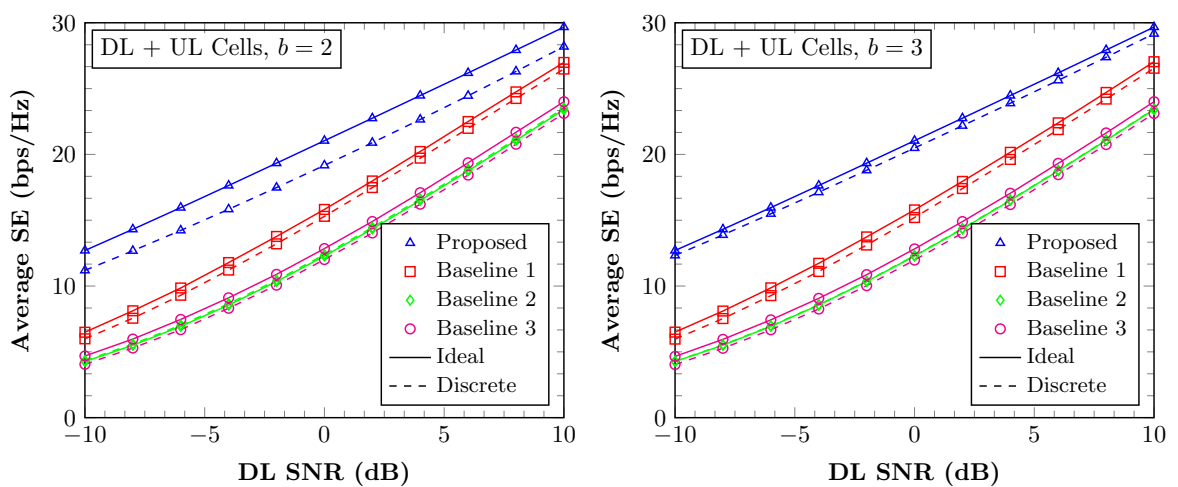


Fig. 5.1: SLNR versus DL transmit power, assuming  $M_S = 256$  and  $M_T = 16$ .

discrete phase levels is  $b = 2$ . From the figure, we can clearly see that the proposed method has better SE performance compared to the other baseline schemes. The figure shows that the SLNR-based schemes (Proposed and Baseline 1) outperform the ZF-based schemes (Baseline 2 and Baseline 3), this is as a result of the fact that the SLNR-based schemes do not suffer from the dimensionality condition in [13] for effective mitigation of the multi-user interference in the system. We note that the system-wide SEs for the ZF-based solutions (**Baseline 2** and **Baseline 3**) are mainly due to the achievable rates in the UL cells. This is because according to the condition in (5.33) the ZF solution for the DL cells is zero, i.e.,  $\mathbf{f}_q^{\text{ZF}} \in \mathbb{C}^{M_T} = \mathbf{0}$ ,  $\forall q \in \mathcal{Q}^{\text{dl}}$ .

Fig. 5.3 compares the SE performance of the considered schemes upper-bounded by their ideal RIS cases (continuous phases) for different values of  $b$ . There is a performance gap in the achievable SE between the ideal case and the discrete case for the considered schemes as a result of the quantization error, which reduces with an increase in the number of quantization bits. The proposed method outperforms the other baseline schemes in both scenarios.

Fig. 5.2: System-wide SE versus DL SNR, assuming  $b = 2$ .Fig. 5.3: SE versus DL SNR, for different quantization bits  $b$ .

## 5.7 Chapter Conclusions

In this chapter, we have considered the transmit beamforming and RIS reflection coefficient design problem in an RIS-aided DTDD wireless network to maximize the signal-to-leakage-and-noise ratio. We have proposed a centralized low-complexity and non-iterative solution for the design of the RIS reflection vector and the constrained optimization of the SLNR for the design of the transmit beamforming vectors. The decoupled nature of the SLNR criterion allows for a characterization of the solution to the multi-user beamforming problem in terms of generalized eigenvalue problems. The proposed design scheme does not impose a restriction on the number of available transmit antennas. The provided simulation results have shown that the proposed method achieves satisfactory performance compared to other baseline schemes.

## 6. ROBUST BEAMFORMING FOR RIS-AIDED DYNAMIC TDD SYSTEMS

In this thesis, RIS-aided DTDD systems have been proposed as a solution to meet the traffic fluctuations in small cells and tune the wireless propagation channels in real time. The performance improvement that can be obtained from this incorporation heavily depends on the accuracy of the channel state information (CSI). However, previous works have considered systems with perfect CSI, without considering the effects of channel estimation errors. In this chapter, we propose robust transmission strategies for an RIS-aided DTDD system with imperfect CSI. The problem is formulated as a sum-power minimization problem for the downlink cells under individual users' SINR constraints, interference temperature constraints for the uplink cells, and unit-modulus constraints of the RIS in the presence of CSI errors. We consider the bounded CSI imperfection and the statistical imperfection models. We adopt the S-procedure to reformulate the bounded CSI model-based design formulation and a Bernstein-type inequality to reformulate the statistical CSI model-based design approach into tractable problems that can be solved efficiently. Numerical results show that the outage probability-based (statistical) approach outperforms the bounded CSI method-based design.

### 6.1 Introduction

In the previous chapters and in [41–43], we demonstrated the potential benefit of employing the RIS to improve the communication efficiency, while reducing the impact of cross-link BS-to-BS interference for an RIS-aided DTDD system. The cross-link interference is effectively mitigated via the joint design of active transmit beamforming vectors and the passive RIS reflection vector. The performance improvement that can be obtained from this joint design of the active and passive beamforming vectors heavily depends on the accuracy of the CSI. In this context, most of the works on RIS-aided communication systems have assumed the availability of perfect CSI, i.e., there are no CSI estimation errors, e.g., [41–43, 74]. Unfortunately, it is impossible

to perfectly acquire the CSI in practice due to channel variations or feedback errors. Hence, assuming perfect CSI for beamforming design either imposes a high burden on communication systems or results in a resource allocation mismatch such that the QoS of the users cannot be guaranteed. Therefore, robust active and passive beamforming designs taking CSI imperfections into account are desirable to fully realize the potential benefits of RIS-aided communication systems.

In [148], the robust transmit beamforming vectors at the BS and the phase shifts at the RIS are jointly designed in order to minimize the total transmit power subject to worst-case QoS constraints, i.e., maintaining a required achievable rate for every user under all possible cases of CSI errors. To that end, an ellipsoid approach was adopted to capture the channel uncertainties, where the Frobenius norm of the channel error vector is assumed to be confined within a given radius of the uncertainty region. This method results in a conservative approach, which requires an exceedingly large amount of system resources to protect rarely occurring worst cases.

The authors in [149] further proposed a robust secure transmission strategy by also applying the worst-case optimization method when the channels from the RIS to the eavesdroppers were imperfect, i.e., the CSI has estimation errors. However, in practice to implement this robust design algorithm one would have to estimate the BS-RIS channel and RIS-UE channels independently. This is difficult to achieve since several active elements would have to be installed at the RIS, increasing the hardware cost and consuming extra power.

In [150], a robust probabilistic-constrained optimization problem is formulated to jointly design the active and passive beamforming vectors at the BS and the RIS. The proposed solution minimizes the total transmit power while maintaining the users' SINR coverage probability above a predefined value. The authors adopted a Bernstein-type inequality to transform the formulated problem into a linear matrix inequality (LMI) form, i.e., into a convex optimization problem and then adopted an alternating optimization (AO) approach to iteratively design the transmit and passive beamforming vectors. Transmit power minimization problems for RIS-aided MISO communication systems are studied in [151, 152]. The authors considered the bounded CSI error and the statistical CSI error models. The CSI uncertainties under a bounded CSI error model were addressed by applying the S-procedure and those under the statistical CSI error model were tackled by using a Bernstein-type inequality. The reformulated problems were efficiently solved under the alternating optimization framework.

However, all the existing contributions on robust beamforming designs for RIS-aided communication systems have been considered for TDD systems. Against this background, we study robust transmission strategies for an RIS-aided DTDD communi-

cation system. Particularly, the work in this chapter is similar to the work in [151,152], but extended to an RIS-aided DTDD system. Both works adopt the S-procedure and a Bernstein-type inequality to respectively recast the resulting intractable problems for the bounded norm and statistical CSI error models, into tractable ones. The difference between an RIS-aided TDD system and that of an RIS-aided DTDD system is the additional cross-link interference in addition to other existing interference (intra-cell and inter-cell interference). The main challenge brought by DTDD is the cross-link interference issue, because adjacent cells may use different TDD frame configurations according to traffic needs at a given time, thereby giving rise to opposite transmission directions among neighboring cells. There are two kinds of cross-link interference: base station-to-base station (BS-to-BS) and user equipment-to-user equipment (UE-to-UE) interference, which may degrade the system performance significantly (see Fig. 6.1). Among the two, the BS-to-BS interference is extremely detrimental due to the large transmit power and LOS propagation characteristics. The robust beamforming problem considered in this chapter is formulated as a sum-power minimization problem for the downlink cells under individual UE's target SINR constraints, interference temperature constraints for the UL cells, and unit-modulus constraints of the RIS in the presence of CSI errors. We assume that the directions of the small cells have been optimized *a priori*, e.g., by using the cell reconfiguration method proposed in [122], and are known at the CPU.

## 6.2 Chapter Contributions and Organization

In this chapter, we consider robust transmission strategies for an RIS-aided DTDD communication system. The contributions of this chapter are summarized as follows:

- Taking the CSI imperfection into consideration, we investigate robust transmission strategies for an RIS-aided DTDD communication system. We address the problem of minimizing the total transmission power of the cells in the downlink direction subject to the following set of QoS constraints:
  1. that the SINR at each UE in the downlink cells is higher than the QoS predefined threshold for all channel realizations;
  2. that the sum interference leakage power at each cell in the uplink direction due to the transmission of the downlink cells is less than the QoS imposed threshold;
  3. that the RIS is a passive device that just changes the phase of the incident signal.

- We consider a conventional worst-case formulation which has deterministic upper bounds on the norms of the channel imperfection. We adopt an SDR technique and S-procedure [131] to reformulate the problem into an SDP form with linear matrix inequality (LMI) constraints. Then, we adopt the AO approach to update the active transmit beamforming vectors and the passive RIS reflection vector sequentially. The worst-case robust beamforming design has been published in [44].
- However, it is impractical to use deterministic upper bounds on the norms of the channel errors. Due to the random nature of the wireless channel, it is more logical to exploit the statistical nature of these imperfections. Motivated by this fact, we introduce a probabilistic-constrained optimization problem, based on the statistical channel error model. Since the adopted probabilistic constraints are non-convex we employ a Bernstein-type inequality [142] to develop a safe (conservative) approximation of the original problem. Then, the SDR technique [140] is used to transform the safe approximation into a tractable SDP which can be optimally solved by a standard interior point method (IPM), e.g., the self-Dual-Minimization (SeDuMi) solver in CVX [135]. Finally, we adopt the AO approach to update the active transmit beamforming vectors and the passive RIS reflection vector iteratively. The probabilistic-constrained robust beamforming design has been published in [45].
- We analyze the performance complexity tradeoff of the considered robust transmission strategies. We show the complexity orders for the design methods when implemented by a generic IPM. Results from our numerical analysis show that the probabilistic-constrained (outage probability) based approach [45] outperforms that of the worst-case design-based robust transmission strategy [44].

The rest of the chapter is organized as follows. The system model is introduced in Section 6.3. The worst-case robust design problem is formulated and solved in Section 6.4. In Section 6.5, the probabilistic-constrained robust design problem is formulated and solved. The computational complexity of the developed robust design methods is analyzed in Section 6.6. Simulation results are then provided in Section 6.7, and conclusions are drawn in Section 6.8.

### 6.3 System Model

In this chapter, we consider an RIS-aided DTDD system consisting of  $Q$  small cells, where each cell has a BS with a ULA of  $M_T$  antennas serving a single UE<sup>1</sup> that is equipped with a single-antenna. As shown in Fig. 6.1, we assume that the communication is aided by an RIS with  $M_S$  passive reflection elements uniformly arranged on a rectangular surface. The RIS has  $M^h$  and  $M^v$  elements in the horizontal and vertical directions, respectively, as shown in Fig. 3.1. Therefore,  $M_S = M^h \cdot M^v$ . The BSs and the RIS are controlled by a CPU via backhaul connections. Similar to [33], we note that due to pathloss the negligible strength of the signals reflected two or more times by the RIS is ignored. We focus on a challenging scenario where the *direct links* are not available due to unfavorable propagation conditions.

Denote  $\mathcal{Q} \triangleq \{1, \dots, Q\}$  as the set of BSs (cells). At the considered time instant, we assume that there are  $|\mathcal{Q}^{\text{ul}}|$  cells operating in the uplink (UL) direction and  $|\mathcal{Q}^{\text{dl}}|$  cells operating in the downlink (DL) direction, such that  $|\mathcal{Q}^{\text{ul}}| + |\mathcal{Q}^{\text{dl}}| = Q$  and  $\mathcal{Q}^{\text{ul}} \cap \mathcal{Q}^{\text{dl}} = \emptyset$ . Note that  $|\mathcal{X}|$  denote the cardinality of set  $\mathcal{X}$ , i.e., the number of elements in set  $\mathcal{X}$ . Let  $\mathbf{H}_q \in \mathbb{C}^{M_S \times M_T}$  be the channel matrix from the  $q$ th BS to the RIS and  $\mathbf{h}_q \in \mathbb{C}^{M_S}$  be the channel vector from the RIS to the  $q$ th UE in the  $q$ th DL cell. Then, the received signal by the UE in the  $q$ th DL cell, i.e.,  $q \in \mathcal{Q}^{\text{dl}}$ , can be expressed as

$$y_q^{(\text{dl})} = \sum_{\forall k \in \mathcal{Q}^{\text{dl}}} (\mathbf{h}_{q,k}^{\text{BS-UE}})^H \mathbf{f}_k x_k + \sum_{\forall r \in \mathcal{Q}^{\text{ul}}} h_{q,r}^{\text{UE-UE}} \sqrt{p_r^{\text{ul}}} x_r + z_q, \quad (6.1)$$

where

$$\mathbf{h}_{q,k}^{\text{BS-UE}} = (\mathbf{h}_q^H \Theta \mathbf{H}_k)^H, \quad (6.2)$$

is the composite BS-UE channel from the BS in the  $q$ th DL cell to the  $q$ th UE in the same cell via the RIS and

$$h_{q,r}^{\text{UE-UE}} = \mathbf{h}_q^H \Theta \mathbf{h}_r, \quad (6.3)$$

is the composite UE-UE channel from the UE in the  $r$ th UL cell to the  $q$ th UE in the  $q$ th DL cell via the RIS. Furthermore,  $\Theta = \text{diag}(\boldsymbol{\theta})$  is the RIS reflection diagonal matrix,  $\boldsymbol{\theta} = [\beta_1 e^{j\phi_1}, \dots, \beta_M e^{j\phi_M}]^T \in \mathbb{C}^{M_S}$ , where  $\beta_m \in [0, 1]$  and  $\phi_m \sim \mathcal{N}(0, 2\pi)$  denote the amplitude and phase shift associated with the  $m$ th element of the RIS, respectively. We assume that  $\beta_m = 1, \forall m$  in this chapter to maximize the signal reflection [32]. Equally,  $\mathbf{f}_k \in \mathbb{C}^{M_T}$  is the transmit beamforming vector with  $\|\mathbf{f}_k\|_2^2 = p_k^{\text{dl}}$ ,  $x_k$  is the zero mean

<sup>1</sup> The extension of the proposed solution to multi-user scenarios is straightforward.

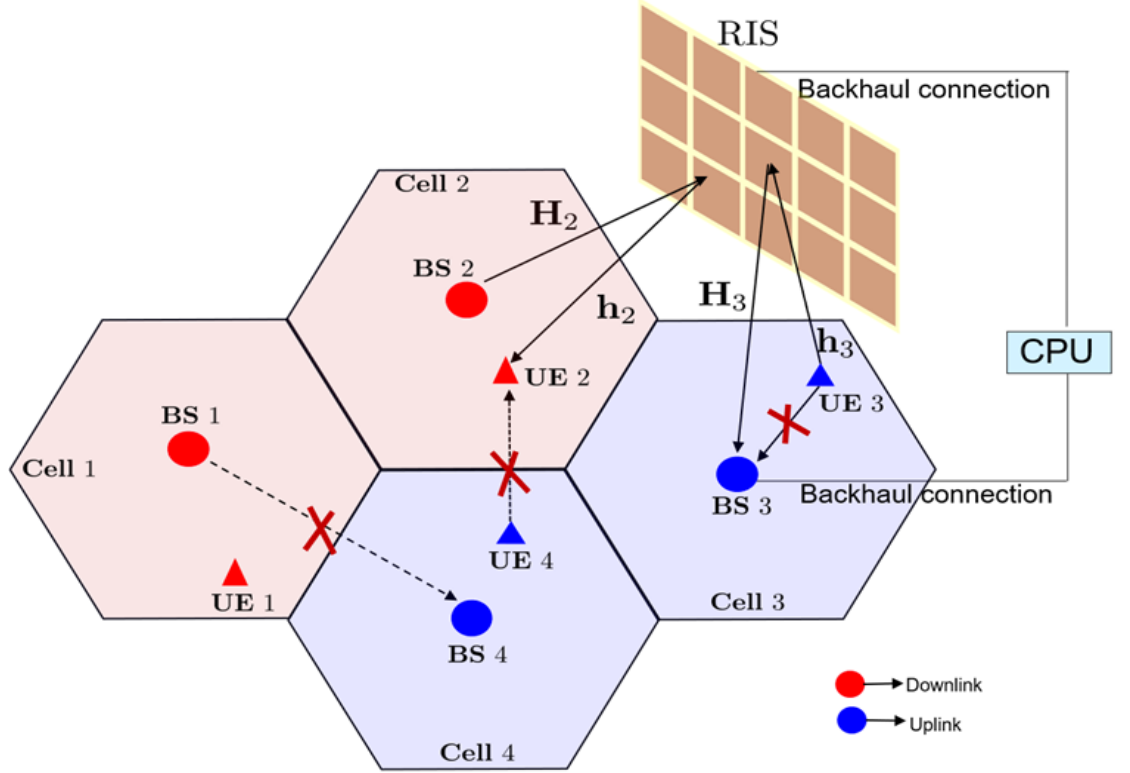


Fig. 6.1: An RIS-aided DTDD system without direct links.

transmit symbol such that  $\mathbb{E}\{|x_k|^2\} = 1$ ,  $z_q$  is additive white complex Gaussian noise with zero mean and variance  $\sigma_q^2$ , and  $p_r^X$  is the transmit power on the  $X \in \{\text{dl}, \text{ul}\}$  direction. Therefore, the SINR of the  $q$ th UE,  $q \in \mathcal{Q}^{\text{dl}}$ , is given as

$$\Gamma_q^{(\text{dl})} = \frac{|(\mathbf{h}_{q,q}^{\text{BS-UE}})^H \mathbf{f}_q|^2}{\sum_{\substack{\forall k \in \mathcal{Q}^{\text{dl}} \\ k \neq q}} |(\mathbf{h}_{q,k}^{\text{BS-UE}})^H \mathbf{f}_k|^2 + \sum_{\forall r \in \mathcal{Q}^{\text{ul}}} |h_{q,r}^{\text{UE-UE}}|^2 p_r^{\text{ul}} + \sigma_q^2}. \quad (6.4)$$

On the other hand, the total received BS-BS interference power at the  $r$ th UL BS, i.e.,  $r \in \mathcal{Q}^{\text{ul}}$ , from the DL BSs, can be expressed as

$$\text{IP}_r = \sum_{\forall q \in \mathcal{Q}^{\text{dl}}} \|\mathbf{H}_{r,q}^{\text{BS-BS}} \mathbf{f}_q\|^2, \quad (6.5)$$

where the effective BS-BS channel from the  $q$ th DL BS to the  $r$ th UL BS is given as

$$\mathbf{H}_{r,q}^{\text{BS-BS}} = \mathbf{H}_r^{\text{H}} \Theta \mathbf{H}_q. \quad (6.6)$$

This interference power should be limited by the interference threshold  $I_{\text{th}}$  in order to guarantee a certain QoS of the UL cells. For ease of computation, we extract the RIS reflection vector in (6.5) as a column vector by using (1.1) and (1.2). As a result, the BS-BS interference power in (6.5) can be written as

$$\text{IP}_r = \sum_{\forall q \in \mathcal{Q}^{\text{dl}}} \|(\mathbf{f}_q^{\text{T}} \otimes \mathbf{I}_{M_{\text{T}}}) \underbrace{(\mathbf{H}_q^{\text{T}} \diamond \mathbf{H}_r^{\text{H}})}_{\mathfrak{J}_{r,q}} \boldsymbol{\theta}\|^2, \quad (6.7)$$

where  $\mathfrak{J}_{r,q} \in \mathbb{C}^{M_{\text{T}}^2 \times M_{\text{S}}}$  is the BS-BS RIS-assisted channel from the  $q$ th DL BS to the  $r$ th UL BS via the RIS. Similarly, to extract the RIS reflection vector as a column vector from (6.4) we apply a change of variable to (6.2) and (6.3), such that the RIS-assisted BS-UE channels from the  $q$ th BS to the UE in the  $q$ th DL cell and from the  $q$ th BS to the UE in the  $k$ th DL cell are given in (6.8) and (6.9), respectively. Furthermore, the RIS-assisted UE-UE channel from the UE in the  $r$ th UL cell to the UE in the  $q$ th DL cell can be written in (6.10),

$$\mathbf{E}_{q,q} = \text{diag}(\mathbf{h}_q^{\text{H}}) \mathbf{H}_q \in \mathbb{C}^{M_{\text{S}} \times M_{\text{T}}}, \quad (6.8)$$

$$\mathbf{E}_{q,k} = \text{diag}(\mathbf{h}_q^{\text{H}}) \mathbf{H}_k \in \mathbb{C}^{M_{\text{S}} \times M_{\text{T}}}, \quad (6.9)$$

$$\mathbf{e}_{q,r} = \text{diag}(\mathbf{h}_q^{\text{H}}) \mathbf{h}_r \in \mathbb{C}^{M_{\text{S}}}. \quad (6.10)$$

To obtain the channel uncertainty model, we adopt the channel estimation protocol proposed in [108, Algorithm 2] for the estimation of the cascaded channels. The estimates of the cascaded channel obtained by using the above channel estimation protocol are given as  $\hat{\mathbf{e}}_{q,r}$ ,  $\hat{\mathbf{E}}_{q,k}$ ,  $\hat{\mathbf{E}}_{q,q}$ , and  $\hat{\mathfrak{J}}_{r,q}$ . Therefore, the exact cascaded channels which are the sum of the estimated cascaded channels and the channel estimation errors, can be represented as

$$\mathbf{e}_{q,r} = \hat{\mathbf{e}}_{q,r} + \boldsymbol{\delta}_{q,r} \quad \forall q, r \in \mathcal{Q}, \quad (6.11)$$

$$\mathbf{E}_{q,q} = \hat{\mathbf{E}}_{q,q} + \boldsymbol{\Delta}_{q,q}, \quad \forall q \in \mathcal{Q}^{\text{dl}}, \quad (6.12)$$

$$\mathbf{E}_{q,k} = \hat{\mathbf{E}}_{q,k} + \boldsymbol{\Delta}_{q,k}, \quad \forall q, k \in \mathcal{Q}^{\text{dl}}, \quad k \neq q, \quad (6.13)$$

$$\mathfrak{J}_{r,q} = \hat{\mathfrak{J}}_{r,q} + \boldsymbol{\Delta}_{r,q}^{(\mathfrak{J})}, \quad \forall q, r \in \mathcal{Q}, \quad (6.14)$$

where  $\boldsymbol{\delta}_{q,r}$ ,  $\boldsymbol{\Delta}_{q,q}$ ,  $\boldsymbol{\Delta}_{q,k}$ , and  $\boldsymbol{\Delta}_{r,q}^{(\mathfrak{J})}$  are the unknown channel estimation errors. These

estimated cascaded channels are known at the BSs through the CPU. Therefore, the SINR  $\Gamma_q^{(\text{dl})}$  of the  $q$ th UE in the  $q$ th DL cell, i.e.,  $q \in \mathcal{Q}^{\text{dl}}$ , given in (6.4) and the UL interference power  $\text{IP}_r$  at the  $r$ th UL cell, i.e.,  $q \in \mathcal{Q}^{\text{dl}}$ , given in (6.5) can be equivalently written as

$$\Gamma_q^{(\text{dl})} = \frac{|\boldsymbol{\theta}^H(\hat{\mathbf{E}}_{q,q} + \boldsymbol{\Delta}_{q,q})\mathbf{f}_q|^2}{\sum_{\substack{\forall k \in \mathcal{Q}^{\text{dl}} \\ k \neq q}} |\boldsymbol{\theta}^H(\hat{\mathbf{E}}_{q,k} + \boldsymbol{\Delta}_{q,k})\mathbf{f}_k|^2 + \sum_{\forall r \in \mathcal{Q}^{\text{ul}}} |\boldsymbol{\theta}^H(\hat{\mathbf{e}}_{q,r} + \boldsymbol{\delta}_{q,r})|^2 p_r^{\text{ul}} + \sigma_q^2}, \quad (6.15)$$

$$\text{IP}_r = \sum_{\forall q \in \mathcal{Q}^{\text{dl}}} \|(\mathbf{f}_q^T \otimes \mathbf{I}_{M_T})(\hat{\boldsymbol{\Delta}}_{r,q} + \boldsymbol{\Delta}_{r,q}^{(\boldsymbol{\Delta})})\boldsymbol{\theta}\|^2. \quad (6.16)$$

We propose a robust approach to minimize the total transmit power of the DL cells in the network, under the constraints of satisfying the SINR requirements at the individual DL UEs, the interference leakage power at each UL cell, and the unit-modulus constraints of the RIS in the presence of channel estimation errors [153].

In the following, we consider two types of robust beamforming designs based on two different channel uncertainty models. First, Section 6.4 considers the worst-case robust beamforming design based on the bounded uncertainty model. Then, we consider the probabilistic-constrained robust beamforming design based on the statistical uncertainty model in Section 6.5.

## 6.4 Worst-case Robust (WCR) Beamforming Design

In this section, we consider the worst-case robust (WCR) beamforming design based on the bounded uncertainty model. We assume that the norm of the channel estimation errors is upper-bounded by some known constants, i.e.,  $\|\boldsymbol{\delta}_{q,r}\|_2 \leq \zeta_{q,r}^{(\boldsymbol{\delta})}$ ,  $\|\boldsymbol{\Delta}_{q,q}\|_{\text{F}} \leq \zeta_{q,q}$ ,  $\|\boldsymbol{\Delta}_{q,k}\|_{\text{F}} \leq \zeta_{q,k}$  and  $\|\boldsymbol{\Delta}_{r,q}^{(\boldsymbol{\Delta})}\|_{\text{F}} \leq \zeta_{r,q}^{(\boldsymbol{\Delta})}$ .

Using this error model, the proposed WCR beamforming approach consists of jointly designing the beamforming vectors  $\mathbf{f}_q \in \mathbb{C}^{M_T}, \forall q \in \mathcal{Q}^{\text{dl}}$ , and the passive reflection vector of the RIS  $\boldsymbol{\theta} \in \mathbb{C}^{M_S}$ , to meet the QoS and interference targets at the DL cells and UL cells, respectively, in all possible error cases described by the error model. The WCR design problem can be mathematically formulated as

$$\min \sum_{\forall q \in \mathcal{Q}^{\text{dl}}} \|\mathbf{f}_q\|^2 \quad (6.17a)$$

$$\text{s.t. } \Gamma_q^{(\text{dl})} \geq \gamma_q \quad \forall q \in \mathcal{Q}^{\text{dl}}, \quad (6.17b)$$

$$\text{IP}_r \leq I_{\text{th}}, \quad \forall r \in \mathcal{Q}^{\text{ul}}, \quad (6.17c)$$

$$\|\boldsymbol{\delta}_{q,r}\|_2 \leq \zeta_{q,r}^{(\boldsymbol{\delta})}, \quad (6.17d)$$

$$\|\boldsymbol{\Delta}_{q,q}\|_F \leq \zeta_{q,q}, \quad (6.17e)$$

$$\|\boldsymbol{\Delta}_{q,k}\|_F \leq \zeta_{q,k}, \quad (6.17f)$$

$$\|\boldsymbol{\Delta}_{r,q}^{(\boldsymbol{\beth})}\|_F \leq \zeta_{r,q}^{(\boldsymbol{\beth})}, \quad (6.17g)$$

$$|\boldsymbol{\theta}[m]| = 1, \quad m = 1, \dots, M_S, \quad (6.17h)$$

where the optimization variables are  $\mathbf{f}_q$  and  $\boldsymbol{\theta}$ . Equation (6.17h) shows the unit-modulus constraints for the RIS reflection coefficients, which indicates that the RIS is a passive device that just changes the phase of the incident signal. Furthermore,  $\gamma_q$  is the QoS-constrained SINR threshold, while  $I_{\text{th}}$  is the uplink interference threshold. Problem (6.17) is non-convex due to its joint optimization of the optimization variables ( $\mathbf{f}_q, q \in \mathcal{Q}^{\text{dl}}, \boldsymbol{\theta}$ ) and the constraints in (6.17h). To obtain a solution, we propose an AO-based algorithm using the S-procedure and SDR techniques (see Appendices D.1 and C.5, respectively).

First, we introduce new slack variables,  $t_{q,k}, \forall k, q \in \mathcal{Q}^{\text{dl}}, k \neq q, I_{r,q}, \forall \{q, r\} \in \mathcal{Q}$ , and  $V_{q,r}, \forall \{q, r\} \in \mathcal{Q}$ . These slack variables will help to decouple the inter-cell interference and the UE-UE cross-link interference terms in (6.15) and the BS-BS cross-link interference term in (6.16). Since  $\boldsymbol{\Delta}_{q,q}$  and  $\boldsymbol{\Delta}_{q,k}$  are independent, problem (6.17) can be recast equivalently as

$$\min \sum_{\forall q \in \mathcal{Q}^{\text{dl}}} \|\mathbf{f}_q\|^2 \quad (6.18a)$$

$$\text{s.t. } |\boldsymbol{\theta}^H(\hat{\mathbf{E}}_{q,q} + \boldsymbol{\Delta}_{q,q})\mathbf{f}_q|^2 \geq \gamma_q \left( \sum_{\substack{\forall k \in \mathcal{Q}^{\text{dl}} \\ k \neq q}} t_{q,k} + \sum_{\forall r \in \mathcal{Q}^{\text{ul}}} V_{q,r} p_r^{\text{ul}} + \sigma_q^2 \right), \quad (6.18b)$$

$$|\boldsymbol{\theta}^H(\hat{\mathbf{E}}_{q,k} + \boldsymbol{\Delta}_{q,k})\mathbf{f}_k|^2 \leq t_{q,k}, \quad (6.18c)$$

$$|\boldsymbol{\theta}^H(\hat{\mathbf{e}}_{q,r} + \boldsymbol{\delta}_{q,r})|^2 \leq V_{q,r}, \quad (6.18d)$$

$$\sum_{\forall q \in \mathcal{Q}^{\text{dl}}} I_{r,q} \leq I_{\text{th}}, \quad \forall r \in \mathcal{Q}^{\text{ul}}, \quad (6.18e)$$

$$\|(\mathbf{f}_q^T \otimes \mathbf{I}_{M_T})(\hat{\boldsymbol{\beth}}_{r,q} + \boldsymbol{\Delta}_{r,q}^{(\boldsymbol{\beth})})\boldsymbol{\theta}\|^2 \leq I_{r,q}, \quad (6.18f)$$

$$\|\boldsymbol{\Delta}_{q,q}\|_F \leq \zeta_{q,q}, \quad (6.18g)$$

$$\|\boldsymbol{\Delta}_{q,k}\|_F \leq \zeta_{q,k}, \quad (6.18h)$$

$$\|\boldsymbol{\delta}_{q,r}\|_2 \leq \zeta_{q,r}^{(\boldsymbol{\delta})}, \quad (6.18i)$$

$$\|\boldsymbol{\Delta}_{r,q}^{(\boldsymbol{\beth})}\|_F \leq \zeta_{r,q}^{(\boldsymbol{\beth})}, \quad (6.18j)$$

$$|\boldsymbol{\theta}[m]| = 1, \quad m = 1, \dots, M_S, \quad (6.18k)$$

where the optimization variables are  $\mathbf{f}_q$ ,  $\boldsymbol{\theta}$ ,  $V_{q,r}$ ,  $t_{q,k}$ , and  $I_{r,q}$ . It can be easily shown (e.g, by contradiction) that the constraints (6.18b), (6.18c), and (6.18d) are tight (i.e., they hold with equality at optimality). Therefore, problem (6.18) is an equivalent reformulation of problem (6.17).

Furthermore, we introduce a new set of variables  $\mathbf{F}_q = \mathbf{f}_q \mathbf{f}_q^H, \forall q \in \mathcal{Q}^{\text{dl}}$  and  $\boldsymbol{\Psi} = \boldsymbol{\theta} \boldsymbol{\theta}^H$ , where  $\mathbf{F}_q \succeq \mathbf{0}, \boldsymbol{\Psi} \succeq \mathbf{0}, \mathbf{F}_q \in \mathbb{H}^{M_T \times M_T}, \boldsymbol{\Psi} \in \mathbb{H}^{M_S \times M_S}$ , and  $\mathbf{F}_q$  and  $\boldsymbol{\Psi}$  are rank-one Hermitian matrices. Using the newly introduced auxiliary variables and the properties given in (1.3), (1.4), and (1.5), the left-hand side (LHS) of the constraints given in (6.18b), (6.18c), (6.18d), and (6.18f) can be expanded, respectively as, (see Appendix D.4 for the detailed derivation),

$$|\boldsymbol{\theta}^H (\hat{\mathbf{E}}_{q,q} + \boldsymbol{\Delta}_{q,q}) \mathbf{f}_q|^2 = \text{vec}^H \{ \boldsymbol{\Delta}_{q,q} \} \underbrace{(\mathbf{F}_q^T \otimes \boldsymbol{\Psi})}_{\mathbf{B}_{q,q}} \text{vec} \{ \boldsymbol{\Delta}_{q,q} \} + 2 \text{Re} \{ \text{vec}^H \{ \boldsymbol{\Delta}_{q,q} \} \underbrace{(\mathbf{F}_q^T \otimes \boldsymbol{\Psi})}_{\mathbf{b}_{q,q}} \text{vec} \{ \hat{\mathbf{E}}_{q,q} \} \} + b_{q,q}, \quad (6.19a)$$

$$|\boldsymbol{\theta}^H (\hat{\mathbf{E}}_{q,k} + \boldsymbol{\Delta}_{q,k}) \mathbf{f}_k|^2 = \text{vec}^H \{ \boldsymbol{\Delta}_{q,k} \} \underbrace{(\mathbf{F}_k^T \otimes \boldsymbol{\Psi})}_{\mathbf{B}_{q,k}} \text{vec} \{ \boldsymbol{\Delta}_{q,k} \} + 2 \text{Re} \{ \text{vec}^H \{ \boldsymbol{\Delta}_{q,k} \} \underbrace{(\mathbf{F}_k^T \otimes \boldsymbol{\Psi})}_{\mathbf{b}_{q,k}} \text{vec} \{ \hat{\mathbf{E}}_{q,k} \} \} + b_{q,k}, \quad (6.19b)$$

$$|\boldsymbol{\theta}^H (\hat{\mathbf{e}}_{q,r} + \boldsymbol{\delta}_{q,r})|^2 = \boldsymbol{\delta}_{q,r}^H \boldsymbol{\Psi} \boldsymbol{\delta}_{q,r} + 2 \text{Re} \{ \boldsymbol{\delta}_{q,r}^H \boldsymbol{\Psi} \hat{\mathbf{e}}_{q,r} \} + \hat{\mathbf{e}}_{q,r}^H \boldsymbol{\Psi} \hat{\mathbf{e}}_{q,r}, \quad (6.19c)$$

$$\|(\mathbf{f}_q^T \otimes \mathbf{I}_{M_T})(\hat{\boldsymbol{\Delta}}_{r,q} + \boldsymbol{\Delta}_{r,q}^{(\boldsymbol{\Delta})}) \boldsymbol{\theta}\|^2 = \text{vec}^H \{ \boldsymbol{\Delta}_{r,q}^{(\boldsymbol{\Delta})} \} \underbrace{(\boldsymbol{\Psi}^T \otimes (\mathbf{F}_q^T \otimes \mathbf{I}_{M_T}))}_{\mathbf{U}_{r,q}} \text{vec} \{ \boldsymbol{\Delta}_{r,q}^{(\boldsymbol{\Delta})} \} + 2 \text{Re} \{ \text{vec}^H \{ \boldsymbol{\Delta}_{r,q}^{(\boldsymbol{\Delta})} \} \underbrace{(\boldsymbol{\Psi}^T \otimes (\mathbf{F}_q^T \otimes \mathbf{I}_{M_T}))}_{\mathbf{u}_{r,q}} \text{vec} \{ \hat{\boldsymbol{\Delta}}_{r,q} \} \} + u_{r,q}, \quad (6.19d)$$

where the scalar terms are given as

$$b_{q,q} = \text{vec}^H \{ \hat{\mathbf{E}}_{q,q} \} (\mathbf{F}_q^T \otimes \boldsymbol{\Psi}) \text{vec} \{ \hat{\mathbf{E}}_{q,q} \}, \quad (6.20a)$$

$$b_{q,k} = \text{vec}^H \{ \hat{\mathbf{E}}_{q,k} \} (\mathbf{F}_k^T \otimes \boldsymbol{\Psi}) \text{vec} \{ \hat{\mathbf{E}}_{q,k} \}, \quad (6.20b)$$

$$u_{r,q} = \text{vec}^H \{ \hat{\boldsymbol{\Delta}}_{r,q} \} (\boldsymbol{\Psi}^T \otimes (\mathbf{F}_q^T \otimes \mathbf{I}_{M_T})) \text{vec} \{ \hat{\boldsymbol{\Delta}}_{r,q} \}. \quad (6.20c)$$

For notational convenience, we define the following variables

$$\mathbf{B}_{q,q} = \mathbf{F}_q^T \otimes \boldsymbol{\Psi} \in \mathbb{C}^{M_T M_S \times M_T M_S} \quad (6.21)$$

$$\mathbf{b}_{q,q} = \mathbf{B}_{q,q} \text{vec} \{ \hat{\mathbf{E}}_{q,q} \} \in \mathbb{C}^{M_T M_S} \quad (6.22)$$

$$\mathbf{B}_{q,k} = \mathbf{F}_k^T \otimes \boldsymbol{\Psi} \quad (6.23)$$

$$\mathbf{b}_{q,k} = \mathbf{B}_{q,k} \text{vec} \{ \hat{\mathbf{E}}_{q,k} \} \in \mathbb{C}^{M_T M_S} \quad (6.24)$$

$$\mathbf{U}_{r,q} = \boldsymbol{\Psi}^T \otimes (\mathbf{F}_q^T \otimes \mathbf{I}_{M_T}) \in \mathbb{C}^{M_S M_T^2 \times M_S M_T^2} \quad (6.25)$$

$$\mathbf{u}_{r,q} = \mathbf{U}_{r,q} \text{vec} \{ \hat{\boldsymbol{\Delta}}_{r,q} \} \in \mathbb{C}^{M_S M_T^2 \times 1}. \quad (6.26)$$

As a result, (6.19) can be written concisely as

$$\begin{aligned}
|\boldsymbol{\theta}^H(\hat{\mathbf{E}}_{q,q} + \boldsymbol{\Delta}_{q,q})\mathbf{f}_q|^2 &= \text{vec}^H\{\boldsymbol{\Delta}_{q,q}\}\mathbf{B}_{q,q}\text{vec}\{\boldsymbol{\Delta}_{q,q}\} + 2\text{Re}\{\text{vec}^H\{\boldsymbol{\Delta}_{q,q}\}\mathbf{b}_{q,q}\} + b_{q,q}, \\
|\boldsymbol{\theta}^H(\hat{\mathbf{E}}_{q,k} + \boldsymbol{\Delta}_{q,k})\mathbf{f}_k|^2 &= \text{vec}^H\{\boldsymbol{\Delta}_{q,k}\}\mathbf{B}_{q,k}\text{vec}\{\boldsymbol{\Delta}_{q,k}\} + 2\text{Re}\{\text{vec}^H\{\boldsymbol{\Delta}_{q,k}\}\mathbf{b}_{q,k}\} + b_{q,k}, \\
|\boldsymbol{\theta}^H(\hat{\mathbf{e}}_{q,r} + \boldsymbol{\delta}_{q,r})|^2 &= \boldsymbol{\delta}_{q,r}^H\boldsymbol{\Psi}\boldsymbol{\delta}_{q,r} + 2\text{Re}\{\boldsymbol{\delta}_{q,r}^H\boldsymbol{\Psi}\hat{\mathbf{e}}_{q,r}\} + \hat{\mathbf{e}}_{q,r}^H\boldsymbol{\Psi}\hat{\mathbf{e}}_{q,r}, \\
\|(\mathbf{f}_q^T \otimes \mathbf{I}_{M_T})(\hat{\boldsymbol{\Delta}}_{r,q} + \boldsymbol{\Delta}_{r,q}^{(\mathfrak{Q})})\boldsymbol{\theta}\|^2 &= \text{vec}^H\{\boldsymbol{\Delta}_{r,q}^{(\mathfrak{Q})}\}\mathbf{U}_{r,q}\text{vec}\{\boldsymbol{\Delta}_{r,q}^{(\mathfrak{Q})}\} + 2\text{Re}\{\text{vec}^H\{\boldsymbol{\Delta}_{r,q}^{(\mathfrak{Q})}\}\mathbf{u}_{r,q}\} + u_{r,q},
\end{aligned}$$

Then, we can rewrite the transmit power minimization problem in (6.18) as

$$\min \sum_{\forall q \in \mathcal{Q}^{\text{dl}}} \text{Tr}\{\mathbf{F}_q\} \quad (6.27\text{a})$$

$$\text{s.t.} \quad \|\boldsymbol{\Delta}_{q,q}\|_F \leq \zeta_{q,q}, \quad (6.27\text{b})$$

$$\|\boldsymbol{\Delta}_{q,k}\|_F \leq \zeta_{q,k}, \quad (6.27\text{c})$$

$$\|\boldsymbol{\delta}_{q,r}\|_2 \leq \zeta_{q,r}^{(\delta)}, \quad (6.27\text{d})$$

$$\|\boldsymbol{\Delta}_{r,q}^{(\mathfrak{Q})}\|_F \leq \zeta_{r,q}^{(\mathfrak{Q})}, \quad (6.27\text{e})$$

$$\sum_{\forall q \in \mathcal{Q}^{\text{dl}}} I_{r,q} \leq I_{\text{th}}, \quad \forall r \in \mathcal{Q}^{\text{ul}}, \quad (6.27\text{f})$$

$$\begin{aligned}
&\text{vec}^H\{\boldsymbol{\Delta}_{q,q}\}\mathbf{B}_{q,q}\text{vec}\{\boldsymbol{\Delta}_{q,q}\} + 2\text{Re}\{\text{vec}^H\{\boldsymbol{\Delta}_{q,q}\}\mathbf{b}_{q,q}\} + b_{q,q} \\
&\quad - \gamma_q \left( \sum_{\substack{\forall k \in \mathcal{Q}^{\text{dl}} \\ k \neq q}} t_{q,k} + \sum_{\forall r \in \mathcal{Q}^{\text{ul}}} V_{q,r} p_r^{\text{ul}} + \sigma_q^2 \right) \geq 0, \quad (6.27\text{g})
\end{aligned}$$

$$t_{q,k} - \text{vec}^H\{\boldsymbol{\Delta}_{q,k}\}\mathbf{B}_{q,k}\text{vec}\{\boldsymbol{\Delta}_{q,k}\} - 2\text{Re}\{\text{vec}^H\{\boldsymbol{\Delta}_{q,k}\}\mathbf{b}_{q,k}\} - b_{q,k} \geq 0 \quad (6.27\text{h})$$

$$V_{q,r} - \boldsymbol{\delta}_{q,r}^H\boldsymbol{\Psi}\boldsymbol{\delta}_{q,r} - 2\text{Re}\{\boldsymbol{\delta}_{q,r}^H\boldsymbol{\Psi}\hat{\mathbf{e}}_{q,r}\} - \hat{\mathbf{e}}_{q,r}^H\boldsymbol{\Psi}\hat{\mathbf{e}}_{q,r} \geq 0 \quad (6.27\text{i})$$

$$I_{r,q} - \text{vec}^H\{\boldsymbol{\Delta}_{r,q}^{(\mathfrak{Q})}\}\mathbf{U}_{r,q}\text{vec}\{\boldsymbol{\Delta}_{r,q}^{(\mathfrak{Q})}\} - 2\text{Re}\{\text{vec}^H\{\boldsymbol{\Delta}_{r,q}^{(\mathfrak{Q})}\}\mathbf{u}_{r,q}\} - u_{r,q} \geq 0 \quad (6.27\text{j})$$

$$\mathbf{F}_q \succeq \mathbf{0}, \quad \text{rank}(\mathbf{F}_q) = 1, \quad (6.27\text{k})$$

$$\text{rank}(\boldsymbol{\Psi}) = 1, \quad \text{diag}\{\boldsymbol{\Psi}\} = \mathbf{1}_{M_S}, \quad \boldsymbol{\Psi} \succeq \mathbf{0}, \quad (6.27\text{l})$$

where the optimization variables are  $\mathbf{F}_q$ ,  $\boldsymbol{\Psi}$ ,  $t_{q,k}$ ,  $V_{q,r}$ , and  $I_{r,q}$ . Problem (6.27) is a semi-infinite optimization problem, i.e., an optimization problem with a finite number of variables and an infinite number of constraints [131]. Furthermore, we can see that constraints (6.27g) and (6.27b) are quadratic in  $\text{vec}\{\boldsymbol{\Delta}_{q,q}\}$ , as it is easy to verify that (6.27b) can be written as  $\text{vec}^H\{\boldsymbol{\Delta}_{q,q}\}\text{vec}\{\boldsymbol{\Delta}_{q,q}\} - \zeta_{q,q}^2 \leq 0$ . Similarly, (6.27h) and (6.27c) are quadratic in  $\text{vec}\{\boldsymbol{\Delta}_{q,k}\}$ ; (6.27i) and (6.27d) are quadratic in  $\boldsymbol{\delta}_{q,r}$ , and also (6.27j) and (6.27e) are quadratic in  $\text{vec}\{\boldsymbol{\Delta}_{r,q}^{(\mathfrak{Q})}\}$ . Therefore, we can leverage on the following lemma to recast these quadratic constraints in such a way that they become linear matrix inequalities (LMIs).

**Lemma 1.** (The *S*-procedure [131, 154]) Let

$$f_i(\mathbf{x}) = \mathbf{x}^H \mathbf{A}_i \mathbf{x} + 2 \operatorname{Re}\{\mathbf{x}^H \mathbf{b}_i\} + c_i, \quad i = 1, 2,$$

where  $\mathbf{A}_i \in \mathbb{H}^{M \times M}$ ,  $\mathbf{b}_i \in \mathbb{C}^M$ , and  $c_i \in \mathbb{R}$ . Suppose that there exists an  $\hat{\mathbf{x}} \in \mathbb{C}^M$  such that  $f_2(\hat{\mathbf{x}}) \leq 0$ . Then, the conditions  $f_1(\mathbf{x}) \geq 0$  and  $f_2(\mathbf{x}) \leq 0$  are satisfied for all  $\mathbf{x} \in \mathbb{C}^M$  if there exists a  $\lambda \geq 0$  such that

$$\begin{bmatrix} \mathbf{A}_1 + \lambda \mathbf{A}_2 & \mathbf{b}_1 + \lambda \mathbf{b}_2 \\ \mathbf{b}_1^H + \lambda \mathbf{b}_2^H & c_1 + \lambda c_2 \end{bmatrix} \succeq \mathbf{0}.$$

The proof of Lemma 1 can be found in Appendix D.1.

Consider first the constraints (6.27g) and (6.27b). According to Lemma 1, the inequality (6.27g) is satisfied for all channel errors  $\operatorname{vec}\{\Delta_{q,q}\}$  that satisfy (6.27b) if there exists  $\lambda_{q,q} \geq 0$  such that the condition

$$\Sigma_{q,q} \triangleq \begin{bmatrix} \mathbf{B}_{q,q} + \lambda_{q,q} \mathbf{I}_{M_T M_S} & \mathbf{b}_{q,q} \\ \mathbf{b}_{q,q}^H & \tilde{k}_{q,q} \end{bmatrix} \succeq \mathbf{0}, \quad \forall q \in \mathcal{Q}^{\text{dl}}, \quad (6.28)$$

is satisfied, where

$$\tilde{k}_{q,q} = b_{q,q} - \gamma_q \left( \sum_{\substack{\forall k \in \mathcal{Q}^{\text{dl}} \\ k \neq q}} t_{q,k} + \sum_{\forall r \in \mathcal{Q}^{\text{ul}}} V_{q,r} p_r^{\text{ul}} + \sigma_q^2 \right) - \lambda_{q,q} \zeta_{q,q}^2. \quad (6.29)$$

Following the same procedure, it follows that the inequality (6.27h) is satisfied for all channel errors  $\operatorname{vec}\{\Delta_{q,k}\}$ , that satisfy (6.27c) if there exists  $\lambda_{q,k} \geq 0$  such that the condition

$$\Phi_{q,k} \triangleq \begin{bmatrix} -\mathbf{B}_{q,k} + \lambda_{q,k} \mathbf{I}_{M_T M_S} & -\mathbf{b}_{q,k} \\ -\mathbf{b}_{q,k}^H & \tilde{k}_{q,k} \end{bmatrix} \succeq \mathbf{0}, \quad \forall k, q \in \mathcal{Q}^{\text{dl}}, \quad k \neq q, \quad (6.30)$$

is satisfied, where  $\tilde{k}_{q,k} = -b_{q,k} - \lambda_{q,k} \zeta_{q,k}^2 + t_{q,k}$ . Equally, the inequality in (6.27i) is satisfied for all channel error  $\delta_{q,r}$ , that satisfy (6.27d) if there exists  $\ell_{q,r} \geq 0$  such that the condition

$$\mathbf{U}_{q,r} \triangleq \begin{bmatrix} -\Psi + \ell_{q,r} \mathbf{I}_{M_S} & -\Psi \hat{\mathbf{e}}_{q,r} \\ -(\Psi \hat{\mathbf{e}}_{q,r})^H & \tilde{k}_{q,r} \end{bmatrix} \succeq \mathbf{0}, \quad \forall r \in \mathcal{Q}^{\text{ul}}, \quad \forall q \in \mathcal{Q}^{\text{dl}} \quad (6.31)$$

is satisfied, where  $\tilde{k}_{q,r} = -\hat{e}_{q,r}^H \Psi \hat{e}_{q,r} - \ell_{q,r} \{\zeta_{q,r}^{(\delta)}\}^2 + V_{q,r}$ . Similarly, the inequality (6.27j) is satisfied for all channel error  $\text{vec}\{\Delta_{r,q}^{(\mathfrak{D})}\}$  that satisfy (6.27e) if there exists  $\varpi_{r,q} \geq 0$  such that the condition

$$\mathbf{\Omega}_{r,q} \triangleq \begin{bmatrix} -\mathbf{U}_{r,q} + \varpi_{r,q} \mathbf{I}_{M_T^2, M_S} & -\mathbf{u}_{r,q} \\ -\mathbf{u}_{r,q}^H & \tilde{k}_{r,q} \end{bmatrix} \succeq \mathbf{0}, \forall r \in \mathcal{Q}^{\text{ul}}, \forall q \in \mathcal{Q}^{\text{dl}} \quad (6.32)$$

is satisfied, where  $\tilde{k}_{r,q} = -u_{r,q} - \varpi_{r,q} \{\zeta_{r,q}^{(\mathfrak{D})}\}^2 + I_{r,q}$ . Thus, we can rewrite problem (6.27) equivalently as follows:

$$\min \sum_{\forall q \in \mathcal{Q}^{\text{dl}}} \text{Tr}\{\mathbf{F}_q\} \quad (6.33a)$$

$$\text{s.t. } \mathbf{\Sigma}_{q,q} \succeq \mathbf{0}, \forall q \in \mathcal{Q}^{\text{dl}} \quad (6.33b)$$

$$\mathbf{\Phi}_{q,k} \succeq \mathbf{0}, \lambda_{q,k} \geq 0, \forall k, q \in \mathcal{Q}^{\text{dl}}, k \neq q \quad (6.33c)$$

$$\mathbf{U}_{q,r} \succeq \mathbf{0}, \mathbf{\Omega}_{r,q} \succeq \mathbf{0}, \forall r \in \mathcal{Q}^{\text{ul}}, \forall q \in \mathcal{Q}^{\text{dl}} \quad (6.33d)$$

$$\ell_{q,r} \geq 0, \varpi_{r,q} \geq 0, \forall q \in \mathcal{Q}^{\text{dl}}, \forall r \in \mathcal{Q}^{\text{ul}} \quad (6.33e)$$

$$\sum_{\forall q \in \mathcal{Q}^{\text{dl}}} I_{r,q} \leq I_{\text{th}}, \forall r \in \mathcal{Q}^{\text{ul}}, \quad (6.33f)$$

$$\mathbf{F}_q \succeq \mathbf{0}, \text{rank}(\mathbf{F}_q) = 1, \quad (6.33g)$$

$$\text{rank}(\mathbf{\Psi}) = 1, \text{diag}\{\mathbf{\Psi}\} = \mathbf{1}_{M_S}, \mathbf{\Psi} \succeq \mathbf{0}, \quad (6.33h)$$

where the optimization variables are  $\mathbf{F}_q, \lambda_{q,k}, \varpi_{r,q}, \mathbf{\Psi}, t_{q,k}, V_{q,r}, \ell_{q,r}$  and  $I_{r,q}$ . Problem (6.33) is still non-convex and hard to solve due to the rank-one constraints, and the coupling between  $\mathbf{F}_q$  and  $\mathbf{\Psi}$  in  $\mathbf{\Sigma}_{q,q}, \mathbf{\Phi}_{q,k}, \mathbf{U}_{q,r}$ , and  $\mathbf{\Omega}_{q,r}$ . In the following, we adopt the AO approach to design  $\mathbf{F}_q$  and  $\mathbf{\Psi}$  alternately in an iterative manner. In particular, for a given  $\mathbf{\Psi}$ , we solve the following sub-problem of  $\mathbf{F}_q$  during the  $i$ th iteration

$$\min \sum_{\forall q \in \mathcal{Q}^{\text{dl}}} \text{Tr}\{\mathbf{F}_q^{(i)}\} \quad (6.34a)$$

$$\text{s.t. } \mathbf{\Sigma}_{q,q} \succeq \mathbf{0}, \forall q \in \mathcal{Q}^{\text{dl}} \quad (6.34b)$$

$$\mathbf{\Phi}_{q,k} \succeq \mathbf{0}, \lambda_{q,k} \geq 0, \forall k, q \in \mathcal{Q}^{\text{dl}}, k \neq q \quad (6.34c)$$

$$\mathbf{U}_{q,r} \succeq \mathbf{0}, \mathbf{\Omega}_{r,q} \succeq \mathbf{0}, \forall r \in \mathcal{Q}^{\text{ul}}, \forall q \in \mathcal{Q}^{\text{dl}} \quad (6.34d)$$

$$\ell_{q,r} \geq 0, \varpi_{r,q} \geq 0, \forall q \in \mathcal{Q}^{\text{dl}}, \forall r \in \mathcal{Q}^{\text{ul}} \quad (6.34e)$$

$$\sum_{\forall q \in \mathcal{Q}^{\text{dl}}} I_{r,q} \leq I_{\text{th}}, \forall r \in \mathcal{Q}^{\text{ul}}, \quad (6.34f)$$

$$\mathbf{F}_q \succeq \mathbf{0}, \quad (6.34g)$$

$$\text{rank}(\mathbf{F}_q) = 1, \quad (6.34h)$$

where the optimization variables are  $\mathbf{F}_q$ ,  $\lambda_{q,k}$ ,  $\varpi_{r,q}$ ,  $t_{q,k}$ ,  $V_{q,r}$ ,  $\ell_{q,r}$ , and  $I_{r,q}$ . Problem (6.34) is a rank-constrained SDP. Therefore, we adopt the SDR technique and relax the rank-one constraint in (6.34h), so problem (6.34) becomes

$$\min \sum_{\forall q \in \mathcal{Q}^{\text{dl}}} \text{Tr}\{\mathbf{F}_q^{(i)}\} \quad (6.35\text{a})$$

$$\text{s.t. } \boldsymbol{\Sigma}_{q,q} \succeq \mathbf{0}, \forall q \in \mathcal{Q}^{\text{dl}} \quad (6.35\text{b})$$

$$\boldsymbol{\Phi}_{q,k} \succeq \mathbf{0}, \lambda_{q,k} \geq 0, \forall k, q \in \mathcal{Q}^{\text{dl}}, k \neq q \quad (6.35\text{c})$$

$$\boldsymbol{\mathcal{U}}_{q,r} \succeq \mathbf{0}, \boldsymbol{\Omega}_{r,q} \succeq \mathbf{0}, \forall r \in \mathcal{Q}^{\text{ul}}, \forall q \in \mathcal{Q}^{\text{dl}} \quad (6.35\text{d})$$

$$\ell_{q,r} \geq 0, \varpi_{r,q} \geq 0, \forall q \in \mathcal{Q}^{\text{dl}}, \forall r \in \mathcal{Q}^{\text{ul}} \quad (6.35\text{e})$$

$$\sum_{\forall q \in \mathcal{Q}^{\text{dl}}} I_{r,q} \leq I_{\text{th}}, \forall r \in \mathcal{Q}^{\text{ul}}, \quad (6.35\text{f})$$

$$\mathbf{F}_q \succeq \mathbf{0}. \quad (6.35\text{g})$$

Therefore, the resulting problem becomes a convex SDP and can be solved via CVX [135] for a given  $\boldsymbol{\Psi}^{(i-1)}$ . With the obtained solution of problem (6.35), the sub-problem of  $\boldsymbol{\Psi}^{(i)}$  becomes a feasibility-check problem given as

$$\text{Find } \boldsymbol{\Psi}^{(i)} \quad (6.36\text{a})$$

$$\text{s.t. } \boldsymbol{\Sigma}_{q,q} \succeq \mathbf{0}, \forall q \in \mathcal{Q}^{\text{dl}} \quad (6.36\text{b})$$

$$\boldsymbol{\Phi}_{q,k} \succeq \mathbf{0}, \lambda_{q,k} \geq 0, \forall k, q \in \mathcal{Q}^{\text{dl}}, k \neq q \quad (6.36\text{c})$$

$$\boldsymbol{\mathcal{U}}_{q,r} \succeq \mathbf{0}, \boldsymbol{\Omega}_{r,q} \succeq \mathbf{0}, \forall r \in \mathcal{Q}^{\text{ul}}, \forall q \in \mathcal{Q}^{\text{dl}} \quad (6.36\text{d})$$

$$\ell_{q,r} \geq 0, \varpi_{r,q} \geq 0, \forall q \in \mathcal{Q}^{\text{dl}}, \forall r \in \mathcal{Q}^{\text{ul}} \quad (6.36\text{e})$$

$$\sum_{\forall q \in \mathcal{Q}^{\text{dl}}} I_{r,q} \leq I_{\text{th}}, \forall r \in \mathcal{Q}^{\text{ul}}, \quad (6.36\text{f})$$

$$\text{diag}\{\boldsymbol{\Psi}\} = \mathbf{1}_{M_S}, \boldsymbol{\Psi} \succeq \mathbf{0}, \quad (6.36\text{g})$$

$$\text{rank}(\boldsymbol{\Psi}) = 1, \quad (6.36\text{h})$$

To further improve the converged solution in the optimization of  $\boldsymbol{\Psi}^{(i)}$ , we introduce a slack variable  $\omega_q$ , which is interpreted as the SINR residual of the users [33]. Therefore, the feasibility-check problem in (6.36) can be reformulated as

$$\max \sum_{\forall q \in \mathcal{Q}^{\text{dl}}} \omega_q \quad (6.37\text{a})$$

$$\text{s.t. } \boldsymbol{\Phi}_{q,k} \succeq \mathbf{0}, \lambda_{q,k} \geq 0, \forall k, q \in \mathcal{Q}^{\text{dl}}, k \neq q \quad (6.37\text{b})$$

$$\boldsymbol{\mathcal{U}}_{q,r} \succeq \mathbf{0}, \boldsymbol{\Omega}_{r,q} \succeq \mathbf{0}, \forall r \in \mathcal{Q}^{\text{ul}}, \forall q \in \mathcal{Q}^{\text{dl}} \quad (6.37\text{c})$$

$$\ell_{q,r} \geq 0, \varpi_{r,q} \geq 0, \forall q \in \mathcal{Q}^{\text{dl}}, \forall r \in \mathcal{Q}^{\text{ul}} \quad (6.37\text{d})$$

$$\sum_{\forall q \in \mathcal{Q}^{\text{dl}}} I_{r,q} \leq I_{\text{th}}, \forall r \in \mathcal{Q}^{\text{ul}}, \quad (6.37\text{e})$$

$$\text{diag}\{\mathbf{\Psi}\} = \mathbf{1}_{M_S}, \mathbf{\Psi} \succeq \mathbf{0}, \quad (6.37\text{f})$$

$$\text{rank}(\mathbf{\Psi}) = 1 \quad (6.37\text{g})$$

$$\text{modified-(6.36b)} \quad (6.37\text{h})$$

$$\omega_q \geq 0, \forall q \in \mathcal{Q}^{\text{dl}}, \quad (6.37\text{i})$$

where the optimization variables are  $\omega_q$ , and  $\mathbf{\Psi}^{(i)}$ . The constraint in (6.37h) is obtained by replacing the constant  $\tilde{k}_{q,q}$  in  $\Sigma_{q,q}$  of (6.28) with

$$\bar{k}_{q,q} = b_{q,q} - \gamma_q \left( \sum_{\substack{\forall k \in \mathcal{Q}^{\text{dl}} \\ k \neq q}} t_{q,k} + \sum_{\forall r \in \mathcal{Q}^{\text{ul}}} V_{q,r} p_r^{\text{ul}} + \sigma_q^2 \right) - \lambda_{q,q} \zeta_{q,q}^2 - \omega_q. \quad (6.38)$$

We adopt the SDR technique to transform the rank-constrained problem (6.37) into a convex SDP by relaxing the rank-one constraint in (6.37g). The resulting convex SDP can be solved using CVX tools.

$$\max \sum_{\forall q \in \mathcal{Q}^{\text{dl}}} \omega_q \quad (6.39\text{a})$$

$$\text{s.t. } \mathbf{\Phi}_{q,k} \succeq \mathbf{0}, \lambda_{q,k} \geq 0, \forall k, q \in \mathcal{Q}^{\text{dl}}, k \neq q \quad (6.39\text{b})$$

$$\mathbf{U}_{q,r} \succeq \mathbf{0}, \mathbf{\Omega}_{r,q} \succeq \mathbf{0}, \forall r \in \mathcal{Q}^{\text{ul}}, \forall q \in \mathcal{Q}^{\text{dl}} \quad (6.39\text{c})$$

$$\ell_{q,r} \geq 0, \varpi_{r,q} \geq 0, \forall q \in \mathcal{Q}^{\text{dl}}, \forall r \in \mathcal{Q}^{\text{ul}} \quad (6.39\text{d})$$

$$\sum_{\forall q \in \mathcal{Q}^{\text{dl}}} I_{r,q} \leq I_{\text{th}}, \forall r \in \mathcal{Q}^{\text{ul}}, \quad (6.39\text{e})$$

$$\text{diag}\{\mathbf{\Psi}\} = \mathbf{1}_{M_S}, \mathbf{\Psi} \succeq \mathbf{0} \quad (6.39\text{f})$$

$$\text{modified-(6.36b)} \quad (6.39\text{g})$$

$$\omega_q \geq 0, \forall q \in \mathcal{Q}^{\text{dl}} \quad (6.39\text{h})$$

It can be seen that (6.35) and (6.39) are convex problems and their feasible domains are convex sets. Hence, the proposed AO-based algorithm will converge to a fixed point solution when the sub-problems (6.35) and (6.39) are feasible.

Finally, we can obtain the active beamforming vector  $\mathbf{f}_q \in \mathbb{C}^{M_T}$ ,  $\forall q \in \mathcal{Q}^{\text{dl}}$  and the passive reflection vector  $\boldsymbol{\theta} \in \mathbb{C}^{M_S}$ , based on the solutions obtained from (6.35) and (6.39), respectively. It is noted that the considered SDP problems have relaxed the rank-one constraint. However, the rank of the obtained solutions may not be 1. If the rank is 1, then  $\mathbf{f}_q \in \mathbb{C}^{M_T}$ ,  $\forall q \in \mathcal{Q}^{\text{dl}}$  and  $\boldsymbol{\theta} \in \mathbb{C}^{M_S}$  can be obtain by using an eigenvalue decomposition. Otherwise, we can obtain a high-quality rank-one solution by applying

Gaussian randomization [139, 140] (see Appendix C.5). The AO-based algorithm for the WCR beamforming design for an RIS-aided DTDD system is outlined in Fig. 6.2.

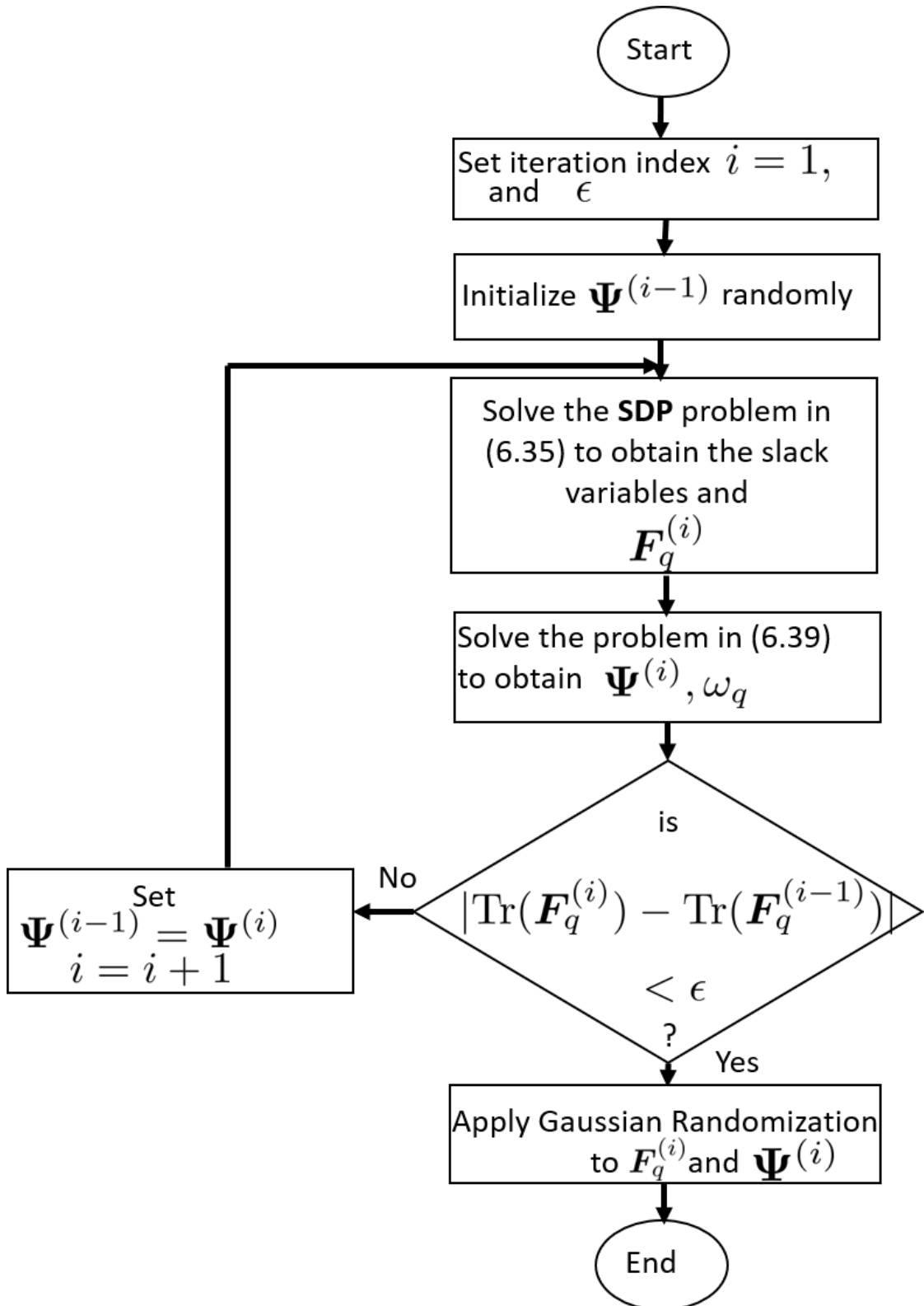


Fig. 6.2: Flow chart for the implementation of the WCR AO-based algorithm.

## 6.5 Probabilistic-Constrained Robust (PCR) Optimization

In the previous section, bounded-norm conditions have been implicitly imposed on the channel estimation errors. However, such a conservative model may not reflect practical channels accurately, since the channel error bound cannot be obtained exactly. Moreover, the worst-case approach in Section 6.5 can be overly pessimistic due to the fact that the probability of the actual worst-case errors may be extremely low [155].

To overcome this problem, we adopt a different approach in this section to obtain another robust formulation using more flexible and realistic probabilistic constraints. In the following, we consider the statistical uncertainty model

$$\text{vec}\{\mathbf{\Delta}_{q,q}\} \sim \mathcal{CN}(\mathbf{0}, \mathbf{\Xi}_{q,q}), \mathbf{\Xi}_{q,q} \succ \mathbf{0}, \forall q \in \mathcal{Q}^{\text{dl}}, \quad (6.40)$$

$$\text{vec}\{\mathbf{\Delta}_{q,k}\} \sim \mathcal{CN}(\mathbf{0}, \mathbf{\Xi}_{q,k}), \mathbf{\Xi}_{q,k} \succ \mathbf{0}, \forall k, q \in \mathcal{Q}^{\text{dl}}, k \neq q, \quad (6.41)$$

$$\text{vec}\{\mathbf{\Delta}_{r,q}^{(\mathfrak{J})}\} \sim \mathcal{CN}(\mathbf{0}, \mathbf{\Xi}_{r,q}^{(\mathfrak{J})}), \mathbf{\Xi}_{r,q}^{(\mathfrak{J})} \succ \mathbf{0}, \forall r, q \in \mathcal{Q}, \quad (6.42)$$

$$\boldsymbol{\delta}_{q,r} \sim \mathcal{CN}(\mathbf{0}, \mathbf{\Xi}_{q,r}^{(\delta)}), \mathbf{\Xi}_{q,r}^{(\delta)} \succ \mathbf{0}, \forall r, q \in \mathcal{Q}, \quad (6.43)$$

where  $\mathbf{\Xi}_{q,q} \in \mathbb{C}^{M_S M_T \times M_S M_T}$ ,  $\mathbf{\Xi}_{q,k} \in \mathbb{C}^{M_S M_T \times M_S M_T}$ ,  $\mathbf{\Xi}_{r,q}^{(\mathfrak{J})} \in \mathbb{C}^{M_T^2 M_S \times M_T^2 M_S}$ , and  $\mathbf{\Xi}_{q,r}^{(\delta)} \in \mathbb{C}^{M_S \times M_S}$  are positive definite error covariance matrices. Since the statistical distributions of the CSI errors are known, the QoS can be only guaranteed in a probabilistic sense. The resulting probabilistic-constrained power minimization problem can be written as

$$\min \sum_{\forall q \in \mathcal{Q}^{\text{dl}}} \|\mathbf{f}_q\|^2 \quad (6.44a)$$

$$\text{s.t.} \quad \Pr \left( |\boldsymbol{\theta}^H (\hat{\mathbf{E}}_{q,q} + \mathbf{\Delta}_{q,q}) \mathbf{f}_q|^2 \geq \gamma_q \left\{ \sum_{\substack{\forall k \in \mathcal{Q}^{\text{dl}} \\ k \neq q}} t_{q,k} + \sum_{\forall r \in \mathcal{Q}^{\text{ul}}} V_{q,r} p_r^{\text{ul}} + \sigma_q^2 \right\} \right) \geq 1 - \rho_{q,q} \quad (6.44b)$$

$$\Pr \left( |\boldsymbol{\theta}^H (\hat{\mathbf{E}}_{q,k} + \mathbf{\Delta}_{q,k}) \mathbf{f}_k|^2 \leq t_{q,k} \right) \geq 1 - \rho_{q,k} \quad (6.44c)$$

$$\Pr \left( |\boldsymbol{\theta}^H (\hat{\mathbf{e}}_{q,r} + \boldsymbol{\delta}_{q,r})|^2 \leq V_{q,r} \right) \geq 1 - \rho_{q,r} \quad (6.44d)$$

$$\Pr \left( \|(\mathbf{f}_q^T \otimes \mathbf{I}_{M_T})(\hat{\mathbf{\Delta}}_{r,q} + \mathbf{\Delta}_{r,q}^{(\mathfrak{J})}) \boldsymbol{\theta}\|^2 \leq I_{r,q} \right) \geq 1 - \tilde{\rho}_{r,q}, \quad (6.44e)$$

$$\sum_{\forall q \in \mathcal{Q}^{\text{dl}}} I_{r,q} \leq I_{\text{th}} \quad (6.44f)$$

$$|\boldsymbol{\theta}[m]| = 1, m = 1, \dots, M_S, \quad (6.44g)$$

where the optimization variables are  $\mathbf{f}_q$ ,  $\boldsymbol{\theta}$ ,  $I_{r,q}$ ,  $t_{q,k}$ , and  $V_{q,r}$ . Similar to Section 6.5 we

have introduced the new slack variables,  $t_{q,k}$ ,  $\forall k, q \in \mathcal{Q}^{\text{dl}}, k \neq q$ ,  $I_{r,q}$ ,  $\forall \{q, r\} \in \mathcal{Q}$ , and  $V_{q,r}$ ,  $\forall \{q, r\} \in \mathcal{Q}$ . These slack variables will help to decouple the inter-cell interference (6.44c) and the UE-UE cross-link interference (6.44d) terms in the SINR of the  $q$ th UE in the  $q$ th DL cell as defined in (6.15) and the BS-BS cross-link interference term (6.44e) in (6.16). Moreover,  $\rho_{q,q} \in (0, 1]$ ,  $\tilde{\varrho}_{r,q} \in (0, 1]$ , and  $\varrho_{q,r} \in (0, 1]$  are the preselected tolerable (small) outage probabilities of SINR-outages and leakage-outages, respectively. The constraints in (6.44b) and (6.44e) ensure that the outage probability of each DL user and the QoS constraint at each UL receiver should be no less than  $\rho_{q,q}$  and  $\tilde{\varrho}_{r,q}$ , respectively.

As in Section 6.4, we introduce the following variables,  $\mathbf{F}_q = \mathbf{f}_q \mathbf{f}_q^H$ , and  $\Psi = \boldsymbol{\theta} \boldsymbol{\theta}^H$ , where  $\mathbf{F}_q \succeq \mathbf{0}$ ,  $\Psi \succeq \mathbf{0}$ ,  $\mathbf{F}_q \in \mathbb{H}^{M_T \times M_T}$ ,  $\Psi \in \mathbb{H}^{M_S \times M_S}$ , and  $\mathbf{F}_q$  and  $\Psi$  are rank-one Hermitian matrices. Furthermore, as in Section 6.4 the power terms in the constraints given in (6.44b)-(6.44e) can be expressed as (see Appendix D.4 for the detailed derivation),

$$|\boldsymbol{\theta}^H(\hat{\mathbf{E}}_{q,q} + \Delta_{q,q})\mathbf{f}_q|^2 = \text{vec}^H\{\Delta_{q,q}\}(\mathbf{F}_q^T \otimes \Psi)\text{vec}\{\Delta_{q,q}\} + 2 \text{Re}\{\text{vec}^H\{\Delta_{q,q}\}(\mathbf{F}_q^T \otimes \Psi)\text{vec}\{\hat{\mathbf{E}}_{q,q}\}\} \\ + \text{vec}^H\{\hat{\mathbf{E}}_{q,q}\}(\mathbf{F}_q^T \otimes \Psi)\text{vec}\{\hat{\mathbf{E}}_{q,q}\}, \quad (6.45a)$$

$$|\boldsymbol{\theta}^H(\hat{\mathbf{E}}_{q,k} + \Delta_{q,k})\mathbf{f}_k|^2 = \text{vec}^H\{\Delta_{q,k}\}(\mathbf{F}_k^T \otimes \Psi)\text{vec}\{\Delta_{q,k}\} + 2 \text{Re}\{\text{vec}^H\{\Delta_{q,k}\}(\mathbf{F}_k^T \otimes \Psi)\text{vec}\{\hat{\mathbf{E}}_{q,k}\}\} \\ + \text{vec}^H\{\hat{\mathbf{E}}_{q,k}\}(\mathbf{F}_k^T \otimes \Psi)\text{vec}\{\hat{\mathbf{E}}_{q,k}\}, \quad (6.45b)$$

$$|\boldsymbol{\theta}^H(\hat{e}_{q,r} + \delta_{q,r})|^2 = \delta_{q,r}^H \Psi \delta_{q,r} + 2 \text{Re}\{\delta_{q,r}^H \Psi \hat{e}_{q,r}\} + \hat{e}_{q,r}^H \Psi \hat{e}_{q,r}, \quad (6.45c)$$

$$\|(\mathbf{f}_q^T \otimes \mathbf{I}_{M_T})(\hat{\boldsymbol{\Sigma}}_{r,q} + \Delta_{r,q}^{(\boldsymbol{\Sigma})})\boldsymbol{\theta}\|^2 = \text{vec}^H\{\Delta_{r,q}^{(\boldsymbol{\Sigma})}\}(\Psi^T \otimes (\mathbf{F}_q^T \otimes \mathbf{I}_{M_T}))\text{vec}\{\Delta_{r,q}^{(\boldsymbol{\Sigma})}\} \\ + 2 \text{Re}\{\text{vec}^H\{\Delta_{r,q}^{(\boldsymbol{\Sigma})}\}(\Psi^T \otimes (\mathbf{F}_q^T \otimes \mathbf{I}_{M_T}))\text{vec}\{\hat{\boldsymbol{\Sigma}}_{r,q}\}\} + \text{vec}^H\{\hat{\boldsymbol{\Sigma}}_{r,q}\}(\Psi^T \otimes (\mathbf{F}_q^T \otimes \mathbf{I}_{M_T}))\text{vec}\{\hat{\boldsymbol{\Sigma}}_{r,q}\}. \quad (6.45d)$$

For simplicity, let us simplify the covariance matrices of the CSI errors given in (6.40)-(6.43) as

$$\begin{aligned} \Xi_{q,q} &= \eta_{q,q}^2 \mathbf{I}_{M_S M_T}, \\ \Xi_{q,k} &= \eta_{q,k}^2 \mathbf{I}_{M_S M_T}, \\ \Xi_{r,q}^{(\boldsymbol{\Sigma})} &= (\eta_{r,q}^{(\boldsymbol{\Sigma})})^2 \mathbf{I}_{M_T^2 M_S}, \\ \Xi_{q,r}^{(\delta)} &= (\eta_{q,r}^{(\delta)})^2 \mathbf{I}_{M_S} \end{aligned}$$

where  $\eta_{q,q}^2$ ,  $\eta_{q,k}^2$ ,  $(\eta_{r,q}^{(\boldsymbol{\Sigma})})^2$ , and  $(\eta_{q,r}^{(\delta)})^2$  are the error variances. Then the CSI errors can be written as

$$\text{vec}\{\Delta_{q,q}\} = \eta_{q,q} \boldsymbol{\lambda}_{q,q}, \quad (6.46a)$$

$$\text{vec}\{\Delta_{q,k}\} = \eta_{q,q} \boldsymbol{\lambda}_{q,k}, \quad (6.46b)$$

$$\text{vec}\{\Delta_{r,q}^{(\boldsymbol{\Sigma})}\} = \eta_{r,q}^{(\boldsymbol{\Sigma})} \boldsymbol{\lambda}_{r,q}^{(\boldsymbol{\Sigma})}, \quad (6.46c)$$

$$\boldsymbol{\delta}_{q,r}^{(\delta)} = \eta_{q,r}^{(\delta)} \boldsymbol{\lambda}_{q,r}^{(\delta)}, \quad (6.46d)$$

where,

$$\boldsymbol{\lambda}_{q,q} \sim \mathcal{CN}(\mathbf{0}, \mathbf{I}_{M_S M_T}) \quad (6.47)$$

$$\boldsymbol{\lambda}_{q,k} \sim \mathcal{CN}(\mathbf{0}, \mathbf{I}_{M_S M_T}) \quad (6.48)$$

$$\boldsymbol{\lambda}_{r,q} \sim \mathcal{CN}(\mathbf{0}, \mathbf{I}_{M_T^2 M_S}) \quad (6.49)$$

$$\boldsymbol{\lambda}_{q,r} \sim \mathcal{CN}(\mathbf{0}, \mathbf{I}_{M_S}), \quad (6.50)$$

are the standard zero mean circularly symmetric complex Gaussian random vectors. Therefore, using (6.45a)-(6.45d) and (6.46a)-(6.46d) the constraints in (6.44b)-(6.44e) can be expressed as

$$\Pr \left( \underbrace{\boldsymbol{\lambda}_{q,q}^H \eta_{q,q}^2 (\mathbf{F}_q^T \otimes \boldsymbol{\Psi}) \boldsymbol{\lambda}_{q,q}}_{D_{q,q}} + 2 \operatorname{Re} \left\{ \underbrace{\boldsymbol{\lambda}_{q,q}^H \eta_{q,q} (\mathbf{F}_q^T \otimes \boldsymbol{\Psi}) \operatorname{vec}\{\hat{\mathbf{E}}_{q,q}\}}_{d_{q,q}} \right\} + d_{q,q} \geq 0 \right) \geq 1 - \rho_{q,q} \quad (6.51a)$$

$$\Pr \left( \underbrace{\boldsymbol{\lambda}_{q,k}^H \eta_{q,k}^2 (\mathbf{F}_k^T \otimes \boldsymbol{\Psi}) \boldsymbol{\lambda}_{q,k}}_{D_{q,k}} + 2 \operatorname{Re} \left\{ \underbrace{\boldsymbol{\lambda}_{q,k}^H \eta_{q,k} (\mathbf{F}_k^T \otimes \boldsymbol{\Psi}) \operatorname{vec}\{\hat{\mathbf{E}}_{q,k}\}}_{d_{q,k}} \right\} + d_{q,k} \leq t_{q,k} \right) \geq 1 - \rho_{q,k} \quad (6.51b)$$

$$\Pr \left( \underbrace{(\boldsymbol{\lambda}_{q,r}^{(\delta)})^H (\eta_{q,r}^{(\delta)})^2 \boldsymbol{\Psi} (\boldsymbol{\lambda}_{q,r}^{(\delta)})}_{A_{q,r}} + 2 \operatorname{Re} \left\{ \underbrace{(\boldsymbol{\lambda}_{q,r}^{(\delta)})^H \eta_{q,r}^{(\delta)} \boldsymbol{\Psi} \hat{\mathbf{e}}_{q,r}}_{a_{q,r}} \right\} + a_{q,r} \leq V_{q,r} \right) \geq 1 - \rho_{q,r} \quad (6.51c)$$

$$\Pr \left( \underbrace{(\boldsymbol{\lambda}_{r,q}^{(\zeta)})^H (\eta_{r,q}^{(\zeta)})^2 (\boldsymbol{\Psi}^T \otimes (\mathbf{F}_q^T \otimes \mathbf{I}_{M_T})) (\boldsymbol{\lambda}_{r,q}^{(\zeta)})}_{U_{r,q}} + 2 \operatorname{Re} \left\{ \underbrace{(\boldsymbol{\lambda}_{r,q}^{(\zeta)})^H (\eta_{r,q}^{(\zeta)}) (\boldsymbol{\Psi}^T \otimes (\mathbf{F}_q^T \otimes \mathbf{I}_{M_T})) \operatorname{vec}\{\hat{\boldsymbol{\zeta}}_{r,q}\}}_{u_{r,q}} \right\} + u_{r,q} \leq I_{r,q} \right) \geq 1 - \tilde{\rho}_{r,q} \quad (6.51d)$$

where

$$d_{q,q} = \operatorname{vec}^H \{ \hat{\mathbf{E}}_{q,q} \} (\mathbf{F}_q^T \otimes \boldsymbol{\Psi}) \operatorname{vec} \{ \hat{\mathbf{E}}_{q,q} \} - \gamma_q \left\{ \sum_{\substack{\forall k \in \mathcal{Q}^{\text{dl}} \\ k \neq q}} t_{q,k} + \sum_{\forall r \in \mathcal{Q}^{\text{ul}}} V_{q,r} p_r^{\text{ul}} + \sigma_q^2 \right\} \quad (6.52)$$

$$d_{q,k} = \operatorname{vec}^H \{ \hat{\mathbf{E}}_{q,k} \} (\mathbf{F}_k^T \otimes \boldsymbol{\Psi}) \operatorname{vec} \{ \hat{\mathbf{E}}_{q,k} \} \quad (6.53)$$

$$a_{q,r} = \hat{\mathbf{e}}_{q,r}^H \boldsymbol{\Psi} \hat{\mathbf{e}}_{q,r} \quad (6.54)$$

$$u_{r,q} = \operatorname{vec}^H \{ \hat{\boldsymbol{\zeta}}_{r,q} \} \tilde{U}_{r,q} \operatorname{vec} \{ \hat{\boldsymbol{\zeta}}_{r,q} \}. \quad (6.55)$$

As a result, the probability-constrained power minimization problem in (6.44) can be

written as

$$\min \sum_{\forall q \in \mathcal{Q}^{\text{dl}}} \text{Tr}\{\mathbf{F}_q\} \quad (6.56a)$$

$$\text{s.t. } \Pr(\boldsymbol{\lambda}_{q,q}^{\text{H}} \mathbf{D}_{q,q} \boldsymbol{\lambda}_{q,q} + 2 \text{Re}\{\boldsymbol{\lambda}_{q,q}^{\text{H}} \mathbf{d}_{q,q}\} + d_{q,q} \geq 0) \geq 1 - \rho_{q,q} \quad (6.56b)$$

$$\Pr(\boldsymbol{\lambda}_{q,k}^{\text{H}} \mathbf{D}_{q,k} \boldsymbol{\lambda}_{q,k} + 2 \text{Re}\{\boldsymbol{\lambda}_{q,k}^{\text{H}} \mathbf{d}_{q,k}\} + d_{q,k} \leq t_{q,k}) \geq 1 - \rho_{q,k} \quad (6.56c)$$

$$\Pr((\boldsymbol{\lambda}_{q,r}^{(\delta)})^{\text{H}} \mathbf{A}_{q,r} (\boldsymbol{\lambda}_{q,r}^{(\delta)}) + 2 \text{Re}\{(\boldsymbol{\lambda}_{q,r}^{(\delta)})^{\text{H}} \mathbf{a}_{q,r}\} + a_{q,r} \leq V_{q,r}) \geq 1 - \varrho_{q,r} \quad (6.56d)$$

$$\Pr((\boldsymbol{\lambda}_{r,q}^{(\mathfrak{I})})^{\text{H}} \mathbf{U}_{r,q} (\boldsymbol{\lambda}_{r,q}^{(\mathfrak{I})}) + 2 \text{Re}\{(\boldsymbol{\lambda}_{r,q}^{(\mathfrak{I})})^{\text{H}} \mathbf{u}_{r,q}\} + u_{r,q} \leq I_{r,q}) \geq 1 - \tilde{\varrho}_{r,q}, \quad (6.56e)$$

$$\sum_{\forall q \in \mathcal{Q}^{\text{dl}}} I_{r,q} \leq I_{\text{th}} \quad (6.56f)$$

$$\mathbf{F}_q \succeq \mathbf{0} \quad (6.56g)$$

$$\text{rank}(\mathbf{F}_q) = 1 \quad (6.56h)$$

$$\boldsymbol{\Psi} \succeq \mathbf{0} \quad (6.56i)$$

$$\text{diag}(\boldsymbol{\Psi}) = \mathbf{1}_{M_S} \quad (6.56j)$$

$$\text{rank}(\boldsymbol{\Psi}) = 1. \quad (6.56k)$$

Problem (6.56) is computationally intractable since it is difficult to derive a closed-form expression for the cumulative distribution function (CDF) of the non-outage probabilities in (6.56b)- (6.56e). To solve this problem, we first adopt a safe (conservative) convex approximation of these constraints. Here "safe" implies that the feasible points for the safe approximation always fulfill the probabilistic constraints. This means that the feasible points must be necessarily feasible also for the original optimization problem. Therefore, the safe approximation is a restriction to the original problem [131]. This convex approximation approach is based on a large deviation inequality, i.e., a Bernstein-type inequality. It transforms the outage constraints into a deterministic form [142]. The Bernstein-type inequality is given in the following lemma.

**Lemma 2.** (*Bernstein-Type Inequality [142, 156]*): Consider the following random variable  $G = \mathbf{v}^{\text{H}} \mathbf{Q} \mathbf{v} + 2 \text{Re}\{\mathbf{v}^{\text{H}} \mathbf{u}\}$ , where  $\mathbf{Q} \in \mathbb{H}^{N \times N}$ ,  $\mathbf{u} \in \mathbb{C}^N$ , and  $\mathbf{v} \sim \mathcal{CN}(\mathbf{0}, \mathbf{I}_N)$ . For all  $\delta \geq 0$ , the following statements hold:

$$\Pr(G \geq \text{Tr}\{\mathbf{Q}\} - \sqrt{2\delta} \sqrt{\|\mathbf{Q}\|_F^2 + 2\|\mathbf{u}\|^2} - \delta s^-(\mathbf{Q})) \geq 1 - e^{-\delta}, \quad (6.57)$$

$$\Pr(G \leq \text{Tr}\{\mathbf{Q}\} + \sqrt{2\delta} \sqrt{\|\mathbf{Q}\|_F^2 + 2\|\mathbf{u}\|^2} + \delta s^+(\mathbf{Q})) \geq 1 - e^{-\delta}, \quad (6.58)$$

where  $s^+(\mathbf{Q}) = \max\{\lambda_{\max}(\mathbf{Q}), 0\}$  in which  $\lambda_{\max}$  denotes the maximum eigenvalue of  $(\mathbf{Q})$  and  $s^-(\mathbf{Q}) = \max\{\lambda_{\max}(-\mathbf{Q}), 0\}$ .

The Bernstein-type inequality bounds the probability that a sum of random vari-

ables deviates from its mean  $\text{Tr}\{\mathbf{Q}\}$  [157] (see Appendix D.2). A detailed explanation of this lemma can be found in Appendix D.2. Let  $\delta \triangleq -\ln(\rho)$  where  $\rho \in (0, 1]$ . Therefore, Lemma 2 implies that the inequality

$$\Pr(\mathbf{v}^H \mathbf{Q} \mathbf{v} + 2 \text{Re}\{\mathbf{v}^H \mathbf{u}\} \geq b) \geq 1 - \rho \quad (6.59)$$

holds if the following inequality is satisfied

$$\text{Tr}\{\mathbf{Q}\} - \sqrt{2\delta} \sqrt{\|\mathbf{Q}\|_{\mathbb{F}}^2 + 2\|\mathbf{u}\|^2} - \delta s^-(\mathbf{Q}) \geq b. \quad (6.60)$$

This shows that (6.60) serves as a conservative formulation for (6.59). However, another important fact about the conservative formulation in (6.60) is that it can be equivalently replaced with the following constraints [142, 157]

$$\text{Tr}\{\mathbf{Q}\} - \sqrt{2\delta}x - \delta y \geq b, \quad (6.61)$$

$$\sqrt{\|\mathbf{Q}\|_{\mathbb{F}}^2 + 2\|\mathbf{u}\|^2} \leq x, \quad (6.62)$$

$$y\mathbf{I}_N + \mathbf{Q} \succeq \mathbf{0}, \quad (6.63)$$

$$y \geq 0, \quad (6.64)$$

where  $x, y \in \mathbb{R}$  are slack variables. The constraint in (6.62) can be further reformulated into a standard second-order-cone (SOC) constraint as

$$\left\| \begin{bmatrix} \sqrt{2}\mathbf{u} \\ \text{vec}(\mathbf{Q}) \end{bmatrix} \right\| \leq x \quad (6.65)$$

To begin, we denote  $\delta = -\ln(\rho_{q,q})$  and introduce new slack variables  $\Upsilon$  and  $\beta$ , so that the probability constraint in (6.56b) can be transformed into the deterministic form by applying Lemma 2 as

$$\text{Tr}\{\mathbf{D}_{q,q}\} - \sqrt{2\ln(1/\rho_{q,q})}\Upsilon_{q,q} + \ln(\rho_{q,q})\beta_{q,q} + d_{q,q} \geq 0 \quad (6.66a)$$

$$\left\| \begin{bmatrix} \sqrt{2}\mathbf{d}_{q,q} \\ \text{vec}\{\mathbf{D}_{q,q}\} \end{bmatrix} \right\| \leq \Upsilon_{q,q}, \forall q \in \mathcal{Q}^{\text{dl}} \quad (6.66b)$$

$$\beta_{q,q}\mathbf{I}_{M_{\text{T}}M_{\text{S}}} + \mathbf{D}_{q,q} \succeq \mathbf{0}, \forall q \in \mathcal{Q}^{\text{dl}}, \quad (6.66c)$$

$$\beta_{q,q} \geq 0. \quad (6.66d)$$

Similarly, the outage constraint in (6.56c) can be transformed into a deterministic form

by applying Lemma 2 and introducing new slack variables  $\mu$  and  $\vartheta$  as

$$\text{Tr}\{\mathbf{D}_{q,k}\} - \sqrt{2 \ln(1/\rho_{q,k})} \mu_{q,k} + \ln(\rho_{q,k}) \vartheta_{q,k} + d_{q,k} \leq t_{q,k} \quad (6.67a)$$

$$\left\| \begin{bmatrix} \sqrt{2} \mathbf{d}_{q,k} \\ \text{vec}\{\mathbf{D}_{q,k}\} \end{bmatrix} \right\| \leq \mu_{q,k}, \forall q \in \mathcal{Q}^{\text{dl}} \quad (6.67b)$$

$$\vartheta_{q,k} \mathbf{I}_{M_{\text{T}} M_{\text{S}}} - \mathbf{D}_{q,k} \succeq \mathbf{0}, \forall q, k \in \mathcal{Q}^{\text{dl}}, k \neq q \quad (6.67c)$$

$$\mu_{q,k} \geq 0. \quad (6.67d)$$

Equally, the constraint in (6.56d) can be transformed into a deterministic form by adopting Lemma 2 and introducing the following slack variables  $\varkappa$  and  $\alpha$  as

$$\text{Tr}\{\mathbf{A}_{q,r}\} - \sqrt{2 \ln(1/\rho_{q,r})} \alpha_{q,r} + \ln(\rho_{q,r}) \varkappa_{q,r} + a_{q,r} \leq V_{q,r} \quad (6.68a)$$

$$\left\| \begin{bmatrix} \sqrt{2} \mathbf{a}_{q,r} \\ \text{vec}\{\mathbf{A}_{q,r}\} \end{bmatrix} \right\| \leq \alpha_{q,r}, \forall q \in \mathcal{Q}^{\text{dl}}, \forall r \in \mathcal{Q}^{\text{ul}} \quad (6.68b)$$

$$\varkappa_{q,r} \mathbf{I}_{M_{\text{S}}} - \mathbf{A}_{q,r} \succeq \mathbf{0}, \forall q \in \mathcal{Q}^{\text{dl}}, \forall r \in \mathcal{Q}^{\text{ul}} \quad (6.68c)$$

$$\varkappa_{q,r} \geq 0. \quad (6.68d)$$

Furthermore, we introduce the following slack variables  $\varphi$  and  $\kappa$  and adopt Lemma 2 to transform the outage constraint in (6.56e) into the deterministic form as

$$\text{Tr}\{\mathbf{U}_{r,q}\} - \sqrt{2 \ln(1/\rho_{r,q})} \kappa_{r,q} + \ln(\rho_{r,q}) \varphi_{r,q} + u_{r,q} \leq I_{r,q} \quad (6.69a)$$

$$\left\| \begin{bmatrix} \sqrt{2} \mathbf{u}_{r,q} \\ \text{vec}\{\mathbf{U}_{r,q}\} \end{bmatrix} \right\| \leq \kappa_{r,q}, \forall q \in \mathcal{Q}^{\text{dl}}, \forall r \in \mathcal{Q}^{\text{ul}} \quad (6.69b)$$

$$\varphi_{r,q} \mathbf{I}_{M_{\text{T}}^2 M_{\text{S}}} - \mathbf{U}_{r,q} \succeq \mathbf{0}, \forall q \in \mathcal{Q}^{\text{dl}}, \forall r \in \mathcal{Q}^{\text{ul}}, \quad (6.69c)$$

$$\varphi_{r,q} \geq 0 \quad (6.69d)$$

Therefore, a safe (conservative) approximation of the transmit power minimization problem in (6.56) can be written as

$$\min \sum_{q \in \mathcal{Q}^{\text{dl}}} \text{Tr}\{\mathbf{F}_q\} \quad (6.70a)$$

$$\text{s.t.} \quad \text{Tr}\{\mathbf{D}_{q,q}\} - \sqrt{2 \ln(1/\rho_{q,q})} \tau_{q,q} + \ln(\rho_{q,q}) \beta_{q,q} + d_{q,q} \geq 0 \quad (6.70b)$$

$$\left\| \begin{bmatrix} \sqrt{2} \mathbf{d}_{q,q} \\ \text{vec}\{\mathbf{D}_{q,q}\} \end{bmatrix} \right\| \leq \tau_{q,q}, \forall q \in \mathcal{Q}^{\text{dl}} \quad (6.70c)$$

$$\beta_{q,q} \mathbf{I}_{M_{\text{T}} M_{\text{S}}} + \mathbf{D}_{q,q} \succeq \mathbf{0}, \forall q \in \mathcal{Q}^{\text{dl}}, \quad (6.70d)$$

$$\beta_{q,q} \geq 0 \quad (6.70e)$$

$$\text{Tr}\{\mathbf{D}_{q,k}\} - \sqrt{2\ln(1/\rho_{q,k})}\mu_{q,k} + \ln(\rho_{q,k})\vartheta_{q,k} + d_{q,k} \leq t_{q,k} \quad (6.70f)$$

$$\left\| \begin{bmatrix} \sqrt{2}\mathbf{d}_{q,k} \\ \text{vec}\{\mathbf{D}_{q,k}\} \end{bmatrix} \right\| \leq \mu_{q,k}, \forall q \in \mathcal{Q}^{\text{dl}} \quad (6.70g)$$

$$\vartheta_{q,k}\mathbf{I}_{M_{\text{T}}M_{\text{S}}} - \mathbf{D}_{q,k} \succeq \mathbf{0}, \forall q, k \in \mathcal{Q}^{\text{dl}}, k \neq q \quad (6.70h)$$

$$\vartheta_{q,k}\mathbf{I}_{M_{\text{T}}M_{\text{S}}} - \mathbf{D}_{q,k} \succeq \mathbf{0}, \forall q, k \in \mathcal{Q}^{\text{dl}}, k \neq q \quad (6.70i)$$

$$\mu_{q,k} \geq 0 \quad (6.70j)$$

$$\text{Tr}\{\mathbf{A}_{q,r}\} - \sqrt{2\ln(1/\rho_{q,r})}\alpha_{q,r} + \ln(\rho_{q,r})\varkappa_{q,r} + a_{q,r} \leq V_{q,r} \quad (6.70k)$$

$$\left\| \begin{bmatrix} \sqrt{2}\mathbf{a}_{q,r} \\ \text{vec}\{\mathbf{A}_{q,r}\} \end{bmatrix} \right\| \leq \alpha_{q,r}, \forall q \in \mathcal{Q}^{\text{dl}}, \forall r \in \mathcal{Q}^{\text{ul}} \quad (6.70l)$$

$$\varkappa_{q,r}\mathbf{I}_{M_{\text{S}}} - \mathbf{A}_{q,r} \succeq \mathbf{0}, \forall q \in \mathcal{Q}^{\text{dl}}, \forall r \in \mathcal{Q}^{\text{ul}} \quad (6.70m)$$

$$\varkappa_{q,r} \geq 0 \quad (6.70n)$$

$$\text{Tr}\{\mathbf{U}_{r,q}\} - \sqrt{2\ln(1/\rho_{r,q})}\kappa_{r,q} + \ln(\rho_{r,q})\varphi_{r,q} + u_{r,q} \leq I_{r,q} \quad (6.70o)$$

$$\left\| \begin{bmatrix} \sqrt{2}\mathbf{u}_{r,q} \\ \text{vec}\{\mathbf{U}_{r,q}\} \end{bmatrix} \right\| \leq \kappa_{r,q}, \forall q \in \mathcal{Q}^{\text{dl}}, \forall r \in \mathcal{Q}^{\text{ul}} \quad (6.70p)$$

$$\varphi_{r,q}\mathbf{I}_{M_{\text{T}}^2M_{\text{S}}} - \mathbf{U}_{r,q} \succeq \mathbf{0}, \forall q \in \mathcal{Q}^{\text{dl}}, \forall r \in \mathcal{Q}^{\text{ul}}, \quad (6.70q)$$

$$\varphi_{r,q} \geq 0 \quad (6.70r)$$

$$\sum_{\forall q \in \mathcal{Q}^{\text{dl}}} I_{r,q} \leq I_{\text{th}} \quad (6.70s)$$

$$\mathbf{F}_q \succeq \mathbf{0} \quad (6.70t)$$

$$\text{rank}(\mathbf{F}_q) = 1 \quad (6.70u)$$

$$\mathbf{\Psi} \succeq \mathbf{0} \quad (6.70v)$$

$$\text{diag}(\mathbf{\Psi}) = \mathbf{1}_{M_{\text{S}}} \quad (6.70w)$$

$$\text{rank}(\mathbf{\Psi}) = 1. \quad (6.70x)$$

The second-order cone (SOC) constraints in (6.70c), (6.70g), (6.70l), and (6.70p) are sub-cases of an SDP and can be recast in linear matrix equality (LMI) [131]. However, problem (6.70) is still difficult to solve as the variables  $\mathbf{F}_q$  and  $\mathbf{\Psi}$  are still coupled. We use an AO approach to update  $\mathbf{F}_q$  and  $\mathbf{\Psi}$  sequentially in an iterative manner. In particular, for a given  $\mathbf{\Psi}^{(i-1)}$ , we adopt the SDR technique to relax the non-convex problem in  $\mathbf{F}_q$  (by relaxing the rank-one constraint in (6.70u)) during the  $i$ th iteration, and the resulting problem can be solved using CVX tools. The convex SDP problem in  $\mathbf{F}_q^{(i)}$ , is given as

$$\min \sum_{\forall q \in \mathcal{Q}^{\text{dl}}} \text{Tr}\{\mathbf{F}_q^{(i)}\} \quad (6.71a)$$

$$\text{s.t.} \quad (6.70\text{b}) - (6.70\text{t}), \quad (6.71\text{b})$$

where we have relaxed the rank-one constraint given in (6.70u) and the optimization variables are  $\mathbf{F}_q^{(i)}$ ,  $\mathfrak{T}_{q,q}$ ,  $\beta_{q,q}$ ,  $\mu_{q,k}$ ,  $\vartheta_{q,k}$ ,  $\alpha_{q,r}$ ,  $\varkappa_{q,r}$ ,  $\kappa_{r,q}$ ,  $\varphi_{r,q}$ ,  $t_{q,k}$ ,  $V_{q,r}$ , and  $I_{r,q}$ . With the obtained solution of problem (6.71), the sub-problem of  $\Psi^{(i)}$  becomes a feasibility-check problem given as

$$\text{Find} \quad \Psi^{(i)} \quad (6.72\text{a})$$

$$\text{s.t.} \quad (6.70\text{b}) - (6.70\text{s}), \quad (6.72\text{b})$$

$$\Psi \succeq \mathbf{0}, \quad (6.72\text{c})$$

$$\text{diag}(\Psi) = \mathbf{1}_{M_S} \quad (6.72\text{d})$$

$$\text{rank}(\Psi) = 1. \quad (6.72\text{e})$$

We adopt the SDR technique to transform the rank-constrained problem (6.72) into a convex SDP by relaxing the rank-one constraint given in (6.72e). The resulting problem can be solved via CVX. Similar to the approach in (6.37) we maximize the SINR residual given as

$$\max \sum_{\forall q \in \mathcal{Q}^{\text{dl}}} \omega_q \quad (6.73\text{a})$$

$$\text{s.t.} \quad \text{modified-(6.70b)}, \quad (6.73\text{b})$$

$$(6.70\text{c}) - (6.70\text{s}), \quad (6.73\text{c})$$

$$\Psi \succeq \mathbf{0}, \quad (6.73\text{d})$$

$$\text{diag}(\Psi) = \mathbf{1}_{M_S}, \quad (6.73\text{e})$$

$$\omega_q \geq 0, \forall q \in \mathcal{Q}^{\text{dl}}, \quad (6.73\text{f})$$

where the optimization variables are  $\Psi^{(i)}$  and  $\omega_q$ , while modified-(6.70b) is given as

$$\text{Tr}\{\mathbf{D}_{q,q}\} - \sqrt{2 \ln(1/\rho_{q,q})} \mathfrak{T}_{q,q} + \ln(\rho_{q,q}) \beta_{q,q} + d_{q,q} - \omega_q \geq 0 \quad (6.74)$$

Finally, we can obtain the active beamforming vector  $\mathbf{f}_q \in \mathbb{C}^{M_T}, \forall q \in \mathcal{Q}^{\text{dl}}$  and the passive reflection vector  $\boldsymbol{\theta} \in \mathbb{C}^{M_S}$ , based on the solutions obtained from (6.71) and (6.73), respectively. It is important to note that the considered SDP problems in (6.71) and (6.73) have relaxed rank-one constraints. Therefore, the rank of the obtained solutions may not be 1. If the rank is 1, then  $\mathbf{f}_q \in \mathbb{C}^{M_T}, \forall q \in \mathcal{Q}^{\text{dl}}$  and  $\boldsymbol{\theta} \in \mathbb{C}^{M_S}$  can be obtained via an eigenvalue decomposition. Otherwise, we can obtain a high-quality

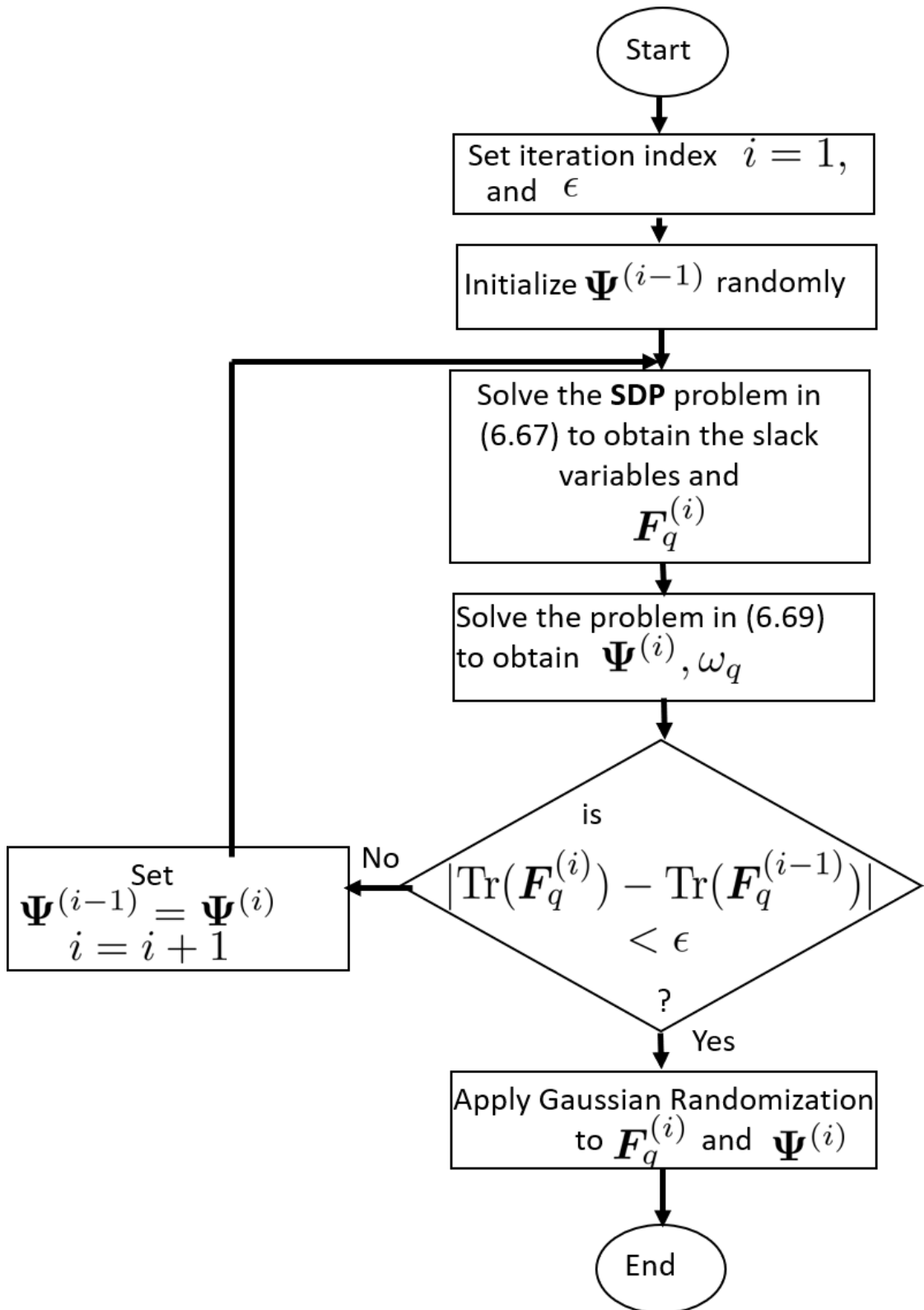


Fig. 6.3: Flow chart for the implementation of the PCR AO-based algorithm.

rank-one solution by applying Gaussian randomization (see Appendix C.5) [139, 140]. The AO-based algorithm for the PCR robust beamforming design for an RIS-aided

DTDD system is outlined in Fig. 6.3.

## 6.6 Complexity Analysis

In the following, we analyze the computational complexities of the different problems of the WCR design in (6.33) and the PCR design in (6.70) by using the number of floating-point operations (FLOPS). A FLOP involves the floating point add, subtract, multiply, or divide. Hence, the total number of FLOPS in any given matrix computation is derived by adding the number of arithmetic operations involved in solving the problem [127]. The total FLOPS for solving the SDP problem in (6.35) is the product of the per iteration cost and the number of iterations. The number of FLOPS per iteration for solving the SDP problem for the design of the DL transmit beamforming vector for the WCR approach given in (6.35) using an interior point method (IPM) is obtained as follows. Problem (6.35) contains  $|\mathcal{Q}^{\text{dl}}|$  constraints for  $\Sigma_{q,q}$ ,  $|\mathcal{Q}^{\text{dl}}| \cdot (|\mathcal{Q}^{\text{dl}}| - 1)$  constraints for  $\Phi_{q,k}$ ,  $q, k \in |\mathcal{Q}^{\text{dl}}|$ ,  $k \neq q$ , and there are  $|\mathcal{Q}^{\text{dl}}||\mathcal{Q}^{\text{ul}}|$  constraints each for  $\mathbf{U}_{q,r}$  and  $\mathbf{\Omega}_{r,q}$ . We note that each of these positive semidefinite matrices involves Cholesky decomposition which has the cost of  $\mathcal{O}(n^3)$  FLOPS and solving linear systems which also cost  $\mathcal{O}(n^3)$  FLOPS, where  $n$  is the dimension of the symmetric matrix [127]. Furthermore, the problem has  $|\mathcal{Q}^{\text{dl}}|$  constraints for  $\lambda_{q,q}$ ,  $|\mathcal{Q}^{\text{dl}}| \cdot (|\mathcal{Q}^{\text{dl}}| - 1)$  constraints for  $\lambda_{q,k}$ ,  $q, k \in |\mathcal{Q}^{\text{dl}}|$ ,  $k \neq q$ , and there are  $|\mathcal{Q}^{\text{dl}}||\mathcal{Q}^{\text{ul}}|$  constraints each for  $\ell_{q,r}$  and  $\varpi_{r,q}$ . These non-negative constraints involve  $\mathcal{O}(1)$  FLOPS each. However, when compared with the number of FLOPS for the matrix operations the number of FLOPS for these non-negative constraints are negligible. Thus the FLOPS per iteration for the problem in (6.35) is given as

$$\begin{aligned} \text{Per iteration cost} &= |\mathcal{Q}^{\text{dl}}| \cdot \mathcal{O}((M_{\text{T}}M_{\text{S}} + 1)^3) + |\mathcal{Q}^{\text{dl}}| \cdot (|\mathcal{Q}^{\text{dl}}| - 1) \cdot \mathcal{O}((M_{\text{T}}M_{\text{S}} + 1)^3) \\ &\quad + |\mathcal{Q}^{\text{dl}}||\mathcal{Q}^{\text{ul}}| \cdot \mathcal{O}((M_{\text{S}} + 1)^3) + |\mathcal{Q}^{\text{dl}}||\mathcal{Q}^{\text{ul}}| \cdot \mathcal{O}((M_{\text{T}}^2M_{\text{S}} + 1)^3). \end{aligned} \quad (6.75)$$

The number of iterations is given as  $\mathcal{O}(\sqrt{\max(M_{\text{T}}, M_{\text{S}})} \log(1/\varepsilon))$ . Therefore, the total FLOPS for solving problem (6.35) is

$$\mathcal{O}_{\mathbf{F}}^{\text{WCR}} = \mathcal{O}(\sqrt{\max(M_{\text{T}}, M_{\text{S}})} \log(1/\varepsilon)) \cdot \text{Per iteration cost} \quad (6.76)$$

The number of FLOPS for solving the problem given in (6.39) is obtained in a similar manner. Therefore, the number of FLOPS for the WCR approach is given as

$$\mathcal{O}_{\mathbf{F}}^{\text{WCR}} + \mathcal{O}_{\boldsymbol{\theta}}^{\text{WCR}}. \quad (6.77)$$

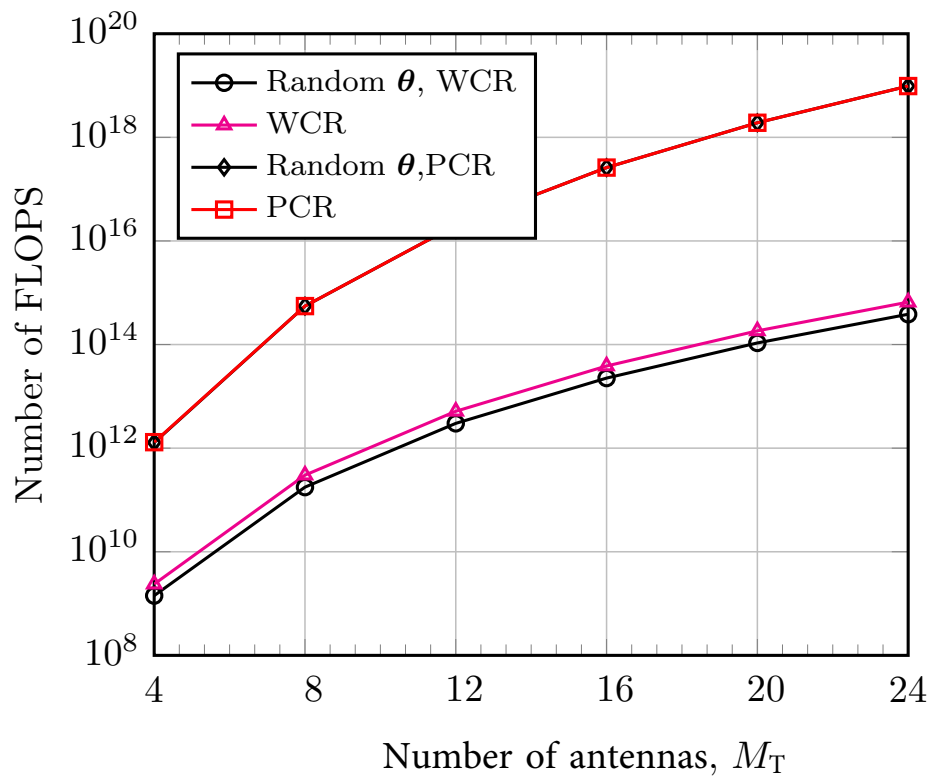
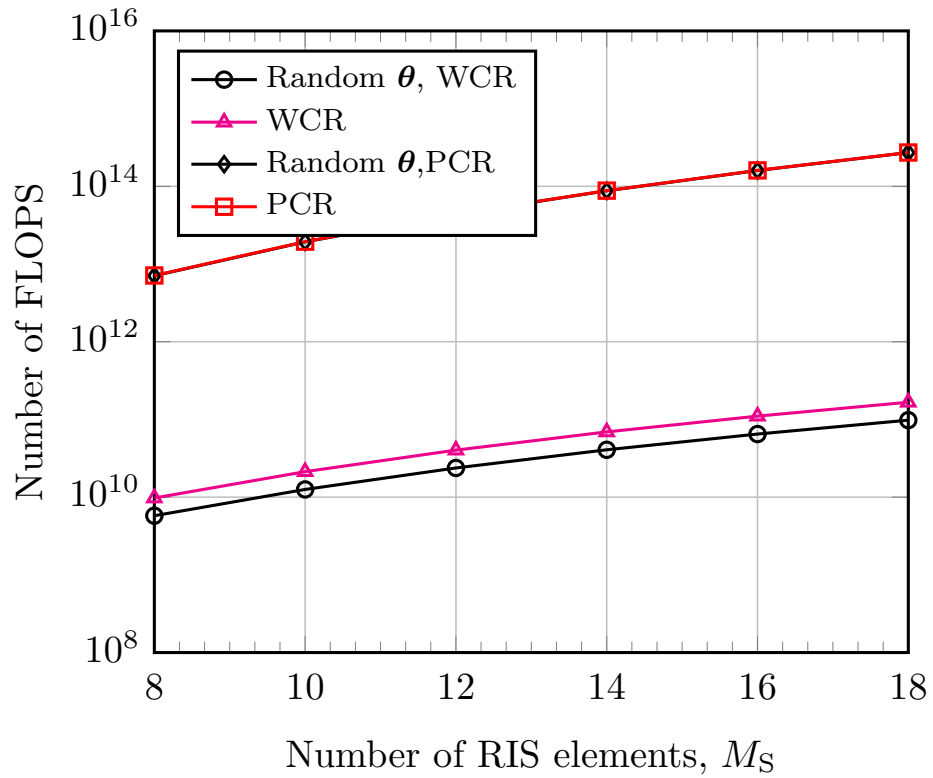
For the probabilistic-constrained robust design problems given in (6.71) and (6.73), the number of FLOPS involved in solving the problems using interior-point methods is obtained by considering the number of FLOPS for the semidefinite constraints, second-order cone constraints, and the linear constraints. For the problem in (6.71) the complexity can be obtained as [127]

$$\mathcal{O}_{\mathbf{F}}^{\text{PCR}} \approx \mathcal{O}((n+c)^2 n^{2.5}), \quad (6.78)$$

where  $n$  corresponds to the size of the largest semidefinite matrix in the problem and  $c$  is the total number of scalar variables. For the given problem the largest semidefinite matrix is  $\mathbf{U}_{r,q} \in \mathbb{C}^{M_{\text{T}}^2 M_{\text{S}} \times M_{\text{T}}^2 M_{\text{S}}}$ . The problem has the following linear constraints  $|\mathcal{Q}^{\text{dl}}|$  constraints for  $\beta_{q,q}$  and  $\Upsilon_{q,q}$ ,  $|\mathcal{Q}^{\text{dl}}| \cdot (|\mathcal{Q}^{\text{dl}}| - 1)$  constraints for  $\mu_{q,k}$ , and  $\vartheta_{q,k}$ ,  $q, k \in |\mathcal{Q}^{\text{dl}}|$ ,  $k \neq q$ , and there are  $|\mathcal{Q}^{\text{dl}}| |\mathcal{Q}^{\text{ul}}|$  constraints each for  $\alpha_{q,r}$ ,  $\varkappa_{q,r}$ ,  $\varphi_{r,q}$  and  $\kappa_{r,q}$ . As a result,  $\mathcal{O}_{\mathbf{F}}^{\text{PCR}} \approx \mathcal{O}((M_{\text{T}}^2 M_{\text{S}} + c)^2 (M_{\text{T}}^2 M_{\text{S}})^{2.5})$ . Similarly, the number of FLOPS for solving the problem given in (6.73) is obtained. Therefore, the number of FLOPS for the PCR approach is given as

$$\mathcal{O}_{\mathbf{F}}^{\text{PCR}} + \mathcal{O}_{\boldsymbol{\theta}}^{\text{PCR}}. \quad (6.79)$$

In figures 6.4 and 6.5 we have provided plots for the number of FLOPS against the number of antennas and the number of RIS elements, respectively. A detailed analysis of the computational complexities is provided in Appendix D.5. From Fig. 6.4 and Fig. 6.5, it can be observed that the WCR design has a lower complexity as compared with the PCR design. With such complexities, the BS must have a strong computational power so that the transmit beamforming vectors and the passive reflection coefficients of the RIS can be computed in real-time. However, the PCR approach is more power-efficient than the WCR approach as shown in Section 6.7. Note that in the figures, Random  $\boldsymbol{\theta}$ , indicates that the entries of the RIS reflection vector are designed randomly as  $[\boldsymbol{\theta}]_{[m]} = e^{j\phi_m}$ ,  $\forall m$ , with  $\phi_m \sim \mathcal{U}(-\pi, \pi)$ .

Fig. 6.4: Number of FLOPs vs. number of transmit antennas,  $M_T$  for  $M_S = 12$ .Fig. 6.5: Number of FLOPs vs. number of RIS elements,  $M_S$  for  $M_T = 6$ .

## 6.7 Numerical Results

This section presents some numerical results illustrating the performance of our proposed robust design methods. We consider a DTDD system with  $Q = 4$  cells, as shown in Fig. 6.1, where  $|\mathcal{Q}^{\text{dl}}| = 2$  and  $|\mathcal{Q}^{\text{ul}}| = 2$  and the interference power threshold is  $I_{\text{th}} = 34$  dBm. We assume the same noise variance for DL cell UEs, i.e.,  $\sigma_q^2 = -80$  dBm,  $\forall q \in \mathcal{Q}^{\text{dl}}$ . The channel models are assumed to include large-scale fading and small-scale fading. The distance-dependent large-scale fading model is given as  $L(d) = C_0(d/D_0)^{-\alpha}$ , where  $C_0 = -30$  dB is the path loss at the reference distance  $D_0 = 1$  m,  $d$  is the individual link distance, and  $\alpha$  denotes the path loss exponent. For the channels  $\mathbf{H}$  and  $\mathbf{h}$  we set  $\alpha$  to be 2 and 2.2, respectively. The small-scale fading model is assumed to be a Rayleigh fading distribution. We set the radii of the uncertainty regions for the bounded CSI model as

$$\zeta_{q,q} = \sqrt{\frac{\eta_{q,q}^2 \text{ICDF}_{2M_S M_T}(1 - \rho_{q,q})}{2}}, \quad (6.80)$$

$$\zeta_{q,k} = \sqrt{\frac{\eta_{q,k}^2 \text{ICDF}_{2M_S M_T}(1 - \rho_{q,k})}{2}}, \quad (6.81)$$

$$\zeta_{q,r}^{(\delta)} = \sqrt{\frac{(\eta_{q,r}^{(\delta)})^2 \text{ICDF}_{2M_S}(1 - \rho_{q,r})}{2}}, \quad (6.82)$$

$$\zeta_{r,q}^{(\mathbf{\Delta})} = \sqrt{\frac{(\eta_{r,q}^{(\mathbf{\Delta})})^2 \text{ICDF}_{2M_T^2 M_S}(1 - \rho_{q,q})}{2}}, \quad (6.83)$$

where  $\text{ICDF}_{2M_S}(\cdot)$ ,  $\text{ICDF}_{2M_S M_T}(\cdot)$ , and  $\text{ICDF}_{2M_T^2 M_S}(\cdot)$  denote the inverse cumulative distribution function of the chi-square distribution with the degrees of freedom equal to  $2M_S$ ,  $2M_S M_T$ , and  $2M_T^2 M_S$ , respectively. For the probabilistic-constrained robust design, we set the variance of the statistical CSI error model  $\text{vec}\{\mathbf{\Delta}_{q,q}\}$ ,  $\delta_{q,r}$ , and  $\text{vec}\{\mathbf{\Delta}_{r,q}^{(\mathbf{\Delta})}\}$  as  $\eta_{q,q}^2 = \epsilon^2 \|\text{vec}\{\hat{\mathbf{E}}_{q,q}\}\|_2^2$ ,  $(\eta_{q,r}^{(\delta)})^2 = \epsilon^2 \|\hat{\mathbf{e}}_{q,r}\|_2^2$ , and  $(\eta_{r,q}^{(\mathbf{\Delta})})^2 = \epsilon^2 \|\text{vec}\{\hat{\mathbf{\Delta}}_{r,q}\}\|_2^2$ , respectively, where  $\epsilon \in [0, 1)$  is a term that controls the relative amount of CSI uncertainty. The outage specifications for all users are set to the same  $\rho_{q,q} = \tilde{\rho}_{r,q} \triangleq \rho$ . The target minimal SINR is set to be the same for different DL cell users, i.e.,  $\gamma_1 = \dots = \gamma_{|\mathcal{Q}^{\text{dl}}|} \triangleq \gamma$ . The stopping criterion for the iteration in the proposed design methods is that the decrease

of the transmit power is less than  $\varepsilon = 10^{-3}$ , i.e., 
$$\frac{\left| \sum_{q \in \mathcal{Q}^{\text{dl}}} \text{Tr}\{\mathbf{F}_q^{(i)}\} - \sum_{q \in \mathcal{Q}^{\text{dl}}} \text{Tr}\{\mathbf{F}_q^{(i-1)}\} \right|}{\left| \sum_{q \in \mathcal{Q}^{\text{dl}}} \text{Tr}\{\mathbf{F}_q^{(i)}\} \right|} \leq \varepsilon.$$

We include results for the following two baseline cases:

- **Random**, where the entries of the RIS reflection vector are designed randomly as  $[\boldsymbol{\theta}]_{[m]} = e^{j\phi_m}$ ,  $\forall m$ , with  $\phi_m \sim \mathcal{U}(-\pi, \pi)$ ,

- **Non Robust scheme**, the case where the beamforming vectors are obtained based only on the estimated cascaded channels and ignoring the uncertainty, i.e.,  $\{\hat{\mathbf{E}}, \hat{\mathbf{e}}, \hat{\mathbf{\Xi}}\}$  are used as if they were for perfect CSI.

In Fig.6.6, we show the minimum transmit power required versus the various target SINR values for the robust transmission strategies (WCR and PCR) while assuming  $M_S = 12$ , and  $M_T = 6$ . The figure shows that the proposed robust strategies and their non-robust counterparts perform better than the random RIS scenario in terms of providing a better power efficiency. This is due to the benefit of the beamforming gains obtained from the joint design of the active transmit beamforming vectors at the DL BSs and the RIS reflection vector. The non-robust design has the best power efficiency compared to the robust design (with a performance gap of about 3 dBm), this performance gap can be seen as the price to pay in order to guarantee the QoS of the users, i.e., robustness to the CSI estimation errors. This is because the SINR constraints are easy to be met in this condition and the outage requirement does not influence the total power. We can clearly see that the average total transmit power increases for a given outage probability as we increase the CSI uncertainty variance. The performance gap can be interpreted as the higher level of robustness against CSI errors comes with the cost of an increment in the total transmit power. This shows that the effects of CSI uncertainty are more difficult to cope with when there is demand for higher SINRs.

Equally, we observe that the transmit power consumption increases for a given CSI uncertainty variance as we decrease the outage probability ( $\rho$ ). The result confirms that achieving robustness at a higher uncertainty level comes at the expense of lower achievable limits of SINR targets at an affordable power level. The PCR approach is more power-efficient than the WCR approach. This is because even though the WCR design approach has a lower computational complexity as shown in Section 6.6, it, however, requires an exceedingly large amount of system resources to protect rarely occurring worst cases.

Fig. 6.7 shows the sum rate of the DL cells, and the SINR target is fixed as  $\gamma_q = 6$  dB. The figure demonstrates the performance benefit of the robust beamforming designs against the non-robust schemes. This indicates the performance trade-off between achieving higher system capacity and power consumption. The non-robust scheme has a lower power consumption but has the worst system sum rate performance.

Next, we investigate the impact of the number of passive reflective elements of the RIS on the downlink transmit power. The average transmit power versus the number of passive reflective elements in the RIS is shown in Fig. 6.8. The number of antennas

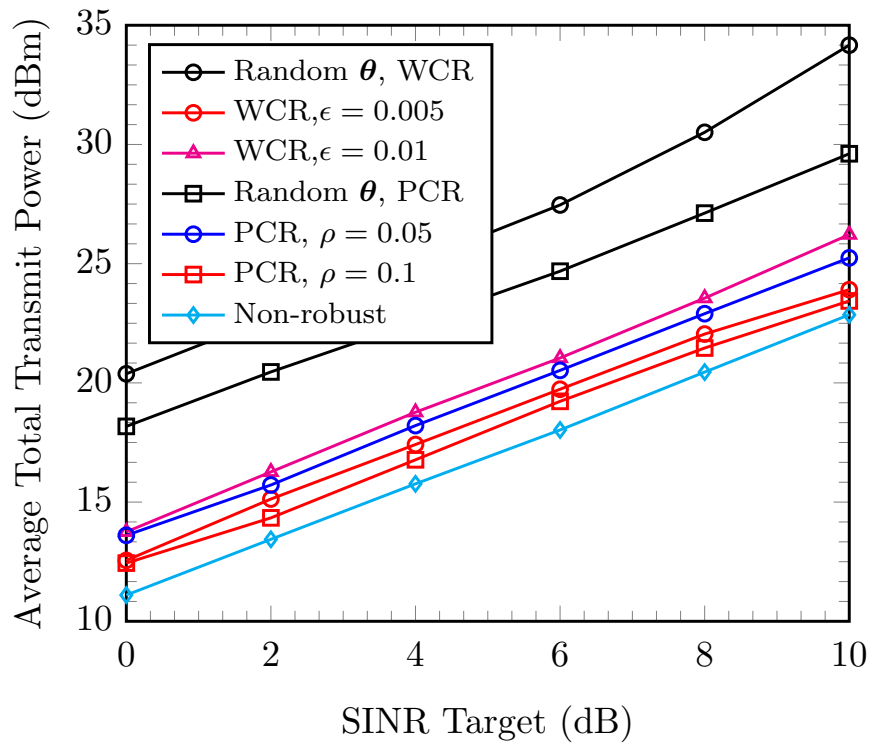


Fig. 6.6: Average total transmit power vs. target SINR for both methods.

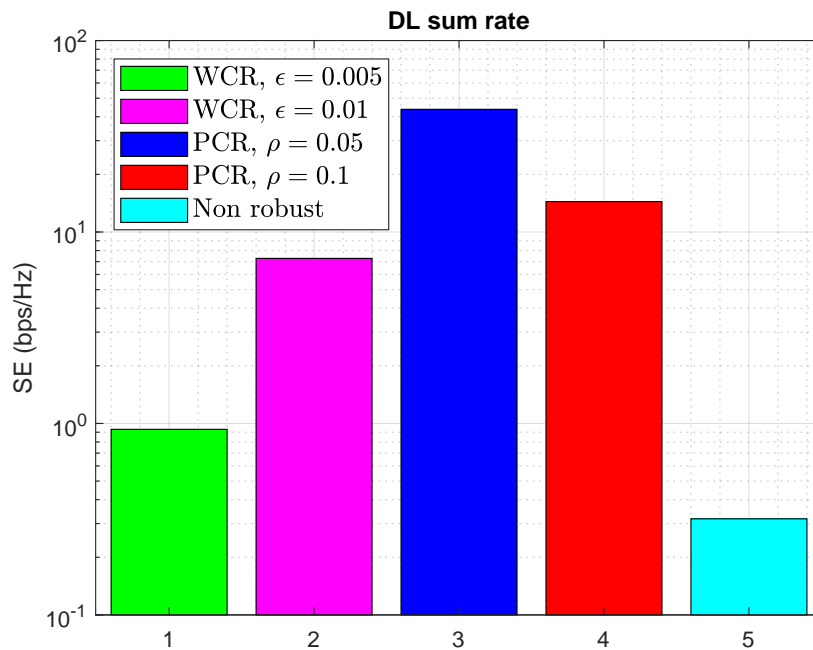


Fig. 6.7: DL sum rate, assuming SINR target  $\gamma = 6$  dB,  $M_S = 12$ , and  $M_T = 6$ .

in each BS is  $M_T = 6$  and the SINR target is fixed as 6 dB. It is seen that the transmit power decreases as the number of the RIS elements  $M$  increases. The reason for this significant drop in the transmit power is that the passive beamforming gain of the

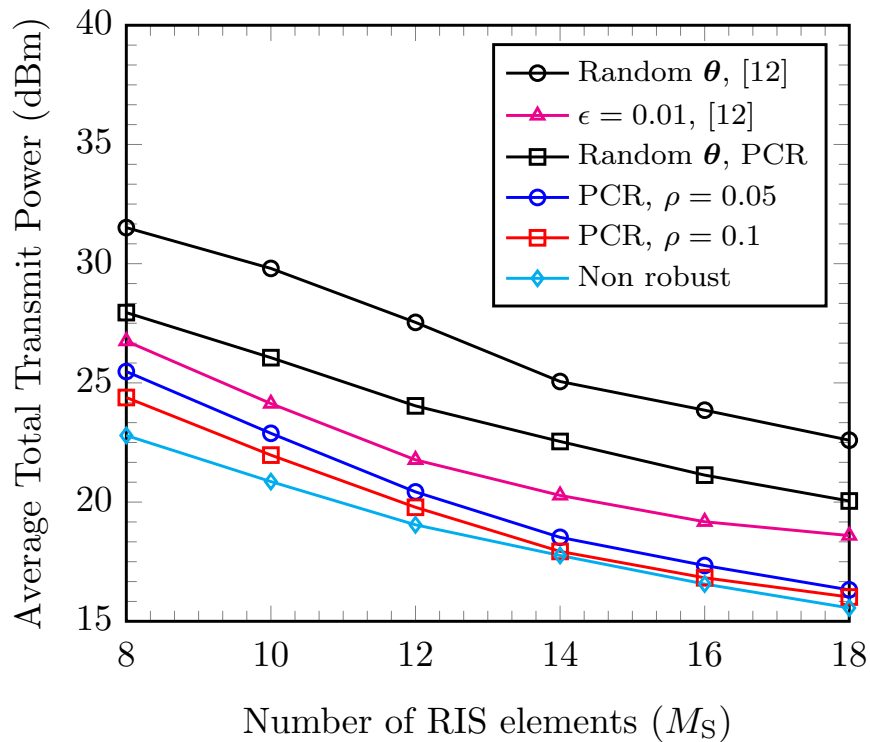


Fig. 6.8: Average total transmit power vs. number of RIS elements  $M_S$ , assuming SINR target = 6 dB and  $M_T = 6$ .

RIS increases with the number of passive reflective elements, pointing to the benefit of the RIS in power savings. The proposed probabilistic-constrained robust transmission strategy stably outperforms the worst-case robust transmission design.

In Fig. 6.9, we show the total leakage power from the DL cells to the UL cells, while assuming that the RIS has  $M_S = 12$  passive reflecting elements and each BS has  $M_T = 6$  antennas. We plot the total DL leakage power for the UL cells separately to demonstrate how the joint design of the active transmit beamforming vectors at the DL BSs and the passive RIS reflection vector of the considered robust transmission schemes have sustained the sum leakage power from the DL cells to the UL cells (BS-BS interference) below the given threshold of 34 dBm. This guarantees the required QoS for the UL cells and supports our findings in [41] that the integration of an RIS in a DTDD system improves the spectral efficiency of the system.

Furthermore, we plot the histograms of the achieved objective function in problem (6.17), the achieved SINR to verify if the constraint in (6.17b) is satisfied, and the achieved DL leakage power to evaluate the satisfaction of the constraint in (6.17c) for all the considered schemes. The achieved objective function is given as

$$\min \sum_{\forall q \in Q^{dl}} \|\hat{\mathbf{f}}_q\|^2, \quad (6.84)$$

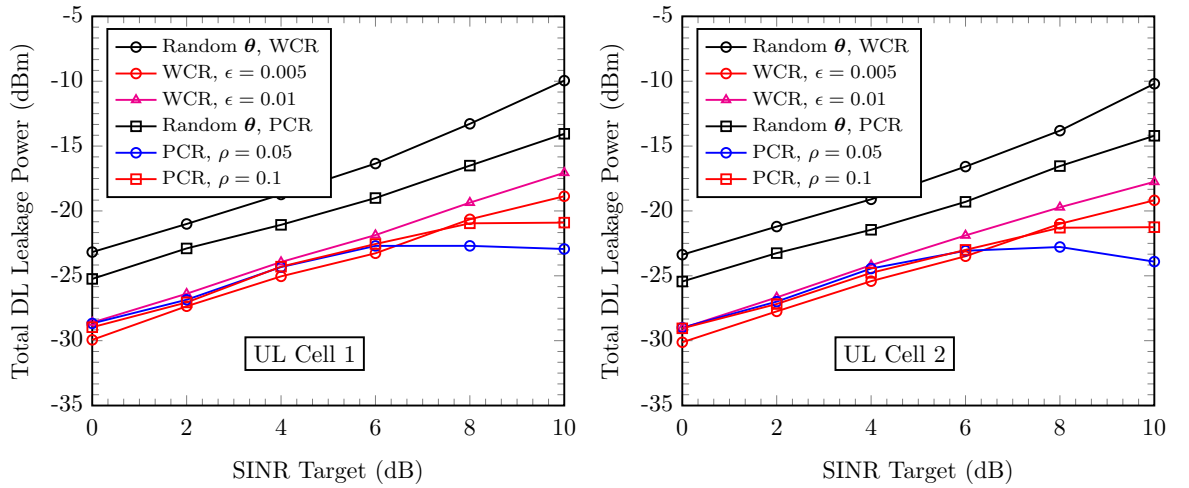


Fig. 6.9: Total DL cells leakage power.

where  $\hat{\mathbf{f}}_q$  is the feasible solution obtained after solving problems (6.35) and (6.71). Fig. 6.10 provides the histogram plots for the achieved DL transmit power for the various schemes obtained from 500 random sets of channel realizations. The SINR target has been fixed to 4 dB.

The figures show the minimum achieved DL transmit power for all the considered schemes. The non-robust scheme achieves the minimum transmit power which supports the results presented earlier. The average of the minimum transmit power is given in Table 6.1.

WCR, Random $\theta$	WCR	PCR, Random $\theta$	PCR	Non robust
38.44	37.95	38.91	37.43	36.86

Tab. 6.1: Mean achieved minimum DL transmit power in dBm.

The achieved SINR is given as

$$\hat{\Gamma}_q^{(dl)} = \frac{|\hat{\boldsymbol{\theta}}^H(\hat{\mathbf{E}}_{q,q} + \boldsymbol{\Delta}_{q,q})\hat{\mathbf{f}}_q|^2}{\sum_{\substack{\forall k \in \mathcal{Q}^{dl} \\ k \neq q}} |\hat{\boldsymbol{\theta}}^H(\hat{\mathbf{E}}_{q,k} + \boldsymbol{\Delta}_{q,k})\hat{\mathbf{f}}_k|^2 + \sum_{\forall r \in \mathcal{Q}^{ul}} |\hat{\boldsymbol{\theta}}^H(\hat{\mathbf{e}}_{q,r} + \boldsymbol{\delta}_{q,r})|^2 p_r^{ul} + \sigma_q^2}, \quad (6.85)$$

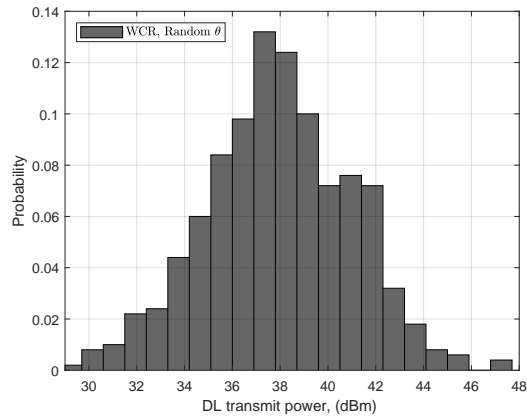
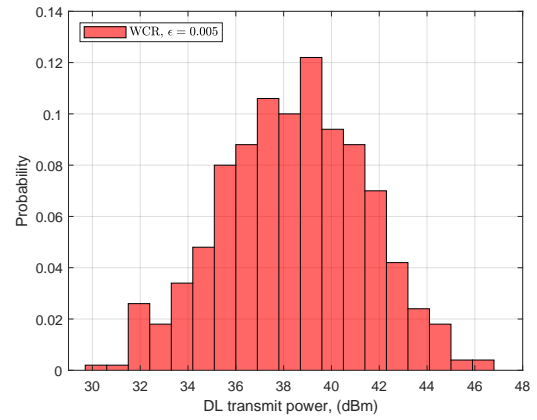
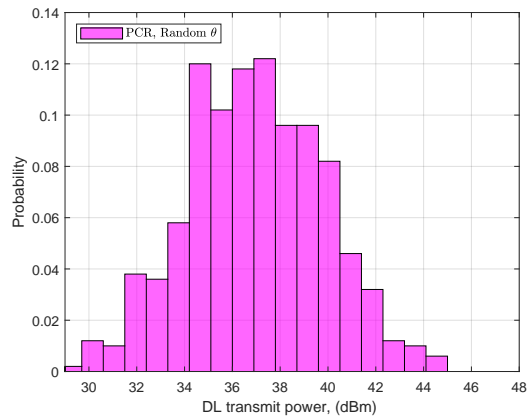
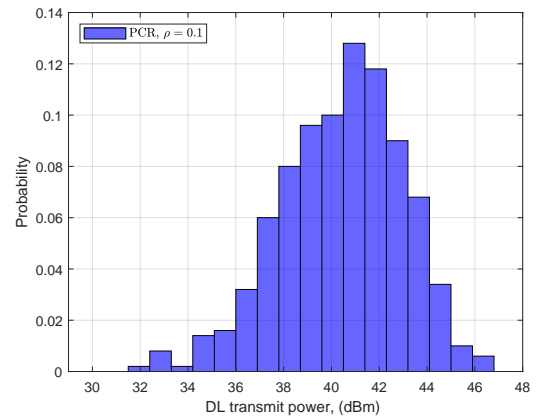
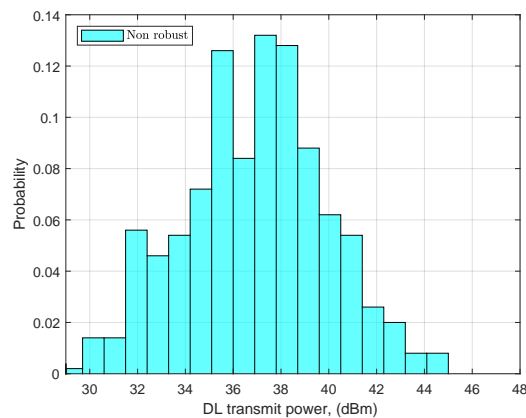
where  $\hat{\mathbf{f}}$  and  $\hat{\boldsymbol{\theta}}$  are the feasible solutions obtained after solving the given optimization problem. Fig. 6.11 provides the histogram plots for the achieved SINR for the various schemes obtained from 500 random sets of channel realizations. The SINR target has been fixed to 4 dB. Achieved SINR values greater or equal to 4 dB indicate that the QoS constraint in (6.17b) is satisfied. From the results, it is observed that in a greater percentage of all the trials, the WCR schemes satisfy the QoS constraints. This shows that the WCR approach is a conservative method, which requires an exceedingly large

amount of system resources to protect rarely occurring worst cases. As shown by the results, the PCR schemes satisfy the QoS constraint with a certain probability ( $\rho = 0.1$ ). This shows that the probabilistic error model has the advantage of being less conservative. It makes a prudent selection of the robustness parameters as compared with the worst-case. Moreover, the QoS constraint is not satisfied in a considerable number of trials (about 89%) for the non-robust scheme.

However, we observe that regrettably in some instances this constraint is violated. This could result from the fact that the resulting optimization problems in (6.35) and (6.39) as well as the problems in (6.71) and (6.73) are approximate SDP problems. The obtained solution may not be a rank-one solution. A rank-one approximation is used to obtain the best rank-one solution. We have used the Gaussian randomization method to obtain the best rank-one solution. In Fig. 6.12 we plot the histogram of the achieved DL leakage power to evaluate the satisfaction of the UL interference constraint given in (6.17c). The UL interference threshold is set at  $I_{\text{th}} = 34$  dBm. Achieved DL leakage power below 34 dBm shows that the UL interference constraint is satisfied. The achieved DL leakage power is given as

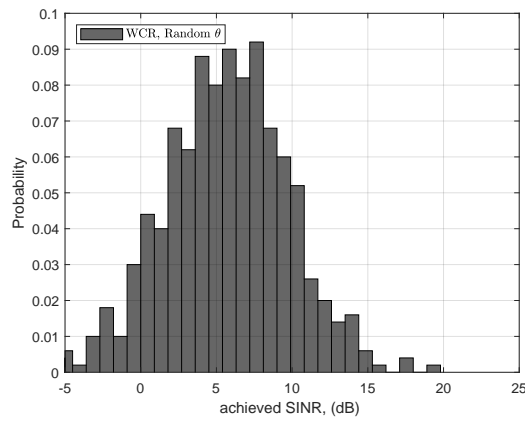
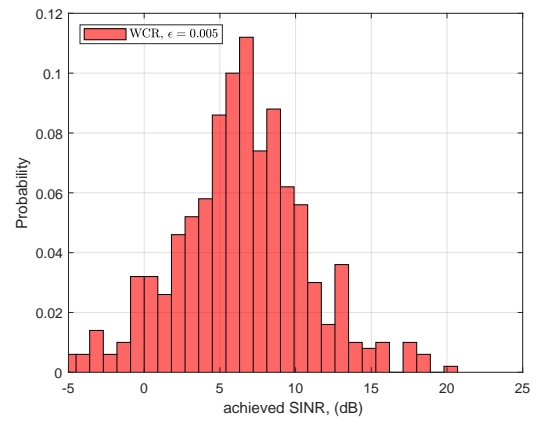
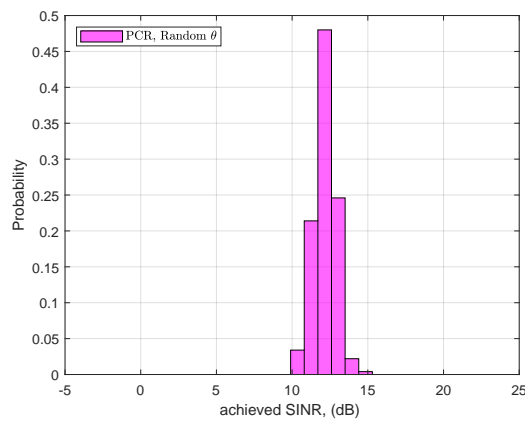
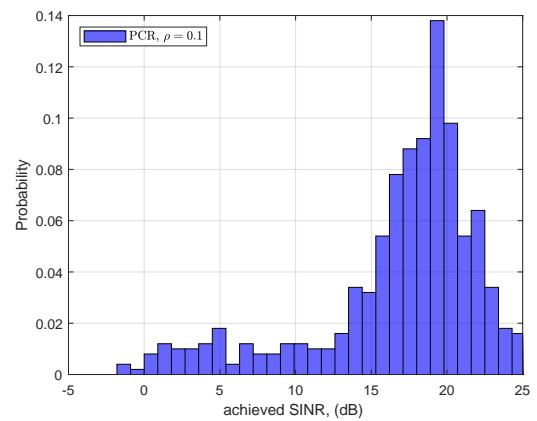
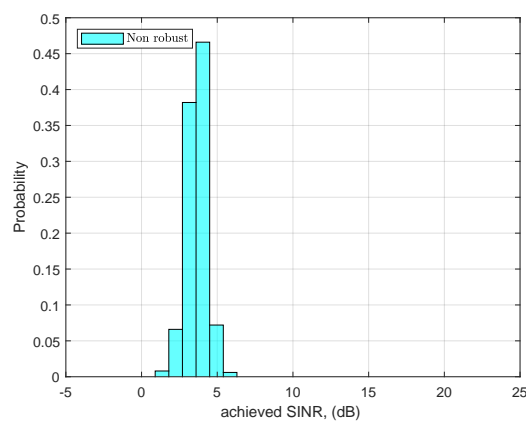
$$\text{IP}_r = \sum_{\forall q \in \mathcal{Q}^{\text{dl}}} \|(\hat{\mathbf{f}}_q^{\text{T}} \otimes \mathbf{I}_{M_{\text{T}}})(\hat{\mathbf{c}}_{r,q} + \Delta_{r,q}^{(\mathbf{c})})\hat{\boldsymbol{\theta}}\|^2. \quad (6.86)$$

From the results, we note that all the considered schemes have a satisfaction rate of 99% for the UL interference constraint given in (6.17c). The few exceptional cases could be due to the rank-one approximation as discussed earlier.

(a) DL transmit power for WCR scheme with random RIS phase shifts,  $\theta$ .(b) DL transmit power for WCR scheme,  $\epsilon = 0.005$ (c) DL transmit power for PCR scheme with random RIS phase shifts,  $\theta$ .(d) DL transmit power for PCR scheme,  $\rho = 0.1$ .

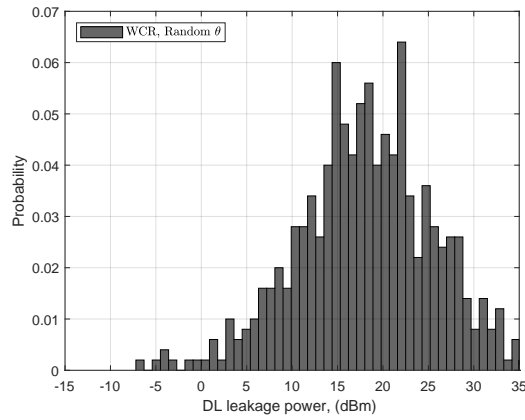
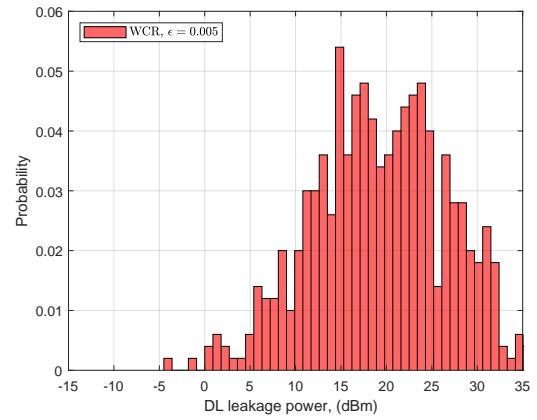
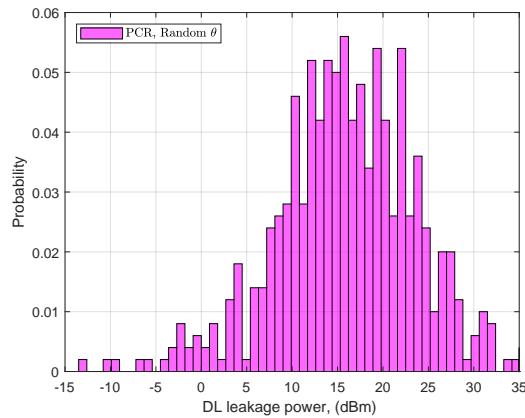
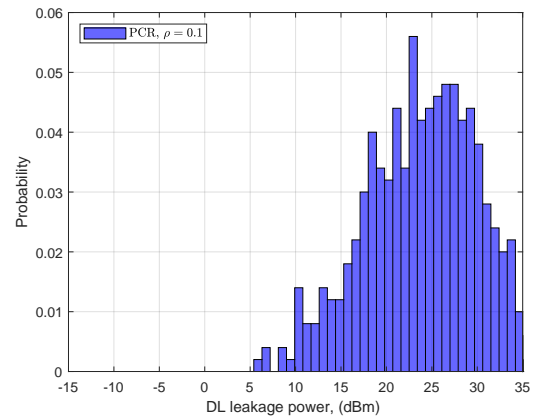
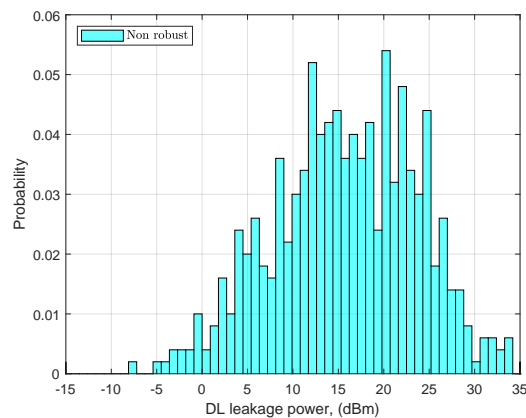
(e) DL transmit power for non-robust scheme.

Fig. 6.10: Histogram of DL transmit power.

(a) Achieved SINR for WCR scheme with random RIS phase shifts,  $\theta$ .(b) Achieved SINR for WCR scheme,  $\epsilon = 0.005$ (c) Achieved SINR for PCR scheme with random RIS phase shifts,  $\theta$ .(d) Achieved SINR for PCR scheme,  $\rho = 0.1$ .

(e) Achieved SINR for non-robust scheme.

Fig. 6.11: Histogram of achieved SINR.

(a) DL leakage power for WCR scheme with random RIS phase shifts,  $\theta$ .(b) DL leakage power for WCR scheme,  $\epsilon = 0.005$ (c) DL leakage power for PCR scheme with random RIS phase shifts,  $\theta$ .(d) DL leakage power for PCR scheme,  $\rho = 0.1$ .

(e) DL leakage power for non-robust scheme.

Fig. 6.12: Histogram of DL leakage power.

## 6.8 Chapter Conclusions

In this chapter, we have considered robust transmission strategies for an RIS-aided DTDD wireless network with imperfect channel state information. The problem is formulated as a sum-power minimization problem for the DL cells under the constraints of satisfying the SINR requirements at the individual DL UEs, the interference leakage power at each UL cell, and unit-modulus constraints of the RIS in the presence of channel estimation errors. We adopted the SDR technique, the S-procedure, and a Bernstein-type inequality for safe convex approximations of the original problems. The beamforming vectors at the downlink BSs and the passive reflecting vector of the RIS are then iteratively computed via an alternating optimization approach. We have utilized the statistical outage probability-based problem as a basis for comparison with a conventional worst-case formulation which has deterministic upper bounds on the norms of the channel imperfections. The proposed probabilistic-constrained beamforming method is seen to be more power efficient than the worst-case approach as shown by the simulation results. The technique minimizes the total transmit power of the downlink cells while maintaining the non-outage probability for all users above a predefined threshold value. The performance gap between the non-robust design and the robust designs can be interpreted as the price for guaranteeing the QoS for the UEs in the DTDD system with certain outage probability, i.e., robustness to the imperfect CSI.

## 7. NEAR FIELD BEAMFORMING FOR MU-MIMO MILLIMETER WAVE COMMUNICATION SYSTEM

Employing a large number of antennas in conjunction with the exploitation of higher frequencies is a promising solution for improving the rate of future wireless systems. The use of large antenna arrays with high transmission frequencies leads to the fact that the devices operate in the near-field region of large-scale antenna arrays. This chapter studies near-field beamforming for a multi-user multiple-input multiple-output (MU-MIMO) millimeter wave (mmWave) communication system. We exploit the distance discrimination potentials of the near-field beamforming to facilitate an efficient deployment of high-rate multi-user downlink MIMO mmWave systems. To this end, we investigate the performance of the near-field beamforming using several precoding schemes. Our numerical results demonstrate a significant performance improvement due to the capability of the near-field beamforming to support reliable communications even for devices that are located in the same angular direction which corresponds to the “worst case” situation.

### 7.1 Introduction

Massive multiple-input-multiple-output (MIMO) and millimeter wave (mmWave) communications have emerged as two key technologies to meet the demands of higher data rates in future wireless systems [158]. Due to the propagation characteristics at mmWave frequencies, BSs operating in these high-frequency bands will be equipped with large antenna arrays [159]. The resulting effect of the combination of large-scale antennas with high transmission frequencies often causes the communicating devices to operate in the near-field (Fresnel) region of the BS antenna. Hence, the far-field assumption often used for conventional wireless systems does not hold [160]. Radiative near-field propagation takes place between the Fraunhofer distance and the Fresnel distance of large-scale antennas operating at mmWave frequencies [161, 162]. The near-field distance can be several dozens of meters for relatively small antennas operating

at mmWave and Terahertz (THz) frequencies [163].

The distinction between plane waves and spherical waves is due to the distance between the antenna array and the user location. Within the radiative near-field region, the wavefronts become spherical, and exploitation of these spherical wavefronts results in flexible transmit beamforming capabilities. The authors in [164] considered near-field communications for a point-to-point short-range MIMO communication system, which consists of two identical transceiver array antennas that face each other at a distance comparable to the size of the antenna aperture. In [165,166], near-field communications was considered for antennas based on large intelligent surfaces or RISs whose large aperture gives rise to operations in the near-field. In particular, in [165], the authors studied a two-user uplink scenario in which the BS is equipped with an RIS. The work studied ideal antenna architectures, where the transceiver has direct access to the signal observed at each element. Near-field modeling and a performance analysis for multi-user extremely large scale MIMO was studied in [167], taking into account the variations of the signal amplitude and the projected aperture across the array elements.

## 7.2 Chapter Contributions and Organization

One of the advantages of near-field beamforming is that it is possible to provide a certain degree of range discrimination. This distance discrimination allows the array to reduce the effects of reflected wavefronts arriving from the same angle of incidence but originating from different distances [168]. However, the potential of range discrimination of near-field beamforming has not been fully exploited from the communication perspective. With this motivation, in this chapter, we exploit the range discrimination capability of near-field beamforming to facilitate the deployment of high-rate multi-user downlink MIMO mmWave systems. We consider the spectral efficiency achievable for a “worst case” scenario where the users are located at the same angular direction but with different distances. Additionally, we constrain the elements of the beamforming vectors to constant modulus, thus employing phase-only beamforming. The performance of the maximum ratio transmission (MRT), ZF, MMSE, and leakage-based precoding schemes is investigated. The results of the near-field beamforming for MU-MIMO mmWave communications presented in this chapter have been published in [46].

The rest of the chapter is organized as follows. The system model and the optimization problem are introduced in Section 7.3. The performance of several precoding schemes is evaluated for MISO and MIMO communication systems in Section 7.4.

Then, simulation results are provided in Section 7.5, and conclusions are drawn in Section 7.6.

### 7.3 System Model

In this chapter, we consider a downlink multi-user MIMO system where the BS is equipped with a ULA of  $M_T$  antennas, serving  $K$  UEs each with  $M_R$  antennas in the radiative near-field of the BS. The radiative near-field lies between the Fraunhofer distance ( $d_F = \frac{2D^2}{\lambda}$ ) and the Fresnel distance ( $d_N = \sqrt{\frac{D^3}{8\lambda}}$ ), where  $D$  is the antenna diameter and  $\lambda$  is the wavelength [162].

For simplicity, we assume a 2-D setup and consider only the LOS path. We assume that  $d$  is the inter-element spacing for arrays at the BS and the UE. The  $(x, y)$  coordinates of the  $n$ -th element of the BS array are given by

$$\mathbf{b}_n = \left[ 0, \left( n - \frac{M_T-1}{2} \right) d \right]^T, \quad 0 \leq n \leq M_T - 1. \quad (7.1)$$

The coordinate system is defined such that its origin is at the phase center of the BS array as indicated in Fig. 7.1. Equally, the position vector for the  $m$ -th element of the  $k$ th UE array is given as

$$\mathbf{u}_m^{(k)} = \left[ \alpha_m^{(k)}, \beta_m^{(k)} \right]^T, \quad 0 \leq m \leq M_R - 1, \quad (7.2)$$

where  $\alpha_m^{(k)} = \left( m - \frac{M_R-1}{2} \right) d \cos \phi_{\text{array}}^{(k)} + r^{(k)} \cos \phi_{\text{UE}}^{(k)}$  and  $\beta_m^{(k)} = \left( m - \frac{M_R-1}{2} \right) d \sin \phi_{\text{array}}^{(k)} + r^{(k)} \sin \phi_{\text{UE}}^{(k)}$ . Furthermore,  $\phi_{\text{array}}^{(k)}$  is the array orientation,  $\phi_{\text{UE}}^{(k)}$  is the angle towards the UE from the BS, and  $r^{(k)}$  is the distance towards the UE. Here we assume that the UE array is orthogonal to the line connecting the phase centers between the BS and UE arrays as depicted in Fig. 7.1. The received signal at the  $k$ th UE is expressed as

$$\mathbf{y}_k = \mathbf{A}_k \mathbf{W}_k \mathbf{d}_k + \sum_{j=1, j \neq k}^K \mathbf{A}_k \mathbf{W}_j \mathbf{d}_j + \mathbf{z}_k \in \mathbb{C}^{M_R}, \quad (7.3)$$

where  $\mathbf{z}_k$  denotes additive white Gaussian noise with variance  $\sigma_n^2$ ,  $\mathbf{W}_k \in \mathbb{C}^{M_T \times Q}$  is the precoding matrix for the  $k$ th UE,  $\mathbf{d}_k \in \mathbb{C}^Q$  represents the data vector for the  $k$ th UE, and  $Q$  is the number of streams for that particular UE. The matrix  $\mathbf{A}_k$  which represents the channel between the BS and the  $k$ th user is given as,

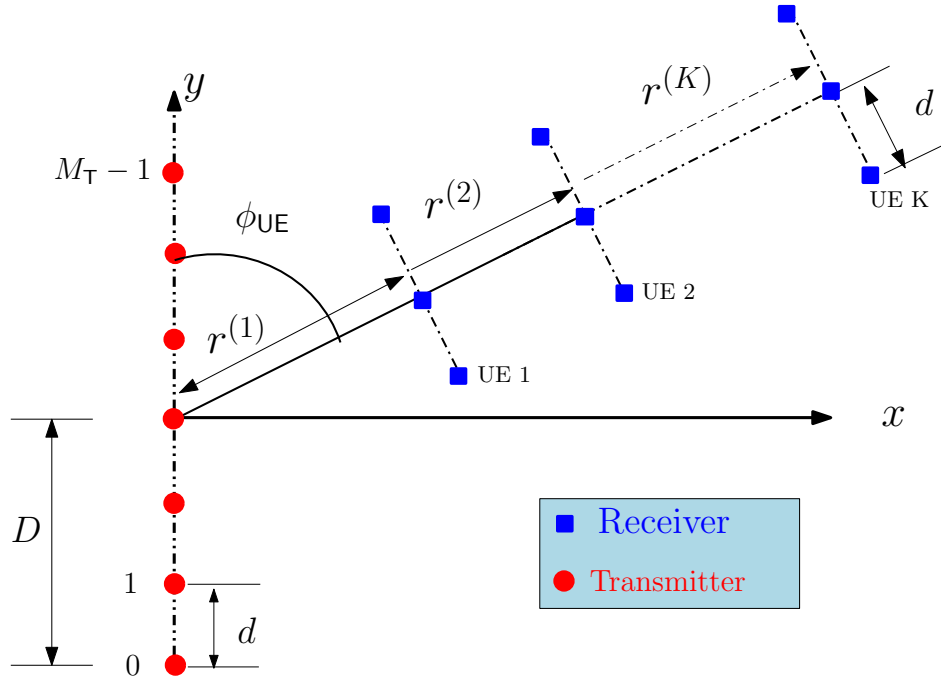


Fig. 7.1: MU-MIMO near-field configuration with ULA at the BS,  $\phi_{\text{UE}}^{(k)} = \phi_{\text{UE}}, \forall k$

$$\mathbf{A}_k = \begin{bmatrix} a_{1,1}^{(k)} & a_{1,2}^{(k)} & \cdots & a_{1,M_T}^{(k)} \\ a_{2,1}^{(k)} & a_{2,2}^{(k)} & \cdots & a_{2,M_T}^{(k)} \\ \vdots & \ddots & \ddots & \vdots \\ a_{M_R,1}^{(k)} & a_{2,2}^{(k)} & \cdots & a_{M_R,M_T}^{(k)} \end{bmatrix} \in \mathbb{C}^{M_R \times M_T}, \quad (7.4)$$

where  $a_{m,n}^{(k)} = e^{-j2\pi \frac{\delta_{m,n}^{(k)}}{\lambda}}$  and  $\delta_{m,n}^{(k)}$  is the path difference between the  $n$ -th element of the array at the BS and the  $m$ -th antenna of the  $k$ th UE given as

$$\begin{aligned} \delta_{m,n}^{(k)} &= \|\mathbf{u}_m^{(k)} - \mathbf{b}_n\|_2 \\ &= \sqrt{(\alpha_m^{(k)})^2 + \left(\beta_m^{(k)} - \left(n - \frac{M_T - 1}{2}\right)d\right)^2}. \end{aligned} \quad (7.5)$$

Note that the exact expression of the array steering vector depends on the path difference expression which is a function of the adopted wavefront model. Let us denote  $\mathbf{A}$  and  $\mathbf{W}$  as the system-wide steering and precoding block matrices, respectively defined as

$$\mathbf{A} = \left[ \mathbf{A}_1^T, \mathbf{A}_2^T, \dots, \mathbf{A}_K^T \right]^T \in \mathbb{C}^{M_R K \times M_T} \quad (7.6)$$

$$\mathbf{W} = \left[ \mathbf{W}_1, \mathbf{W}_2, \dots, \mathbf{W}_K \right] \in \mathbb{C}^{M_T \times QK}, \quad (7.7)$$

we normalize  $\mathbf{W}$  such that  $\|\mathbf{W}\|_F = 1$ . Additionally, we denote the multi-user interference channel block matrix relative to the  $k$ th UE as

$$\tilde{\mathbf{A}}_k = [\mathbf{A}_1^\top, \dots, \mathbf{A}_{k-1}^\top, \mathbf{A}_{k+1}^\top, \dots, \mathbf{A}_K^\top]^\top \in \mathbb{C}^{M_R(K-1) \times M_T}. \quad (7.8)$$

As a performance metric we adopt the system-wide achievable rate, which is expressed as

$$R = \log_2 \det \left( \mathbf{I}_{M_R K} + \frac{P}{M_T \sigma_n^2} \mathbf{A} \mathbf{W} \mathbf{W}^H \mathbf{A}^H \right), \quad (7.9)$$

where  $P$  is the maximum power available at the BS. In the following, we consider several precoding schemes for the near-field beamforming in the multi-user mmWave communication systems to maximize the achievable rate. The elements of the overall beamforming matrix  $\mathbf{W}$  are constrained to be constant modulus, thus representing phase-only beamforming. The resulting problem is given as

$$\max_{\mathbf{W}} \log_2 \det \left( \mathbf{I}_{M_R K} + \frac{P}{M_T \sigma_n^2} \mathbf{A} \mathbf{W} \mathbf{W}^H \mathbf{A}^H \right) \quad (7.10a)$$

$$\text{s.t. } |\mathbf{W}(x, y)| = 1, \quad x = 1, 2, \dots, M_T, \quad y = 1, 2, \dots, QK, \quad (7.10b)$$

where  $P$  is the maximum power available at the BS. The problem in (7.10) is non-convex due to the constant modulus constraints (CMCs) on the precoding matrix given in (7.10b). In the following we relax the CMCs on the precoding matrix to obtain a sub-optimal solution and evaluate the performance of the near-field beamforming using several precoding schemes.

## 7.4 Precoding Methods

In this section, we relax the constant modulus constraints on the precoding matrix and design the precoding matrix, and thereafter project the resulting continuous-amplitude precoding matrix onto the unit circle to obtain the solution that satisfy the constraints given in (7.10b). We consider the following two setups for the multi-user MIMO mmWave communication system.

### 7.4.1 MU-MISO transmission

In the first case, we assume a single antenna ( $M_R = 1$ ) at each of the  $K$  UEs. We consider near-field beamforming for the MU-MISO mmWave system using the following precoding methods.

### Maximum Ratio Transmission

The maximum ratio transmission (MRT) precoder  $\mathbf{w}_k^{\text{MRT}}$  is designed to maximize the received signal power at the desired UE [9]. It can be expressed as

$$\mathbf{w}_k^{\text{MRT}} = \underset{\mathbf{w}}{\operatorname{argmax}} \quad |\mathbf{w}_k^{\text{H}} \mathbf{a}_k|^2 = \frac{\mathbf{a}_k}{\|\mathbf{a}_k\|_2}, \quad (7.11)$$

while the beamforming vector after constraining to only phases is denoted by

$$\mathbf{w}_{\text{CMC},k}^{\text{MRT}} = \operatorname{Proj}(\mathbf{w}_k^{\text{MRT}}), \quad (7.12)$$

where  $\operatorname{Proj}(z_i) = \frac{z_i}{|z_i|}$  is the element-wise projection function. The vector  $\mathbf{a}_k \in \mathbb{C}^{M_{\text{T}} \times 1}$  is a special case of the matrix  $\mathbf{A}_k \in \mathbb{C}^{M_{\text{R}} \times M_{\text{T}}}$  assuming a single antenna at the  $k$ th receiver, i.e., ( $M_{\text{R}} = 1$ ). Note that the MRT precoder does not attempt to cancel the multi-user interference [9].

### Zero-Forcing

In the zero-forcing (ZF) scheme, the beamforming vectors are designed in such a way as to avoid interference among users, i.e.,  $\mathbf{w}_k^{\text{H}} \mathbf{a}_j = 0$ . Such beamforming weights can be easily found by inverting the composite channel matrix of the users [9, 13]. By doing this, the multi-user interference can be completely removed, which eases implementation as well as performance analysis. The ZF scheme is given as

$$\mathbf{W}^{\text{ZF}} = \frac{\mathbf{A}_{\text{MISO}}^+}{\|\mathbf{A}_{\text{MISO}}^+\|_{\text{F}}}, \quad (7.13)$$

and the constrained beamforming as

$$\mathbf{W}_{\text{CMC}}^{\text{ZF}} \leftarrow \operatorname{Proj}(\mathbf{W}^{\text{ZF}}), \quad (7.14)$$

where  $\mathbf{A}_{\text{MISO}}^+$  is the pseudo-inverse of  $\mathbf{A}_{\text{MISO}}$ . Moreover,  $\mathbf{A}_{\text{MISO}}$  is given as

$$\mathbf{A}_{\text{MISO}} = \begin{bmatrix} \mathbf{a}_1^{\text{T}} \\ \vdots \\ \mathbf{a}_K^{\text{T}} \end{bmatrix} \in \mathbb{C}^{K \times M_{\text{T}}}. \quad (7.15)$$

The ZF scheme enforces the zero multi-user interference condition  $\tilde{\mathbf{A}}_{\text{MISO}}^k \mathbf{w}_k^{\text{ZF}} = \mathbf{0}$  by basically forcing the  $\mathbf{w}_k^{\text{ZF}}$  to lie in the null space of  $\tilde{\mathbf{A}}_{\text{MISO}}^k$  so as to avoid the interference

from user  $k$  to other users, where  $\mathbf{w}_k^{\text{ZF}}$  denotes the  $k$ th column of  $\mathbf{W}^{\text{ZF}}$ . Note that

$$\tilde{\mathbf{A}}_{\text{MISO}}^k = \begin{bmatrix} \mathbf{a}_1^\top \\ \vdots \\ \mathbf{a}_{k-1}^\top \\ \mathbf{a}_{k+1}^\top \\ \vdots \\ \mathbf{a}_K^\top \end{bmatrix} \in \mathbb{C}^{(K-1) \times M_T} \quad (7.16)$$

is the multi-user interference matrix relative to the  $k$ th UE which is a special case of the block interference matrix defined in (7.8) for  $M_R = 1$ , i.e., a matrix containing all other steering vectors except for the  $k$ th steering vector. We assume that we implement a large antenna array at the BS, which means  $M_T$  is very large such that  $M_T \gg K$  to ensure that the null space of  $\tilde{\mathbf{A}}_{\text{MISO}}^k$  (i.e.,  $\tilde{\mathbf{V}}_k^{(0)}$ ) exists. This solution results in good performance since it completely cancels the multi-user interference at every receiver. However, this solution is sensitive to unmodeled interference and other sources of distortion and may not result to the optimal signal-to-interference-plus-noise ratio [9]. Moreover, choosing the precoding vector according to (7.13) imposes a strong condition on the system configuration in terms of the number of antennas that are needed [13].

### Minimum Mean Square Error

The minimum mean square error (MMSE) scheme is a form of a regularized ZF process, which is seen as a solution to the noise enhancement problem of the ZF precoder [126]. The precoder that minimizes the mean squared error is given as

$$\mathbf{W}^{\text{MMSE}} = \frac{\bar{\mathbf{A}}_{\text{MISO}}}{\|\bar{\mathbf{A}}_{\text{MISO}}\|_F}, \quad (7.17)$$

$$\mathbf{W}_{\text{CMC}}^{\text{MMSE}} \leftarrow \text{Proj}(\mathbf{W}^{\text{MMSE}}), \quad (7.18)$$

where  $\bar{\mathbf{A}}_{\text{MISO}} = (\mathbf{A}_{\text{MISO}}^H \mathbf{A}_{\text{MISO}} + \sigma_n^2 \mathbf{I}_{M_T})^{-1} \mathbf{A}_{\text{MISO}}^H$ . The matrix  $\mathbf{A}_{\text{MISO}}$  is defined in (7.15).

### Leakage-Based Precoder

The *leakage*-based precoder is designed to maximize the signal-to-leakage-noise ratio (SLNR) defined as

$$\Omega_k = \frac{|\mathbf{w}_k^H \mathbf{a}_k|^2}{\|\tilde{\mathbf{A}}_{\text{MISO}}^k \mathbf{w}_k\|^2 + \sigma_k^2}. \quad (7.19)$$

Maximizing the SLNR for all the users is an efficient way of designing the transmit precoding vectors because it limits the search space and also lowers the complexity involved in finding efficient transmit precoders [23, 143]. According to the generalized Rayleigh-Ritz quotient method (see Appendix D.3) [127], the optimal  $\mathbf{w}_k^{\text{SLNR}}$  is given as

$$\mathbf{w}_k^{\text{SLNR}} = \mathbf{v}_{\max} \left\{ \left( (\tilde{\mathbf{A}}_{\text{MISO}}^k)^H \tilde{\mathbf{A}}_{\text{MISO}}^k + \sigma_n^2 \mathbf{I}_{M_T} \right)^{-1} \mathbf{a}_k \mathbf{a}_k^H \right\}, \quad (7.20)$$

where  $\mathbf{v}_{\max}\{\cdot\}$  is the eigenvector corresponding to the largest eigenvalue of the matrix. The solution that satisfies the CMCs is given as

$$\mathbf{w}_{\text{CMC},k}^{\text{SLNR}} \leftarrow \text{Proj}(\mathbf{w}^{\text{SLNR},k}). \quad (7.21)$$

## 7.4.2 MU-MIMO transmission

Next, we consider the general MU-MIMO setup and use all the above precoding methods. In addition, we use the block diagonalization (BD) scheme for the cancellation of the MUI. The BD scheme is a more generalized ZF solution applicable for a scenario when the receiver has multiple antennas [13, 169]. The BD scheme enforces the following zero MUI condition  $\tilde{\mathbf{A}}_k \mathbf{W}_k = \mathbf{0}$ , which can be expressed as

$$\mathbf{W}_k^{\text{BD}} = \tilde{\mathbf{V}}_k^{(0)} \mathbf{V}_k^{\max}, \quad (7.22)$$

$$\mathbf{W}_{\text{CMC},k}^{\text{BD}} \leftarrow \text{Proj}(\mathbf{W}^{\text{BD},k}), \quad (7.23)$$

where  $\tilde{\mathbf{V}}_k^{(0)} \in \mathbb{C}^{M_T \times (M_T - M_R(K-1))}$  holds the basis for the null-space of  $\tilde{\mathbf{A}}_k \in \mathbb{C}^{M_R(K-1) \times M_T}$ , which can be obtained from the singular value decomposition (SVD) of  $\tilde{\mathbf{A}}_k$  [13] and  $\mathbf{V}_k^{\max} \in \mathbb{C}^{(M_T - M_R(K-1)) \times M_R}$  is a matrix whose columns are the right singular vectors corresponding to the  $M_R$  largest singular values of  $\mathbf{A}_k \tilde{\mathbf{V}}_k^{(0)} \in \mathbb{C}^{M_R \times (M_T - M_R(K-1))}$ . Note that the matrices  $\mathbf{A}$  and  $\tilde{\mathbf{A}}_k$  are defined in (7.6) and (7.8), respectively. We assume that  $Q$  in (7.3) is given as  $Q = M_R$  .i.e., the number of streams for that particular UE is equal to the number of antenna at the UE.

## 7.5 Numerical Results

In this section, we show simulation results to evaluate the performance of the transmit precoding methods considered for the near-field beamforming for MU-MIMO mmWave systems. We assume that the BS uses a ULA with  $M_T = 128$  antennas which are

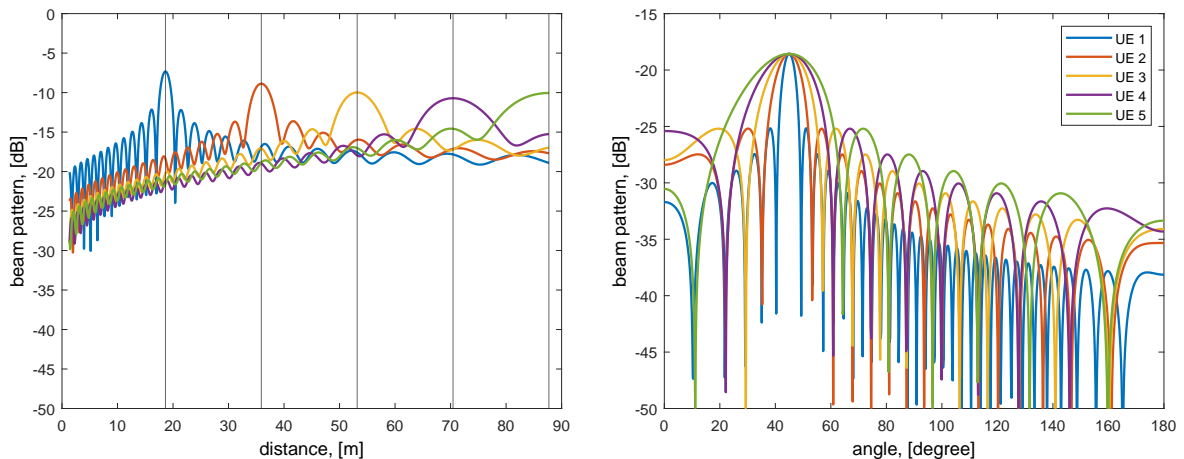


Fig. 7.2: Beam pattern for MRT. Left: Beam pattern vs. distance. Right: Beam pattern vs. angle.

uniformly spaced with  $d = \lambda/2$  at a carrier frequency of 28 GHz. We consider a system with  $\sigma_n^2 = 1$  and  $K = 5$  UEs each with  $M_R = 4$  antennas. The number of streams  $Q$  transmitted to each UE is equal to the number of antenna at the UE i.e.,  $Q = M_R = 4$ . With the above simulation parameters, the matrix that spans the null-space of  $\tilde{\mathbf{A}}_k \in \mathbb{C}^{M_R(K-1) \times M_T}$  matrix is given as  $\tilde{\mathbf{V}}_k^{(0)} \in \mathbb{C}^{128 \times 112}$  and the matrix whose columns are the right singular vectors corresponding to the  $M_R$  largest singular values of  $\mathbf{A}_k \tilde{\mathbf{V}}_k^{(0)} \in \mathbb{C}^{M_R \times (M_T - M_R(K-1))}$  is given as  $\mathbf{V}_k^{\max} \in \mathbb{C}^{112 \times 4}$ .

We present a worst-case scenario where the UEs are uniformly spaced at the same angle in the radiative near-field of the BS antenna as shown in Fig. 7.1. We assume that the UEs have the same AoA  $\theta_1 = \theta_K = 45^\circ$  where the angle is with respect to the phase center of the BS array. In our numerical experiments, the distance between the UEs and the BS is given as  $r = [18.63, 35.90, 53.17, 70.44, 87.71]m$ .

Fig. 7.2 shows the normalized beam pattern for the MRT scheme for the different users versus their distance from the transmitting antenna for the MU-MISO setup on the left. The result depicts the distance discrimination potentials of the near-field beamforming, as the UEs can be separated by their respective distance to the BS. It is seen that the MRT schemes do not cancel the MUI and that the UE closer to the BS has a more focused beam, while the beam focus expands for UEs farther away from the BS. Furthermore, the figure on the right depicts the normalized beam pattern with the AoA of  $\theta = 45^\circ$  for all the UEs, with the range  $\theta \in [0^\circ, 180^\circ]$ . It is observed that similar to the previous result the UE farthest from the BS has a directivity similar to the far-field scenario (see [170]), while the closet UE has the best directivity.

In Fig. 7.3 we show the normalized beam pattern versus distance for the ZF and MMSE schemes for the MU-MISO setup, respectively. Both precoding schemes improve

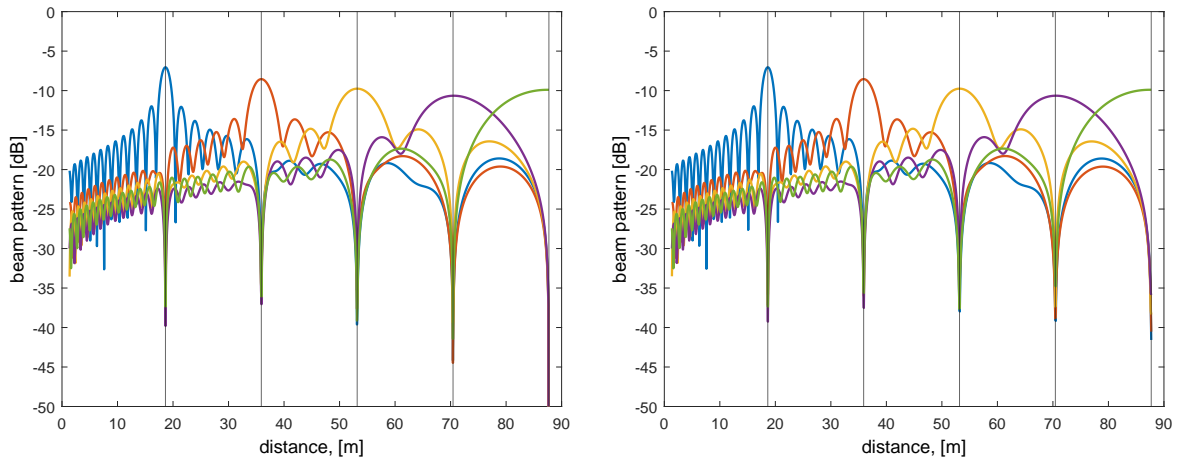
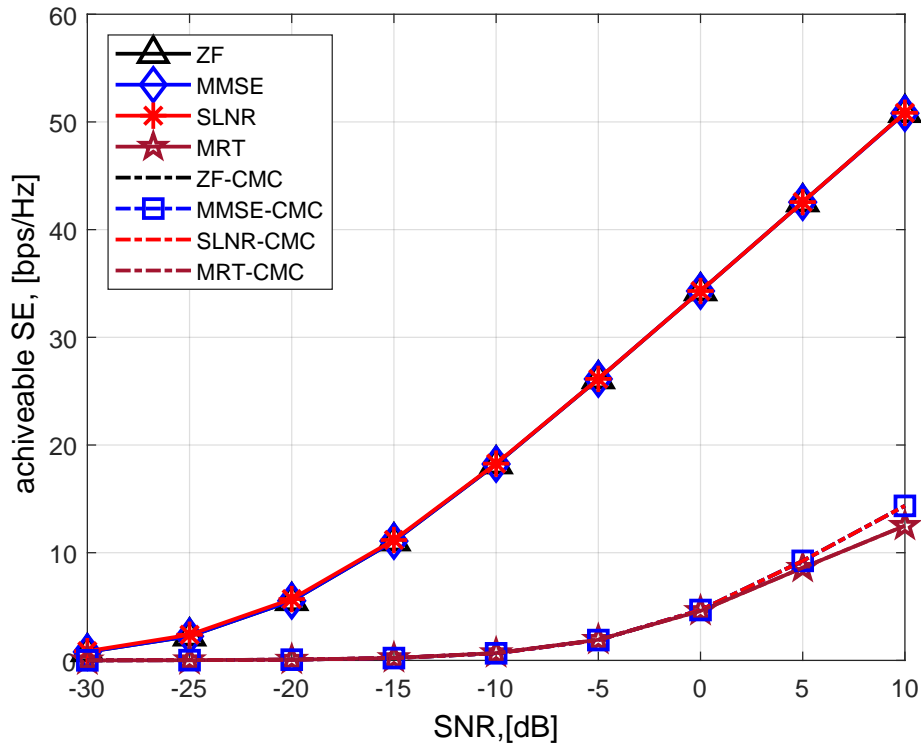


Fig. 7.3: Beam pattern vs. distance. Left: ZF. Right: MMSE.

Fig. 7.4: Achievable rate for MU-MISO setup ( $M_T = 128$ ,  $M_R = 1$ ,  $K = 5$ ).

the performance of the system by canceling the multi-user interference and improving the directivity of the beam for the desired users. This can be seen by the schemes successively placing nulls for the MUI at the desired UE locations as compared to the MRT scheme where there are no nulls placed for the MUI. Moreover, Fig. 7.4 shows the achievable rate given in (7.9) for the MU-MISO setup for different SNRs. It is observed that the MRT scheme has the worst performance as it does not attempt to cancel the MUI in the system. Furthermore, we observe a comparable performance improvement

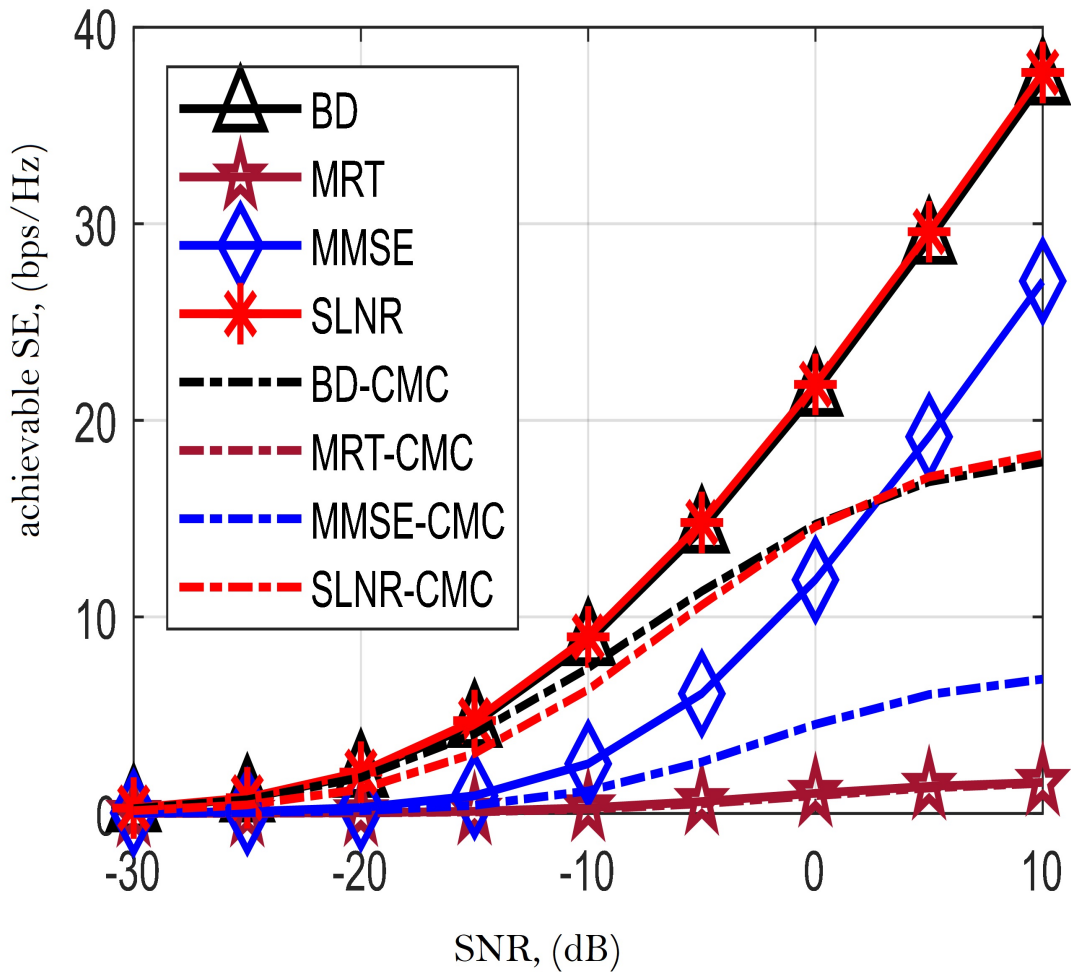


Fig. 7.5: Achievable rate for MU-MIMO setup ( $M_T = 128$ ,  $M_R = 4$ ,  $K = 5$ ).

with respect to the achievable rate for the other considered precoding schemes. The MMSE scheme depends on the levels of interference and noise: if the SNR is low the MMSE scheme looks more like an MRT, if the SNR is high the MMSE scheme looks like a ZF scheme.

In Fig. 7.5, the achievable rate (given in (7.9)) for the MU-MIMO setup is evaluated with respect to different values of SNRs. The SLNR scheme outperforms the other schemes in the high SNR regime, while the BD scheme has a better performance than the MMSE scheme because the BD scheme has the ability to make optimal use of the excess degrees of freedom available at the transmitter. We observe that there is a performance degradation between the continuous amplitude solution and the constant modulus (CMC) solution.

Furthermore, Fig. 7.6 depicts the achievable rate for the MU-MIMO setup with respect to increasing array size, which is given as  $M_T d$ . We consider various values

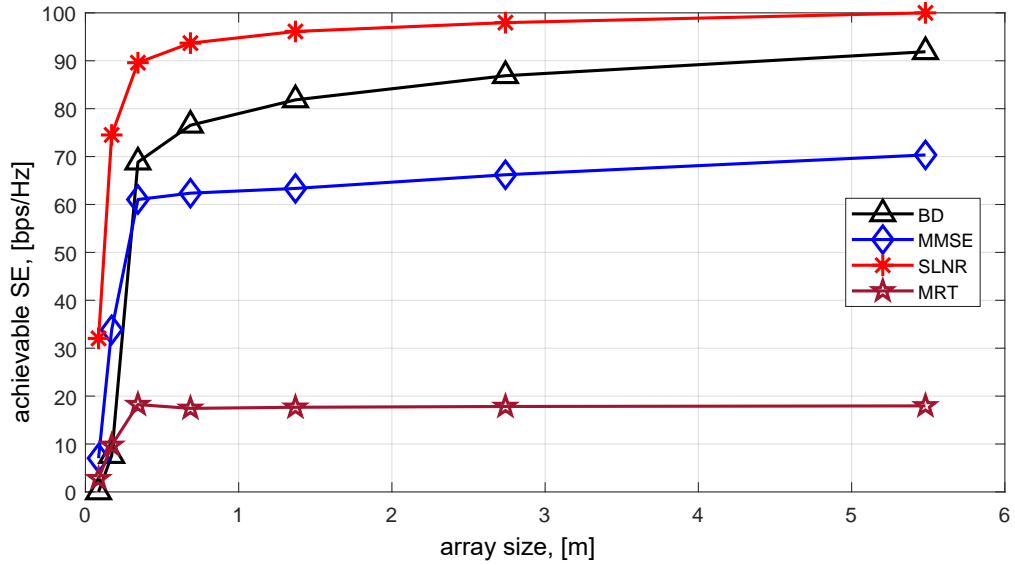


Fig. 7.6: Achievable rate vs array size ( $M_T d$ ) for MU-MIMO setup ( $M_R = 4$ ,  $K = 5$ ).

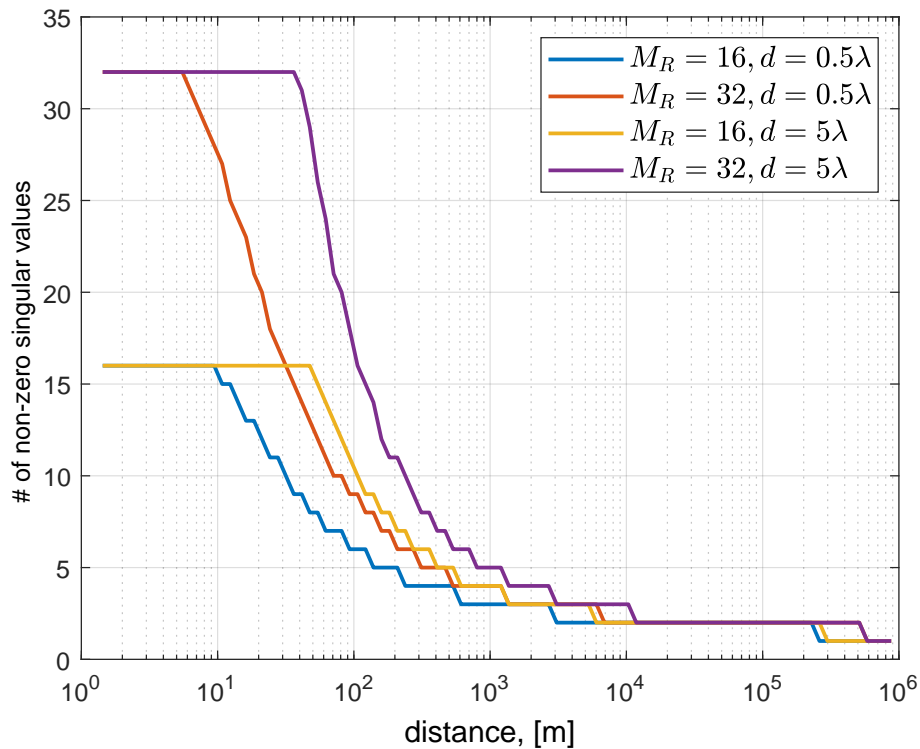


Fig. 7.7: Non-zero singular values vs distance.

of  $M_T$  with a fixed  $d = \lambda/2$  assuming that the SNR is 20 dB. It is observed that the achievable spectral efficiency improves with an increase in the array size for the considered precoding schemes with the MRT having the worst performance.

In Fig. 7.7, we show the profile of the number of non-zero singular values of the

steering matrix as a function of the distance for the various combinations of the number of antennas at the UE and inter-element spacing,  $d$ . From the figure, we observe that spatial multiplexing is possible in the near-field, and that the number of streams  $Q$  that can be transmitted to a UE depends on distance. The range of distances for the maximum possible streams (full rank) is increased with an increase in the aperture of the antenna array.

## 7.6 Chapter Conclusions

In this chapter, we have exploited the distance discrimination potential of near-field beamforming from a communications perspective to facilitate the deployment of high-rate MU-MIMO millimeter wave systems. We have studied the system's performance with the MRT, ZF, MMSE, and SLNR precoding schemes. Simulation results have shown that the SLNR scheme performs better for the MU-MIMO setup than the other schemes. The block diagonalization (BD) scheme, which is a generalized ZF scheme, has an improved performance than the MMSE scheme due to the ability of the BD algorithm to make optimal use of the excess degrees of freedom available at the BS.

## 8. ROBUST NEAR FIELD BEAMFORMING FOR MILLIMETER WAVE COMMUNICATION SYSTEMS WITH APERTURE PERTURBATIONS

Due to the potentially large size of the antenna array at the base station, it is difficult to ensure a perfect aperture geometry during the installation of the antenna, which might consist of multiple panels being stacked together. This leads to inevitable aperture deformations that degrade the overall performance of the communication system. Motivated by this, in this chapter, we develop near-field beamforming algorithms that are robust against aperture deformations. We consider the worst-case design approach and derive an analytical expression on the bound of the elements of the steering vector as a function of the known bounds of the coordinate displacement. Simulation results show that the proposed robust near-field beamforming algorithm outperforms the available benchmarks in the literature.

### 8.1 Introduction

To meet the demands for higher spectral efficiency, employing a large number of antennas in conjunction with the exploitation of higher frequencies has been recognized as a promising solution for future wireless systems [171,172]. Base stations (BSs) that operate in the mmWave band will employ large antenna arrays, as a result of the propagation conditions at these high frequencies [159]. Therefore, this will cause the communicating devices to operate within the BS antennas' near-field [173]. As a result, the far-field assumption used regularly in conventional wireless systems does not hold. This fact underlines the motivation for the research on near-field beamforming that has recently attracted a lot of attention from the research community. Radiative near-field propagation takes place between the Fraunhofer distance and the Fresnel distance of large-scale antenna arrays operating at mmWave frequencies [161,162]. The near-field distance can be several dozens of meters for relatively small antennas operating at

---

mmWave and Terahertz (THz) frequencies [46, 159].

At the same time, due to the potentially large size of the antenna arrays operating at mmWave frequencies, there might be different reasons for the emergence of perturbations in the aperture geometry. For example, these errors might occur during the installation of the antenna array. Due to the size of the antenna array, it is difficult to ensure a perfect aperture geometry during the installation of the antenna, which might consist of multiple panels being stacked together. This leads to inevitable aperture deformations that degrade the overall performance of the communication system, such as a reduction in the power gain, lower directivity, or a change in the direction of the main beam, as well as deviations in other performance standards [174, 175].

Most of the conventional methods for robust beamforming are designed for far-field scenarios. Moreover, most of them are focused on the robustness against the steering vector mismatch, which is caused by an estimation error of the angle of arrival (AoA) or angle of departure (AoD) [170, 176, 177]. For example, the authors in [170] proposed a robust algorithm based on prior information about a bound on the steering vector mismatch to avoid self-nulling of the desired signal even in the case of worst-case perturbations. On the other hand, the authors in [178] considered a beamforming design that is robust to aperture deformations caused by thermal deformations. Unfortunately, this work has a limited application for the problem we consider, since the system model is based on the far-field assumption and considers non-terrestrial networks. There are also a few references related to the design of robust beamforming algorithms for near-field users. The authors in [179] proposed a near-field beamforming algorithm robust to steering vector mismatches, which is a similar problem to [170]. In [180], the authors proposed a near-field beamforming algorithm with robustness against distance errors for acoustic signals. However, even though there are many excellent references on the topic of robust beamforming design, the number of publications for the implementation of robust beamforming methods for near-field users with respect to aperture deformations stays rather limited. In this chapter, we consider robust near-field beamforming for mmWave networks under aperture perturbations of the base station (BS) antenna array.

## 8.2 Chapter Contributions and Organization

In this chapter, we consider robust near-field beamforming for mmWave networks under aperture perturbations of the base station (BS) antenna array. The main contributions are as follows.

- We cast the problem as a worst-case optimization problem which has a deterministic upper bound on the norm of the steering vector error. To this end, for the considered near-field model we derive a closed-form expression for the bound on the norms of the perturbations of the array steering vector as a function of the bound on the coordinate displacements.
- We apply this bound during the optimization procedure to design beamformers that are robust to aperture perturbations.
- The performance of our proposed scheme is evaluated in terms of the output signal-to-inference-plus-noise ratio (SINR) and transmit power. Results from our numerical analysis show that the proposed robust near-field beamforming scheme outperforms the benchmark schemes. The concept of the robust near-field beamforming design presented in this chapter has been published in [47].

The rest of the chapter is organized as follows. The system model is introduced in Section 8.3. The aperture perturbation model considered in this chapter is presented in Section 8.4. In Section 8.5 the SINR maximization problem is formulated, while the worst-case robust beamforming solution is introduced in Section 8.6. Simulation results are then provided in Section 8.7, and conclusions are drawn in Section 8.8.

### 8.3 System Model

We consider a downlink multi-user MIMO system where the BS is equipped with a uniform rectangular array (URA) in the  $x$ - $y$  plane consisting of  $M_x$  and  $M_y$  antennas along the  $X$ - and  $Y$ - directions such that  $M_T = M_x \cdot M_y$  is the total number of BS antennas. Furthermore, we assume that  $M_x$  and  $M_y$  are even integers. We assume that the phase center of the BS antenna array is in the center of the URA at the origin of the coordinate system as shown in Fig. 8.1. The inter-element spacing between the elements along the  $x$ -axis and the  $y$ -axis is denoted as  $\Delta_x$  and  $\Delta_y$ , respectively.

The BS serves a single antenna user equipment (UE) in the radiative near-field of the BS. The spherical coordinates of the UE are given as  $(\theta_{rx}, \phi_{rx}, r_{rx})$ , where  $\theta_{rx} \in [-180^\circ, 180^\circ]$  and  $\phi_{rx} \in [-90^\circ, 90^\circ]$  are the azimuth and elevation angles in the direction of the phase center of the transmitter, respectively, while  $r_{rx}$  is the distance towards it. The received signal at the UE can be written as

$$y(k) = \mathbf{w}^H \mathbf{x}(k), \quad (8.1)$$

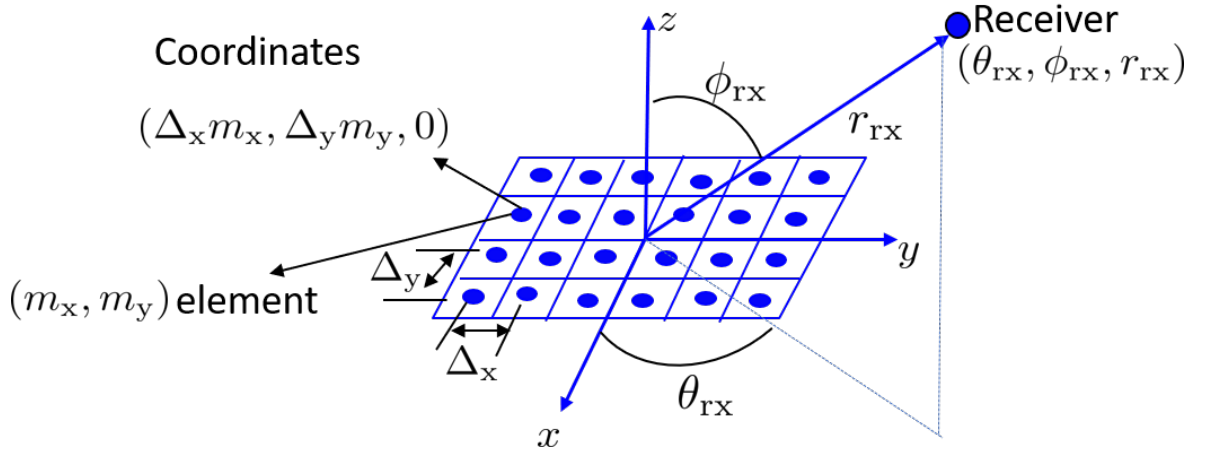


Fig. 8.1: Configuration and Orientation of URA at the BS

where  $\mathbf{w} \in \mathbb{C}^{M_T \times 1}$  denotes the vector of beamforming weights,  $\mathbf{x}(k) \in \mathbb{C}^{M_T \times 1}$  is the input vector, and  $k$  denotes the time index. The input vector can be described as

$$\mathbf{x}(k) = \mathbf{a}s(k) + \mathbf{i}(k) + \mathbf{n}(k), \quad (8.2)$$

where  $\mathbf{a} = \text{vec}\{\mathbf{A}\} \in \mathbb{C}^{M_T \times 1}$  is the vectorization of the near-field steering matrix  $\mathbf{A} \in \mathbb{C}^{M_x \times M_y}$  comprising the response between every element of the BS antenna array and the UE. Furthermore,  $s(k)$  is the desired signal,  $\mathbf{i}(k)$  is the interference, and  $\mathbf{n}(k) \in \mathbb{C}^{M_T \times 1}$  is the noise assumed as zero-mean circularly symmetric complex Gaussian.

The  $(m_x, m_y)$  element of the near-field steering matrix  $\mathbf{A}$  where  $0 \leq m_x \leq m_x - 1$ ,  $0 \leq m_y \leq m_y - 1$  can be described as

$$\mathbf{A}(m_x, m_y) = \frac{1}{\delta_{m_x, m_y}} e^{-j \frac{2\pi}{\lambda} \delta_{m_x, m_y}} \in \mathbb{C}, \quad (8.3)$$

where  $\delta_{m_x, m_y}$  is the distance between the  $(m_x, m_y)$  element of the BS antenna array and the receive antenna given as

$$\delta_{m_x, m_y} = \sqrt{(x_{rx} - m_x \Delta_x)^2 + (y_{rx} - m_y \Delta_y)^2 + (z_{rx} - 0)^2}, \quad (8.4)$$

where  $(x_{rx}, y_{rx}, z_{rx})$  represent the cartesian coordinates of the UE, which are given as  $x_{rx} = r_{rx} \sin \phi_{rx} \cos \theta_{rx}$ ,  $y_{rx} = r_{rx} \sin \phi_{rx} \sin \theta_{rx}$ , and  $z_{rx} = r_{rx} \cos \phi_{rx}$ , respectively. Using a first order approximation, (8.4) can be further simplified as

$$\delta_{m_x, m_y} = L_{\text{rx}} \sqrt{1 - \frac{2m_x \Delta_x x_{\text{rx}} + 2m_y \Delta_y y_{\text{rx}} - m_x^2 \Delta_x^2 - m_y^2 \Delta_y^2}{L_{\text{rx}}^2}}, \quad (8.5a)$$

$$\approx L_{\text{rx}} - \frac{2m_x \Delta_x x_{\text{rx}} - m_x^2 \Delta_x^2}{2L_{\text{rx}}} - \frac{2m_y \Delta_y y_{\text{rx}} - m_y^2 \Delta_y^2}{2L_{\text{rx}}}, \quad (8.5b)$$

where  $L_{\text{rx}} = \sqrt{x_{\text{rx}}^2 + y_{\text{rx}}^2 + z_{\text{rx}}^2}$  and we used the approximation  $\sqrt{1+x} \approx 1 + \frac{x}{2}$  for small  $x$ . We note that  $L_{\text{rx}}$  is the distance between the receiver and the antenna at the BS, which is the cartesian coordinate equivalent of  $r_{\text{rx}}$ , i.e.,  $L_{\text{rx}} = r_{\text{rx}}$

## 8.4 Aperture Perturbation Model

In this section, we introduce the BS antenna array aperture perturbation model and describe its impact on the components of the received signal given in (8.1). One of the possible causes of aperture perturbation may be as a result of imperfect installation of the antenna array. We use a deterministic uncertainty region model in which the error is bounded. We assume that the imperfections due to aperture perturbation lead to a displacement in the  $(x, y, z)$  coordinates of the elements of the BS antenna array. We assume that different coordinates are uncorrelated, while the perturbation of one coordinate can be defined by the corresponding known bound.

Let us denote  $\boldsymbol{\sigma} = [\sigma_x, \sigma_y, \sigma_z]^T \in \mathbb{R}^3$  as a vector that contains the known bounds of the perturbation for each axis as shown in Fig. 8.2. In this chapter, we assume that the displacements for the  $x$  and  $y$  coordinates are much smaller in comparison to the displacement for the  $z$  coordinate, i.e.,  $\sigma_z \gg \sigma_x \approx \sigma_y$ . On the other hand, the uncertainty region can be described as an ellipsoid of known shape [177]. The uncertainty ellipse  $\mathcal{E}$  for the vector displacement  $\mathbf{p} \in \mathbb{R}^3$  is defined as  $\mathcal{E}_p = \{\text{diag}(\boldsymbol{\sigma}) \cdot \mathbf{u} \mid \|\mathbf{u}\| \leq 1, \mathbf{u} \in \mathbb{R}^3\}$ . We assume that we have information only about the statistics of the perturbation but not the instantaneous realizations of them. The  $(m_x, m_y)$  element of the steering matrix of the input signal affected by the perturbations is given by

$$\tilde{\mathbf{A}}(m_x, m_y) = \frac{1}{\tilde{\delta}_{m_x, m_y}} e^{-j \frac{2\pi}{\lambda} \tilde{\delta}_{m_x, m_y}} \in \mathbb{C}, \quad (8.6)$$

where  $\tilde{\delta}_{m_x, m_y}$  is defined as

$$\tilde{\delta}_{m_x, m_y} = \sqrt{(x_{\text{rx}} - m_x \Delta_x + p_{m_x, m_y}^{\text{err}, x})^2 + (y_{\text{rx}} - m_y \Delta_y + p_{m_x, m_y}^{\text{err}, y})^2 + (z_{\text{rx}} - 0 + p_{m_x, m_y}^{\text{err}, z})^2}, \quad (8.7)$$

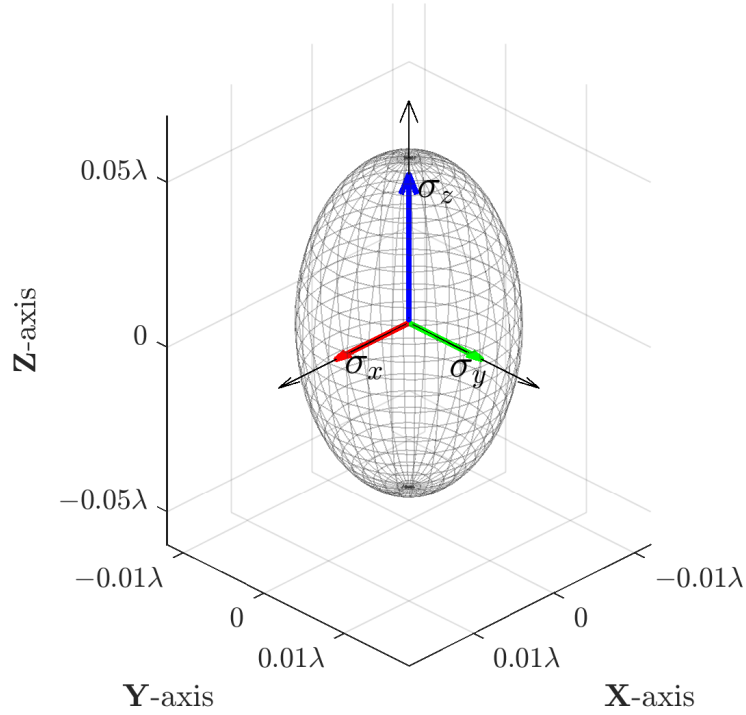


Fig. 8.2: Bounds of the perturbation for each axis of URA at the BS

and the variable,  $p_{m_x, m_y}^{\text{err}, i}$  is the random displacement along the  $i$  axis,  $i \in \{x, y, z\}$ . Similarly, using a first order approximation we can approximate  $\tilde{\delta}_{m_x, m_y}$  as

$$\tilde{\delta}_{m_x, m_y} = L_{\text{rx}} \sqrt{1 - \frac{2m_x \Delta_x x_{\text{rx}} + 2m_y \Delta_y y_{\text{rx}} - m_x^2 \Delta_x^2 - m_y^2 \Delta_y^2 + \xi_{m_x, m_y}^{\text{err}}}{L_{\text{rx}}^2}}, \quad (8.8)$$

$$\approx L_{\text{rx}} - \frac{2m_x \Delta_x x_{\text{rx}} - m_x^2 \Delta_x^2}{2L_{\text{rx}}} - \frac{2m_y \Delta_y y_{\text{rx}} - m_y^2 \Delta_y^2}{2L_{\text{rx}}} - \frac{\xi_{m_x, m_y}^{\text{err}}}{2L_{\text{rx}}}, \quad (8.9)$$

$$\approx \delta_{m_x, m_y} + \Delta \delta_{m_x, m_y}, \quad (8.10)$$

where  $\Delta \delta_{m_x, m_y} = -\frac{\xi_{m_x, m_y}^{\text{err}}}{2L_{\text{rx}}}$  and

$$\xi_{m_x, m_y}^{\text{err}} = 2(x_{\text{rx}} - m_x \Delta_x) p_{m_x, m_y}^{\text{err}, x} + 2(y_{\text{rx}} - m_y \Delta_y) p_{m_x, m_y}^{\text{err}, y} + 2(z_{\text{rx}} - 0) p_{m_x, m_y}^{\text{err}, z}.$$

Next, we compute a first-order Taylor expansion for small perturbations given as

$$\begin{aligned} e^{j(\alpha + \Delta\alpha)} &= e^{j\alpha} + j\Delta\alpha e^{j\alpha} + \mathcal{O}(\Delta^2) \\ &\approx e^{j\alpha} + \Delta_\alpha, \end{aligned} \quad (8.11)$$

where  $\Delta_\alpha = j\Delta\alpha e^{j\alpha}$ . Then by applying (8.11) to (8.6), we can find the first-order Taylor approximation for the expression of the  $(m_x, m_y)$  element of the perturbed matrix  $\tilde{\mathbf{A}}$  as

$$\tilde{\mathbf{A}}(m_x, m_y) = \frac{1}{\tilde{\delta}_{m_x, m_y}} e^{-j\frac{2\pi}{\lambda}\tilde{\delta}_{m_x, m_y}} \quad (8.12)$$

$$\approx \frac{1}{\delta_{m_x, m_y}} e^{j\frac{2\pi}{\lambda}(\delta_{m_x, m_y} + \Delta\delta_{m_x, m_y})} \quad (8.13)$$

$$\approx \frac{1}{\delta_{m_x, m_y}} e^{-j\frac{2\pi}{\lambda}\delta_{m_x, m_y}} - j\frac{2\pi}{\lambda} \frac{\Delta\delta_{m_x, m_y}}{\delta_{m_x, m_y}} e^{-j\frac{2\pi}{\lambda}\delta_{m_x, m_y}} \quad (8.14)$$

$$= \mathbf{A}(m_x, m_y) + \Delta\mathbf{A}(m_x, m_y) \in \mathbb{C}, \quad (8.15)$$

where  $\Delta\mathbf{A}(m_x, m_y) = -j\frac{2\pi}{\lambda}\Delta\delta_{m_x, m_y}\mathbf{A}(m_x, m_y)$ . Additionally, we represent the expression  $j\frac{2\pi}{\lambda}\Delta\delta_{m_x, m_y}$  in vector format after back substitution as

$$= j\frac{2\pi}{\lambda} \left( \frac{(x_{\text{rx}} - m_x\Delta_x)p_{m_x, m_y}^{\text{err}, x} + (y_{\text{rx}} - m_y\Delta_y)p_{m_x, m_y}^{\text{err}, y} + (z_{\text{rx}} - 0)p_{m_x, m_y}^{\text{err}, z}}{L_{\text{rx}}} \right), \quad (8.16)$$

$$= j\frac{2\pi}{\lambda} \left[ \frac{(x_{\text{rx}} - m_x\Delta_x)}{L_{\text{rx}}}, \frac{(y_{\text{rx}} - m_y\Delta_y)}{L_{\text{rx}}}, \frac{z_{\text{rx}}}{L_{\text{rx}}} \right] \cdot [p_{m_x, m_y}^{\text{err}, x}, p_{m_x, m_y}^{\text{err}, y}, p_{m_x, m_y}^{\text{err}, z}]^T, \quad (8.17)$$

$$= \mathbf{q}_{m_x, m_y}^T \mathbf{p}_{m_x, m_y}, \quad (8.18)$$

where

$$\mathbf{q}_{m_x, m_y} = j\frac{2\pi}{\lambda} \left[ \frac{(x_{\text{rx}} - m_x\Delta_x)}{L_{\text{rx}}}, \frac{(y_{\text{rx}} - m_y\Delta_y)}{L_{\text{rx}}}, \frac{z_{\text{rx}}}{L_{\text{rx}}} \right]^T,$$

and

$$\mathbf{p}_{m_x, m_y} = [p_{m_x, m_y}^{\text{err}, x}, p_{m_x, m_y}^{\text{err}, y}, p_{m_x, m_y}^{\text{err}, z}]^T.$$

As a result, we can write

$$\Delta\mathbf{A}(m_x, m_y) = \mathbf{p}_{m_x, m_y}^T \mathbf{q}_{m_x, m_y} \mathbf{A}(m_x, m_y). \quad (8.19)$$

After that, we find the bound on the norm of the mismatch of each element of the near-field steering matrix  $\mathbf{A}$  caused by aperture perturbation with a known norm of the bound of error  $\|\mathbf{p}_{m_x, m_y}\|_2 \in \mathcal{E}_p$ . The bound on the norm of the mismatch is given as

$$\begin{aligned}
 \|\Delta\mathbf{A}(m_x, m_y)\|_2 &= \sqrt{\Delta\mathbf{A}^*(m_x, m_y)\Delta\mathbf{A}(m_x, m_y)}, \\
 &= \sqrt{\mathbf{A}^*(m_x, m_y)\mathbf{q}_{m_x, m_y}^H \mathbf{p}_{m_x, m_y}^* \mathbf{p}_{m_x, m_y}^T \mathbf{q}_{m_x, m_y} \mathbf{A}(m_x, m_y)}, \\
 &\leq \frac{1}{\delta_{m_x, m_y}} \|\boldsymbol{\sigma}\|_2 \|\mathbf{q}_{m_x, m_y}\|_2 = \epsilon_{m_x, m_y},
 \end{aligned} \tag{8.20}$$

where we apply the *Cauchy-Bunyakovsky-Schwarz* inequality for inner products, i.e.,  $\|\mathbf{b}^H \mathbf{d}\|_2 \leq \|\mathbf{b}\|_2 \cdot \|\mathbf{d}\|_2$ ,  $\forall \mathbf{b}, \mathbf{d} \in \mathbb{C}^m$ .

## 8.5 Problem Formulation

The signal-to-interference-plus-noise ratio (SINR) at the receiver can be written as [181]

$$\text{SINR} = \frac{\sigma_s^2 |\mathbf{w}^H \mathbf{a}|^2}{\mathbf{w}^H \mathbf{R}_{i+n} \mathbf{w}}, \tag{8.21}$$

where  $\mathbf{R}_{i+n} = \mathbb{E}\{[\mathbf{i}(k) + \mathbf{n}(k)][\mathbf{i}(k) + \mathbf{n}(k)]^H\} \in \mathbb{C}^{M_T \times M_T}$  is the interference-plus-noise covariance matrix,  $\sigma_s^2$  is the signal power, and  $\mathbb{E}\{\cdot\}$  denotes the statistical expectation. The optimal weight vector can be found via a maximization of the SINR in (8.21) which is equivalently written as

$$\min_{\mathbf{w}} \quad \mathbf{w}^H \mathbf{R}_{i+n} \mathbf{w} \tag{8.22a}$$

$$\text{s. t.} \quad \mathbf{w}^H \mathbf{a} = 1, \tag{8.22b}$$

where the optimal weight vector is given as [182]

$$\mathbf{w}_{\text{opt}} = \beta \mathbf{R}_{i+n}^{-1} \mathbf{a}, \tag{8.23}$$

and  $\beta = 1/\mathbf{a}^H \mathbf{R}_{i+n}^{-1} \mathbf{a}$ . However, the matrix is commonly replaced by the sample covariance matrix due to the unavailability of the true interference-plus-noise covariance matrix in practice. The sample covariance matrix given as

$$\hat{\mathbf{R}} = \frac{1}{N_s} \sum_{k=1}^{N_s} \mathbf{x}(k) \mathbf{x}(k)^H, \tag{8.24}$$

where  $N_s$  is the number of snapshots. Therefore, problem (8.22a) can be rewritten as

$$\min_{\mathbf{w}} \quad \mathbf{w}^H \hat{\mathbf{R}} \mathbf{w} \tag{8.25a}$$

$$\text{s. t.} \quad \mathbf{w}^H \mathbf{a} = 1. \tag{8.25b}$$

A direct solution to the minimum variance distortionless response (MVDR) problem in (8.25a) is known as the sample matrix inversion (SMI) beamformer, where the optimal weight vector is given as

$$\mathbf{w}_{\text{SMI}} = \alpha \hat{\mathbf{R}}^{-1} \mathbf{a}, \quad (8.26)$$

and  $\alpha = 1/\mathbf{a}^H \hat{\mathbf{R}}^{-1} \mathbf{a}$ . However, this solution essentially lacks the necessary robustness to handle a mismatch between the presumed and actual steering vectors. As a result, this leads to self-nulling of the desired signal. In the following, we develop a new robust near-field beamformer that takes into account the prior information about the bound on the perturbation of the  $(m_x, m_y)$  element of the steering matrix  $\mathbf{A}$ . We denote the actual steering vector comprising the effect of the random perturbations of the surface on the BS antenna array as  $\tilde{\mathbf{a}}$ . The relationship between the actual and the presumed steering vector is given as

$$\tilde{\mathbf{a}} = \mathbf{a} + \mathbf{e}, \quad (8.27)$$

where  $\mathbf{a} = \text{vec}(\mathbf{A})$  and the vector  $\mathbf{e} \in \mathbb{C}^{M_T \times 1}$  models the effect of the random perturbations on the steering vector due to aperture perturbations.

## 8.6 Worst-Case Robust beamforming

For the conventional worst-case steering vector error model, the norm of the error vector is bounded by some known constant. In this section, the norm of the error vector is bounded by  $\gamma$ , i.e.,  $\|\mathbf{e}\| \leq \gamma$  where  $\gamma$  is obtained from (8.20) as  $\gamma = \sqrt{M_T} \max(\epsilon_m), \forall m \in M_T$  which represents the worst-case bound on the perturbations. Next, we denote  $\mathcal{A}$  as the set of all possible realizations of the steering vector impacted by random perturbations

$$\mathcal{A} = \{\tilde{\mathbf{a}} | \tilde{\mathbf{a}} = \mathbf{a} + \mathbf{e}, \|\mathbf{e}\| \leq \gamma\}. \quad (8.28)$$

Therefore, the robust near-field beamforming that tries to maximize the SINR for the worst-case perturbation in the case of steering vector mismatch can be written as

$$\min_{\mathbf{w}} \quad \mathbf{w}^H \hat{\mathbf{R}} \mathbf{w}, \quad (8.29a)$$

$$\text{s. t. } \min_{\tilde{\mathbf{a}} \in \mathcal{A}} |\mathbf{w}^H \tilde{\mathbf{a}}| \geq 1, \quad (8.29b)$$

where (8.29) designs the beamforming weight by minimizing the worst-case output power subject to the distortionless response constraint which must be satisfied for the steering vector bounded by the worst-case norm  $\mathbf{e}$  [170]. The constraint in problem

(8.29) will be satisfied by a worst-case vector  $\tilde{\mathbf{a}}$  that lies on the boundary of the uncertainty set  $\mathcal{A}$ . The nonlinear constraint in (8.29b) can be equivalently written as

$$\min_{\mathbf{e} \in \mathcal{D}(\gamma)} |\mathbf{w}^H(\mathbf{a} + \mathbf{e})| \geq 1, \quad (8.30a)$$

where the set  $\mathcal{D}(\gamma) \triangleq \{\mathbf{e} \mid \|\mathbf{e}\| \leq \gamma\}$ . Following [170], we can show that the vector that achieves the minimum can be found by solving the problem

$$|\mathbf{w}^H(\mathbf{a} + \mathbf{e})| = |\mathbf{w}^H\mathbf{a}| - \gamma\|\mathbf{w}\|, \quad (8.31)$$

such that the solution with respect to the vector  $\mathbf{e}$  can be written as  $\mathbf{e} = -\frac{\mathbf{w}}{\|\mathbf{w}\|}\gamma e^{j\phi}$ , where  $\phi = \angle(\mathbf{w}^H\mathbf{a})$ . From [170], it is required that  $|\mathbf{w}^H\mathbf{a}| \geq \gamma\|\mathbf{w}\|$ , otherwise the white noise gain of the robust beamformer may be insufficient, where the white noise gain is the array gain when the noise term  $\mathbf{n}$  is spatially white. Therefore, the constraint in (8.29b) can be replaced by  $|\mathbf{w}^H\mathbf{a}| - \gamma\|\mathbf{w}\| \geq 1$ .

Then, the worst-case robust near-field beamforming problem can be written as

$$\min_{\mathbf{w}} \mathbf{w}^H \hat{\mathbf{R}} \mathbf{w}, \quad (8.32a)$$

$$\text{s. t. } |\mathbf{w}^H\mathbf{a}| - \gamma\|\mathbf{w}\| \geq 1. \quad (8.32b)$$

Since the cost function of (8.32a) is unchanged when  $\mathbf{w}$  undergoes an arbitrary phase rotation [170], then the problem can be rewritten as

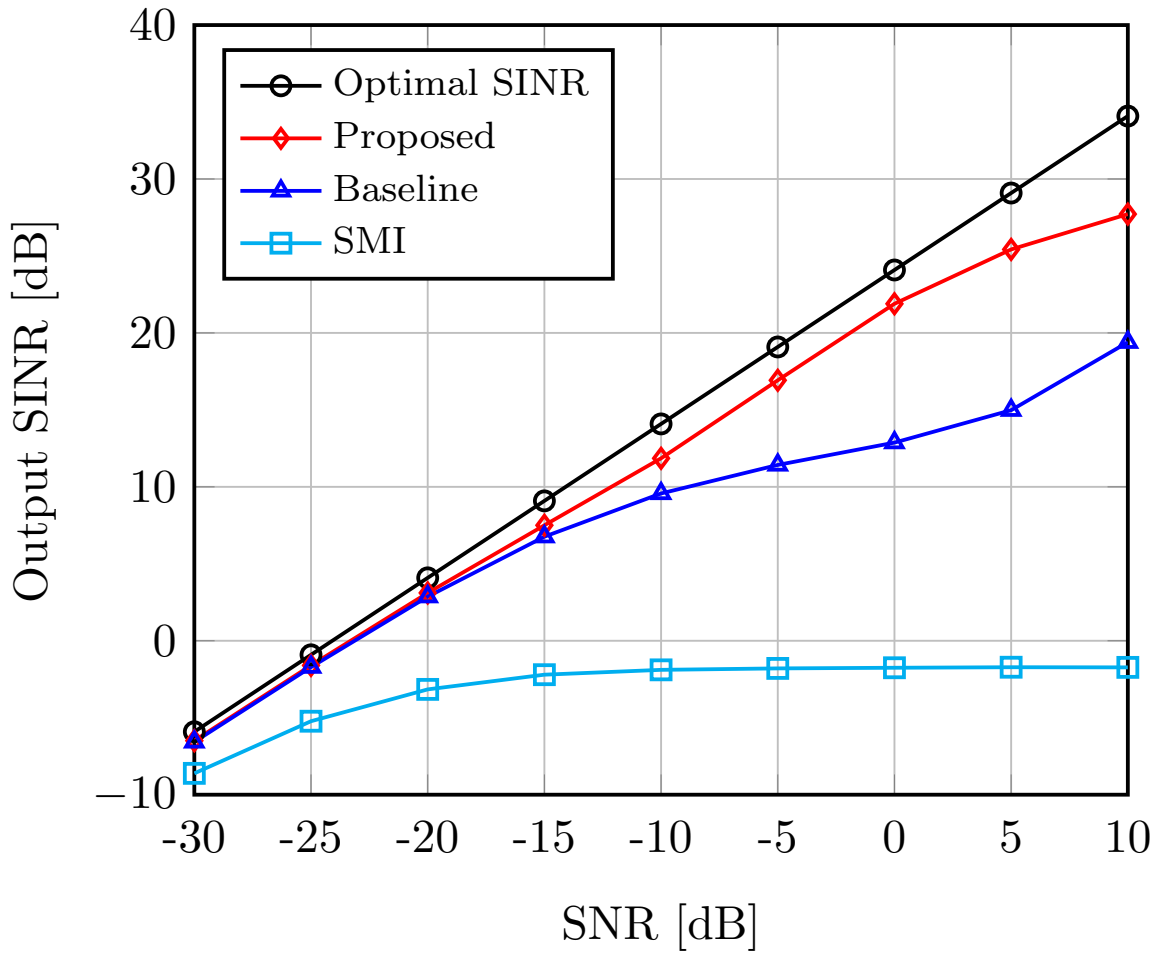
$$\min_{\mathbf{w}} \mathbf{w}^H \hat{\mathbf{R}} \mathbf{w} \quad (8.33a)$$

$$\text{s. t. } \mathbf{w}^H\mathbf{a} \geq \gamma\|\mathbf{w}\| + 1, \text{Im}\{\mathbf{w}^H\mathbf{a}\} = 0. \quad (8.33b)$$

The optimization problem (8.33) is convex, and can easily be reformulated as a second-order cone program (SOCP) similar to [170, 179] which can be solved using interior point methods with a complexity of  $\mathcal{O}(M_T^{3.5})$  [131].

## 8.7 Numerical Results

In this section, we show simulation results to evaluate the performance of the proposed and existing algorithms. We assume that the BS uses a URA with  $M_x = 64$  and  $M_y = 4$  antennas which are uniformly spaced. For simplicity we assume that  $\Delta_x = \Delta_y = \Delta = \lambda/2$  at a carrier frequency of 28 GHz. The azimuth and elevation angles of the desired UE are given as  $\{90^\circ, 45^\circ\}$ . We assume that there are two interferers whose azimuth and

Fig. 8.3: Output SINR versus SNR,  $N_s = 1000$ 

elevation angles are respectively given as  $\{50^\circ, 120^\circ\}$  and  $\{120^\circ, 90^\circ\}$ . The interference-to-noise ratio (INR) is 30 dB. The UEs are uniformly spaced in the radiative near-field of the BS antenna.

The proposed algorithm is compared with the optimal solution given in (8.23) according to [182], the sample matrix inversion (SMI) beamforming scheme given in (8.26), and the worst-case near-field beamforming design with a mismatch in the steering vector due to AoA errors (Baseline) according to [179] i.e., the solution to problem (8.33) with a mismatch due to AOA errors. In our simulations, the known bounds on the norm of the perturbations for each of the axes are given as  $(0.01\lambda, 0.01\lambda, 0.05\lambda)$ , for the steering vector mismatch algorithm we modified the known bound given in [179], to take into account the number of sensors,  $\epsilon = c\sqrt{M_T}$ ,  $c = 0.01$ .

Fig. 8.3 shows the SINR performance over the SNR for  $N_s = 1000$  samples. The result is averaged over 1000 realizations. From the figure, it is observed that the proposed algorithm outperforms the other existing schemes.

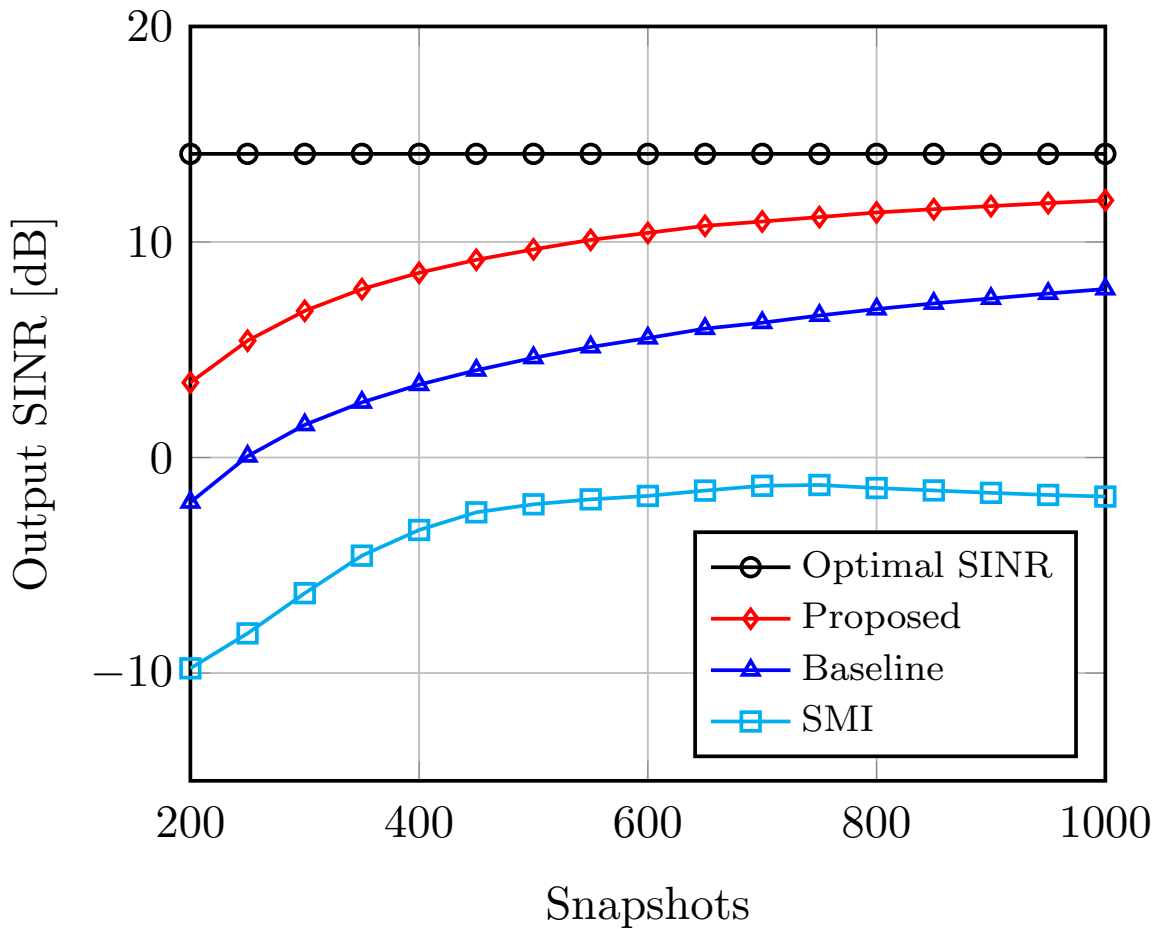
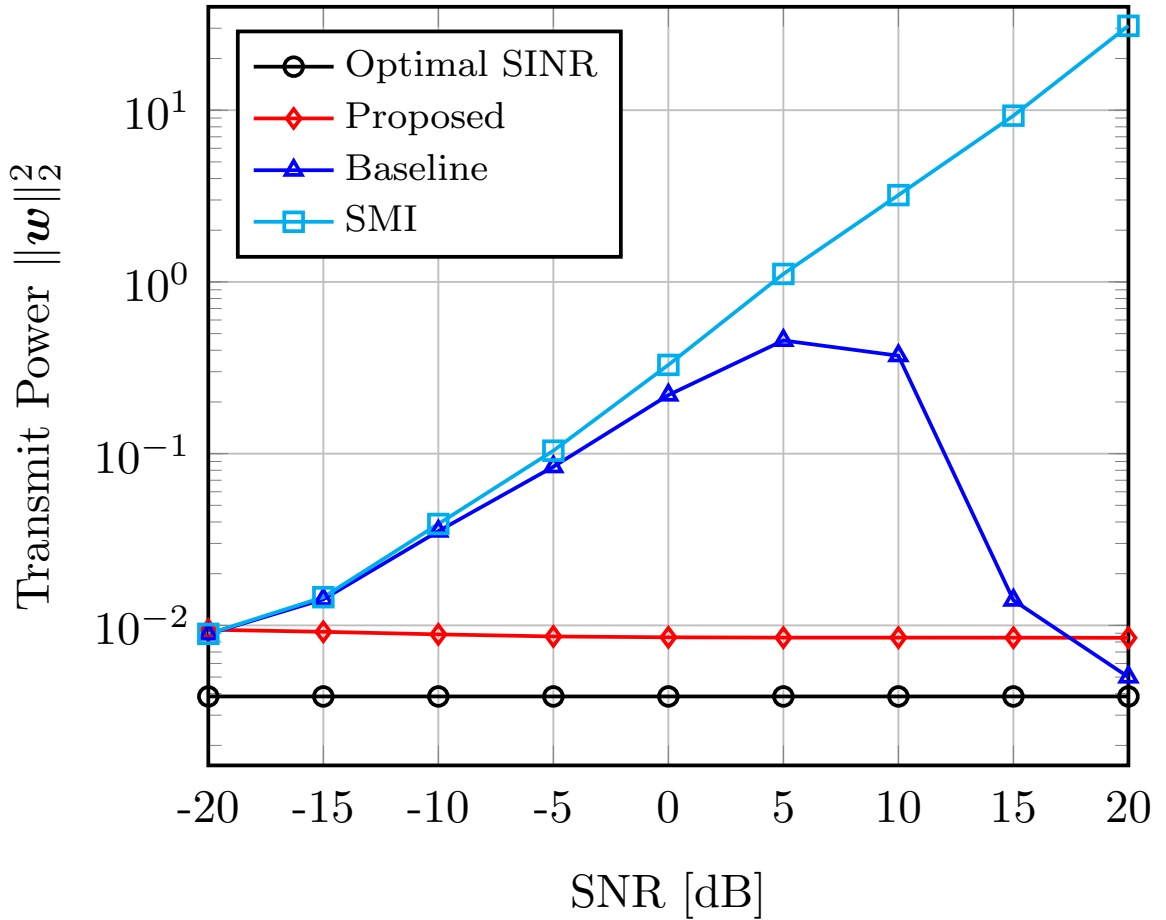


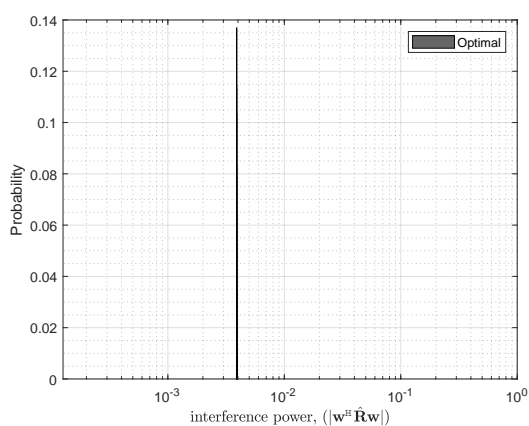
Fig. 8.4: Output SINR versus  $N_s$ , SNR= -15 dB

Fig. 8.4 presents the output SINR as a function of the number of snapshots. The considered SNR is -15 dB, and the result is averaged over 1000 realizations. Here the comparison of the convergence of the proposed robust near-field beamforming algorithm and the existing schemes is demonstrated. The proposed algorithm outperforms the existing solutions. In Fig. 8.5 the power consumption of the schemes is evaluated. From the figure, the proposed worst-case robust beamforming approach has a better power efficiency than the other existing schemes.

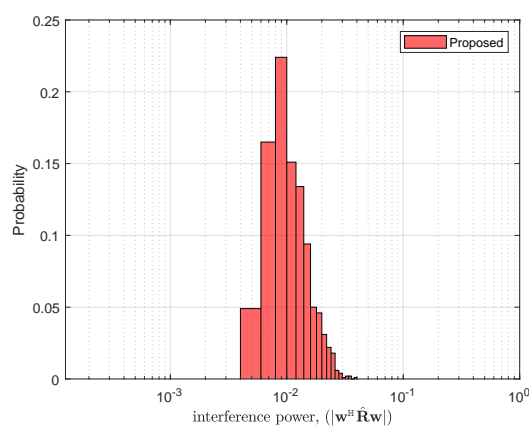
Additionally, we plot the histograms of the achieved objective function in problem (8.29), and the constraint in (8.29b) for all the considered schemes to verify that they are satisfied. The achieved solutions for the interference power and the desired power using the feasible solution  $\hat{\mathbf{w}}$  are given as  $|\hat{\mathbf{w}}^H \hat{\mathbf{R}} \hat{\mathbf{w}}|$  and  $|\hat{\mathbf{w}}^H \hat{\mathbf{a}}|$ , respectively. Fig. 8.6 provides the histogram plots for the achieved interference power for the various schemes obtained from 1000 random sets of channel realizations. The SINR target has been fixed to 5 dB. The results show that the proposed algorithm has a better performance in terms of minimizing the interference power in comparison with the other schemes, with the SMI

Fig. 8.5: Transmit power versus SINR,  $N_s = 1000$ 

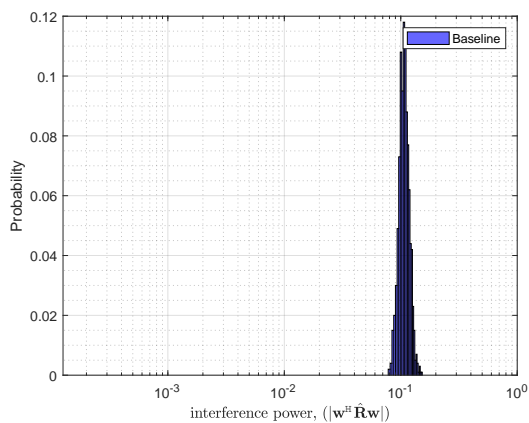
approach having the worst performance. This is because the SMI scheme in (8.26) lacks the necessary robustness to handle a mismatch between the presumed and actual steering vectors. As a result, this leads to self-nulling of the desired signal. In Fig. 8.7 we present the histogram plots for the achieved desired power. An achieved value greater than or equal to 1 indicates that the constraint in (8.29b) is satisfied. As shown in the figure, our proposed scheme achieves the best result as the constraint is satisfied in all cases. Furthermore, the constraint is satisfied by the Baseline scheme, whereas the SMI scheme satisfies the constraint only in a few cases. In both Figures 8.6 and 8.7 the optimal scheme in (8.23) which is the solution to the problem in (8.22a) has the desirable result compared to the other schemes. However, the solution is impractical as the true interference-plus-noise covariance matrix  $\mathbf{R}_{i+n}$  is not available in practice. Therefore, the matrix is commonly replaced by the sample covariance matrix  $\hat{\mathbf{R}}$ .



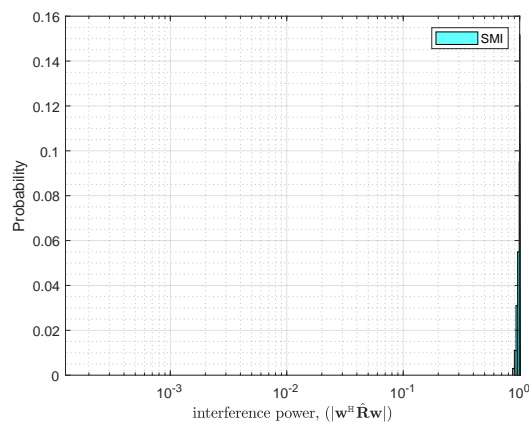
(a) Minimized interference power for the Optimal solution.



(b) Minimized interference power for the Proposed solution.

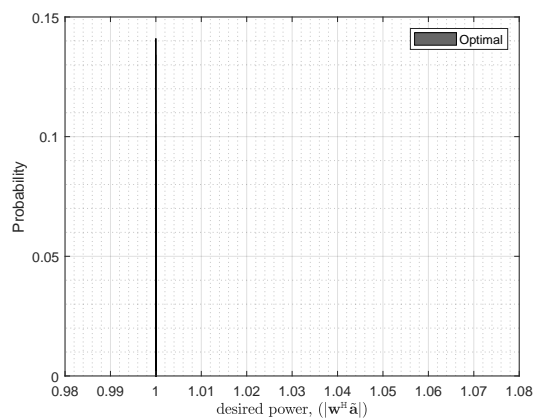


(c) Minimized interference power for the Baseline solution.

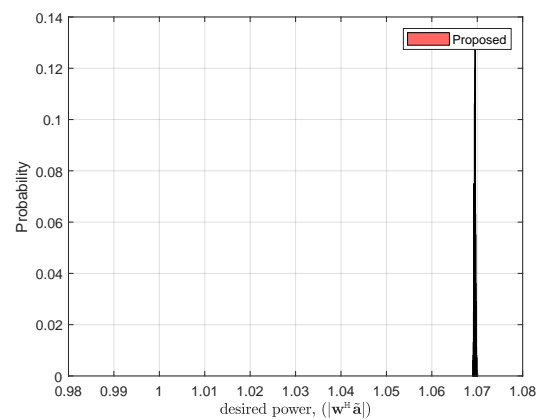


(d) Minimized interference power for the SMI solution.

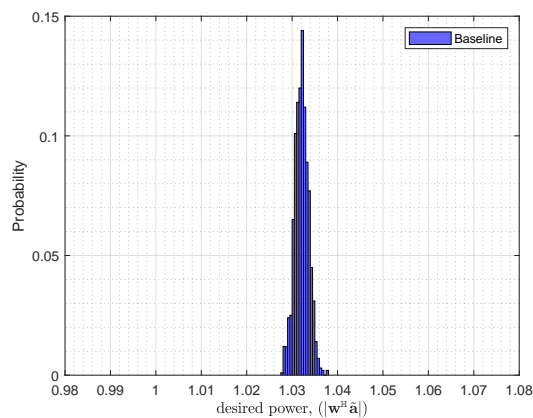
Fig. 8.6: Histogram of minimized interference power.



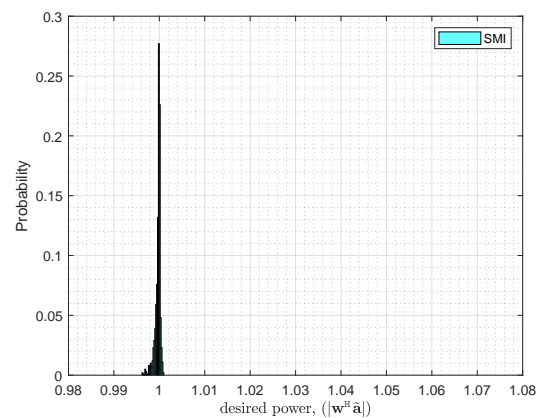
(a) Achieved desired power for the Optimal solution.



(b) Achieved desired power for the Proposed solution.



(c) Achieved desired power for the Baseline solution.



(d) Achieved desired power for the SMI solution.

Fig. 8.7: Histogram of achieved desired power.

---

## 8.8 Conclusions

In this chapter, we have proposed a robust near-field beamforming algorithm. The proposed algorithm demonstrated robustness due to BS antenna array aperture perturbations. We analytically derived the bounds on the perturbations of the steering vector as a function of the known norm of the coordinate displacements for the worst-case robust beamforming scheme. The simulation results confirm that the proposed robust near-field algorithm outperforms the other benchmark schemes, in terms of the output SINR and power consumption.

## 9. CONCLUSIONS AND FUTURE WORK

In this thesis, we focus on developing signal processing algorithms for multicell multi-user MIMO wireless communication systems. The main goal of the thesis is to fulfill some of the requirements for future wireless cellular networks, such as enhanced spectral and energy efficiencies, reduced latency, and greater flexibility in traffic handling. In this thesis, we address the major interference problem occasioned by the densification of communication networks and the advent of small cells for future wireless communication networks. We have shown in this thesis, that by exploiting the advantages offered by the DTDD system along with the potential benefits of the RIS, an efficient interference management scheme can be implemented to improve the overall system performance. The main contributions are summarized as follows.

Chapter 1 introduces the concept of signal processing for multicell multi-user MIMO communication systems. The motivation and the state of the art as well as the contributions of the thesis are provided in this chapter.

Chapter 2 is dedicated to the fundamental concepts of Reconfigurable Intelligent Surface (RIS) technology, its benefits, use cases, and applications in B5G and 6G networks. In addition, the channel estimation problem and the RIS reflection coefficient optimization methods are discussed, where we present the current state-of-the-art model for RIS-aided wireless communications. In Chapter 3, we address the joint optimization of the transmit beamforming and the passive beamforming for an RIS-aided DTDD wireless system to minimize the cross-link interference and maximize the system-wide spectral efficiency. However, the problem is shown to be non-convex as a result of the coupling of the optimization variables and the constant modulus constraints of the RIS. Therefore, to obtain a solution, we propose two different novel non-iterative algorithms for solving the problem. The first algorithm designs a single RIS passive reflection vector for the cells in the DTDD system and designs the transmit beamforming vector using the zero-forcing scheme. In the first algorithm we intuitively design the RIS reflection coefficient vector to mitigate the cross-link interference and maximize the SE. However, to reduce overhead and complexity, we propose a heuristic approach in designing the RIS reflection coefficient vector in order to address the issue of the cross-link interference and further improve the system performance. The second algorithm designs the RIS passive reflection vector to maximize the desired user signal

power of each cell independently. We investigate the performance of the two proposed algorithms using numerical examples. Results from our numerical experiments show that the proposed algorithms have a better sum rate performance as compared to a DTDD system without RIS. This shows that the integration of the RIS in a DTDD system has the potential to mitigate cross-link interference. This cross-link interference is one of the major challenges of DTDD wireless systems, as the interference can severely degrade the system performance, especially the performance of the cells operating in the uplink direction, if not properly managed.

Chapter 4 is devoted to designing a decentralized coordinated algorithm for an RIS-aided DTDD system. Future wireless communication systems are expected to be much more densified with small cells. Therefore, the implementation of a centralized scheme as presented in Chapter 3 may be impractical as a result of the high signaling overhead involved in the collection of all the channel state information at the CPU. As a result, a distributed solution is much more desirable. The design objective is to maximize the minimum SINR of the DL users while satisfying the total power constraint of the DL BSs. Additionally, the problem guarantees that the maximum interference seen by the UL users due to the transmission of the DL cells is below a pre-defined level. Therefore, in this case, the performance of the cells operating in both uplink and downlink directions can be guaranteed. Similarly, the problem is shown to be non-convex and NP-hard. To obtain a solution, we propose a novel distributed algorithm based on the relaxed SDP and ADMM techniques for solving the problem. One of the major benefits of the ADMM schemes is that it is a powerful decomposition technique that combines the superior convergence properties of the dual decomposition method and the numerical robustness of augmented Lagrangian method. Therefore, it is a favourable choice for practical implementation. The results demonstrate that the ADMM-based algorithm converges to the centralized solution after a few iterations.

In Chapter 5, we address the issue of further reducing the complexity involved with the joint design of the transmit beamforming and the passive beamforming for an RIS-aided DTDD wireless system. In this chapter, we consider a discrete phase-shift model for the RIS and the concept of signal leakage for the design of the transmit beamforming for an RIS-aided DTDD system controlled by a CPU. It has been shown that maximizing the SLNR for all the users in the downlink cells is an efficient way of designing the transmit beamforming vectors because it limits the search space and also lowers the complexity involved in finding efficient transmit beamformers. The decoupled nature of the SLNR criterion allows for a characterization of the solution to the multi-user beamforming problem in terms of generalized eigenvalue problems. The resulting optimization problem is solved by decoupling it among the variables. We

propose a low-complexity and non-iterative method for the design of the RIS reflection vector and the Rayleigh-Ritz method for the design of the transmit beamforming vectors. Moreover, we investigate the performance of the proposed algorithm using numerical examples, which show that the proposed algorithm achieves satisfactory performance compared to other baseline schemes.

Chapter 6 is devoted to the design of a robust transmit beamforming algorithm that minimizes the sum transmit power while satisfying the users' QoS targets in the presence of channel errors. The performance improvement obtainable from the joint design of the active and passive beamforming vectors for an RIS-aided DTDD wireless system heavily depends on the accuracy of the channel state information (CSI). However, due to estimation errors and limited feedback channels, the transmitters can never have perfect CSI. As a result, the performance targets can no longer be guaranteed if the CSI errors are not taken into account. To this end, robust beamforming solutions are much desired. We consider a conventional worst-case robust (WCR) formulation which has deterministic upper bounds on the norms of the channel estimation errors. However, it is impractical to use deterministic upper bounds on the norms of the channel errors. Due to the random nature of the wireless channel, it is more logical to exploit the statistical nature of these imperfections. Hence, we also consider a probabilistic-constrained robust (PCR) optimization problem, based on the statistical channel error model. We propose two algorithms based on the relaxed SDP to solve the two problems, respectively. Results from our numerical analysis show that the outage probability-based approach outperforms that of the worst-case design-based robust transmission strategy.

In Chapter 7, we carry out a preliminary investigation on the concept of near-field beamforming. As a result of the combination of massive MIMO and operations at mmWave frequencies, communicating devices will operate in the near-field of the BS antenna. We exploit the distance discrimination potential of the near-field beamforming from a communication perspective to facilitate the deployment of high-rate MU-MIMO millimeter wave systems. We investigate the system's performance using several precoding strategies. Our numerical results demonstrate a significant performance improvement due to the capability of the near-field beamforming to support reliable communications even for devices that are located in the same angular direction which corresponds to the "worst case" situation.

Finally, in Chapter 8, we study the robust near-field beamforming design. We propose a robust near-field beamforming algorithm that is robust against BS antenna array aperture perturbations. We analytically derive the bounds on the perturbations of the steering vector as a function of the known norm of the coordinate displacements

for the worst-case robust beamforming scheme. The simulation results confirm that the proposed robust near-field algorithm outperforms the other benchmark schemes.

## 9.1 Future works

Due to the densification of the small cells and the amount of CSI involved in an RIS-aided DTDD system, there is still the need to carry out further work to develop and implement solutions that will further reduce the complexity involved in the joint design of the RIS reflection coefficients and active beamforming in order to further reduce the burden on the CPU and the backhaul connections. In the following, we list some of the possible areas for the extension of the contents of this thesis.

### 9.1.1 Acquisition of channel state information

The channel estimation scheme adopted in this thesis and most of the works in the literature are mostly focused on the design of all the cascaded channel coefficients of all the RIS reflecting elements at once. Unfortunately, this approach requires a long training time which may not be practically available in the DTDD-based small cells due to their short packet transmissions with insufficient pilot length and/or fast-fading channels with a short coherence time. Therefore, the development of efficient and flexible channel estimation protocols for the RIS-aided DTDD systems with adjustable pilot duration to adapt to different transmission requirements and channel coherence time is worth investigating. One efficient way to tackle this problem may be the exploitation of machine learning techniques to predict the optimal RIS phase shifts for the UEs without the need for their explicit CSI.

### 9.1.2 Orthogonal frequency-division multiplexing System

Another possible extension of this thesis is the extension to orthogonal frequency-division multiplexing (OFDM) system subject to frequency-selective fading channels. The optimization of the RIS reflection design for rate maximization for OFDM-based systems is more challenging, as a result of the need to cater to more channels in both space and frequency. Additionally, the RIS phase shifts need to be jointly optimized with multiple transmit covariance matrices on different sub-carriers. This could be even more involved for an RIS-aided DTDD system. Therefore, there is a need to investigate and implement low-complexity and efficient algorithms for the OFDM-based

RIS-aided DTDD system. A possible solution is to adopt an successive convex approximation-based algorithm or an alternating optimization-based algorithm to extend the algorithms presented in this thesis for OFDM-based systems.

### 9.1.3 Integration of double RISs

Further performance improvement for RIS-aided DTDD systems could be obtained by extending the contents of this thesis to a DTDD system assisted by double RISs with direct LOS between the RISs [183]. Tensor-based signal processing techniques could be exploited to reduce the complexity that might be associated with such an implementation.

### 9.1.4 Effects of CSI estimation error on Near-field beamforming

The robust near-field beamforming implementation in Chapter 8 has considered the worst-case error model. However, the worst-case approach can be overly pessimistic because the probability of the actual worst-case errors occurring in practice may be extremely low. Therefore, it is interesting for near-field communications to investigate the effects of CSI estimation errors on the system performance and develop a robust beamforming algorithm based on the probabilistic error model as discussed in Chapter 6. The probabilistic error model has the advantage of being less conservative. It makes a prudent selection of the robustness parameters as compared with the worst-case approach by explicitly specifying them in terms of the covariance matrix and the outage probability.

## APPENDIX A. SYMBOLS AND NOTATION

$x, y$	Scalars
$\mathbf{x}, \mathbf{y}$	Vectors
$\mathbf{X}, \mathbf{Y}$	Matrices
$\mathbf{x}^\top, \mathbf{X}^\top$	Transpose of a vector or a matrix
$\mathbf{x}^H, \mathbf{X}^H$	conjugate transpose (Hermitian) of a vector or a matrix
$\mathbf{I}_p$	Identity matrix of size $p \times p$
$\mathbb{E}\{\cdot\}$	Expectation operator
$\text{Diag}(\boldsymbol{\lambda})$	Forms a square matrix with $\boldsymbol{\lambda}$ on its diagonal
$\text{diag}(\mathbf{\Lambda})$	Extracts the diagonal of matrix $\mathbf{\Lambda}$ into a vector
$\text{vec}(\cdot)$	Vectorization operator
$\circ$	Outer product
$\otimes$	Kronecker product
$\diamond$	Khatri-Rao product
$\ \mathbf{x}\ _1$	$L^1$ norm of the vector $\mathbf{x}$
$\ \mathbf{x}\ _2$	Euclidean norm ( $L^2$ norm) of the vector $\mathbf{x}$
$\ \mathbf{X}\ _F$	Frobenius norm of the matrix $\mathbf{X}$
$\text{Pr}(\cdot)$	Probability operator
$\text{Tr}(\mathbf{X})$	The trace of the matrix $\mathbf{X}$
$\mathbb{C}^n$	$n \times n$ complex-valued matrix
$\mathbb{H}^n$	$n \times n$ complex Hermitian matrix
$\mathbb{S}^n$	$n \times n$ symmetric matrix
$\mathbb{R}^n$	$n \times n$ real-valued matrix
$\mathbf{X} \succeq \mathbf{0}$	$\mathbf{X}$ is positive semidefinite
$\mathbf{X} \succ \mathbf{0}$	$\mathbf{X}$ is positive definite
$\lambda_{\min}(\mathbf{X}), \lambda_{\max}(\mathbf{X})$	minimum and maximum eigenvalue of $\mathbf{X}$ respectively
$\text{Re}\{\mathbf{X}\}, \text{Im}\{\mathbf{X}\}$	real and imaginary part of a complex $\mathbf{X}$ respectively

## APPENDIX B. ACRONYMS

<b>2G</b>	<b>S</b> econd <b>G</b> eneration
<b>3GPP</b>	<b>3</b> rd <b>G</b> eneration <b>P</b> artnership <b>P</b> roject
<b>5G</b>	<b>F</b> ifth <b>G</b> eneration
<b>6G</b>	<b>S</b> ixth <b>G</b> eneration
<b>ADMM</b>	<b>A</b> lternating <b>D</b> irection <b>M</b> ethod of <b>M</b> ultipliers
<b>ALS</b>	<b>A</b> lternating <b>L</b> east <b>S</b> quares
<b>AO</b>	<b>A</b> lternating <b>O</b> ptimization
<b>AP</b>	<b>A</b> ccess <b>P</b> oint
<b>AWGN</b>	<b>A</b> dditive <b>W</b> hite <b>G</b> aussian <b>N</b> oise
<b>B5G</b>	<b>B</b> eyond <b>F</b> ifth <b>G</b> eneration
<b>BD</b>	<b>B</b> lock <b>D</b> iagonalization
<b>BS</b>	<b>B</b> ase <b>S</b> tation
<b>CE</b>	<b>C</b> hannel <b>E</b> stimation
<b>CDF</b>	<b>C</b> umulative <b>D</b> istribution <b>F</b> unction
<b>CL</b>	<b>C</b> ross- <b>L</b> ink
<b>CMC</b>	<b>C</b> onstant <b>M</b> odulus <b>C</b> onstraint
<b>CNN</b>	<b>C</b> onvolutional <b>N</b> eural <b>N</b> etwork
<b>CP</b>	<b>C</b> anonical <b>P</b> olyadic
<b>CPU</b>	<b>C</b> entral <b>P</b> rocessing <b>U</b> nit
<b>CSI</b>	<b>C</b> hannel <b>S</b> tate <b>I</b> nformation
<b>CSCG</b>	<b>C</b> ircularly <b>S</b> ymmetric <b>C</b> omplex <b>G</b> aussian
<b>DL</b>	<b>D</b> own <b>L</b> ink
<b>DoA</b>	<b>D</b> irection-of- <b>A</b> rrival
<b>DoD</b>	<b>D</b> irection-of- <b>D</b> eparture
<b>DTDD</b>	<b>D</b> ynamic <b>T</b> ime <b>D</b> ivision <b>D</b> uplex

---

<b>EE</b>	<b>E</b> nergy <b>E</b> fficiency
<b>EM</b>	<b>E</b> xpectation- <b>M</b> aximization
<b>eMBB</b>	enhanced <b>M</b> obile <b>B</b> roadband
<b>FD</b>	<b>F</b> ull- <b>D</b> uplex
<b>FDD</b>	<b>F</b> requency <b>D</b> ivision <b>D</b> uplex
<b>FPGA</b>	<b>F</b> ield <b>P</b> rogrammable <b>G</b> ate <b>A</b> rray
<b>HD</b>	<b>H</b> alf- <b>D</b> uplex
<b>ICI</b>	<b>I</b> nter <b>C</b> ell <b>I</b> nterference
<b>IRS</b>	<b>I</b> ntelligent <b>R</b> eflecting <b>S</b> urface
<b>IoT</b>	<b>I</b> nternet of <b>T</b> hings
<b>IPM</b>	<b>I</b> nterior <b>P</b> oint <b>M</b> ethod
<b>LMI</b>	<b>L</b> inear <b>M</b> atrix <b>I</b> nequality
<b>LOS</b>	<b>L</b> east-of- <b>S</b> quares
<b>LS</b>	<b>L</b> east <b>S</b> quares
<b>LTE</b>	<b>L</b> ong <b>T</b> erm <b>E</b> volution
<b>MIMO</b>	<b>M</b> ultiple <b>I</b> nter <b>M</b> ultiple <b>O</b> utput
<b>MISO</b>	<b>M</b> ultiple <b>I</b> nter <b>S</b> ingle <b>O</b> utput
<b>MMSE</b>	<b>M</b> inimum <b>M</b> ean <b>S</b> quared <b>E</b> rror
<b>mmWave</b>	<b>M</b> illimeter <b>W</b> ave
<b>MRT</b>	<b>M</b> aximum <b>R</b> atio <b>T</b> ransmission
<b>MSE</b>	<b>M</b> ean <b>S</b> quared <b>E</b> rror
<b>MU</b>	<b>M</b> ultiple <b>U</b> ser
<b>MUI</b>	<b>M</b> ultiple <b>U</b> ser <b>I</b> nterference
<b>MU-MIMO</b>	<b>M</b> ulti-user- <b>M</b> IMO
<b>NLOS</b>	<b>N</b> on <b>L</b> ine-of- <b>S</b> ight
<b>NN</b>	<b>N</b> eural <b>N</b> etwork
<b>NP</b>	<b>N</b> ondeterministic <b>P</b> olynomial-time
<b>QoS</b>	<b>Q</b> uality-of- <b>S</b> ervice
<b>RE</b>	<b>R</b> esource <b>E</b> fficiency

<b>RF</b>	<b>R</b> adio <b>F</b> requency
<b>RIS</b>	<b>R</b> econfigurable <b>I</b> ntelligent <b>S</b> urface
<b>SCA</b>	<b>S</b> uccessive <b>C</b> onvex <b>A</b> pproximation
<b>SDMA</b>	<b>S</b> pace <b>D</b> ivision <b>M</b> ultiple <b>A</b> ccess
<b>SDP</b>	<b>S</b> emi <b>D</b> efinite <b>P</b> rogramming
<b>SDR</b>	<b>S</b> emi <b>D</b> efinite <b>R</b> elaxation
<b>SE</b>	<b>S</b> pectral <b>E</b> fficiency
<b>SER</b>	<b>S</b> ymbol <b>E</b> rror <b>R</b> ate
<b>SIC</b>	<b>S</b> uccessive <b>I</b> nterference <b>C</b> ancellation
<b>SIMO</b>	<b>S</b> ingle- <b>I</b> nterference <b>M</b> ultiple- <b>O</b> utput
<b>SINR</b>	<b>S</b> ignal-to- <b>I</b> nterference-plus- <b>N</b> oise <b>R</b> atio
<b>SISO</b>	<b>S</b> ingle- <b>I</b> nterference <b>S</b> ingle- <b>O</b> utput
<b>SLNR</b>	<b>S</b> ignal-to- <b>L</b> eakage-and- <b>N</b> oise <b>R</b> atio
<b>SNR</b>	<b>S</b> ignal-to- <b>N</b> oise <b>R</b> atio
<b>SOC</b>	<b>S</b> econd- <b>O</b> rders <b>C</b> one
<b>SOCP</b>	<b>S</b> econd- <b>O</b> rders <b>C</b> one <b>P</b> rogramming
<b>SQUAREM</b>	<b>S</b> QUARed <b>E</b> xtrapolation <b>M</b> ethods
<b>SU-MIMO</b>	<b>S</b> ingle <b>U</b> ser- <b>M</b> IMO
<b>SVD</b>	<b>S</b> ingular <b>V</b> alue <b>D</b> ecomposition
<b>TDD</b>	<b>T</b> ime <b>D</b> ivision <b>D</b> uplex
<b>TDMA</b>	<b>T</b> ime <b>D</b> ivision <b>M</b> ultiple <b>A</b> ccess
<b>UAV</b>	<b>U</b> nmanned <b>A</b> erial <b>V</b> ehicle
<b>UE</b>	<b>U</b> ser <b>E</b> quipment
<b>UL</b>	<b>U</b> p <b>L</b> ink
<b>ULA</b>	<b>U</b> niform <b>L</b> inear <b>A</b> rray
<b>ZF</b>	<b>Z</b> ero <b>F</b> orcing

## APPENDIX C. CONVEX OPTIMIZATION

In this appendix, we present a basic overview of convex optimization and some of the optimization techniques used in this work. These techniques are used to recast the problems considered in this thesis into equivalent convex optimization problems. In Appendices C.1-C.5 we present these techniques for the optimization of a real-valued variable. However, since the considered optimization problems in this work are complex-valued, we present the concept for the extension of the optimization of a real-valued variable to a complex-valued variable in Appendix C.6. In Appendix C.5 we present the basic idea of a semidefinite programming SDP and semidefinite relaxation (SDR) techniques as well as Gaussian randomization that are used in Sections 4.6, 6.4, and 6.5.

Convex optimization is a major class of mathematical optimization problems [131, 184]. The special role of convex optimization and recent advances in the development of powerful solvers have led to an increase in the use of convex optimization techniques in various applications, such as signal and image processing, estimation and inverse problems, modeling, finance, automatic control, and statistics. Understanding and formulating convex optimization problems is beneficial as there exist methods that can solve such problems efficiently and reliably.

### C.1 Convex Sets

A set  $\mathcal{D}$  is convex if and only if any line segment between any two points in  $\mathcal{D}$  is in  $\mathcal{D}$ , [131] i.e., if for any  $\mathbf{x}_1, \mathbf{x}_2 \in \mathcal{D}$  and any  $\phi$  with  $0 \leq \phi \leq 1$ , we have

$$\phi \mathbf{x}_1 + (1 - \phi) \mathbf{x}_2 \in \mathcal{D}. \quad (\text{C.1.1})$$

This simply implies that a set is convex if every point within the set can be seen by every other point within the set. The set  $\mathcal{D}$  is said to be closed if any converging sequence in  $\mathcal{D}$  converges to a point in  $\mathcal{D}$ , i.e., if  $\{\mathbf{x}_n\}_{n \in \mathbb{N}}$  is a sequence such that  $\mathbf{x}_n \in \mathcal{D}, \forall n \in \mathbb{N}$  and  $\mathbf{x}_n \rightarrow \mathbf{x}_0$ , then  $\mathbf{x}_0 \in \mathcal{D}$ . If  $\mathcal{D}_1$  and  $\mathcal{D}_2$  are convex, then  $\mathcal{D}_1 \cap \mathcal{D}_2$  is also convex, i.e., intersection preserves convexity [131]. The following are some important examples of

convex sets

1. **Hyperplane:** A hyperplane is a set of the form

$$\{\mathbf{x} \in \mathbb{R}^n \mid \mathbf{a}^\top \mathbf{x} = b\}, \quad (\text{C.1.2})$$

where  $\mathbf{a} \in \mathbb{R}^n$ ,  $\mathbf{a} \neq 0$ , and  $b \in \mathbb{R}$ . A hyperplane is a convex set since for any  $\mathbf{x}_1, \mathbf{x}_2 \in \mathcal{D}$ , and  $0 \leq \phi \leq 1$  we have

$$\phi \mathbf{a}^\top \mathbf{x}_1 + (1 - \phi) \mathbf{a}^\top \mathbf{x}_2 = \phi b + (1 - \phi)b = b. \quad (\text{C.1.3})$$

2. **Half-space:** A half-space is defined as

$$\{\mathbf{x} \in \mathbb{R}^n \mid \mathbf{a}^\top \mathbf{x} \leq b\}, \quad (\text{C.1.4})$$

where  $\mathbf{a} \in \mathbb{R}^n$ ,  $\mathbf{a} \neq 0$ , and  $b \in \mathbb{R}$ . A hyperplane divides the  $\mathbb{R}^n$  into two half-spaces. Half-spaces are convex. An open half-space is the interior of the half-space given as [131]

$$\{\mathbf{x} \in \mathbb{R}^n \mid \mathbf{a}^\top \mathbf{x} < b\}. \quad (\text{C.1.5})$$

3. **Polyhedra:** A polyhedra is defined as

$$\{\mathbf{x} \in \mathbb{R}^n \mid \mathbf{a}_j^\top \mathbf{x} \leq b_j, j \in \{1, \dots, J\}\}, \quad (\text{C.1.6})$$

where  $\mathbf{a}_j \neq 0$ , and  $b_j \in \mathbb{R}, \forall j \in J$ . Since the polyhedron is the intersection of a finite number of half-spaces and hyperplanes it is a convex set [131].

4. **Euclidean ball:** A Euclidean ball is of the form

$$B(\mathbf{x}_c, r) = \{\mathbf{x} \in \mathbb{R}^n \mid \|\mathbf{x} - \mathbf{x}_c\|_2 \leq r\} = \{\mathbf{x} \in \mathbb{R}^n \mid (\mathbf{x} - \mathbf{x}_c)^\top (\mathbf{x} - \mathbf{x}_c) \leq r^2\}, \quad (\text{C.1.7})$$

where  $r > 0$ , and  $\|\cdot\|_2$  is the Euclidean norm. Here  $\mathbf{x}_c$  is the center of the ball with radius  $r$ . The Euclidean ball  $B(\mathbf{x}_c, r)$  consists of all the points within a distance  $r$  of the center  $\mathbf{x}_c$  [131]. If  $\|\mathbf{x}_1 - \mathbf{x}_c\|_2 \leq r$ ,  $\|\mathbf{x}_2 - \mathbf{x}_c\|_2 \leq r$ , and  $0 \leq \phi \leq 1$ , we have

$$\begin{aligned} \|\phi \mathbf{x}_1 + (1 - \phi) \mathbf{x}_2 - \mathbf{x}_c\|_2 &= \|\phi(\mathbf{x}_1 - \mathbf{x}_c) + (1 - \phi)(\mathbf{x}_2 - \mathbf{x}_c)\|_2 \\ &\leq \phi \|\mathbf{x}_1 - \mathbf{x}_c\|_2 + (1 - \phi) \|\mathbf{x}_2 - \mathbf{x}_c\|_2 \\ &\leq r, \end{aligned} \quad (\text{C.1.8})$$

which shows that the Euclidean ball is a convex set.

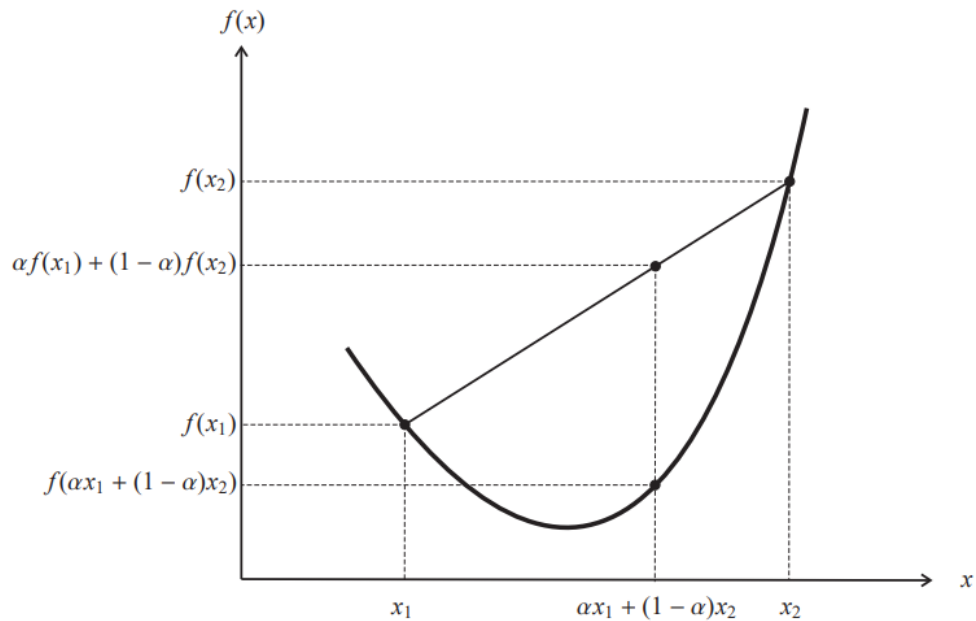


Fig. C.1: Graphical representation of a convex function, (adapted from [131] )

5. **Ellipsoid:** An Ellipsoid is a convex set that is of the form

$$\mathcal{E} = \{\mathbf{x} \in \mathbb{R}^n \mid (\mathbf{x} - \mathbf{x}_c)^\top \mathbf{P}^{-1}(\mathbf{x} - \mathbf{x}_c) \leq 1\}, \quad (\text{C.1.9})$$

where  $\mathbf{P} = \mathbf{P}^\top \succ 0$  is a matrix that determines how far the ellipsoid extends in every direction from the center of the ellipsoid  $\mathbf{x}_c$  [131].

6. **Affine sets:** A set  $\mathcal{Q} \subseteq \mathbb{R}^n$  is affine if the line passing through any two points in  $\mathcal{Q}$  lies in  $\mathcal{Q}$ . This implies that for any  $\mathbf{x}_1, \mathbf{x}_2 \in \mathcal{Q}$  and  $\phi \in \mathbb{R}$ , we have

$$\phi \mathbf{x}_1 + (1 - \phi) \mathbf{x}_2 \in \mathcal{Q}. \quad (\text{C.1.10})$$

## C.2 Convex Functions

Let the set  $\mathcal{D}$  be a convex set. Then a function  $f : \mathcal{D} \rightarrow \mathbb{R}$  is said to be convex if  $\forall \phi \in [0, 1]$ ,

$$f(\phi \mathbf{x}_1 + (1 - \phi) \mathbf{x}_2) \leq \phi f(\mathbf{x}_1) + (1 - \phi) f(\mathbf{x}_2), \forall \mathbf{x}_1, \mathbf{x}_2 \in \mathcal{D}. \quad (\text{C.2.1})$$

Let us consider the convex function  $f(x)$ ,  $x \in \mathbb{R}$  and the line segment joining two points  $(x_1, f(x_1))$  and  $(x_2, f(x_2))$ . Then, geometrically, it implies that a function is a convex function if the graph of the given function lies below the line segment that joins any two points of the graph as shown in Fig. C.1 [131]. Equally,  $f$  is said to be strictly

convex if  $\forall \phi \in (0, 1)$  and  $\forall \mathbf{x}_1 \neq \mathbf{x}_2, \mathbf{x}_1, \mathbf{x}_2 \in \mathcal{D}$ , we have

$$f(\phi \mathbf{x}_1 + (1 - \phi) \mathbf{x}_2) < \phi f(\mathbf{x}_1) + (1 - \phi) f(\mathbf{x}_2). \quad (\text{C.2.2})$$

The function  $f$  is said to be strongly convex if  $F : \mathcal{D} \rightarrow \mathbb{R}$  defined as  $F(\mathbf{x}) = f(\mathbf{x}) - \alpha |\mathbf{x}|^2$  is convex for some  $\alpha > 0$ .

### C.3 Convex Optimization Problem

A constrained convex optimization problem can be written as

$$\begin{aligned} \min_{\mathbf{x}} \quad & f(\mathbf{x}), \quad \mathbf{x} \in \mathbb{R}^n \\ \text{s.t.} \quad & g_i(\mathbf{x}) \leq 0, \quad \forall i = 1, \dots, K \\ & h_j(\mathbf{x}) = 0, \quad \forall j = 1, \dots, P, \end{aligned} \quad (\text{C.3.1})$$

where equality constraints  $h_j(\mathbf{x}) = \mathbf{a}_j^\top \mathbf{x} - b_j$  are linear, the inequality constraint functions  $g_i(\mathbf{x})$ , and the objective function  $f(\mathbf{x})$  are convex [131, 184]. A problem is said to be a convex problem if  $g_i, \forall i = 0, \dots, K$  are convex and  $h_j, \forall j = 1, \dots, P$ , are affine. Convex optimization problems are a category of optimization problems that can be solved using efficient algorithms [131]. The set of input values  $\mathbf{x}$  for which the objective function and the constraints of the optimization problem are defined is known as the *domain* of the convex optimization problem. The set of all the members of the domain that satisfies all the constraints is called the *feasible set or constraint set*.

A convex optimization problem can be transformed into an equivalent form. According to [131, 185], two optimization problems are said to be equivalent when the optimal solution of one of the problems can be found from the optimal solution of the other problem, and vice versa. This problem transformation can be achieved by using some useful tricks, these include a monotone transformation of the constraints and the objective function, introduction of some slack variables, replacing the equality constraints with inequality, reformulation as an epigraph, change of variables, etc.

For example, with the use of slack variables the problem in (C.3.1) can be trans-

formed as

$$\begin{aligned}
\min_{\mathbf{x}} \quad & f(\mathbf{x}), & \mathbf{x} \in \mathbb{R}^n \\
\text{s.t.} \quad & \mathbf{q}_i \geq 0, & \forall i = 1, \dots, K \\
& g_i(\mathbf{x}) \leq +\mathbf{q}_i, & \forall i = 1, \dots, K \\
& h_j(\mathbf{x}) = 0, & \forall j = 1, \dots, P,
\end{aligned} \tag{C.3.2}$$

where the new variable  $\mathbf{q}_i$  is the slack variable introduced that is associated with inequality constraint in (C.3.1). The slack variables replace each inequality constraint with equality and nonnegative constraints.

Equally, using a slack variable the generic convex objective function of the optimization problem in (C.3.1) can be transformed into a linear objective function given as

$$\begin{aligned}
\min_{\mathbf{x}, t} \quad & t, & \mathbf{x} \in \mathbb{R}^n, t \in \mathbb{R} \\
\text{s.t.} \quad & f(\mathbf{x}) \leq t \\
& g_i(\mathbf{x}) \leq 0, & \forall i = 1, \dots, K \\
& h_j(\mathbf{x}) = 0, & \forall j = 1, \dots, P,
\end{aligned} \tag{C.3.3}$$

where  $t$  is a new slack variable. The problem in (C.3.3) is referred to as the *epigraph form* of the original optimization problem in (C.3.1) [131, 185]. Problem (C.3.3) can easily be seen as an optimization problem in the "graph space"  $(x, t)$ . The addition of the slack variable  $t$  is essentially the price to pay for having a linear objective function [185].

The duality principle in convex optimization implies that any given optimization problem can be considered from either of two contexts, the original problem (known as the primal problem) or the dual problem [131]. One important function in constrained convex optimization is the *Lagrangian* given as

$$L(\mathbf{x}, \boldsymbol{\lambda}, \boldsymbol{\nu}) = f(\mathbf{x}) + \sum_{i=1}^K \lambda_i g_i(\mathbf{x}) + \sum_{j=1}^P \nu_j h_j(\mathbf{x}), \tag{C.3.4}$$

where  $\boldsymbol{\lambda} \in \mathbb{R}^K$  and  $\boldsymbol{\nu} \in \mathbb{R}^P$  are known as the Lagrange multipliers or the dual variables. The basic concept involved in obtaining the Lagrangian in (C.3.4) is to augment the objective function of (C.3.1) with a weighted sum of the constraints. The Lagrange

dual problem of the primal problem in (C.3.1) is then given as

$$\begin{aligned} \max_{\boldsymbol{\lambda}, \boldsymbol{\nu}} \quad & r(\boldsymbol{\lambda}, \boldsymbol{\nu}) \\ \text{s.t.} \quad & \lambda_i \geq 0, \quad \forall i = 1, \dots, K \end{aligned} \quad (\text{C.3.5})$$

where  $r(\boldsymbol{\lambda}, \boldsymbol{\nu})$  is the dual function define as  $r(\boldsymbol{\lambda}, \boldsymbol{\nu}) = \inf_{\mathbf{x}} L(\mathbf{x}, \boldsymbol{\lambda}, \boldsymbol{\nu})$ . The optimal solution  $\hat{\boldsymbol{\nu}}$  of the problem in (C.3.5) gives the best lower bound on the optimal solution  $\hat{\mathbf{x}}$  of problem (C.3.1). If we have

$$r_i(\hat{\boldsymbol{\nu}}) \leq f_i(\hat{\mathbf{x}}), \quad \forall i = 1, \dots, K \quad (\text{C.3.6})$$

then, this is known as *weak duality*. This inequality holds when the two optimal solutions are infinite [131]. However, if the equality

$$r_i(\hat{\boldsymbol{\nu}}) = f_i(\hat{\mathbf{x}}), \quad \forall i = 1, \dots, K \quad (\text{C.3.7})$$

holds, then we have that *strong duality* exists between the primal and dual function, i.e., the optimal duality gap is zero. Generally, there is no analytical formula for the solution of convex optimization [131]. However, constrained convex optimization problems can be efficiently solved using interior point polynomial time algorithms [186]. In [187], the fundamental concepts behind these interior point algorithms are presented.

The necessary and sufficient conditions for the optimality of the primal and dual functions of a convex optimization problem with a differentiable objective and constraint functions are given by the Karush-Kuhn-Tucker (KKT) conditions [131]

$$\begin{aligned} f_i(\hat{\mathbf{x}}) &\leq 0, \quad \forall i = 1, \dots, K \\ h_j(\hat{\mathbf{x}}) &= 0, \quad \forall j = 1, \dots, P \\ \hat{\lambda}_i &\geq 0, \quad \forall i = 1, \dots, K \\ \hat{\lambda}_i f_i(\hat{\mathbf{x}}) &= 0, \quad \forall i = 1, \dots, K \\ \nabla f(\hat{\mathbf{x}}) + \sum_{i=1}^K \hat{\lambda}_i \nabla g_i(\hat{\mathbf{x}}) + \sum_{j=1}^P \hat{\nu}_j \nabla h_j(\hat{\mathbf{x}}) &= 0, \end{aligned} \quad (\text{C.3.8})$$

where  $\hat{\mathbf{x}}$  represents the optimal solution and  $\nabla$  denotes the differential operator.

## C.4 Second-order Cone Programming

Second-order cone programming (SOCP) problem can be seen as a generalization of linear and quadratic programming that permits affine mixtures of variables to be re-

stricted within a unique convex set, known as a second-order cone [141]. SOCP is a convex programming problem, and just like linear programming, semidefinite programming, and quadratic programming, it can be solved in polynomial time using interior point methods [131]. Due to its computational tractability, SOCP is used in diverse formulations and applications, such as in approximation problems, geometry problems, and probabilistic problems [186].

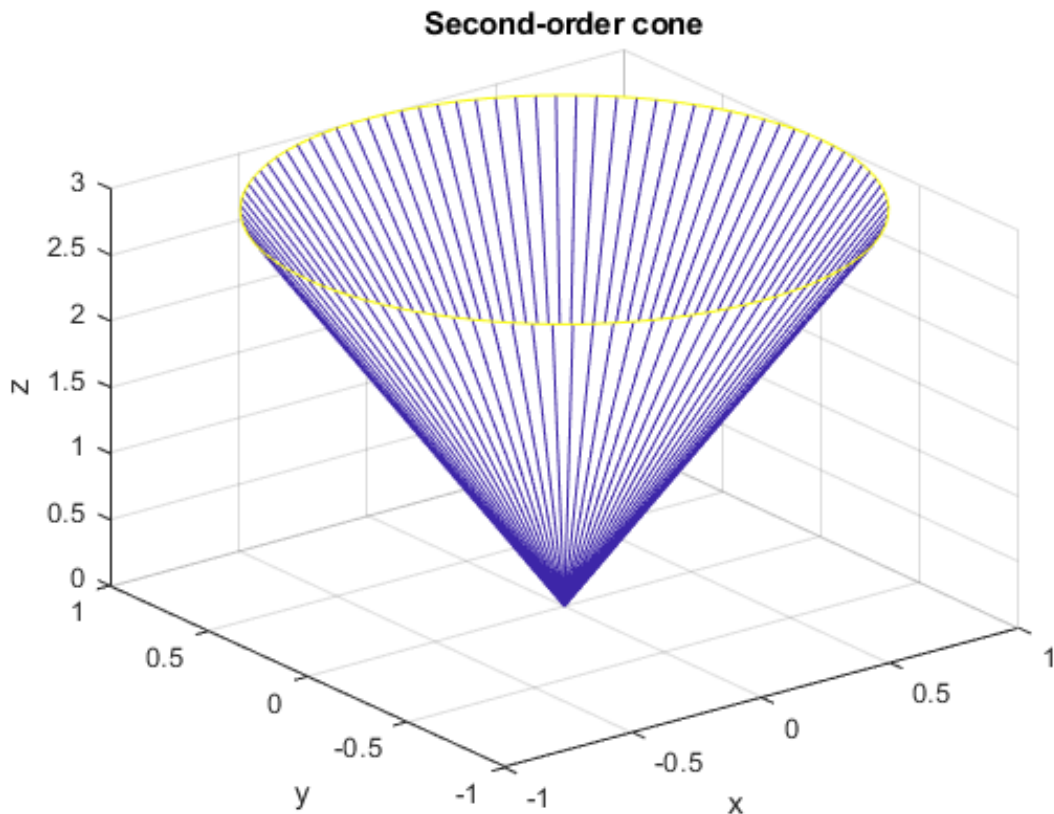


Fig. C.2: Second-order cone

The standard second-order cone (SOC) in  $\mathbb{R}^3$  is a set of triples  $\{x, y, z\}$  such that

$$\sqrt{x^2 + y^2} \leq z. \quad (\text{C.4.1})$$

The disks of radius  $\alpha$  are the horizontal sections of the set at the level  $\alpha \geq 0$ . The geometric interpretation of SOC is given in Fig. C.2. However, in general, the SOC for an  $(n + 1)$  dimension is given as the following set

$$\mathcal{S}_n = \{(\mathbf{x}, t), \mathbf{x} \in \mathbb{R}^n, t \in \mathbb{R} \mid \|\mathbf{x}\|_2 \leq t\}. \quad (\text{C.4.2})$$

Also, the rotated SOC in  $\mathbb{R}^{n+2}$  is represented by the following set

$$\mathcal{S}_n^r = \{(\mathbf{x}, y, t), \mathbf{x} \in \mathbb{R}^n, y \in \mathbb{R}, t \in \mathbb{R} \mid \mathbf{x}^\top \mathbf{x} \leq 2yt, y \geq 0, t \geq 0\}. \quad (\text{C.4.3})$$

Intuitively, this rotated SOC can be reformulated as a linear transformation of the plain as

$$\|\mathbf{x}\|_2^2 \iff \left\| \begin{bmatrix} \mathbf{x} \\ \frac{1}{\sqrt{2}(y-t)} \end{bmatrix} \right\| \leq \frac{1}{\sqrt{2}(y+t)}, \quad (\text{C.4.4})$$

which implies that  $(\mathbf{x}, y, t) \in \mathcal{S}_n^r$  if and only if  $(a, b) \in \mathcal{S}_n$ , where  $a = (\mathbf{x}, (y-t)/\sqrt{2})$ , and  $b = (y+t)/\sqrt{2}$ . This reformulation is the basis for notably increasing the set of problems that can be formulated as SOCPs [141].

### C.4.1 Formulating Problems as SOCP

A convex optimization problem with linear objective function and SOC constraints is known as SOCP. The standard form of SOCP is given as [131, 141]

$$\begin{aligned} \min_{\mathbf{x}} \quad & \mathbf{c}^\top \mathbf{x} \\ \text{s.t.} \quad & \|\mathbf{A}_i \mathbf{x} + \mathbf{b}_i\|_2 \leq \mathbf{c}_i^\top \mathbf{x} + d_i, \quad i = 1, \dots, m, \end{aligned} \quad (\text{C.4.5})$$

where  $\mathbf{A}_i \in \mathbb{R}^{m_i \times n}$ ,  $\mathbf{b}_i \in \mathbb{R}^{m_i}$ ,  $\mathbf{c}_i \in \mathbb{R}^n$ , and  $d_i \in \mathbb{R}$ . A majority of convex optimization problems can be represented as SOCPs. These include linear program (LP), quadratic program (QP), quadratically constrained quadratic program (QCQP), etc. In the following, we present some of the optimization problems that can be cast as SOCPs.

1. **Linear Programs as SOCPs:** A standard LP in inequality form given as

$$\begin{aligned} \min_{\mathbf{x}} \quad & \mathbf{c}^\top \mathbf{x} \\ \text{s.t.} \quad & \mathbf{a}_i^\top \mathbf{x} \leq b_i, \quad i = 1, \dots, m \end{aligned} \quad (\text{C.4.6})$$

can easily be formulated in SOCP form as

$$\begin{aligned} \min_{\mathbf{x}} \quad & \mathbf{c}^\top \mathbf{x} \\ \text{s.t.} \quad & \|\mathbf{C}_i \mathbf{x} + \mathbf{d}_i\|_2 \leq b_i - \mathbf{a}_i^\top \mathbf{x}, \quad i = 1, \dots, m, \end{aligned} \quad (\text{C.4.7})$$

where  $\mathbf{C}_i = 0$  and  $\mathbf{d}_i = 0$ .

2. **Quadratic Programs as SOCPs:** A standard QP in the form

$$\begin{aligned} \min_{\mathbf{x}} \quad & \mathbf{x}^\top \mathbf{D} \mathbf{x} + \mathbf{c}^\top \mathbf{x} \\ \text{s.t.} \quad & \mathbf{a}_i^\top \mathbf{x} \leq b_i, \quad i = 1, \dots, m \end{aligned} \quad (\text{C.4.8})$$

where  $\mathbf{D} = \mathbf{D}^\top \succeq \mathbf{0}$ , can be readily be expressed as an SOCP as

$$\begin{aligned} \min_{\mathbf{x}, y} \quad & \mathbf{c}^\top \mathbf{x} \\ \text{s.t.} \quad & \left\| \begin{bmatrix} 2\mathbf{D}^{1/2} \mathbf{x} \\ y - 1 \end{bmatrix} \right\| \leq y + 1, \\ & \mathbf{a}_i^\top \mathbf{x} \leq b_i. \end{aligned} \quad (\text{C.4.9})$$

3. **Quadratic-Constrained Quadratic Programs as SOCPs :** A convex QCQP program given as

$$\begin{aligned} \min_{\mathbf{x}} \quad & \mathbf{x}^\top \mathbf{D}_0 \mathbf{x} + \mathbf{a}_0^\top \mathbf{x} \\ \text{s.t.} \quad & \mathbf{x}^\top \mathbf{D}_i + \mathbf{a}_i^\top \mathbf{x} \leq b_i, \quad i = 1, \dots, m \end{aligned} \quad (\text{C.4.10})$$

$\mathbf{D}_i = \mathbf{D}_i^\top \succeq \mathbf{0}$ , can be formulated as an SOCP as

$$\begin{aligned} \min_{\mathbf{x}, g} \quad & \mathbf{a}_0^\top \mathbf{x} + g \\ \text{s.t.} \quad & \left\| \begin{bmatrix} 2\mathbf{D}_0^{1/2} \mathbf{x} \\ g - 1 \end{bmatrix} \right\| \leq g + 1, \\ & \left\| \begin{bmatrix} 2\mathbf{D}_i^{1/2} \mathbf{x} \\ b_i - \mathbf{a}_i^\top \mathbf{x} - 1 \end{bmatrix} \right\| \leq \mathbf{a}_i^\top \mathbf{x} + 1, \end{aligned} \quad (\text{C.4.11})$$

4. **Minimization of Sum of Norms as SOCPs:** The following norm minimization problem

$$\min_{\mathbf{x}} \quad \sum_{i=1}^r \|\mathbf{A}_i \mathbf{x} - \mathbf{b}_i\|_2, \quad (\text{C.4.12})$$

where  $\mathbf{A}_i \in \mathbb{R}^{m \times n}$ ,  $\mathbf{b}_i \in \mathbb{R}^m$  are the available data, then the problem can be cast

as an SOCP given as

$$\begin{aligned} \min_{\mathbf{x}, v} \quad & \sum_{i=1}^r v_i \\ \text{s.t.} \quad & \|\mathbf{A}_i \mathbf{x} + \mathbf{b}_i\| \leq v_i, \dots, r, \end{aligned} \quad (\text{C.4.13})$$

where  $v_1, \dots, r$  are the introduced auxiliary variables.

5. **Minimization of the Maximum Norm as SOCPs:** The problem

$$\min_{\mathbf{x}} \max_{i=1, \dots, r} \|\mathbf{A}_i \mathbf{x} - \mathbf{b}_i\|_2, \quad (\text{C.4.14})$$

has the SOCP formulation as

$$\begin{aligned} \min_{\mathbf{x}, v} \quad & v \\ \text{s.t.} \quad & \|\mathbf{A}_i \mathbf{x} + \mathbf{b}_i\| \leq v, \dots, r, \end{aligned} \quad (\text{C.4.15})$$

## C.5 Semidefinite Programming

Semidefinite programming (SDP) problem can be defined as the optimization problem over the intersection of an affine set and the cone of positive semidefinite matrices [139, 140]. SDPs can be solved in polynomial time (up to any prescribed accuracy) using interior-point algorithms [131], and as a result, have been effectively used in the design of approximation algorithms for many NP-hard problems. Note that NP-hard problems are problems for which we cannot prove that a polynomial time solution exists [131].

The semidefinite relaxation (SDR) technique is the technique adopted to approximately solve any given SDP problem. It is a powerful and computationally efficient approximation technique for a lot of difficult optimization problems such as non-convex QCQP, Boolean quadratic program (BQP), etc [140].

To demonstrate the concept of SDR, let us consider the QCOP problem given as

$$\begin{aligned} \min_{\mathbf{x} \in \mathbb{R}^n} \quad & \mathbf{x}^\top \mathbf{Y} \mathbf{x} \\ \text{s.t.} \quad & \mathbf{x}^\top \mathbf{Q}_i \mathbf{x} \geq b_i, i = 1, \dots, m, \end{aligned} \quad (\text{C.5.1})$$

where  $\mathbf{Y} \in \mathbb{S}^n$ ,  $b_i \in \mathbb{R}$ ,  $\forall i \in m$ , and  $\mathbf{Q}_i \in \mathbb{S}^n$ ,  $\forall i \in m$ . We note that both the objective function and the constraint are linear in  $\mathbf{x}\mathbf{x}^\top$ . This is evident from the trace of the

both functions,

$$\begin{aligned}\mathbf{x}^\top \mathbf{Y} \mathbf{x} &= \text{Tr}(\mathbf{x}^\top \mathbf{Y} \mathbf{x}) = \text{Tr}(\mathbf{Y} \mathbf{x} \mathbf{x}^\top) \\ \mathbf{x}^\top \mathbf{Q}_i \mathbf{x} &= \text{Tr}(\mathbf{x}^\top \mathbf{Q}_i \mathbf{x}) = \text{Tr}(\mathbf{Q}_i \mathbf{x} \mathbf{x}^\top).\end{aligned}$$

As a result, we define a new rank-one matrix as  $\mathbf{X} = \mathbf{x} \mathbf{x}^\top \in \mathbb{S}^n$ ,  $\mathbf{X} \succeq \mathbf{0}$ , therefore, the QCQP problem can be recast as

$$\begin{aligned}\min_{\mathbf{X} \in \mathbb{S}^n} \quad & \text{Tr}(\mathbf{Y} \mathbf{X}) \\ \text{s.t.} \quad & \text{Tr}(\mathbf{Q}_i \mathbf{X}) \geq b_i, \quad i = 1, \dots, m, \\ & \mathbf{X} \succeq \mathbf{0}, \\ & \text{rank}(\mathbf{X}) = 1.\end{aligned}\tag{C.5.2}$$

Problem (C.5.2) is a convex-SDP problem since the objective function and the first two constraints are convex. However, the existence of the rank-one constraint makes it difficult to solve the problem. To obtain a solution for the above problem the rank-one constraint is relaxed, and the relaxed version is known as SDR which is given as

$$\begin{aligned}\min_{\mathbf{X} \in \mathbb{S}^n} \quad & \text{Tr}(\mathbf{Y} \mathbf{X}) \\ \text{s.t.} \quad & \text{Tr}(\mathbf{Q}_i \mathbf{X}) \geq b_i, \quad i = 1, \dots, m, \\ & \mathbf{X} \succeq \mathbf{0}.\end{aligned}\tag{C.5.3}$$

One important feature of the SDR problem in (C.5.3) is that it can be efficiently solved to any arbitrary accuracy using interior point methods [131, 140]. Unfortunately, the global optimal solution  $\hat{\mathbf{X}}$  of the SDR problem in (C.5.3) may not be a feasible solution  $\bar{\mathbf{x}}$  for the original QCQP problem given in (C.5.1) [188]. This is due to the fact that the obtained solution  $\hat{\mathbf{X}}$  may not be a rank-one solution. If the solution is rank-one, then there is nothing to worry about because its principal component will be a feasible solution to the original problem in (C.5.1). However, if the solution is not rank-one, then the vector  $\bar{\mathbf{x}}$  that is feasible for the original problem is somehow extracted from the solution of the SDR problem. This can be achieved using either eigenvalue decomposition (EVD) or Gaussian randomization as discussed below [139, 140].

1. **Eigenvalue Decomposition Based Approach:** EVD-based procedure is used to extract rank-one solution from the optimal solution of the relaxed problem. In this approach, EVD operation is applied to  $\hat{\mathbf{X}}$  obtained from solving (C.5.3). Then, the maximum eigenvalue and its corresponding eigenvector are used to reconstruct the rank-one matrix that is feasible for the original problem in (C.5.1).

The EVD-based approach is summarized below in Algorithm 4.

---

**Algorithm 4: EVD-Based Approach**


---

- (a) Input: an optimal solution  $\hat{\mathbf{X}}$  to (C.5.3)  
 (b) Let  $r = \text{rank}(\hat{\mathbf{X}})$   
 (c) Let

$$\hat{\mathbf{X}} = \sum_{i=1}^r \lambda_i \mathbf{v}_i \mathbf{v}_i^{\top},$$

be the EVD of  $\hat{\mathbf{X}}$ , and  $\lambda_1 \geq \lambda_2 \cdots \geq \lambda_r > 0$  are the eigenvalues and  $\mathbf{v}_1, \cdots, \mathbf{v}_r \in \mathbb{R}^n$  are the corresponding eigenvectors.

- (d) Reconstruct  $\hat{\mathbf{X}}_1$  as  $\hat{\mathbf{X}}_1 = \lambda_1 \mathbf{v}_1 \mathbf{v}_1^{\top}$ , as the best rank-one approximation to  $\hat{\mathbf{X}}$ .  
 (e) Extract  $\bar{\mathbf{x}} = \sqrt{\lambda_1} \mathbf{v}_1$  as a feasible solution to the problem in (C.5.1)
- 

2. **Gaussian Randomization Based Approach:** The Gaussian randomization approach is a heuristic procedure that uses  $\hat{\mathbf{X}}$  to generate a set of candidate  $\mathbf{x}_l, \forall l \in L$  vectors, from which the “best”, i.e., the solution that yields the best objective will be selected [188]. The number of randomizations is given by  $L$ . The idea is to calculate the EVD of  $\hat{\mathbf{X}} = \mathbf{U}\mathbf{\Sigma}\mathbf{U}^{\text{H}}$  and select  $\mathbf{x}_l = \mathbf{U}\mathbf{\Sigma}^{1/2}\mathbf{w}_l$ , where the elements of the vector  $\mathbf{w}_l$  are complex circularly symmetric uncorrelated Gaussian random variables with zero-mean and unit-variance. This guarantees that  $\mathbb{E}\{\mathbf{w}_l \mathbf{w}_l^{\text{H}}\} = \hat{\mathbf{X}}$ . However, it is important to note that the design of the Gaussian randomization algorithm is problem-dependent. In [140], it has been shown that the rank-one approximation obtained using the Gaussian randomization procedure outperforms that obtained using the EVD-based procedure. The higher the number of randomizations used, the better the performance that will be obtained<sup>1</sup>. The Gaussian randomization procedure is summarized in Algorithm 5.

---

<sup>1</sup> The typical range of values for  $L$  is between 500 and 1000 to have a good rank-one approximation. In all our experiments in this thesis where Gaussian randomization is applied, we used  $L = 500$ .

---

**Algorithm 5: Gaussian Randomization Approach**


---

1. Input: an optimal solution  $\hat{\mathbf{X}}$  to (C.5.3) and number of randomizations  $L$
  2. Let  $\hat{\mathbf{X}} = \mathbf{U}\mathbf{\Sigma}\mathbf{U}^H$ , be the EVD of  $\hat{\mathbf{X}}$ .
  3. for  $l = 1 : L$ 
    - generate  $\mathbf{w}_l \sim \mathcal{CN}(0, 1)$ ,
    - $\mathbf{x}_l = \mathbf{U}\mathbf{\Sigma}^{1/2}\mathbf{w}_l$ .
  - end
  4. find  $\hat{l} = \operatorname{argmin} \mathbf{x}_l^T \mathbf{Y} \mathbf{x}_l$ .
  5. Extract  $\bar{\mathbf{x}} = \mathbf{x}_{\hat{l}}$  as a feasible solution to the problem in (C.5.1)
- 

## C.6 Optimization Problems of Real Functions in Complex Variables

Many practical optimization problems found in many applications such as signal and array processing, beamforming, adaptive filter, remote sensing, etc., deal with real-valued functions with complex arguments. Because the complex domain provides a natural way to conserve the phase information of the signals involved and also provides a convenient way to represent these signals [189]. As a result, the accuracy of the derivatives of real functions estimated using complex variables is increased by an order of magnitude [190]. A simple complex-variables nonlinear convex programming problem is given as:

$$\begin{aligned} \min_{\mathbf{q} \in \mathbb{C}^n} g(\mathbf{q}) \\ \text{s.t. } \mathbf{q} \in \Omega, \end{aligned} \tag{C.6.1}$$

where  $g(\mathbf{q}), \Omega \subset \mathbb{C}^n \rightarrow \mathbb{R}, \Omega = \{\mathbf{q} \in \mathbb{C}^n \mid \mathbf{A}\mathbf{z} = \mathbf{b}\}, \mathbf{b} \in \mathbb{C}^m$ , and  $\mathbf{A} \in \mathbb{C}^{m \times n}$ . However, for the real-valued function with complex variables given in (C.6.1), the Cauchy-Riemann conditions are not satisfied. As a result, such functions do not have Taylor series expansion.

Consequently, for this group of functions, the optimization methods based on derivatives cannot be directly applied. One of the ways to overcome this problem is by converting the problem to the field of real-valued one. This is achieved by separating the real and imaginary parts of the complex variables and considering them as new

independent variables. After that, the real-valued optimization methods can be applied. Regrettably, this will increase the dimension of the original problem which will inadvertently lead to slow convergence and high computational complexity when the problem size is big.

In (C.6.1), a point  $\mathbf{q}$  is feasible if  $\mathbf{q} \in \Omega$ . A feasible point  $\hat{\mathbf{q}}$  is locally optimal if there exists an open ball around  $\hat{\mathbf{q}}, B_\epsilon(\hat{\mathbf{q}}) \subseteq \Omega$  such that  $g(\mathbf{q}) \geq g(\hat{\mathbf{q}}), \forall \mathbf{q} \in B_\epsilon(\hat{\mathbf{q}}) \cap \Omega$  and  $\hat{\mathbf{q}}$  is globally optimal if  $g(\mathbf{q}) \geq g(\hat{\mathbf{q}}), \forall \mathbf{q} \in \Omega$ . It is important to note that the  $g(\mathbf{q})$  in (C.6.1) is not analytic since the Cauchy-Riemann conditions are not satisfied. However, with the help of Wirtinger Calculus (also known as a relaxed  $\mathbb{C}\mathbb{R}$  calculus it is possible to turn  $g(\mathbf{q})$  into an analytic function [191, 192]. This is achieved by constructing an expansion of the objective function in its original complex variables, given as  $g(\mathbf{q}, \mathbf{q}^*)$ , where  $\mathbf{q}^*$  is the complex conjugate of  $\mathbf{q}$ . Note that functions of complex variables can be analytic in their argument and its complex conjugate as a whole [191].

Denote  $\mathbf{q} = \mathbf{x} + i\mathbf{y}$  where  $i = \sqrt{-1}$  is the imaginary unit. As a result, we can view  $g(\mathbf{q})$  as a real bivariate function of its real and imaginary components  $f(\mathbf{x}, \mathbf{y}) : \mathbb{R}^n \times \mathbb{R}^n \mapsto \mathbb{R}$ . On the other side, from  $x = (\mathbf{q} + \mathbf{q}^*)/2$  and  $y = -i(\mathbf{q} - \mathbf{q}^*)/2$  we see that  $g(\mathbf{q}) = g(\mathbf{q}, \mathbf{q}^*)$ . In the following, we give some important definitions of the real-valued function of a complex variable  $\mathbf{q}$

1. *Convex set*: A set  $\Omega$  is called a convex set if for any two points  $\mathbf{q}_1$  and  $\mathbf{q}_2$  in  $\Omega$  and any  $\phi, 0 \leq \phi \leq 1$ , we have

$$\phi\mathbf{q}_1 + (1 - \phi)\mathbf{q}_2 \in \Omega \quad (\text{C.6.2})$$

2. *Convex function*: A real-valued function of a complex vector  $\mathbf{q}, g(\mathbf{q}) \mathbb{C} \mapsto \mathbb{R}$  defined on convex set  $\Omega \in \mathbb{C}^n$  is said to be convex if for any given two points  $\mathbf{q}_1$  and  $\mathbf{q}_2$  and  $a \in [0, 1]$ , we have

$$g(t\mathbf{q}_1 + (1 - t)\mathbf{q}_2) \leq tg(\mathbf{q}_1) + (1 - t)g(\mathbf{q}_2). \quad (\text{C.6.3})$$

A function is called strictly convex if the above strictly.

3. *Linear mappings*: For a real-valued function with complex variables, the following two linear mappings from the complex space to the real space exist:

- For  $\forall \mathbf{q} \in \mathbb{C}^n$ , then we have

$$\varphi_1(\mathbf{q}) = \begin{bmatrix} \text{Re}(\mathbf{q}) \\ \text{Im}(\mathbf{q}) \end{bmatrix} \in \mathbb{R}^{2n}, \quad (\text{C.6.4})$$

- For  $\forall \mathbf{A} \in \mathbb{C}^{m \times n} (n > 1)$ , then

$$\varphi_2(\mathbf{A}) = \begin{bmatrix} \text{Re}(\mathbf{A}) & -\text{Im}(\mathbf{A}) \\ \text{Im}(\mathbf{A}) & \text{Re}(\mathbf{A}) \end{bmatrix} \in \mathbb{R}^{2m \times 2n}, \quad (\text{C.6.5})$$

where  $\text{Re}(\cdot)$  and  $\text{Im}(\cdot)$  denote the real and imaginary parts of a complex matrix or vector, respectively. Furthermore,  $\varphi_1$  and  $\varphi_2$  are the one-to-one mapping from the complex domain to the real matrix space.

Assume that the partial derivatives of  $f(\mathbf{x}, \mathbf{y})$ ,  $\frac{\partial f}{\partial \mathbf{x}}$  and  $\frac{\partial f}{\partial \mathbf{y}}$ , exist. Then  $\mathbb{R}$ -derivative of a real function of a complex variable  $g(\mathbf{q}) = g(\mathbf{q}, \mathbf{q}^*)$  is given by

$$\frac{\partial g}{\partial \mathbf{q}} = \frac{1}{2} \left( \frac{\partial f}{\partial \mathbf{x}} - i \frac{\partial f}{\partial \mathbf{y}} \right), \quad (\text{C.6.6})$$

and the conjugate  $\mathbb{R}$ -derivative ( $\mathbb{R}^*$ -derivative) of a function  $g(\mathbf{q}) = g(\mathbf{q}, \mathbf{q}^*)$  is given by

$$\frac{\partial g}{\partial \mathbf{q}^*} = \frac{1}{2} \left( \frac{\partial f}{\partial \mathbf{x}} + i \frac{\partial f}{\partial \mathbf{y}} \right). \quad (\text{C.6.7})$$

The Lagrangian function for the real-valued function with complex variables given in (C.6.1) can be written as [193, 194]

$$\mathbf{L}(\mathbf{z}, \mathbf{u}) = g(\mathbf{z}) - \text{Re} (2\mathbf{u}^H (\mathbf{A}\mathbf{z} - \mathbf{b})), \quad (\text{C.6.8})$$

where  $\mathbf{u} \in \mathbb{C}^n$  is the Lagrange multiplier. From (C.6.7) we have for any  $\mathbf{d} \in \mathbb{C}^n$

$$\begin{aligned} \frac{\partial}{\partial \mathbf{z}^*} \text{Re} (\mathbf{d}^H \mathbf{z}) &= \frac{\partial}{\partial \mathbf{z}^*} \left( (\mathbf{d}_R - i\mathbf{d}_I)^T (\mathbf{x} + i\mathbf{y}) \right) = \frac{\partial}{\partial \mathbf{z}^*} (\mathbf{d}_R^T \mathbf{x} + \mathbf{d}_I^T \mathbf{y}) \\ &= \frac{1}{2} \left( \frac{\partial}{\partial \mathbf{x}} (\mathbf{d}_R^T \mathbf{x} + \mathbf{d}_I^T \mathbf{y}) + i \frac{\partial}{\partial \mathbf{y}} (\mathbf{d}_R^T \mathbf{x} + \mathbf{d}_I^T \mathbf{y}) \right) \\ &= \frac{1}{2} (\mathbf{d}_R + i\mathbf{d}_I) = \mathbf{d}/2. \end{aligned} \quad (\text{C.6.9})$$

Then

$$\begin{aligned} \frac{\partial}{\partial \mathbf{z}^*} (g(\mathbf{z}) - \text{Re} (2\mathbf{u}^H (\mathbf{A}\mathbf{z} - \mathbf{b}))) &= \nabla g(\mathbf{z}) - \frac{\partial}{\partial \mathbf{z}^*} \text{Re} (2\mathbf{u}^H (\mathbf{A}\mathbf{z} - \mathbf{b})) \\ &= \nabla g(\mathbf{z}) - \frac{\partial}{\partial \mathbf{z}^*} \text{Re} (2(\mathbf{A}^H \mathbf{u})^H \mathbf{z}) = \nabla g(\mathbf{z}) - \mathbf{A}^H \mathbf{u}. \end{aligned} \quad (\text{C.6.10})$$

Similarly,

$$\begin{aligned}\frac{\partial}{\partial \mathbf{u}} (g(\mathbf{z}) - \operatorname{Re}(2\mathbf{u}^H(\mathbf{A}\mathbf{z} - \mathbf{b}))) &= -\frac{\partial}{\partial \mathbf{u}} \operatorname{Re}(2\mathbf{u}^H(\mathbf{A}\mathbf{z} - \mathbf{b})) \\ &= -\mathbf{A}\mathbf{z} + \mathbf{b}.\end{aligned}\tag{C.6.11}$$

Then

$$\nabla L_{\mathbf{z}}(\mathbf{z}, \mathbf{u}) = \nabla g(\mathbf{z}) - \mathbf{A}^H \mathbf{u}$$

$$\nabla L_{\mathbf{u}}(\mathbf{z}, \mathbf{u}) = -\mathbf{A}\mathbf{z} + \mathbf{b}.$$

## APPENDIX D. PROOFS AND DERIVATIONS

This appendix provides detailed explanations and proofs of the theorems and lemmas used in this work. It also provides detailed derivations for some of the equations used in the work. In Appendix D.1 we provide a detailed explanation and proof of the S-procedure as used in Lemma 1 of Section 6.4 to recast the quadratic constraints in (6.27) into linear matrix inequalities. Similarly, in Appendix D.2 we present a detailed explanation of a Bernstein-type inequality used in Lemma 2 of Section 6.5 to obtain a safe (conservative) approximation of the intractable outage probability constraints in (6.44). Furthermore, in Appendix D.3 we provide detailed explanations and derivations for the generalized Rayleigh quotient or generalized Rayleigh-Ritz problem which is used in Section 5.4 to decouple the leakage-based optimization problem for an RIS-aided DTDD system. Moreover, in Appendix D.4 We provide a detailed derivation process for the expansion of the power constraints used in robust beamforming strategies considered in Chapter 6.

### D.1 Detailed explanation of the S-procedure

The S-procedure or S-lemma tries to solve a system of quadratic inequalities via LMI relaxation. It is a theorem of alternatives for a pair of (nonconvex) quadratic inequalities. The results in this section can be found in the literature under different names in different disciplines, for detailed surveys and references see [154].

**Theorem D.1.1.** *Let us denote  $\mathbf{F}_1$ , and  $\mathbf{F}_2 \in \mathbb{H}^{k \times k}$  as  $k \times k$  Hermitian matrices and the following complex-valued vectors and scalars  $\mathbf{b}_1, \mathbf{b}_2 \in \mathbb{C}^{k \times 1}$ ,  $c_1, c_2 \in \mathbb{R}$ . Suppose that there exists an  $\hat{\mathbf{x}}$  with*

$$\hat{\mathbf{x}}^H \mathbf{F}_s \hat{\mathbf{x}} + 2\mathbf{b}_2^H \hat{\mathbf{x}} + c_2 \leq 0. \quad (\text{D.1.1})$$

*Then there exist an  $\mathbf{x} \in \mathbb{C}^{k \times 1}$  satisfying*

$$\mathbf{x}^H \mathbf{F}_1 \mathbf{x} + 2\mathbf{b}_1^H \mathbf{x} + c_1 \leq 0, \quad \mathbf{x}^H \mathbf{F}_2 \mathbf{x} + 2\mathbf{b}_2^H \mathbf{x} + c_2 \leq 0, \quad (\text{D.1.2})$$

if and only if there exists no  $\lambda$  such that

$$\lambda \geq 0, \quad \begin{bmatrix} \mathbf{F}_1 & \mathbf{b}_1 \\ \mathbf{b}_1^H & c_1 \end{bmatrix} + \lambda \begin{bmatrix} \mathbf{F}_2 & \mathbf{b}_2 \\ \mathbf{b}_2^H & c_2 \end{bmatrix} \succeq 0. \quad (\text{D.1.3})$$

This shows that (D.1.2) and (D.1.3) are strong alternatives.

*Proof.* By assuming that  $\hat{\mathbf{x}}$  is strictly feasible, then it implies that

$$\begin{bmatrix} \mathbf{F}_2 & \mathbf{b}_2 \\ \mathbf{b}_2^H & c_2 \end{bmatrix}$$

has at least one negative eigenvalue. Therefore,

$$\tau \geq 0, \quad \tau \begin{bmatrix} \mathbf{F}_2 & \mathbf{b}_2 \\ \mathbf{b}_2^H & c_2 \end{bmatrix} \succeq 0 \implies \tau = 0.$$

Then, we can apply the theorem of alternatives for non-strict linear matrix inequalities, which states that (D.1.3) is infeasible if and only if

$$\mathbf{X} \succeq 0, \quad \text{Tr} \left\{ \mathbf{X} \begin{bmatrix} \mathbf{F}_1 & \mathbf{b}_1 \\ \mathbf{b}_1^H & c_1 \end{bmatrix} \right\} < 0, \quad \text{Tr} \left\{ \begin{bmatrix} \mathbf{F}_2 & \mathbf{b}_2 \\ \mathbf{b}_2^H & c_2 \end{bmatrix} \right\} \leq 0$$

is feasible. This is equivalent to the feasibility of

$$\begin{bmatrix} \mathbf{v} & \mathbf{w} \end{bmatrix} \begin{bmatrix} \mathbf{F}_1 & \mathbf{b}_1 \\ \mathbf{b}_1^H & c_1 \end{bmatrix} \begin{bmatrix} \mathbf{v} \\ \mathbf{w} \end{bmatrix} < 0, \quad \begin{bmatrix} \mathbf{v} & \mathbf{w} \end{bmatrix} \begin{bmatrix} \mathbf{F}_2 & \mathbf{b}_2 \\ \mathbf{b}_2^H & c_2 \end{bmatrix} \begin{bmatrix} \mathbf{v} \\ \mathbf{w} \end{bmatrix} \leq 0.$$

If  $\mathbf{w} \neq 0$ , then  $\mathbf{x} = \mathbf{v}/\mathbf{w}$  is feasible in (D.1.2). If  $\mathbf{w} = 0$ , we have  $\mathbf{v}^H \mathbf{F}_1 \mathbf{v} < 0$ ,  $\mathbf{v}^H \mathbf{F}_2 \mathbf{v} \leq 0$ , so  $\mathbf{x} = \hat{\mathbf{x}} + d\mathbf{v}$  satisfies

$$\begin{aligned} \mathbf{x}^H \mathbf{F}_1 \mathbf{x} + 2\mathbf{b}_1^H \mathbf{x} + c_1 &= \hat{\mathbf{x}}^H \mathbf{F}_1 \hat{\mathbf{x}} + 2\mathbf{b}_1^H \hat{\mathbf{x}} + c_1 + d^2 \mathbf{v}^H \mathbf{F}_1 \mathbf{v} + 2d(\mathbf{F}_1 \hat{\mathbf{x}} + \mathbf{b}_1)^H \mathbf{v} \\ \mathbf{x}^H \mathbf{F}_2 \mathbf{x} + 2\mathbf{b}_2^H \mathbf{x} + c_2 &= \hat{\mathbf{x}}^H \mathbf{F}_2 \hat{\mathbf{x}} + 2\mathbf{b}_2^H \hat{\mathbf{x}} + c_2 + d^2 \mathbf{v}^H \mathbf{F}_2 \mathbf{v} + 2d(\mathbf{F}_2 \hat{\mathbf{x}} + \mathbf{b}_2)^H \mathbf{v} \\ &< 2d(\mathbf{F}_2 \hat{\mathbf{x}} + \mathbf{b}_2)^H \mathbf{v}, \end{aligned}$$

i.e.,  $\mathbf{x}$  becomes feasible as  $d \rightarrow \pm\infty$ , depending on the sign of  $(\mathbf{F}_2 \hat{\mathbf{x}} + \mathbf{b}_2)^H \mathbf{v}$ .  $\square$

## D.2 Detailed explanation of Bernstein-type inequality

In this section, we present a detailed explanation of a Bernstein-type inequality used in Lemma 2 of Section 6.5 to obtain a safe (conservative) approximation of the intractable outage probability constraints in (6.44). Here "safe" implies that the feasible points for the safe approximation always fulfill the probabilistic constraints. This means that the feasible points must be necessarily feasible also for the original optimization problem. Therefore, the safe approximation is a restriction to the original problem [131]. A Bernstein-type inequality bounds the probability that a sum of random variables deviates from its mean [142]. It can exploit the variance of random variables. Consider the following random variable  $G = \mathbf{v}^H \mathbf{Q} \mathbf{v} + 2 \operatorname{Re}(\mathbf{v}^H \mathbf{u})$ , where  $\mathbf{Q} \in \mathbb{H}^N$ ,  $\mathbf{u} \in \mathbb{C}^N$ , and  $\mathbf{v} \sim \mathcal{CN}(\mathbf{0}, \mathbf{I}_N)$ . For all  $\delta \geq 0$ , the following statements hold:

$$\Pr \left( G \geq \operatorname{Tr}(\mathbf{Q}) - \sqrt{2\delta} \sqrt{\|\mathbf{Q}\|_F^2 + 2\|\mathbf{u}\|^2} - \delta s^-(\mathbf{Q}) \right) \geq 1 - e^{-\delta}, \quad (\text{D.2.1})$$

$$\Pr \left( G \leq \operatorname{Tr}(\mathbf{Q}) + \sqrt{2\delta} \sqrt{\|\mathbf{Q}\|_F^2 + 2\|\mathbf{u}\|^2} + \delta s^+(\mathbf{Q}) \right) \geq 1 - e^{-\delta}, \quad (\text{D.2.2})$$

where  $s^+(\mathbf{Q}) = \max\{\lambda_{\max}(\mathbf{Q}), 0\}$  in which  $\lambda_{\max}$  denotes the maximum eigenvalue of  $\mathbf{Q}$  and  $s^-(\mathbf{Q}) = \max\{\lambda_{\max}(-\mathbf{Q}), 0\}$ . The proof of this Lemma 2 is obtained by extending the result of [156, Lemma 0.2] from a real Gaussian quadratic form to a complex Gaussian quadratic form.

Let  $\tilde{\mathbf{v}} \sim \mathcal{N}(\mathbf{0}, \mathbf{I}_N)$  be a standard random vector,  $\tilde{\mathbf{Q}} \in \mathbb{S}^N$  be the  $N \times N$  symmetric matrix, and  $\tilde{\mathbf{u}} \in \mathbb{R}^N$ . Hence, for any given  $\delta \geq 0$  we have

$$\Pr \left( \tilde{\mathbf{v}}^T \tilde{\mathbf{Q}} \tilde{\mathbf{v}} + 2\tilde{\mathbf{v}}^T \tilde{\mathbf{u}} \geq \operatorname{Tr}(\tilde{\mathbf{Q}}) - \sqrt{2\delta} \sqrt{\|\tilde{\mathbf{Q}}\|_F^2 + 2\|\tilde{\mathbf{u}}\|^2} - \delta s^-(\tilde{\mathbf{Q}}) \right) \geq 1 - e^{-\delta}.$$

To extend to complex Gaussian quadratic form, we observe that  $\mathbf{Q} \in \mathbb{H}^N$ ,  $\mathbf{u} \in \mathbb{C}^N$ , and  $\mathbf{v} \sim \mathcal{CN}(\mathbf{0}, \mathbf{I}_N)$ , then we have

$$\begin{aligned} \tilde{\mathbf{v}} &= \sqrt{2} \begin{bmatrix} \operatorname{Re}(\mathbf{v}) \\ \operatorname{Im}(\mathbf{v}) \end{bmatrix} \sim \mathbb{N}(\mathbf{0}, \mathbf{I}_{2N}) \\ \tilde{\mathbf{Q}} &= \frac{1}{2} \begin{bmatrix} \operatorname{Re}(\mathbf{Q}) & -\operatorname{Im}(\mathbf{Q}) \\ \operatorname{Im}(\mathbf{Q}) & \operatorname{Re}(\mathbf{Q}) \end{bmatrix} \in \mathbb{S}^{2N} \\ \tilde{\mathbf{u}} &= \frac{1}{\sqrt{2}} \begin{bmatrix} \operatorname{Re}(\mathbf{u}) \\ \operatorname{Im}(\mathbf{u}) \end{bmatrix} \in \mathbb{R}^{2N} \end{aligned}$$

It is easy to verify that  $\mathbf{v}^H \mathbf{Q} \mathbf{v} + 2 \operatorname{Re}(\mathbf{v}^H \mathbf{u}) = \tilde{\mathbf{v}}^T \tilde{\mathbf{Q}} \tilde{\mathbf{v}} + 2\tilde{\mathbf{v}}^T \tilde{\mathbf{u}}$ . Therefore, we can adopt [156, Lemma 0.2] to obtain the desired result.

Denote  $\delta = -\ln \rho$  and  $\rho \in (0, 1]$ , then from Lemma 2 it shows that the probability inequality of a quadratic form of complex Gaussian random variables

$$\Pr(\mathbf{v}^H \mathbf{Q} \mathbf{v} + 2 \operatorname{Re}\{\mathbf{v}^H \mathbf{u}\} \geq b) \geq 1 - \rho \quad (\text{D.2.3})$$

holds if the following inequality is satisfied

$$\operatorname{Tr}(\mathbf{Q}) - \sqrt{2\delta} \sqrt{\|\mathbf{Q}\|_{\mathbb{F}}^2 + 2\|\mathbf{u}\|^2} - \delta s^-(\mathbf{Q}) \geq b. \quad (\text{D.2.4})$$

This shows that (D.2.4) serves as a conservative formulation for (D.2.3). However, another important fact about the conservative formulation in (D.2.4) is that it can be equivalently replaced with the following [142, 157]

$$\operatorname{Tr}(\mathbf{Q}) - \sqrt{2\delta}x - \delta y \geq b, \quad (\text{D.2.5})$$

$$\sqrt{\|\mathbf{Q}\|_{\mathbb{F}}^2 + 2\|\mathbf{u}\|^2} \leq x, \quad (\text{D.2.6})$$

$$y\mathbf{I}_N + \mathbf{Q} \succeq \mathbf{0}, \quad (\text{D.2.7})$$

$$y \geq 0, \quad (\text{D.2.8})$$

where  $x, y \in \mathbb{R}$  are slack variables. The constraint in (D.2.6) can be further reformulated into a standard second-order-cone (SOC) constraint as

$$\left\| \begin{bmatrix} \sqrt{2}\mathbf{u} \\ \operatorname{vec}(\mathbf{Q}) \end{bmatrix} \right\| \leq x \quad (\text{D.2.9})$$

Similarly, from Lemma 2 it implies that

$$\Pr(\mathbf{v}^H \mathbf{Q} \mathbf{v} + 2 \operatorname{Re}\{\mathbf{v}^H \mathbf{u}\} \leq c) \geq 1 - \rho \quad (\text{D.2.10})$$

holds if the following inequality is satisfied

$$\operatorname{Tr}(\mathbf{Q}) + \sqrt{2\delta} \sqrt{\|\mathbf{Q}\|_{\mathbb{F}}^2 + 2\|\mathbf{u}\|^2} + \delta s^+(\mathbf{Q}) \leq D. \quad (\text{D.2.11})$$

Also (D.2.11) can be equivalently replaced with the following

$$\operatorname{Tr}(\mathbf{Q}) + \sqrt{2\delta}z + \delta w \leq c, \quad (\text{D.2.12})$$

$$\sqrt{\|\mathbf{Q}\|_{\mathbb{F}}^2 + 2\|\mathbf{u}\|^2} \leq z, \quad (\text{D.2.13})$$

$$w\mathbf{I}_N - \mathbf{Q} \succeq \mathbf{0}, \quad (\text{D.2.14})$$

$$w \geq 0, \quad (\text{D.2.15})$$

where  $z, w \in \mathbb{R}$  are slack variables. The Bernstein-type inequality bounds the probability that a sum of random variables deviates from its mean  $\text{Tr}\{\mathbf{Q}\}$  [157]. The mean of a given random variable  $T = \mathbf{v}^H \mathbf{Q} \mathbf{v}$  is given as

$$\begin{aligned} \mathbb{E}\{\mathbf{v}^H \mathbf{Q} \mathbf{v}\} &= \text{Tr}\{\mathbb{E}\{\mathbf{v}^H \mathbf{Q} \mathbf{v}\}\} \\ &= \text{Tr}\{\mathbf{Q} \cdot \mathbb{E}\{\mathbf{v} \mathbf{v}^H\}\} \\ &= \text{Tr}\{\mathbf{Q}(\text{Cov}(\mathbf{v}) + \boldsymbol{\mu} \boldsymbol{\mu}^H)\} \\ &= \text{Tr}\{\mathbf{Q} \boldsymbol{\Sigma}_{\mathbf{v}\mathbf{v}}\} + \text{Tr}\{\mathbf{Q} \boldsymbol{\mu} \boldsymbol{\mu}^H\} \\ &= \text{Tr}\{\mathbf{Q} \boldsymbol{\Sigma}_{\mathbf{v}\mathbf{v}}\} + \boldsymbol{\mu}^H \mathbf{Q} \boldsymbol{\mu}. \end{aligned}$$

Since the random vector is define as  $\mathbf{v} \sim \mathcal{CN}(\mathbf{0}, \mathbf{I}_N)$ , then  $\boldsymbol{\mu} = \mathbf{0}$  and  $\boldsymbol{\Sigma}_{\mathbf{v}\mathbf{v}} = \mathbf{I}_N$ . Therefore, the mean of the random variable is  $\text{Tr}\{\mathbf{Q}\}$ . The mean of the sum of random variables  $G = \mathbf{v}^H \mathbf{Q} \mathbf{v} + 2 \text{Re}\{\mathbf{v}^H \mathbf{u}\}$  is given as

$$\begin{aligned} \mathbb{E}\{\mathbf{v}^H \mathbf{Q} \mathbf{v}\} + \mathbb{E}\{2 \text{Re}\{\mathbf{v}^H \mathbf{u}\}\} &= \text{Tr}\{\mathbb{E}\{\mathbf{v}^H \mathbf{Q} \mathbf{v}\}\} + 2N \\ &= \text{Tr}\{\mathbf{Q} \cdot \mathbb{E}\{\mathbf{v} \mathbf{v}^H\}\} + 2N \\ &= \text{Tr}\{\mathbf{Q}(\text{Cov}(\mathbf{v}) + \boldsymbol{\mu} \boldsymbol{\mu}^H)\} + 2N \\ &= \text{Tr}\{\mathbf{Q} \boldsymbol{\Sigma}_{\mathbf{v}\mathbf{v}}\} + \text{Tr}\{\mathbf{Q} \boldsymbol{\mu} \boldsymbol{\mu}^H\} + 2N \\ &= \text{Tr}\{\mathbf{Q} \boldsymbol{\Sigma}_{\mathbf{v}\mathbf{v}}\} + \boldsymbol{\mu}^H \mathbf{Q} \boldsymbol{\mu} + 2N. \end{aligned}$$

Since the random vector is define as  $\mathbf{v} \sim \mathcal{CN}(\mathbf{0}, \mathbf{I}_N)$ , then  $\boldsymbol{\mu} = \mathbf{0}$  and  $\boldsymbol{\Sigma}_{\mathbf{v}\mathbf{v}} = \mathbf{I}_N$ . Hence, the mean of  $G$  is  $\text{Tr}\{\mathbf{Q}\} + 2N$ . Note that because the real part of a real number is the number itself, therefore,  $\mathbb{E}\{2 \text{Re}\{\mathbf{v}^H \mathbf{u}\}\} = 2\mathbb{E}\{\text{Re}\{\mathbf{v}^H \mathbf{u}\}\} = 2N$ .

### D.3 Rayleigh Quotient and Eigenvalue Problem

In this section, we provide detailed explanations and derivations for the generalized Rayleigh quotient or generalized Rayleigh-Ritz problem which is used in Section 5.4 to decouple the leakage-based optimization problem for an RIS-aided DTDD system.

For a given Hermitian matrix  $\mathbf{A} \in \mathbb{H}^{n \times n}$ , and non-zero vector  $\mathbf{x} \in \mathbb{C}^n$ , the *Rayleigh-Ritz quotient* or *Rayleigh quotient* is defined as the normalized quadratic form

$$\frac{\mathbf{x}^H \mathbf{A} \mathbf{x}}{\mathbf{x}^H \mathbf{x}} \tag{D.3.1}$$

The maximum or minimum of (D.3.1) is given by the largest  $\lambda_{\max}$  eigenvalue or smallest

eigenvalue  $\lambda_{\max}$  of  $\mathbf{A}$ , respectively, i.e.,

$$\max_{\mathbf{x} \in \mathbb{C}^n} \frac{\mathbf{x}^H \mathbf{A} \mathbf{x}}{\mathbf{x}^H \mathbf{x}} = \lambda_{\max} \quad (\text{when } \mathbf{x} = \text{"largest" eigenvector of } \mathbf{A}) \quad (\text{D.3.2})$$

$$\min_{\mathbf{x} \in \mathbb{C}^n} \frac{\mathbf{x}^H \mathbf{A} \mathbf{x}}{\mathbf{x}^H \mathbf{x}} = \lambda_{\min} \quad (\text{when } \mathbf{x} = \text{"smallest" eigenvector of } \mathbf{A}) \quad (\text{D.3.3})$$

This implies that the eigenvector  $\mathbf{x}_1$  corresponding to the largest eigenvalue  $\lambda_1$  of  $\mathbf{A}$  is the global maximizer in (D.3.2) that gives the maximum value of  $\lambda_1$ . Equally, the eigenvector  $\mathbf{x}_n$  corresponding to the smallest eigenvalue  $\lambda_n$  of  $\mathbf{A}$  is the global minimizer in (D.3.3) that will yield the minimum value  $\lambda_n$ . As a result, the matrix  $\mathbf{A}$  and the extreme values of  $\lambda_i$  and their corresponding vectors  $\mathbf{v}_i$  (D.3.2) and (D.3.3) can be written as

$$\mathbf{A} \mathbf{v}_i = \lambda_i \mathbf{v}_i, \quad \forall i \in \{1, \dots, n\}. \quad (\text{D.3.3})$$

The problem in (D.3.3) is known as the *eigenvalue problem*. This can be written in matrix form as

$$\mathbf{A} \mathbf{V} = \mathbf{V} \mathbf{\Lambda}, \quad (\text{D.3.4})$$

where  $\mathbf{V} = [\mathbf{v}_1, \dots, \mathbf{v}_n] \in \mathbb{C}^{n \times n}$  are the eigenvectors and the diagonal elements of  $\mathbf{\Lambda} = \text{diag}([\lambda_1, \dots, \lambda_n]^T) \in \mathbb{R}^{n \times n}$  are the eigenvalues. Furthermore, let us denote  $\mathbf{B}$  as a Hermitian matrix of the same size that is positive definite, i.e.,  $\mathbf{B} \succ 0$ . Therefore, the *generalized Rayleigh quotient* or *generalized Rayleigh-Ritz* is defined as [127]

$$\frac{\mathbf{x}^H \mathbf{A} \mathbf{x}}{\mathbf{x}^H \mathbf{B} \mathbf{x}}, \quad (\text{D.3.5})$$

where  $\mathbf{A}$  and  $\mathbf{B}$  are Hermitian matrices and  $\mathbf{x}$  is a non-zero vector, i.e.,  $\mathbf{A} = \mathbf{A}^H$ ,  $\mathbf{B} = \mathbf{B}^H$ , and  $\mathbf{x} \neq 0$ . Note that a matrix is said to be **positive semidefinite (PSD)** if for all  $\mathbf{x} \in \mathbb{C}^n$  the quadratic form  $Q(\mathbf{x}) = \mathbf{x}^H \mathbf{A} \mathbf{x} \geq 0$ . When the equality holds true only for  $\mathbf{x} = 0$ , i.e.,  $\mathbf{x}^H \mathbf{A} \mathbf{x} > 0, \forall \mathbf{x} \neq 0$ , therefore matrix  $\mathbf{A}$  is **positive definite (PD)** [131]. Similarly, for the given generalized Rayleigh quotient in (D.3.5) the extreme values of the  $\lambda_i$  and their corresponding eigenvectors that satisfy the problem can be defined as

$$\mathbf{A} \mathbf{v}_i = \lambda_i \mathbf{B} \mathbf{v}_i, \quad \forall i \in \{1, \dots, n\}. \quad (\text{D.3.6})$$

The problem in (D.3.6) is known as the *generalized eigenvalue problem*. This can be

written in matrix form as

$$\mathbf{A}\mathbf{V} = \mathbf{B}\mathbf{V}\mathbf{\Lambda}, \quad (\text{D.3.7})$$

where  $\mathbf{V} = [\mathbf{v}_1, \dots, \mathbf{v}_n] \in \mathbb{C}^{n \times n}$  are the eigenvectors and the diagonal elements of  $\mathbf{\Lambda} = \text{diag}([\lambda_1, \dots, \lambda_n]^T) \in \mathbb{R}^{n \times n}$  are the eigenvalues.

In many fields of science, such as mathematics, statistics, signal processing, and machine learning the eigenvalue and generalized eigenvalue problems play important roles. The eigenvectors of a matrix contain the most important directions of that matrix in the eigenvalue problem. For instance, the eigenvector gives the directions of spread (variance of data) for a covariance matrix. In contrast, the magnitude of the spread in these directions is provided by the eigenvalues [127, 195].

### D.3.1 Generalized Eigenvalue Optimization

A generalized eigenvalue optimization problem is an optimization problem that yields to the generalized eigenvalue problem. For example, consider the following problem

$$\max_{\mathbf{x} \in \mathbb{C}^n} \mathbf{x}^H \mathbf{A} \mathbf{x} \quad (\text{D.3.8})$$

$$\text{s.t. } \mathbf{x}^H \mathbf{B} \mathbf{x} = 1, \quad (9.12)$$

where  $\mathbf{A} \in \mathbb{H}^{n \times n}$ ,  $\mathbf{B} \in \mathbb{H}^{n \times n}$ , and  $\mathbf{x} \in \mathbb{C}^{n \times 1}$ . The Lagrangian of the above problem is given as [131]

$$\mathcal{L} = \mathbf{x}^H \mathbf{A} \mathbf{x} - \lambda(\mathbf{x}^H \mathbf{B} \mathbf{x} - 1), \quad (\text{D.3.9})$$

where  $\lambda \in \mathbb{R}$  is the Lagrange multiplier. Differentiating the Lagrangian with respect to  $\mathbf{x}$  and equating it to zero we have

$$\frac{\partial \mathcal{L}}{\partial \mathbf{x}} = 2\mathbf{A}\mathbf{x} - 2\lambda\mathbf{B}\mathbf{x} \stackrel{\text{set}}{=} 0 \implies \mathbf{A}\mathbf{x} = \lambda\mathbf{B}\mathbf{x}. \quad (\text{D.3.10})$$

According to (D.3.7), we note that (D.3.10) is a generalized eigenvalue problem. The  $\mathbf{x}$  is the eigenvector and the  $\lambda$  is the eigenvalue for this problem. As the optimization in (D.3.8) is a maximization problem, the eigenvector is the one having the largest eigenvalue. In contrast, if the optimization in (D.3.8) is a minimization problem, the eigenvector is the one having the smallest eigenvalue [127, 131].

## D.4 Detailed Expansion of the Power Constraints in WCR and PCR Methods

We provide a detailed derivation process for the expansion of the power constraints used in robust beamforming strategies considered in Chapter 6 in this section. In Appendix D.4.1, we provide these details for the worst-case robust (WCR) formulation in (6.18b) and in Appendix D.4.2 for the probabilistic-constrained robust (PCR) design approach in (6.44).

### D.4.1 Power Constraints in WCR method

**Desired power constraint:** Let us introduce the following variables  $\mathbf{F}_q = \mathbf{f}_q \mathbf{f}_q^H, \forall q \in \mathcal{Q}^{\text{dl}}$  and  $\mathbf{\Psi} = \boldsymbol{\theta} \boldsymbol{\theta}^H$ , where  $\mathbf{F}_q \succeq \mathbf{0}, \mathbf{\Psi} \succeq \mathbf{0}, \mathbf{F}_q \in \mathbb{H}^{M_T \times M_T}, \mathbf{\Psi} \in \mathbb{H}^{M_S \times M_S}$ , and  $\mathbf{F}_q$  and  $\mathbf{\Psi}$  are rank-one Hermitian matrices. Therefore, the desired power for the  $q$ th UE in the  $q$ th DL cell as given in (6.18b) can be expanded as follows

$$\begin{aligned}
|\boldsymbol{\theta}^H (\hat{\mathbf{E}}_{q,q} + \boldsymbol{\Delta}_{q,q}) \mathbf{f}_q|^2 &= \boldsymbol{\theta}^H (\hat{\mathbf{E}}_{q,q} + \boldsymbol{\Delta}_{q,q}) \mathbf{f}_q \mathbf{f}_q^H (\hat{\mathbf{E}}_{q,q} + \boldsymbol{\Delta}_{q,q})^H \boldsymbol{\theta} \\
&\stackrel{(a)}{=} \text{Tr} \left\{ \mathbf{f}_q \mathbf{f}_q^H (\hat{\mathbf{E}}_{q,q} + \boldsymbol{\Delta}_{q,q})^H \boldsymbol{\theta} \boldsymbol{\theta}^H (\hat{\mathbf{E}}_{q,q} + \boldsymbol{\Delta}_{q,q}) \right\} \\
&= \text{Tr} \left\{ \mathbf{F}_q (\hat{\mathbf{E}}_{q,q} + \boldsymbol{\Delta}_{q,q})^H \mathbf{\Psi} (\hat{\mathbf{E}}_{q,q} + \boldsymbol{\Delta}_{q,q}) \right\} \\
&\stackrel{(b)}{=} \text{Tr} \left\{ (\hat{\mathbf{E}}_{q,q} + \boldsymbol{\Delta}_{q,q})^H \mathbf{\Psi} (\hat{\mathbf{E}}_{q,q} + \boldsymbol{\Delta}_{q,q}) \mathbf{F}_q \right\} \\
&\stackrel{(c)}{=} \text{vec}^H \left\{ (\hat{\mathbf{E}}_{q,q} + \boldsymbol{\Delta}_{q,q}) \right\} \text{vec} \left\{ \mathbf{\Psi} (\hat{\mathbf{E}}_{q,q} + \boldsymbol{\Delta}_{q,q}) \mathbf{F}_q \right\} \\
&\stackrel{(d)}{=} \text{vec}^H \left\{ (\hat{\mathbf{E}}_{q,q} + \boldsymbol{\Delta}_{q,q}) \right\} (\mathbf{F}_q^T \otimes \mathbf{\Psi}) \text{vec} \left\{ (\hat{\mathbf{E}}_{q,q} + \boldsymbol{\Delta}_{q,q}) \right\} \\
&= \text{vec}^H \left\{ \boldsymbol{\Delta}_{q,q} \right\} (\mathbf{F}_q^T \otimes \mathbf{\Psi}) \text{vec} \left\{ \boldsymbol{\Delta}_{q,q} \right\} \\
&\quad + 2 \text{Re} \left\{ \text{vec}^H \left\{ \boldsymbol{\Delta}_{q,q} \right\} (\mathbf{F}_q^T \otimes \mathbf{\Psi}) \text{vec}(\hat{\mathbf{E}}_{q,q}) \right\} \\
&\quad + \text{vec}^H \left\{ \hat{\mathbf{E}}_{q,q} \right\} (\mathbf{F}_q^T \otimes \mathbf{\Psi}) \text{vec} \left\{ \hat{\mathbf{E}}_{q,q} \right\}, \tag{D.4.1.1}
\end{aligned}$$

where (a) is obtained by using the property defined in (1.3), i.e.,  $\mathbf{x}^H \mathbf{A} \mathbf{x} = \text{Tr}\{\mathbf{A} \mathbf{x} \mathbf{x}^H\}$  and in (b) we have used the cyclic property of the trace operation as given in (1.7), i.e.,  $\text{Tr}\{\mathbf{A} \mathbf{B} \mathbf{C} \mathbf{D}\} = \text{Tr}\{\mathbf{B} \mathbf{C} \mathbf{D} \mathbf{A}\}$ . Additionally, (c) is due to the trace property given in (1.4), which is  $\text{Tr}\{\mathbf{A}^H \mathbf{B}\} = \text{vec}^H\{\mathbf{A}\} \text{vec}\{\mathbf{B}\}$  and the operation in (d) is due to the property given in (1.5), i.e.,  $\text{vec}\{\mathbf{A} \mathbf{B} \mathbf{C}\} = (\mathbf{C}^T \otimes \mathbf{A}) \text{vec}\{\mathbf{B}\}$ .

The expansion of the power constraint in (6.18c) representing the inter-cell interference power received by the  $q$ th UE in the  $q$ th DL cell from the transmission of the  $k$ th DL BS, and the power constraint in (6.18d) which the UE-UE cross-link interference power received by the UE in the  $q$ th DL cell from the UE in  $r$ th UL can be done similarly as in (D.4.1.1).

**BS-BS power constraint:** The BS-BS cross-link interference power received by the BS in the  $r$ th UL cell due to the transmission of the  $q$ th DL BS as given in (6.18f) can be expanded as follows

$$\begin{aligned}
\|(\mathbf{f}_q^\top \otimes \mathbf{I}_{M_T})(\hat{\mathbf{z}}_{r,q} + \Delta_{r,q}^{(\mathfrak{z})})\boldsymbol{\theta}\|^2 &= (\mathbf{f}_q^\top \otimes \mathbf{I}_{M_T})(\hat{\mathbf{z}}_{r,q} + \Delta_{r,q}^{(\mathfrak{z})})\boldsymbol{\theta}\boldsymbol{\theta}^\text{H}(\hat{\mathbf{z}}_{r,q} + \Delta_{r,q}^{(\mathfrak{z})})^\text{H}(\mathbf{f}_q^\top \otimes \mathbf{I}_{M_T})^\text{H} \\
&\stackrel{(i)}{=} \text{Tr} \left\{ (\hat{\mathbf{z}}_{r,q} + \Delta_{r,q}^{(\mathfrak{z})})\boldsymbol{\Psi}(\hat{\mathbf{z}}_{r,q} + \Delta_{r,q}^{(\mathfrak{z})})^\text{H}(\mathbf{f}_q^\top \otimes \mathbf{I}_{M_T})^\text{H}(\mathbf{f}_q^\top \otimes \mathbf{I}_{M_T}) \right\} \\
&\stackrel{(ii)}{=} \text{Tr} \left\{ (\hat{\mathbf{z}}_{r,q} + \Delta_{r,q}^{(\mathfrak{z})})\boldsymbol{\Psi}(\hat{\mathbf{z}}_{r,q} + \Delta_{r,q}^{(\mathfrak{z})})^\text{H}(\mathbf{f}_q^* \mathbf{f}_q^\top \otimes \mathbf{I}_{M_T}) \right\} \\
&\stackrel{(iii)}{=} \text{Tr} \left\{ (\hat{\mathbf{z}}_{r,q} + \Delta_{r,q}^{(\mathfrak{z})})\boldsymbol{\Psi}(\hat{\mathbf{z}}_{r,q} + \Delta_{r,q}^{(\mathfrak{z})})^\text{H}(\mathbf{F}_q^\top \otimes \mathbf{I}_{M_T}) \right\} \\
&\stackrel{(iv)}{=} \text{Tr} \left\{ (\hat{\mathbf{z}}_{r,q} + \Delta_{r,q}^{(\mathfrak{z})})^\text{H}(\mathbf{F}_q^\top \otimes \mathbf{I}_{M_T})(\hat{\mathbf{z}}_{r,q} + \Delta_{r,q}^{(\mathfrak{z})})\boldsymbol{\Psi} \right\} \\
&\stackrel{(v)}{=} \text{vec}^\text{H} \{ (\hat{\mathbf{z}}_{r,q} + \Delta_{r,q}^{(\mathfrak{z})}) \} \text{vec} \left\{ (\mathbf{F}_q^\top \otimes \mathbf{I}_{M_T})(\hat{\mathbf{z}}_{r,q} + \Delta_{r,q}^{(\mathfrak{z})})\boldsymbol{\Psi} \right\} \\
&\stackrel{(vi)}{=} \text{vec}^\text{H} \{ (\hat{\mathbf{z}}_{r,q} + \Delta_{r,q}^{(\mathfrak{z})}) \} (\boldsymbol{\Psi}^\top \otimes (\mathbf{F}_q^\top \otimes \mathbf{I}_{M_T})) \text{vec} \{ (\hat{\mathbf{z}}_{r,q} + \Delta_{r,q}^{(\mathfrak{z})}) \} \\
&= \text{vec}^\text{H} \{ \Delta_{r,q}^{(\mathfrak{z})} \} (\boldsymbol{\Psi}^\top \otimes (\mathbf{F}_q^\top \otimes \mathbf{I}_{M_T})) \text{vec} \{ \Delta_{r,q}^{(\mathfrak{z})} \} \\
&\quad + 2 \text{Re} \{ \text{vec}^\text{H} \{ \Delta_{r,q}^{(\mathfrak{z})} \} (\boldsymbol{\Psi}^\top \otimes (\mathbf{F}_q^\top \otimes \mathbf{I}_{M_T})) \text{vec} \{ \hat{\mathbf{z}}_{r,q} \} \} + u_{r,q},
\end{aligned} \tag{D.4.1.2}$$

where  $u_{r,q} = \text{vec}^\text{H} \{ \hat{\mathbf{z}}_{r,q} \} (\boldsymbol{\Psi}^\top \otimes (\mathbf{F}_q^\top \otimes \mathbf{I}_{M_T})) \text{vec} \{ \hat{\mathbf{z}}_{r,q} \}$ . We note that the (i) and (iv) are due to the cyclic property of the trace operation as given in (1.7) and the operation in (ii) is due to the property given in (1.6), i.e.,  $(\mathbf{A} \otimes \mathbf{B})(\mathbf{C} \otimes \mathbf{D}) = \mathbf{AC} \otimes \mathbf{BD}$ . In (iii), it can easily be verified that  $\mathbf{f}_q^* \mathbf{f}_q^\top = (\mathbf{f}_q \mathbf{f}_q^\text{H})^\top = \mathbf{F}_q^\top$ . Furthermore, (v) is due to the trace property given in (1.4), which is  $\text{Tr} \{ \mathbf{A}^\text{H} \mathbf{B} \} = \text{vec}^\text{H} \{ \mathbf{A} \} \text{vec} \{ \mathbf{B} \}$  and the operation in (vi) is due to the property given in (1.5), i.e.,  $\text{vec} \{ \mathbf{ABC} \} = (\mathbf{C}^\top \otimes \mathbf{A}) \text{vec} \{ \mathbf{B} \}$ .

## D.4.2 Power Constraints in PCR

All the power constraints in (6.44) can be expanded in the same manner as those of Section D.4.1, the only difference is that we will replace the channel estimation errors with the statistical uncertainty models. For example, the desired power for the  $q$ th UE

in the  $q$ th DL cell as given in (6.44b) can be expanded as follows

$$\begin{aligned}
|\boldsymbol{\theta}^H(\hat{\mathbf{E}}_{q,q} + \boldsymbol{\Delta}_{q,q})\mathbf{f}_q|^2 &= \boldsymbol{\theta}^H(\hat{\mathbf{E}}_{q,q} + \boldsymbol{\Delta}_{q,q})\mathbf{f}_q\mathbf{f}_q^H(\hat{\mathbf{E}}_{q,q} + \boldsymbol{\Delta}_{q,q})^H\boldsymbol{\theta} \\
&\stackrel{(a)}{=} \text{Tr} \left\{ \mathbf{f}_q\mathbf{f}_q^H(\hat{\mathbf{E}}_{q,q} + \boldsymbol{\Delta}_{q,q})^H\boldsymbol{\theta}\boldsymbol{\theta}^H(\hat{\mathbf{E}}_{q,q} + \boldsymbol{\Delta}_{q,q}) \right\} \\
&= \text{Tr} \left\{ \mathbf{F}_q(\hat{\mathbf{E}}_{q,q} + \boldsymbol{\Delta}_{q,q})^H\boldsymbol{\Psi}(\hat{\mathbf{E}}_{q,q} + \boldsymbol{\Delta}_{q,q}) \right\} \\
&\stackrel{(b)}{=} \text{Tr} \left\{ (\hat{\mathbf{E}}_{q,q} + \boldsymbol{\Delta}_{q,q})^H\boldsymbol{\Psi}(\hat{\mathbf{E}}_{q,q} + \boldsymbol{\Delta}_{q,q})\mathbf{F}_q \right\} \\
&\stackrel{(c)}{=} \text{vec}^H \left\{ (\hat{\mathbf{E}}_{q,q} + \boldsymbol{\Delta}_{q,q}) \right\} \text{vec} \left\{ \boldsymbol{\Psi}(\hat{\mathbf{E}}_{q,q} + \boldsymbol{\Delta}_{q,q})\mathbf{F}_q \right\} \\
&\stackrel{(d)}{=} \text{vec}^H \left\{ (\hat{\mathbf{E}}_{q,q} + \boldsymbol{\Delta}_{q,q}) \right\} (\mathbf{F}_q^T \otimes \boldsymbol{\Psi}) \text{vec} \left\{ (\hat{\mathbf{E}}_{q,q} + \boldsymbol{\Delta}_{q,q}) \right\} \\
&= \text{vec}^H \left\{ \boldsymbol{\Delta}_{q,q} \right\} (\mathbf{F}_q^T \otimes \boldsymbol{\Psi}) \text{vec} \left\{ \boldsymbol{\Delta}_{q,q} \right\} \\
&\quad + 2 \text{Re} \left\{ \text{vec}^H \left\{ \boldsymbol{\Delta}_{q,q} \right\} (\mathbf{F}_q^T \otimes \boldsymbol{\Psi}) \text{vec} \left\{ \hat{\mathbf{E}}_{q,q} \right\} \right\} \\
&\quad + \text{vec}^H \left\{ \hat{\mathbf{E}}_{q,q} \right\} (\mathbf{F}_q^T \otimes \boldsymbol{\Psi}) \text{vec} \left\{ \hat{\mathbf{E}}_{q,q} \right\} \\
&\stackrel{(e)}{=} \boldsymbol{\lambda}_{q,q}^H \eta_{q,q}^2 (\mathbf{F}_q^T \otimes \boldsymbol{\Psi}) \boldsymbol{\lambda}_{q,q} + 2 \text{Re} \left\{ \boldsymbol{\lambda}_{q,q}^H \eta_{q,q} (\mathbf{F}_q^T \otimes \boldsymbol{\Psi}) \text{vec} \left\{ \hat{\mathbf{E}}_{q,q} \right\} \right\} \\
&\quad + \text{vec}^H \left\{ \hat{\mathbf{E}}_{q,q} \right\} (\mathbf{F}_q^T \otimes \boldsymbol{\Psi}) \text{vec} \left\{ \hat{\mathbf{E}}_{q,q} \right\}, \tag{D.4.2.1}
\end{aligned}$$

where (a) is obtained by using the property defined in (1.3), i.e.,  $\mathbf{x}^H\mathbf{A}\mathbf{x} = \text{Tr}\{\mathbf{A}\mathbf{x}\mathbf{x}^H\}$  and in (b) we have used the cyclic property of the trace operation as given in (1.7), i.e.,  $\text{Tr}\{\mathbf{A}\mathbf{B}\mathbf{C}\mathbf{D}\} = \text{Tr}\{\mathbf{B}\mathbf{C}\mathbf{D}\mathbf{A}\}$ . Additionally, (c) is due to the trace property given in (1.4), which is  $\text{Tr}\{\mathbf{A}^H\mathbf{B}\} = \text{vec}^H\{\mathbf{A}\}\text{vec}\{\mathbf{B}\}$  and the operation in (d) is due to the property given in (1.5), i.e.,  $\text{vec}\{\mathbf{A}\mathbf{B}\mathbf{C}\} = (\mathbf{C}^T \otimes \mathbf{A})\text{vec}\{\mathbf{B}\}$ . The operation in (e) is as a result of replacing  $\text{vec}\{\boldsymbol{\Delta}_{q,q}\} = \eta_{q,q}\boldsymbol{\lambda}_{q,q}$  as defined in (6.46a).

## D.5 Complexity Analysis for WCR and PCR Designs in Chapter 6

Since the resulting problems of the WCR design in (6.33) and the PCR design in (6.70) contain linear matrix inequality (LMI) and second-order cone (SOC) constraints, a standard interior point method (IPM) can be used to find their optimal solutions [131, 141]. In the following, we analyze the computational complexities of the different problems by using the worst-case runtime of the IPM, while ignoring the complexity of the linear constraints. The complexity of a generic IPM consists of two parts: the iteration complexity and the per-iteration computation cost [142], and is given as

$$\mathcal{O} \left\{ \left( \sum_{j=1}^J k_j + 2I \right)^{1/2} \left( \underbrace{n \sum_{j=1}^J k_j^3 + n^2 \sum_{j=1}^J k_j^2}_{\text{due to LMI}} + \underbrace{n \sum_{i=1}^I k_i^2 + n^3}_{\text{due to SOC}} \right) \right\}, \tag{D.5.1}$$

where  $n$  is the number of decision variables,  $J$  is the number of LMIs of size  $k_j$ , and  $I$  is the number of SOC constraints of size  $k_i$ .

### D.5.1 Worst-case Complexity Analysis

Let  $v = |\mathcal{Q}^{\text{dl}}| \cdot |\mathcal{Q}^{\text{ul}}|$  and  $\tau = |\mathcal{Q}^{\text{dl}}|$ . Problem (6.35) has  $(2\tau + 5v)$  LMI constraints of size 1,  $\tau$  LMI constraints of size  $M_T$ ,  $2\tau$  LMI constraints of size  $(M_T M_S + 1)$ ,  $v$  LMI constraints of size  $(M_S + 1)$ , and  $v$  LMI constraints of size  $(M_S M_T^2 + 1)$ . Therefore, using (D.5.1) the computational complexity per iteration of (6.35) is given in (D.5.2), where  $n_1 = Q M_T$ . In a similar manner, the computational complexity per iteration of (6.39) is given in (D.5.3) and  $n_2 = M_S$ . Here, problem (6.39) has  $(3\tau + 5v)$  LMI constraints of size 1, 1 LMI constraint of size  $M_S$ ,  $2\tau$  LMI constraints of size  $(M_T M_S + 1)$ ,  $v$  LMI constraints of size  $(M_S + 1)$ , and  $v$  LMI constraints of size  $(M_S M_T^2 + 1)$ . Finally, the approximate complexity of the worst-case robust design per iteration is  $o_{\mathbf{F}} + o_{\boldsymbol{\theta}}$ .

$$o_{\mathbf{F}} = \mathcal{O}\left(\left(2\tau(M_T M_S + \frac{M_T}{2} + 2) + v(M_S M_T^2 + M_S + 7)\right)^{1/2} n_1 [\tilde{a} + n_1 \tilde{b} + n_1^2]\right), \quad (\text{D.5.2})$$

$$o_{\boldsymbol{\theta}} = \mathcal{O}\left(\left(\tau(2M_T M_S + 5) + v(M_S M_T^2 + M_S + 7) + M_S\right)^{1/2} n_2 [\tilde{c} + n_2 \tilde{d} + n_2^2]\right), \quad (\text{D.5.3})$$

where

$$\begin{aligned} \tilde{a} &= [2\tau((M_T M_S + 1)^3 + \frac{M_T^3}{2} + 1) + 5v(\frac{(M_S M_T^2 + 1)^3 + (M_S + 1)^3}{5} + 1)], \\ \tilde{b} &= [2\tau((M_T M_S + 1)^2 + \frac{M_T^2}{2} + 1) + 5v(\frac{(M_S M_T^2 + 1)^2 + (M_S + 1)^2}{5} + 1)], \\ \tilde{c} &= [4\tau(\frac{(M_T M_S + 1)^3}{2} + 1) + 5v(\frac{(M_S M_T^2 + 1)^3 + (M_S + 1)^2}{5} + 1) + M_S^3], \\ \tilde{d} &= [4\tau(\frac{(M_T M_S + 1)^2}{2} + 1) + 5v(\frac{(M_S M_T^2 + 1)^2 + (M_S + 1)^2}{5} + 1) + M_S^2]. \end{aligned}$$

### D.5.2 Probabilistic-constrained Complexity Analysis

Following a similar approach, the computational complexity per iteration of (6.71) and (6.73) for the probabilistic-constrained robust design are given in (D.5.4) and (D.5.5) respectively. It can be observed that problem (6.71) has  $(3\tau + 3v)$  LMI constraints of size 1,  $\tau$  LMI constraints of size  $M_T$ ,  $v$  LMI constraints of size  $(M_S M_T^2)$ ,  $v$  LMI constraints of size  $(M_S)$ ,  $2\tau$  SOC constraints of size  $((M_T M_S)^2 + M_T M_S + 1)$ ,  $v$  SOC constraints of size  $(M_S^2 + M_S + 1)$ , and  $v$  SOC constraints of size  $((M_S M_T^2)^2 + M_S M_T^2 + 1)$ . Further, problem (6.73) has  $(4\tau + 3v)$  LMI constraints of size 1, 1 LMI constraint of size  $M_S$ ,  $v$

LMI constraints of size  $(M_S M_T^2)$ ,  $v$  LMI constraints of size  $(M_S)$ ,  $2\tau$  SOC constraints of size  $((M_T M_S)^2 + M_T M_S + 1)$ ,  $v$  SOC constraints of size  $(M_S^2 + M_S + 1)$ , and  $v$  SOC constraints of size  $((M_S M_T^2)^2 + M_S M_T^2 + 1)$ . Finally, the approximate complexity of the probabilistic-constrained robust design per iteration is  $o_{\mathbf{F}} + o_{\boldsymbol{\theta}}$ .

$$o_{\mathbf{F}} = \mathcal{O}\left(\left(\tau(2M_T M_S + M_T + 4) + v(M_S M_T^2 + M_S + 3) + 2(2\tau + v)\right)^{1/2} n_1 [\bar{z}_1 + n_1 \bar{z}_2 + \bar{z}_3 + n_1^2]\right), \quad (\text{D.5.4})$$

$$o_{\boldsymbol{\theta}} = \mathcal{O}\left(\left(\tau(2M_S M_T + 5) + v(M_S M_T^2 + M_S + 3) + 2(2\tau + v)\right)^{1/2} n_2 [\bar{z}_4 + n_2 \bar{z}_5 + \bar{z}_6 + n_2^2]\right), \quad (\text{D.5.5})$$

where

$$\bar{z}_1 = \left[4\tau\left(\frac{2(M_T M_S + 1)^3}{4} + \frac{M_T^3}{4} + 1\right) + 3v\left(\frac{(M_S M_T^2 + M_S)^3}{3} + 1\right)\right],$$

$$\bar{z}_2 = \left[4\tau\left(\frac{2(M_T M_S + 1)^2}{4} + \frac{M_T^2}{4} + 1\right) + 3v\left(\frac{(M_S M_T^2 + M_S)^2}{3} + 1\right)\right],$$

$$\bar{z}_3 = \left[2\tau((M_T M_S)^2 + M_T M_S + 1)^2 + v((M_S M_T^2)^2 + M_S M_T^2 + 1)^2 + v(M_S^2 + M_S + 1)^2\right],$$

$$\bar{z}_4 = \left[4\tau\left(\frac{(M_T M_S)^3}{2} + 1\right) + 3v\left(\frac{(M_S M_T^2 + M_S)^3}{3} + 1\right) + M_S^3\right],$$

$$\bar{z}_5 = \left[4\tau\left(\frac{(M_T M_S)^2}{2} + 1\right) + 3v\left(\frac{(M_S M_T^2 + M_S)^2}{3} + 1\right) + M_S^2\right],$$

$$\bar{z}_6 = \left[2\tau((M_T M_S)^2 + M_T M_S + 1)^2 + v((M_S M_T^2)^2 + M_S M_T^2 + 1)^2 + v(M_S^2 + M_S + 1)^2\right].$$

## BIBLIOGRAPHY

- [1] A. Yadav and O. A. Dobre, “All technologies work together for good: A glance at future mobile networks,” *IEEE Wireless Communications*, vol. 25, no. 4, pp. 10–16, 2018.
- [2] C. A. Gutierrez, O. Caicedo, and D. U. Campos-Delgado, “5G and beyond: Past, present and future of the mobile communications,” *IEEE Latin America Transactions*, vol. 19, no. 10, pp. 1702–1736, 2021.
- [3] Cisco, “Cisco Annual Internet Report (2018–2023) White Paper.” Cisco, Annual Report (AR) c11-741490, March 2020.
- [4] L. Bariah, L. Mohjazi, S. Muhaidat, P. C. Sofotasios, G. K. Kurt, H. Yanikomeroğlu, and O. A. Dobre, “A prospective look: Key enabling technologies, applications and open research topics in 6G networks,” *IEEE access*, vol. 8, pp. 174 792–174 820, 2020.
- [5] A. Dogra, R. K. Jha, and S. Jain, “A Survey on Beyond 5G Network With the Advent of 6G: Architecture and Emerging Technologies,” *IEEE Access*, vol. 9, pp. 67 512–67 547, 2021.
- [6] C. Dietrich, K. Dietze, J. Nealy, and W. Stutzman, “Spatial, polarization, and pattern diversity for wireless handheld terminals,” *IEEE Transactions on Antennas and Propagation*, vol. 49, no. 9, pp. 1271–1281, 2001.
- [7] L. Lu, G. Y. Li, A. L. Swindlehurst, A. Ashikhmin, and R. Zhang, “An overview of massive MIMO: Benefits and challenges,” *IEEE Journal of Selected Topics in Signal Processing*, vol. 8, no. 5, pp. 742–758, 2014.
- [8] L. Zheng and D. Tse, “Diversity and multiplexing: a fundamental tradeoff in multiple-antenna channels,” *IEEE Transactions on Information Theory*, vol. 49, no. 5, pp. 1073–1096, 2003.
- [9] E. Björnson, M. Bengtsson, and B. Ottersten, “Optimal multiuser transmit beamforming: A difficult problem with a simple solution structure [lecture notes],” *IEEE Signal Processing Magazine*, vol. 31, no. 4, pp. 142–148, 2014.
- [10] M. Haardt, V. Stankovic, and G. Del Galdo, “Efficient multi-user MIMO downlink precoding and scheduling,” in *Proc. of 1st IEEE International Workshop on Computational Advances in Multi-Sensor Adaptive Processing, 2005.*, 2005, pp. 237–240.
- [11] H. Weingarten, Y. Steinberg, and S. Shamai, “The capacity region of the Gaussian multiple-input multiple-output broadcast channel,” *IEEE Transactions on Information Theory*, vol. 52, no. 9, pp. 3936–3964, 2006.
- [12] N. Chiurtu, B. Rimoldi, and E. Telatar, “On the capacity of multi-antenna Gaussian channels,” in *Proc. of IEEE International Symposium on Information Theory (IEEE Cat. No.01CH37252)*, 2001, pp. 53–.

- [13] Q. Spencer, A. Swindlehurst, and M. Haardt, "Zero-forcing methods for downlink spatial multiplexing in multiuser MIMO channels," *IEEE Transactions on Signal Processing*, vol. 52, no. 2, pp. 461–471, 2004.
- [14] D. A. Schmidt, C. Shi, R. A. Berry, M. L. Honig, and W. Utschick, "Comparison of distributed beamforming algorithms for MIMO interference networks," *IEEE Transactions on Signal Processing*, vol. 61, no. 13, pp. 3476–3489, 2013.
- [15] T. E. Bogale and L. Vandendorpe, "Weighted sum rate optimization for downlink multiuser MIMO systems with per antenna power constraint: Downlink-uplink duality approach," in *Proc. of IEEE International Conference on Acoustics, Speech and Signal Processing (ICASSP)*, 2012, pp. 3245–3248.
- [16] A. Paulraj, R. Nabar, and D. Gore, *Introduction to Space-Time Wireless Communications*. Cambridge University Press, 2003.
- [17] J. Li, D. Wang, P. Zhu, L. Tang, and X. You, "Coordinated beamforming design using duality theory with dynamic cooperation clusters," *IET Commun.*, vol. 6, no. 12, pp. 1662–1669, 2012. [Online]. Available: <https://doi.org/10.1049/iet-com.2011.0853>
- [18] B. Song, F. Roemer, and M. Haardt, "Efficient channel quantization scheme for multi-user mimo broadcast channels with RBD precoding," in *2008 IEEE International Conference on Acoustics, Speech and Signal Processing*, 2008, pp. 2389–2392.
- [19] C. Song, J. Park, B. Clerckx, I. Lee, and K.-J. Lee, "Generalized precoder designs based on weighted MMSE criterion for energy harvesting constrained MIMO and multi-user MIMO channels," *IEEE Transactions on Wireless Communications*, vol. 15, no. 12, pp. 7941–7954, 2016.
- [20] 3GPP, "LTE: Scenarios and requirements for small cell enhancements for E-UTRA and E-UTRAN." 3GPP, Technical Report (TR) TR 36.932, Jan 2016.
- [21] W. Liu, S. Han, C. Yang, and C. Sun, "Massive MIMO or small cell network: Who is more energy efficient?" in *Proc. of IEEE Wireless Communications and Networking Conference Workshops (WCNCW)*, 2013, pp. 24–29.
- [22] M. Haardt, C. F. Mecklenbräuker, M. Vollmer, and P. Slanina, "Smart antennas for UTRA TDD," *European Transactions on Telecommunications*, vol. 12, no. 5, pp. 393–406, 2001. [Online]. Available: <https://onlinelibrary.wiley.com/doi/abs/10.1002/ett.4460120505>
- [23] M. Haardt, A. Klein, R. Koehn, S. Oestreich, M. Purat, V. Sommer, and T. Ulrich, "The TD-CDMA based UTRA TDD mode," *IEEE Journal on Selected Areas in Communications*, vol. 18, no. 8, pp. 1375–1386, 2000.
- [24] 3GPP Tech. Spec. Group RAN, "NR; physical layer procedures for control," 3GPP, Tech. Rep. TS 38.213, March 2019.
- [25] 3GPP, "Evolved Universal Terrestrial Radio Access (E-UTRA): Further enhancements to LTE Time Division Duplex (TDD) for Downlink-Uplink (DL-UL) interference management and traffic adaptation," 3GPP, Tech. Rep. TS 36.828, Jun 2012.
- [26] A. K. Gupta, M. N. Kulkarni, E. Visotsky, F. W. Vook, A. Ghosh, J. G. Andrews, and R. W. H. Jr., "Rate analysis and feasibility of dynamic TDD in 5G cellular

- systems,” in *Proc. of IEEE International Conference on Communications, ICC 2016, Kuala Lumpur, Malaysia, May 22-27, 2016*. IEEE, 2016, pp. 1–6. [Online]. Available: <https://doi.org/10.1109/ICC.2016.7511412>
- [27] Y.-T. Lin, C.-C. Chao, and H.-Y. Wei, “Dynamic TDD interference mitigation by using soft reconfiguration,” in *Proc. of 11th International Conference on Heterogeneous Networking for Quality, Reliability, Security and Robustness (QSHINE)*, 2015, pp. 352–357.
- [28] Y. S. Choi, I. Sohn, and K. B. Lee, “A novel decentralized time slot allocation algorithm in dynamic TDD system,” in *Proc. of 3rd IEEE Consumer Communications and Networking Conference, 2006.*, vol. 2, 2006, pp. 1268–1272.
- [29] H. Takahashi, K. Yokomakura, and K. Imamura, “A transmit power control based interference mitigation scheme for small cell networks using dynamic TDD in LTE-advanced systems,” in *Proc. of 79th IEEE Vehicular Technology Conference (VTC Spring)*, 2014, pp. 1–5.
- [30] P. Jayasinghe, A. Tölli, J. Kaleva, and M. Latva-aho, “Bi-directional signaling for dynamic TDD with decentralized beamforming,” in *Proc. of IEEE International Conference on Communication Workshop (ICCW)*, 2015, pp. 185–190.
- [31] C. Na, X. Hou, and H. Jiang, “Interference alignment based dynamic TDD for small cells,” in *Proc. of IEEE Globecom Workshops (GC Wkshps)*, 2014, pp. 700–705.
- [32] Q. Wu and R. Zhang, “Towards smart and reconfigurable environment: Intelligent reflecting surface aided wireless network,” *IEEE Communications Magazine*, vol. 58, no. 1, pp. 106–112, 2020.
- [33] Q. Wu, S. Zhang, B. Zheng, C. You, and R. Zhang, “Intelligent reflecting surface-aided wireless communications: A tutorial,” *IEEE Transactions on Communications*, vol. 69, no. 5, pp. 3313–3351, 2021.
- [34] X. Wang, Z. Fei, J. Huang, and H. Yu, “Joint waveform and discrete phase shift design for RIS-assisted integrated sensing and communication system under Cramer-Rao bound constraint,” *IEEE Transactions on Vehicular Technology*, vol. 71, no. 1, pp. 1004–1009, 2022.
- [35] S. Gong, X. Lu, D. T. Hoang, D. Niyato, L. Shu, D. I. Kim, and Y.-C. Liang, “Toward smart wireless communications via intelligent reflecting surfaces: A contemporary survey,” *IEEE Communications Surveys Tutorials*, vol. 22, no. 4, pp. 2283–2314, 2020.
- [36] Y. Cao, T. Lv, Z. Lin, and W. Ni, “Delay-constrained joint power control, user detection and passive beamforming in intelligent reflecting surface-assisted uplink mmwave system,” *IEEE Transactions on Cognitive Communications and Networking*, vol. 7, no. 2, pp. 482–495, 2021.
- [37] K. Ardah, S. Gherekhloo, A. L. F. de Almeida, and M. Haardt, “TRICE: A Channel Estimation Framework for RIS-Aided Millimeter-Wave MIMO Systems,” *IEEE Signal Processing Letters*, vol. 28, pp. 513–517, 2021.
- [38] J. Yuan, Y.-C. Liang, J. Joung, G. Feng, and E. G. Larsson, “Intelligent reflecting surface-assisted cognitive radio system,” *IEEE Transactions on Communications*, vol. 69, no. 1, pp. 675–687, 2021.

- [39] A. Taha, M. Alrabeiah, and A. Alkhateeb, “Enabling large intelligent surfaces with compressive sensing and deep learning,” *IEEE Access*, vol. 9, pp. 44 304–44 321, 2021.
- [40] A. C. Pogaku, D.-T. Do, B. M. Lee, and N. D. Nguyen, “UAV-assisted RIS for future wireless communications: A survey on optimization and performance analysis,” *IEEE Access*, vol. 10, pp. 16 320–16 336, 2022.
- [41] G. C. Nwalozie, K. Ardah, and M. Haardt, “Reflection Design methods for Reconfigurable Intelligent Surfaces-aided Dynamic TDD Systems,” in *Proc. of 12th IEEE Sensor Array and Multichannel Signal Processing Workshop (SAM 2022)*, Trondheim, Norway, June 2022.
- [42] G. C. Nwalozie and M. Haardt, “Distributed Coordinated Beamforming for RIS-aided Dynamic TDD Systems,” in *Proc. of 26th International ITG Workshop on Smart Antennas and 13th Conference on Systems, Communications, and Coding (WSA and SCC 2023)*, Braunschweig, Germany, March 2023.
- [43] —, “Leakage-based Coordinated Beamforming for RIS-aided Dynamic TDD Systems,” in *Proc. of 31st European Signal Processing Conference (EUSIPCO 2023)*, Helsinki, Finland, September 2023.
- [44] —, “Robust Beamforming for RIS-aided Dynamic TDD Systems,” in *Proc. of 31st European Signal Processing Conference (EUSIPCO 2023)*, Helsinki, Finland, September 2023.
- [45] —, “Probabilistic-constrained robust Beamforming for RIS-aided Dynamic TDD Systems,” in *Proc. of 19th International Symposium on Wireless Communication Systems (ISWCS 2024)*, Rio de Janeiro, Brazil, July 2024.
- [46] G. C. Nwalozie, D. Rakhimov, and M. Haardt, “Near-field beamforming for MU-MIMO millimeter wave communication system,” in *Proc. of 31st European Signal Processing Conference (EUSIPCO 2023)*, Helsinki, Finland, September 2023.
- [47] —, “Robust near-field beamforming for millimeter wave communication system with aperture perturbation,” in *Proc. of 49th IEEE International Conference on Acoustics, Speech, and Signal Processing (ICASSP 2024)*, Seoul, Korea, April 2024.
- [48] Q. Wu and R. Zhang, “Intelligent reflecting surface enhanced wireless network via joint active and passive beamforming,” *IEEE Transactions on Wireless Communications*, vol. 18, no. 11, pp. 5394–5409, 2019.
- [49] E. Basar, M. Di Renzo, J. De Rosny, M. Debbah, M.-S. Alouini, and R. Zhang, “Wireless communications through reconfigurable intelligent surfaces,” *IEEE Access*, vol. 7, pp. 116 753–116 773, 2019.
- [50] Y. Liu, X. Liu, X. Mu, T. Hou, J. Xu, M. Di Renzo, and N. Al-Dhahir, “Reconfigurable intelligent surfaces: Principles and opportunities,” *IEEE Communications Surveys & Tutorials*, vol. 23, no. 3, pp. 1546–1577, 2021.
- [51] M. Di Renzo, K. Ntontin, J. Song, F. H. Danufane, X. Qian, F. Lazarakis, J. De Rosny, D.-T. Phan-Huy, O. Simeone, R. Zhang, M. Debbah, G. Lerosey, M. Fink, S. Tretyakov, and S. Shamai, “Reconfigurable intelligent surfaces vs. relaying: Differences, similarities, and performance comparison,” *IEEE Open Journal of the Communications Society*, vol. 1, pp. 798–807, 2020.

- [52] M. A. ElMossallamy, H. Zhang, L. Song, K. G. Seddik, Z. Han, and G. Y. Li, “Reconfigurable intelligent surfaces for wireless communications: Principles, challenges, and opportunities,” *IEEE Transactions on Cognitive Communications and Networking*, vol. 6, no. 3, pp. 990–1002, 2020.
- [53] C. Huang, S. Hu, G. C. Alexandropoulos, A. Zappone, C. Yuen, R. Zhang, M. D. Renzo, and M. Debbah, “Holographic MIMO Surfaces for 6G wireless networks: Opportunities, challenges, and trends,” *IEEE Wireless Communications*, vol. 27, no. 5, pp. 118–125, 2020.
- [54] X. Yuan, Y.-J. A. Zhang, Y. Shi, W. Yan, and H. Liu, “Reconfigurable-intelligent-surface empowered wireless communications: Challenges and opportunities,” *IEEE Wireless Communications*, vol. 28, no. 2, pp. 136–143, 2021.
- [55] X. Pei, H. Yin, L. Tan, L. Cao, Z. Li, K. Wang, K. Zhang, and E. Björnson, “RIS-aided wireless communications: Prototyping, adaptive beamforming, and indoor/outdoor field trials,” *IEEE Transactions on Communications*, vol. 69, no. 12, pp. 8627–8640, 2021.
- [56] H. Yang, X. Chen, F. Yang, S. Xu, X. Cao, M. Li, and J. Gao, “Design of resistor-loaded reflectarray elements for both amplitude and phase control,” *IEEE Antennas and Wireless Propagation Letters*, vol. 16, pp. 1159–1162, 2017.
- [57] Q. Ma, G. D. Bai, H. B. Jing, C. Yang, L. Li, and T. J. Cui, “Smart metasurface with self-adaptively reprogrammable functions,” *Light: Science & Applications*, vol. 8, no. 1, p. 98, Oct. 2019. [Online]. Available: <https://doi.org/10.1038/s41377-019-0205-3>
- [58] S. Abeywickrama, R. Zhang, Q. Wu, and C. Yuen, “Intelligent reflecting surface: Practical phase shift model and beamforming optimization,” *IEEE Transactions on Communications*, vol. 68, no. 9, pp. 5849–5863, 2020.
- [59] T. J. Cui, M. Q. Qi, X. Wan, J. Zhao, and Q. Cheng, “Coding metamaterials, digital metamaterials and programmable metamaterials,” *Light: Science & Applications*, vol. 3, no. 10, pp. e218–e218, Oct. 2014.
- [60] Q. Wu and R. Zhang, “Beamforming optimization for intelligent reflecting surface with discrete phase shifts,” in *Proc. of IEEE International Conference on Acoustics, Speech and Signal Processing (ICASSP)*, 2019, pp. 7830–7833.
- [61] E. Basar, “Reconfigurable Intelligent Surface-Based Index Modulation: A New Beyond MIMO Paradigm for 6G,” *IEEE Transactions on Communications*, vol. 68, no. 5, pp. 3187–3196, 2020.
- [62] M. H. Khoshafa, T. M. N. Ngatched, M. H. Ahmed, and A. R. Ndjiongue, “Active reconfigurable intelligent surfaces-aided wireless communication system,” *IEEE Communications Letters*, vol. 25, no. 11, pp. 3699–3703, 2021.
- [63] R. Long, Y.-C. Liang, Y. Pei, and E. G. Larsson, “Active reconfigurable intelligent surface-aided wireless communications,” *IEEE Transactions on Wireless Communications*, vol. 20, no. 8, pp. 4962–4975, 2021.
- [64] G. Zhou, C. Pan, and H. Ren, “Active reconfigurable intelligent surface aided communication with partial CSI,” in *Proc. of 14th International Conference on Wireless Communications and Signal Processing (WCSP)*, 2022, pp. 1137–1143.

- [65] L. Dong and W. Yan, "Active reconfigurable intelligent surface (RIS) aided secure wireless transmission under a shared power source between transmitter and RIS," in *Proc. of 14th International Conference on Wireless Communications and Signal Processing (WCSP)*, 2022, pp. 996–1000.
- [66] G. C. Alexandropoulos and E. Vlachos, "A hardware architecture for reconfigurable intelligent surfaces with minimal active elements for explicit channel estimation," in *Proc. of IEEE International Conference on Acoustics, Speech and Signal Processing (ICASSP)*, 2020, pp. 9175–9179.
- [67] S. Tripathi, O. J. Pandey, L. R. Cenkeramaddi, and R. M. Hegde, "Optimal Active Elements Selection in RIS-Assisted Edge Networks for Improved QoS," in *Proc. of 12th IEEE Sensor Array and Multichannel Signal Processing Workshop (SAM)*, 2022, pp. 21–25.
- [68] E. Björnson, O. Özdogan, and E. G. Larsson, "Intelligent reflecting surface versus decode-and-forward: How large surfaces are needed to beat relaying?" *IEEE Wireless Communications Letters*, vol. 9, no. 2, pp. 244–248, 2020.
- [69] K. Zhi, C. Pan, H. Ren, and K. Wang, "Power scaling law analysis and phase shift optimization of RIS-Aided Massive MIMO Systems With Statistical CSI," *IEEE Transactions on Communications*, vol. 70, no. 5, pp. 3558–3574, 2022.
- [70] E. Björnson and L. Sanguinetti, "Power scaling laws and near-field behaviors of massive MIMO and intelligent reflecting surfaces," *IEEE Open Journal of the Communications Society*, vol. 1, pp. 1306–1324, 2020.
- [71] Q. Wu and R. Zhang, "Intelligent reflecting surface enhanced wireless network: Joint active and passive beamforming design," in *Proc. of IEEE Global Communications Conference (GLOBECOM)*, 2018, pp. 1–6.
- [72] J. Gao, C. Zhong, X. Chen, H. Lin, and Z. Zhang, "Unsupervised learning for passive beamforming," *IEEE Communications Letters*, vol. 24, no. 5, pp. 1052–1056, 2020.
- [73] Y. Song, M. R. A. Khandaker, F. Tariq, K.-K. Wong, and A. Toding, "Truly intelligent reflecting surface-aided secure communication using deep learning," in *Proc. of 93rd IEEE Vehicular Technology Conference (VTC2021-Spring)*, 2021, pp. 1–6.
- [74] S. Zhang and R. Zhang, "Capacity characterization for intelligent reflecting surface aided MIMO communication," *IEEE Journal on Selected Areas in Communications*, vol. 38, no. 8, pp. 1823–1838, 2020.
- [75] Z. Yigit, E. Basar, and I. Altunbas, "Low complexity adaptation for reconfigurable intelligent surface-based MIMO systems," *IEEE Communications Letters*, vol. 24, no. 12, pp. 2946–2950, 2020.
- [76] M. Jung, W. Saad, M. Debbah, and C. S. Hong, "On the optimality of reconfigurable intelligent surfaces (RISs): Passive beamforming, modulation, and resource allocation," *IEEE Transactions on Wireless Communications*, vol. 20, no. 7, pp. 4347–4363, 2021.
- [77] E. Ibrahim, R. Nilsson, and J. van de Beek, "Intelligent reflecting surfaces for MIMO Communications in LOS environments," in *Proc. of IEEE Wireless Communications and Networking Conference (WCNC)*, 2021, pp. 1–6.

- [78] O. Özdoğan, E. Björnson, and E. G. Larsson, "Using intelligent reflecting surfaces for rank improvement in MIMO communications," in *Proc. of IEEE International Conference on Acoustics, Speech and Signal Processing (ICASSP)*, 2020, pp. 9160–9164.
- [79] N. S. Perović, M. Di Renzo, and M. F. Flanagan, "Channel capacity optimization using reconfigurable intelligent surfaces in Indoor mmwave environments," in *Proc. of IEEE International Conference on Communications (ICC)*, 2020, pp. 1–7.
- [80] S. Sarp, H. Tang, and Y. Zhao, "Use of intelligent reflecting surfaces for and against wireless communication security," in *Proc. of 4th IEEE 5G World Forum (5GWF)*, 2021, pp. 374–377.
- [81] Z. Tang, T. Hou, Y. Liu, J. Zhang, and C. Zhong, "A novel design of RIS for enhancing the physical layer security for RIS-Aided NOMA networks," *IEEE Wireless Communications Letters*, vol. 10, no. 11, pp. 2398–2401, 2021.
- [82] Z. Tang, T. Hou, Y. Liu, J. Zhang, and L. Hanzo, "Physical layer security of intelligent reflective surface aided NOMA networks," *IEEE Transactions on Vehicular Technology*, vol. 71, no. 7, pp. 7821–7834, 2022.
- [83] Z. Huang, B. Zheng, and R. Zhang, "Transforming fading channel from fast to slow: IRS-assisted high-mobility communication," in *Proc. of IEEE International Conference on Communications*, 2021, pp. 1–6.
- [84] S. Zhou, W. Xu, K. Wang, M. Di Renzo, and M.-S. Alouini, "Spectral and energy efficiency of IRS-Assisted MISO communication with hardware impairments," *IEEE Wireless Communications Letters*, vol. 9, no. 9, pp. 1366–1369, 2020.
- [85] B. Yang, X. Cao, C. Huang, C. Yuen, L. Qian, and M. D. Renzo, "Intelligent spectrum learning for wireless networks with reconfigurable intelligent surfaces," *IEEE Transactions on Vehicular Technology*, vol. 70, no. 4, pp. 3920–3925, 2021.
- [86] P. Wang, J. Fang, X. Yuan, Z. Chen, and H. Li, "Intelligent reflecting surface-assisted millimeter wave communications: Joint active and passive precoding design," *IEEE Transactions on Vehicular Technology*, vol. 69, no. 12, pp. 14 960–14 973, 2020.
- [87] M. Jung, W. Saad, M. Debbah, and C. S. Hong, "Asymptotic optimality of reconfigurable intelligent surfaces: Passive beamforming and achievable rate," in *Proc. of IEEE International Conference on Communications (ICC)*, 2020, pp. 1–6.
- [88] W. Ni, X. Liu, Y. Liu, H. Tian, and Y. Chen, "Resource allocation for multi-cell IRS-Aided NOMA Networks," *IEEE Transactions on Wireless Communications*, vol. 20, no. 7, pp. 4253–4268, 2021.
- [89] W. Cai, R. Liu, M. Li, Y. Liu, Q. Wu, and Q. Liu, "IRS-Assisted multicell multiband systems: Practical reflection model and joint beamforming design," *IEEE Transactions on Communications*, vol. 70, no. 6, pp. 3897–3911, 2022.
- [90] H. Xie, J. Xu, and Y.-F. Liu, "Max-min fairness in IRS-aided multi-cell MISO systems via joint transmit and reflective beamforming," in *Proc. of IEEE International Conference on Communications (ICC)*, 2020, pp. 1–6.
- [91] L. You, J. Xiong, D. W. K. Ng, C. Yuen, W. Wang, and X. Gao, "Energy efficiency and spectral efficiency tradeoff in RIS-Aided Multiuser MIMO uplink transmission," *IEEE Transactions on Signal Processing*, vol. 69, pp. 1407–1421, 2021.

- [92] J. Tang, D. K. C. So, E. Alsusa, and K. A. Hamdi, "Resource efficiency: A new paradigm on energy efficiency and spectral efficiency tradeoff," *IEEE Transactions on Wireless Communications*, vol. 13, no. 8, pp. 4656–4669, 2014.
- [93] H. Yang, Z. Xiong, J. Zhao, D. Niyato, Q. Wu, H. V. Poor, and M. Tornatore, "Intelligent reflecting surface assisted anti-jamming communications: A fast reinforcement learning approach," *IEEE Transactions on Wireless Communications*, vol. 20, no. 3, pp. 1963–1974, 2021.
- [94] Z. Xiao, B. Gao, S. Liu, and L. Xiao, "Learning based power control for mmwave massive MIMO against jamming," in *Proc. of IEEE Global Communications Conference (GLOBECOM)*, 2018, pp. 1–6.
- [95] X. Yu, D. Xu, and R. Schober, "Enabling secure wireless communications via intelligent reflecting surfaces," in *Proc. of IEEE Global Communications Conference (GLOBECOM)*, 2019, pp. 1–6.
- [96] F. Oggier and B. Hassibi, "The secrecy capacity of the MIMO wiretap channel," *IEEE Transactions on Information Theory*, vol. 57, no. 8, pp. 4961–4972, 2011.
- [97] S. Asaad, Y. Wu, A. Berekhi, R. R. Müller, R. F. Schaefer, and H. V. Poor, "Secure active and passive beamforming in IRS-aided MIMO systems," *IEEE Transactions on Information Forensics and Security*, vol. 17, pp. 1300–1315, 2022.
- [98] H. Shen, W. Xu, S. Gong, Z. He, and C. Zhao, "Secrecy rate maximization for intelligent reflecting surface assisted multi-antenna communications," *IEEE Communications Letters*, vol. 23, no. 9, pp. 1488–1492, 2019.
- [99] M. Jian, G. C. Alexandropoulos, E. Basar, C. Huang, R. Liu, Y. Liu, and C. Yuen, "Reconfigurable intelligent surfaces for wireless communications: Overview of hardware designs, channel models, and estimation techniques," *Intelligent and Converged Networks*, vol. 3, no. 1, pp. 1–32, 2022.
- [100] Q.-U.-A. Nadeem, H. Alwazani, A. Kammoun, A. Chaaban, M. Debbah, and M.-S. Alouini, "Intelligent reflecting surface-assisted multi-user MISO communication: Channel estimation and beamforming design," *IEEE Open Journal of the Communications Society*, vol. 1, pp. 661–680, 2020.
- [101] D. Mishra and H. Johansson, "Channel estimation and low-complexity beamforming design for passive intelligent surface assisted MISO wireless energy transfer," in *Proc. of IEEE International Conference on Acoustics, Speech and Signal Processing (ICASSP)*, 2019, pp. 4659–4663.
- [102] Z. Wang, L. Liu, and S. Cui, "Channel estimation for intelligent reflecting surface assisted multiuser communications: Framework, algorithms, and analysis," *IEEE Transactions on Wireless Communications*, vol. 19, no. 10, pp. 6607–6620, 2020.
- [103] Z.-Q. He and X. Yuan, "Cascaded channel estimation for large intelligent metasurface assisted massive MIMO," *IEEE Wireless Communications Letters*, vol. 9, no. 2, pp. 210–214, 2020.
- [104] Y. Yang, B. Zheng, S. Zhang, and R. Zhang, "Intelligent reflecting surface meets OFDM: Protocol design and rate maximization," *IEEE Transactions on Communications*, vol. 68, no. 7, pp. 4522–4535, 2020.

- [105] T. L. Jensen and E. De Carvalho, "An optimal channel estimation scheme for intelligent reflecting surfaces based on a minimum variance unbiased estimator," in *Proc. of IEEE International Conference on Acoustics, Speech and Signal Processing (ICASSP)*, 2020, pp. 5000–5004.
- [106] P. Wang, J. Fang, H. Duan, and H. Li, "Compressed channel estimation for intelligent reflecting surface-assisted millimeter wave systems," *IEEE Signal Processing Letters*, vol. 27, pp. 905–909, 2020.
- [107] J. He, M. Leinonen, H. Wymeersch, and M. Juntti, "Channel estimation for RIS-Aided mmWave MIMO systems," in *Proc. of IEEE Global Communications Conference*, 2020, pp. 1–6.
- [108] G. T. de Araújo and A. L. F. de Almeida, "PARAFAC-based channel estimation for intelligent reflective surface assisted MIMO system," in *Proc. of 11th IEEE Sensor Array and Multichannel Signal Processing Workshop (SAM)*, 2020, pp. 1–5.
- [109] T. G. Kolda and B. W. Bader, "Tensor decompositions and applications," *SIAM review*, vol. 51, no. 3, pp. 455–500, 2009.
- [110] P. Comon, X. Luciani, and A. L. de Almeida, "Tensor decompositions, alternating least squares and other tales," *Journal of Chemometrics: A Journal of the Chemometrics Society*, vol. 23, no. 7-8, pp. 393–405, 2009.
- [111] A. L. F. de Almeida, G. Favier, J. da Costa, and J. C. M. Mota, "Overview of tensor decompositions with applications to communications," *Signals and images: advances and results in speech, estimation, compression, recognition, filtering, and processing*, pp. 325–356, 2016.
- [112] N. D. Sidiropoulos, L. De Lathauwer, X. Fu, K. Huang, E. E. Papalexakis, and C. Faloutsos, "Tensor decomposition for signal processing and machine learning," *IEEE Transactions on Signal Processing*, vol. 65, no. 13, pp. 3551–3582, 2017.
- [113] S. Gherekhloo, K. Ardah, A. L. F. de Almeida, and M. Haardt, "Tensor-based channel estimation and beamforming design for RIS-aided millimeter-wave MIMO systems," in *Proc. of 55th Asilomar Conf. on Signals, Systems, and Computers (Asilomar 2021)*, Nov. 2021.
- [114] L. Wei, C. Huang, G. C. Alexandropoulos, C. Yuen, Z. Zhang, and M. Debbah, "Channel estimation for RIS-empowered multi-user MISO wireless communications," *IEEE Transactions on Communications*, vol. 69, no. 6, pp. 4144–4157, 2021.
- [115] A. Albanese, F. Devoti, V. Sciancalepore, M. Di Renzo, and X. Costa-Pérez, "MARISA: A self-configuring metasurfaces absorption and reflection solution towards 6G," in *IEEE INFOCOM 2022 - IEEE Conference on Computer Communications*, 2022, pp. 250–259.
- [116] G. C. Alexandropoulos, N. Shlezinger, I. Alamzadeh, M. F. Imani, H. Zhang, and Y. C. Eldar, "Hybrid reconfigurable intelligent metasurfaces: Enabling simultaneous tunable reflections and sensing for 6G wireless communications," *IEEE Vehicular Technology Magazine*, vol. 19, no. 1, pp. 75–84, 2024.
- [117] W. Lu and M. Di Renzo, "Stochastic geometry modeling and system-level analysis & optimization of relay-aided downlink cellular networks," *IEEE Transactions on Communications*, vol. 63, no. 11, pp. 4063–4085, 2015.

- [118] T. S. Rappaport, Y. Xing, O. Kanhere, S. Ju, A. Madanayake, S. Mandal, A. Alkhateeb, and G. C. Trichopoulos, “Wireless communications and applications above 100 GHz: Opportunities and challenges for 6G and beyond,” *IEEE Access*, vol. 7, pp. 78 729–78 757, 2019.
- [119] T. Nakamura, S. Nagata, A. Benjebbour, Y. Kishiyama, T. Hai, S. Xiaodong, Y. Ning, and L. Nan, “Trends in small cell enhancements in LTE advanced,” *IEEE Communications Magazine*, vol. 51, no. 2, pp. 98–105, 2013.
- [120] C. Wang, X. Hou, A. Harada, S. Yasukawa, and H. Jiang, “HARQ Signalling Design for Dynamic TDD System,” in *Proc. of 80th IEEE Vehicular Technology Conference (VTC2014-Fall)*, 2014, pp. 1–5.
- [121] M. Di Renzo, A. Zappone, M. Debbah, M.-S. Alouini, C. Yuen, J. de Rosny, and S. Tretjakov, “Smart radio environments empowered by reconfigurable intelligent surfaces: How it works, state of research, and the road ahead,” *IEEE Journal on Selected Areas in Communications*, vol. 38, no. 11, pp. 2450–2525, 2020.
- [122] K. Ardah, G. Fodor, Y. C. B. Silva, W. C. Freitas, and F. R. P. Cavalcanti, “A novel cell reconfiguration technique for dynamic TDD wireless networks,” *IEEE Wireless Communications Letters*, vol. 7, no. 3, pp. 320–323, 2018.
- [123] A. A. M. Saleh and R. Valenzuela, “A statistical model for indoor multipath propagation,” *IEEE J. Sel. Areas Commun.*, vol. 5, no. 2, pp. 128–137, Feb. 1987.
- [124] G. Del Galdo, “Geometry-based channel modeling for multi-user MIMO systems and applications,” Ph.D. dissertation, Dept. Elect. Eng. Inf. Tech., Ilmenau University of Technology, Ilmenau, Germany, Jul. 2008.
- [125] G. Del Galdo, M. Haardt, and C. Schneider, “Geometry-based channel modelling of mimo channels in comparison with channel sounder measurements,” *Advances in Radio Science*, vol. 2, no. BC, pp. 117–126, 2005.
- [126] C.-Y. Hung and W.-H. Chung, “An improved MMSE-based MIMO detection using low-complexity constellation search,” in *Proc. of IEEE Globecom Workshops*, 2010, pp. 746–750.
- [127] G. H. Golub and C. F. Van Loan, *Matrix computation*. Johns Hopkins University Press, 2013.
- [128] S. Boyd, N. Parikh, E. Chu, B. Peleato, and J. Eckstein, “Distributed optimization and statistical learning via the alternating direction method of multipliers,” *Foundations and Trends in Machine Learning*, vol. 3, no. 1, pp. 1–122, 2011.
- [129] A. Tolli, H. Pennanen, and P. Komulainen, “SINR balancing with coordinated multi-cell transmission,” in *Proc. of IEEE Wireless Communications and Networking Conference*, 2009, pp. 1–6.
- [130] A. Wiesel, Y. Eldar, and S. Shamai, “Linear precoding via conic optimization for fixed MIMO receivers,” *IEEE Transactions on Signal Processing*, vol. 54, no. 1, pp. 161–176, 2006.
- [131] S. Boyd and L. Vandenberghe, *Convex optimization*. Cambridge Univ. Press, 2004.

- [132] H. Du, T. Ratnarajah, M. Pesavento, and C. B. Papadias, "Joint transceiver beamforming in MIMO cognitive radio network via second-order cone programming," *IEEE Transactions on Signal Processing*, vol. 60, no. 2, pp. 781–792, 2012.
- [133] D. Bertsekas and J. Tsitsiklis, *Parallel and distributed computation: Numerical methods*. Athena Scientific, 2015, tex.lccn: 2014070648. [Online]. Available: [https://books.google.de/books?id=n\\_Q5EAAAQBAJ](https://books.google.de/books?id=n_Q5EAAAQBAJ)
- [134] D. Bertsekas and W. Rheinboldt, *Constrained optimization and lagrange multiplier methods*, ser. Computer science and applied mathematics. Elsevier Science, 2014. [Online]. Available: <https://books.google.de/books?id=j6LiBQAAQBAJ>
- [135] M. Grant and S. Boyd. (2018, Dec.) CVX: MATLAB software for disciplined convex programming. [Online]. Available: <http://cvxr.com/cvx>
- [136] S. K. Joshi, M. Codreanu, and M. Latva-aho, "Distributed resource allocation for MISO downlink systems via the alternating direction method of multipliers," *EURASIP Journal on Wireless Communications and Networking*, vol. 2014, pp. 1–19, 2014.
- [137] M. Hong and Z. Luo, "On the linear convergence of the alternating direction method of multipliers," *Math. Program*, vol. 162, p. 165–199, 2017.
- [138] Y. Wang, W. Yin, and Z. J, "Global convergence of ADMM in nonconvex nonsmooth optimization," *J Sci Comput*, vol. 78, pp. 26–63, 2019.
- [139] A. M.-C. So, J. Zhang, and Y. Ye, "On approximating complex quadratic optimization problems via semidefinite programming relaxations," in *Integer Programming and Combinatorial Optimization*, M. Jünger and V. Kaibel, Eds. Berlin, Heidelberg: Springer Berlin Heidelberg, 2005, pp. 125–135.
- [140] Z.-Q. Luo, W.-K. Ma, A. M.-C. So, Y. Ye, and S. Zhang, "Semidefinite relaxation of quadratic optimization problems," *IEEE Signal Processing Magazine*, vol. 27, no. 3, pp. 20–34, 2010.
- [141] A. Ben-Tal and A. Nemirovski, *Lectures on Modern Convex Optimization*. Society for Industrial and Applied Mathematics, 2001. [Online]. Available: <https://epubs.siam.org/doi/abs/10.1137/1.9780898718829>
- [142] K.-Y. Wang, A. M.-C. So, T.-H. Chang, W.-K. Ma, and C.-Y. Chi, "Outage constrained robust transmit optimization for multiuser MISO downlinks: Tractable approximations by conic optimization," *IEEE Transactions on Signal Processing*, vol. 62, no. 21, pp. 5690–5705, 2014.
- [143] M. Sadek, A. Tarighat, and A. H. Sayed, "A leakage-based precoding scheme for downlink multi-user MIMO channels," *IEEE Transactions on Wireless Communications*, vol. 6, no. 5, pp. 1711–1721, 2007.
- [144] A. Tarighat, M. Sadek, and A. Sayed, "A multi user beamforming scheme for downlink MIMO channels based on maximizing signal-to-leakage ratios," in *Proc. of IEEE International Conference on Acoustics, Speech, and Signal Processing, 2005.*, vol. 3, 2005, pp. iii/1129–iii/1132 Vol. 3.
- [145] S. Park, J. Park, A. Yazdan, and R. W. Heath, "Exploiting spatial channel covariance for hybrid precoding in massive MIMO systems," *IEEE Transactions on Signal Processing*, vol. 65, no. 14, pp. 3818–3832, 2017.

- [146] R. Chen, J. Andrews, and R. Health, "Multiuser space-time block coded MIMO with downlink precoding," in *Proc. of IEEE International Conference on Communications (IEEE Cat. No.04CH37577)*, vol. 5, 2004, pp. 2689–2693 Vol.5.
- [147] J. Zhang, X. Hu, and C. Zhong, "Phase calibration for intelligent reflecting surfaces assisted millimeter wave communications," *IEEE Transactions on Signal Processing*, vol. 70, pp. 1026–1040, 2022.
- [148] G. Zhou, C. Pan, H. Ren, K. Wang, M. Di Renzo, and A. Nallanathan, "Robust beamforming design for intelligent reflecting surface aided MISO communication systems," *IEEE Wireless Communications Letters*, vol. 9, no. 10, pp. 1658–1662, 2020.
- [149] X. Yu, D. Xu, Y. Sun, D. W. K. Ng, and R. Schober, "Robust and secure wireless communications via intelligent reflecting surfaces," *IEEE Journal on Selected Areas in Communications*, vol. 38, no. 11, pp. 2637–2652, 2020.
- [150] T. A. Le, T. Van Chien, and M. Di Renzo, "Robust probabilistic-constrained optimization for IRS-aided MISO communication systems," *IEEE Wireless Communications Letters*, vol. 10, no. 1, pp. 1–5, 2021.
- [151] G. Zhou, C. Pan, H. Ren, K. Wang, and A. Nallanathan, "A framework of robust transmission design for IRS-aided MISO communications with imperfect cascaded channels," *IEEE Transactions on Signal Processing*, vol. 68, pp. 5092–5106, 2020.
- [152] G. Zhou, "Transmission design for reconfigurable intelligent surface-aided wireless systems," Ph.D. dissertation, School of Electronic Engineering and Computer Science, Queen Mary University of London, May. 2022.
- [153] I. Wajid, M. Pesavento, Y. C. Eldar, and D. Ciochina, "Robust downlink beamforming with partial channel state information for conventional and cognitive radio networks," *IEEE Transactions on Signal Processing*, vol. 61, no. 14, pp. 3656–3670, 2013.
- [154] S. Boyd, L. El Ghaoui, E. Feron, and V. Balakrishnan, *Linear Matrix Inequalities in System and Control Theory*. Society for Industrial and Applied Mathematics, 1994. [Online]. Available: <https://epubs.siam.org/doi/abs/10.1137/1.9781611970777>
- [155] B. Chalise and A. Czulwik, "Robust downlink beamforming based upon outage probability criterion [cellular radio]," in *Proc. of 60th IEEE Vehicular Technology Conference, 2004. VTC2004-Fall. 2004*, vol. 1, 2004, pp. 334–338 Vol. 1.
- [156] I. Bechar, "A Bernstein-type inequality for stochastic processes of quadratic forms of gaussian variables," *arXiv preprint arXiv:0909.3595*, 2009.
- [157] K.-Y. Wang, T.-H. Chang, W.-K. Ma, A. M.-C. So, and C.-Y. Chi, "Probabilistic SINR constrained robust transmit beamforming: A bernstein-type inequality based conservative approach," in *Proceedings of IEEE International Conference on Acoustics, Speech and Signal Processing (ICASSP)*, 2011, pp. 3080–3083.
- [158] J. G. Andrews, S. Buzzi, W. Choi, S. V. Hanly, A. Lozano, A. C. K. Soong, and J. C. Zhang, "What will 5G be?" *IEEE Journal on Selected Areas in Communications*, vol. 32, no. 6, pp. 1065–1082, 2014.
- [159] J. Zhang, E. Björnson, M. Matthaiou, D. W. K. Ng, H. Yang, and D. J. Love, "Prospective multiple antenna technologies for beyond 5G," *IEEE Journal on Selected Areas in Communications*, vol. 38, no. 8, pp. 1637–1660, 2020.

- [160] M. N. El Korso and M. Pesavento, "Performance analysis for near field source localization," in *2012 IEEE 7th Sensor Array and Multichannel Signal Processing Workshop (SAM)*, 2012, pp. 197–200.
- [161] K. T. Selvan and R. Janaswamy, "Fraunhofer and Fresnel distances : Unified derivation for aperture antennas." *IEEE Antennas and Propagation Magazine*, vol. 59, no. 4, pp. 12–15, 2017.
- [162] H. Zhang, N. Shlezinger, F. Guidi, D. Dardari, M. F. Imani, and Y. C. Eldar, "Beam focusing for near-field multiuser MIMO communications," *IEEE Transactions on Wireless Communications*, vol. 21, no. 9, pp. 7476–7490, 2022.
- [163] F. Guidi and D. Dardari, "Radio positioning with EM processing of the spherical wavefront," *IEEE Transactions on Wireless Communications*, vol. 20, no. 6, pp. 3571–3586, 2021.
- [164] K. Nishimori, N. Honma, T. Seki, and K. Hiraga, "On the transmission method for short-range MIMO communication," *IEEE Transactions on Vehicular Technology*, vol. 60, no. 3, pp. 1247–1251, 2011.
- [165] A. de Jesus Torres, L. Sanguinetti, and E. Björnson, "Near- and far-field communications with large intelligent surfaces," in *Proc. of 54th Asilomar Conference on Signals, Systems, and Computers*, 2020, pp. 564–568.
- [166] W. Tang, M. Z. Chen, X. Chen, J. Y. Dai, Y. Han, M. Di Renzo, Y. Zeng, S. Jin, Q. Cheng, and T. J. Cui, "Wireless communications with reconfigurable intelligent surface: Path loss modeling and experimental measurement," *IEEE Transactions on Wireless Communications*, vol. 20, no. 1, pp. 421–439, 2021.
- [167] H. Lu and Y. Zeng, "Near-field modeling and performance analysis for multi-user extremely large-scale MIMO communication," *IEEE Communications Letters*, vol. 26, no. 2, pp. 277–281, 2022.
- [168] R. Liu and K. Wu, "Antenna array for amplitude and phase specified near-field multifocus," *IEEE Transactions on Antennas and Propagation*, vol. 67, no. 5, pp. 3140–3150, 2019.
- [169] G. Del Galdo and M. Haardt, "Comparison of zero-forcing methods for downlink spatial multiplexing in realistic multi-user MIMO channels," in *Proc. of 59th IEEE Vehicular Technology Conference. VTC 2004-Spring (IEEE Cat. No.04CH37514)*, vol. 1, 2004, pp. 299–303 Vol.1.
- [170] S. A. Vorobyov, A. B. Gershman, and Z.-Q. Luo, "Robust adaptive beamforming using worst-case performance optimization: A solution to the signal mismatch problem," *IEEE Transactions on Signal Processing*, vol. 51, no. 2, pp. 313–324, 2003.
- [171] E. De Carvalho, A. Ali, A. Amiri, M. Angjelichinoski, and R. W. Heath, "Non-stationarities in extra-large-scale massive MIMO," *IEEE Wireless Communications*, vol. 27, no. 4, pp. 74–80, 2020.
- [172] M. Giordani, M. Polese, M. Mezzavilla, S. Rangan, and M. Zorzi, "Toward 6G networks: Use cases and technologies," *IEEE Communications Magazine*, vol. 58, no. 3, pp. 55–61, 2020.

- [173] M. Cui, Z. Wu, Y. Lu, X. Wei, and L. Dai, “Near-field MIMO communications for 6G: Fundamentals, challenges, potentials, and future directions,” *IEEE Communications Magazine*, vol. 61, no. 1, pp. 40–46, 2022.
- [174] Y. Rahmat-Samii, “Effects of deterministic surface distortions on reflector antenna performance,” *Annales des télécommunications*, vol. 40, pp. 350–360, 1985.
- [175] R. Sharp, M. Liao, J. Giriunas, J. Heighway, A. Lagin, and R. Steinbach, “Reflector surface distortion analysis techniques (thermal distortion analysis of antennas in space),” *NASA, Langley Research Center, Earth Science Geostationary Platform Technology*, 1989.
- [176] L. Landau, R. C. de Lamare, and M. Haardt, “Robust adaptive beamforming algorithms using low-complexity mismatch estimation,” in *Proc. of Statistical Signal Processing Workshop (SSP-2011)*, 2011, pp. 445–448.
- [177] R. Lorenz and S. Boyd, “Robust minimum variance beamforming,” *IEEE Transactions on Signal Processing*, vol. 53, no. 5, pp. 1684–1696, 2005.
- [178] D. Rakhimov, B. Peng, E. Jorswieck, and M. Haardt, “Robust reflective beamforming for non-terrestrial networks under thermal deformations,” in *Proc. of International Conference on Acoustics, Speech, and Signal Processing Workshops (ICASSPW-2023)*, 2023, pp. 1–5.
- [179] L. Yan-ping, J. Yan-min, and Z. Chao-zhu, “Robust near-field beamforming with worst case performance based on convex optimization,” in *Proc. of 5th Global Symposium on Millimeter-Waves*, 2012, pp. 608–611.
- [180] Y. Zheng, R. Goubran, and M. El-Tanany, “Robust near-field adaptive beamforming with distance discrimination,” *IEEE Transactions on Speech and Audio Processing*, vol. 12, no. 5, pp. 478–488, 2004.
- [181] H. Van Trees, *Optimum array processing*. John Wiley & Sons, Inc., 2001.
- [182] J. Li and P. Stoica, *Robust adaptive beamforming*. Wiley, 2005.
- [183] S. Gherekhloo, K. Ardah, G. C. Nwalozie, A. L. F. de Almeida, and M. Haardt, “An efficient channel training protocol for channel estimation in double RIS-aided MIMO systems,” in *Proc. of 32nd European Signal Processing Conference (EUSIPCO 2024)*, Lyon, France, August 2024.
- [184] J. Dattoro, *Convex Optimization and Euclidean Distance Geometry*. Meboo Publishing USA, California, 2012.
- [185] G. Calafiore and L. Ghaoui, *Optimization models*. Cambridge University Press, 2014.
- [186] Y. Nesterov and A. Nemirovskii, *Interior point polynomial time methods in convex programming*. SIAM, Philadelphia, 1994.
- [187] H. Hindi, “A tutorial on convex optimization,” in *Proc. of the American Control Conference*, 2004, pp. 3252–3265,.
- [188] N. Sidiropoulos, T. Davidson, and Z.-Q. Luo, “Transmit beamforming for physical-layer multicasting,” *IEEE Transactions on Signal Processing*, vol. 54, no. 6, pp. 2239–2251, 2006.

- [189] S. Zhang and Y. Xia, "Solving nonlinear optimization problems of real functions in complex variables by complex-valued iterative methods," *IEEE Transactions on Cybernetics*, vol. 48, no. 1, pp. 277–287, 2018.
- [190] W. Squire and G. Trapp, "Using complex variables to estimate derivatives of real functions," *SIAM Review*, vol. 40, no. 1, p. 110 – 112, 1998, cited by: 431; All Open Access, Green Open Access. [Online]. Available: <https://www.scopus.com/inward/record.uri?eid=2-s2.0-0032014469&doi=10.1137%2fS003614459631241X&partnerID=40&md5=b0a450adbf2004e5673c9e46993f26f8>
- [191] R. Remmert, *Theory of complex functions*. New York: Springer-Verlag, 1991.
- [192] D. Brandwood, "A complex gradient operator and its application in adaptive array theory," *IEE Proceedings F: Communications Radar and Signal Processing*, vol. 130, no. 1, p. 11 – 16, 1983, cited by: 654. [Online]. Available: <https://www.scopus.com/inward/record.uri?eid=2-s2.0-0020706753&doi=10.1049%2fip-f-1.1983.0003&partnerID=40&md5=60f1e7d6a739d7daea624aac7b3f02fa>
- [193] G. Costantini, R. Perfetti, and M. Todisco, "Quasi-lagrangian neural network for convex quadratic optimization," *IEEE Transactions on Neural Networks*, vol. 19, no. 10, pp. 1804–1809, 2008.
- [194] S. Zhang and A. Constantinides, "Lagrange programming neural networks," *IEEE Transactions on Circuits and Systems II: Analog and Digital Signal Processing*, vol. 39, no. 7, p. 441 – 452, 1992, cited by: 340. [Online]. Available: <https://www.scopus.com/inward/record.uri?eid=2-s2.0-0026897309&doi=10.1109%2f82.160169&partnerID=40&md5=866e0a58b6eb345d3e3f85142621aedc>
- [195] I. Jolliffe, *Principal component analysis*. Springer, 2011.

## ERKLÄRUNG

Die vorliegende Arbeit habe ich selbstständig ohne Benutzung anderer als der angegebenen Quellen angefertigt. Alle Stellen, die wörtlich oder sinngemäß aus veröffentlichten Quellen entnommen wurden, sind als solche kenntlich gemacht. Die Arbeit ist in gleicher oder ähnlicher Form oder auszugsweise im Rahmen einer oder anderer Prüfungen noch nicht vorgelegt worden.

Ilmenau, den 20. August 2024

Gerald Chetachi Nwalozie